Bioanalysis of eukaryotic organelles

Chad P. Satori[1], **Michelle M. Henderson**[1], **Elyse A. Krautkramer**[1], **Vratislav Kostal**[2,3], **Mark M. Distefano**[1], and **Edgar A. Arriaga**[1,*]

[1]Department of Chemistry, University of Minnesota, Twin Cities, Minneapolis, MN, USA, 55455

[2]Tescan, Libusina trida 21, Brno, 623 00, Czech Republic

[3]Institute of Analytical Chemistry ASCR, Veveri 97, Brno, 602 00, Czech Republic

1. Introduction

The function of biological cells is intimately associated with their internal organization, in which multiple subcellular structures have specialized roles. Such subcellular structures hold the secrets to normal cellular function, progression of disease, and the universe of interactions among biomolecules that define life. Initially observed in unicellular organisms, these subcellular structures were termed organelles because of the parallel to the organ/body relationship in multicellular organisms. Currently, the term "organelle" loosely describes a confined subcellular environment of any cell in which specific functions occur. Thus, organelles comprise large protein complexes (e.g. signalosomes), large protein-RNA complexes (e.g. ribosomes), and membrane bound structures (e.g. mitochondria). The interest in subcellular organization continues to increase as new biological functions, unique molecular features, and therapeutic potential continue being discovered. This interest has fueled recent advances in the bioanalysis of organelles reviewed here.

Because of their diversity in general architecture, taxonomical origin, and function, the approaches and methodologies to investigate organelles are not unique. From an analytical perspective, prokaryotic organelles, biomolecular complexes (membrane-less and non-membranous organelles) and membrane bound structures all require different strategies, which would be impossible to cover in a single review.

Based on the relevance of membrane bound eukaryotic organelles in recent key biomedical discoveries, we focus this review on these organelle types (Table 1). They include: subcellular structures bound by a single lipid layer (e.g., lipid droplets), by single phospholipid bilayer (e.g., lysosomes) or a double phospholipid bilayer (e.g. autophagosomes); it also includes membranous structures with complex topologies (e.g., Golgi). This review excludes all prokaryotic organelles as well as eukaryotic membrane-less and non-membranous organelles. The interested reader on these organelle types will find several relevant references in Table 2.

The membranes of organelles are natural boundaries to processes occurring within the respective organelles. As a consequence, bioanalysis of such organelles enables measurements and observations on composition, biochemistry, and function associated with subcellular processes. Clearly, bulk studies of cell lysates that contain organelle mixtures or when organelles are not clearly identified in imaging-based studies cannot provide the detailed information of subcellular processes. Thus, organelle analysis enables a more specific description of the molecular, biochemical, and physiological processes associated

*Corresponding Author;arriaga@umn.edu.

with diseases, embryonic development, tissue differentiation, organism aging, disease treatments, and organism response to pathogens. Subcellular analysis is also a valuable component in species or tissue comparisons, is instrumental in the development of many novel tools and assays, and its use is leading to many advances in biotechnology.

This review highlights the role that organelle analysis has played in understanding biology. In defining this, we took into consideration the types of organelles that have been of interest in recent reports, other reviews dealing with topics related to subcellular analysis, and the time period covered by such reviews. Table 1 lists important features of organelles that are the subject of recent subcellular analysis reports and that are reviewed here. Because subcellular isolation procedures based on centrifugation are included in the majority of subcellular analysis methods published to date, we chose not to describe details on centrifugation that are used in many of the reports reviewed here.

Another consideration used to define the scope of this review was previous reviews related to subcellular analysis that were published on sub-themes such as the technologies used to analyze isolated organelles[90] or prepare subcellular fractions for proteomic analysis.[91] For the interested reader, Table 2 compiles topical, specialized reviews that were published recently. We also published a review in 2005 assessing the impact of individual organelle analysis in biology, which covered work done prior to that year.[86] To avoid overlap, this current review focuses on advances that have occurred since 2006.

2. History of subcellular analysis

The history of subcellular analysis (Figure 1) began with the discovery of the nucleus in cod and salmon red blood cells by microscopist Antonie Van Leeuwenhoek in 1682.[92] Franz Bauer rediscovered the nucleus in the 1800s. The meaning and significance of the organelle that Van Leeuwenhoek and Bauer discovered were not purposefully investigated for over 150 years from van Leeuwenhoek's original work. In 1833, botanist Robert Brown in orchid cells again identified the nucleus. He identified and coined the term nucleus and his work led to additional studies observing the nucleus in multiple cell types and determining its function in cell division.[94] Another organelle discovered in the 1800s was the mitochondrion. Mitochondria were first discovered using microscopy in the 1850s by Rudolph Albert von Kolliker and were not described again until the 1890s when Richard Altman published his discovery of the "bioblast" (mitochondria) in his book *Die Elementarorganism*. Carl Benda coined the term mitochondria in 1898. The function of mitochondria would not be proposed until the 1910s when Kingbury suggested that mitochondria participated in cell respiration.[95]

In addition to the nucleus and mitochondria, other organelles were first discovered with microscopy. The Golgi apparatus was discovered in the 1890s by Camillo Golgi when he described an "internal reticular apparatus".[96] Andreas Schimper named chloroplasts following their observation in the 1890s.[97] Transmission electron microscopy was first used to observe the subcellular structure of cells in the 1940s and its use led to the discovery of the endoplasmic reticulum (ER) by Albert Claude in that same period.[98] Peroxisomes were first observed by Johannes Rhodin in the 1950s, also using transmission electron microscopy.[94] In addition to organelle discovery, the first reports describing organelle-organelle interactions were also based on transmission electron microscopy. The first report of that phenomenon we could locate occurred in the late 1960s when Sue Ellen Frederick and Eldon H. Newcomb used transmission electron microscopy to observe interactions between storage vacuoles and mitochondria or chloroplasts.[99]

A new era of subcellular discoveries began with the use of cellular fractionation by centrifugation. Differential centrifugation was developed by Albert Claude in the 1940s to

determine the distribution of enzymes within the cell. The Claude lab separated rat and guinea p ig liver fractions into a "large granule fraction" containing mitochondria, a "microsome" fraction containing particulates, and the "supernate" which contained particulates that could not be centrifuged.[100] Differential centrifugation was extended by Claude, George Hogeboom, Walter Schneider, and George Palade who used the technique to enrich mitochondria-containing fractions.[101]

Christian de Duve first discovered lysosomes in 1955. He observed that in rat liver cell fractions prepared by centrifugation, fractions contained overlapping activities of multiple enzymes including acid phosphatase. Acid phosphatase activity was found to be the most abundant in the mitochondria and homogenate fractions. After refrigerated storage of the fractions for further analysis, reanalysis of the fractions indicated acid phosphatase activity had *increased*, a surprising result since they were expected to decrease due to storage. These results suggested that the acid phosphatase enzymes were contained within a membrane-bound body that had likely deteriorated during storage. The body was concluded to be a new type of organelle, the lysosome.[102] By optimizing his centrifugation strategy, de Duve also isolated the lysosome fraction. Alex Novikoff obtained the first e lectron m icrographs of lysosome-enriched fractions shortly thereafter with acid phosphatase used as a marker. De Duve later discovered peroxisomes using a combination of enzymatic analysis of uricase activity and centrifugation fractionation performed in a manner similar to that employed for the study of lysosomes.[103] A closely related organelle to the lysosome, the endosome, was first observed in the 1970s by Ralph M. Steinman using transmission electron microscopy.[104] The role and function of endosomes were first proposed by Ari Helenius, Ira Mellman, Doris Wall, and Ann Hubbard.[105]

To use microscopy to visualize organelles, organelle-specific stains and probes had to first be developed and optimized. This technique originated with the use of haematoxylin to observe nuclei in the 1860s by Franz Bohmer.[106] A few decades later, in the 1900s, Leonor Michaelis used the stain Janus Green B to observe mitochondria in living cells.[107] In the 1930s, W.H. Lewis observed Neutral Red-stained vacuoles present in cultured cells from the chicken heart and embryo.[108] Reports on the subcellular localization of synthetic dyes observed by fluorescence microscopy appeared in the 1960s. In that decade, Boris Rotman and Ben W. Papermaster studied the subcellular distribution of fluorescein,[109] Elliott Robbins and Phillip Marcus observed the intracellular accumulation of acridine orange,[110] and Guido Marinetti investigated that of rhodamine B.[111]

The simultaneous analysis of organelles, beginning in 1915, has proved to be a powerful tool for observing interacting organelles, minimizing experiment duration, and for tracking organelle functions in response to specific conditions, such as osmotic stress.[112] The introduction of transmission electron microscopy allowed for visualization of organelles. The first image of organelles was captured in 1945 by Keith Porter, Albert Claude, and Ernest Fullam from chicken embryo cells.[98] This image also contained the first simultaneous detection of many organelle types such as the nucleus with Golgi and the nucleus with mitochondria. Many organelles were subsequently observed with transmission electron microscopy including the endoplasmic reticulum,[113] Golgi,[114] and lysosomes.[115] The cristae structure of mitochondria was also first observed using transmission electron microscopy.[116]

The use of organelle-specific dyes to enhance visualization by microscopy was first discussed by D. Wittekind[117] who described in his review the simultaneous detection of the Golgi, nuclei and acidic vacuoles using acridine orange for the first two and basic dyes for the latter. Simultaneous organelle detection using fluorescence detection could not be performed prior to technical advances made by Michael R. Loken, David R. Parks, and

Leonard A. Herzenberg, who demonstrated the use of a single excitation wavelength to visualize two fluorophores in instrumentation unrelated to microscopy.[118] The first simultaneous colocalization of proteins was demonstrated in baby hamster kidney cells with immunofluorescence by the Goldman lab in 1985.[119] It was n ot until 1 993 that the first simultaneous fluorescent organelle detection appeared.[120] Hyman M. Schipper, Soriba Cisse, and Paul A. Walton investigated the colocalization of peroxisomes with the Golgi, ER, and lysosomes using immunofluorescence and f luorescent dyes in a strocytes.

The next critical advance in organelle visualization was the development and use of fluorescent proteins. In 1962, green fluorescent protein (GFP) was first isolated and characterized from the *A. victoria* jellyfish by Osamu Shimomura.[121] Cloning and insertion of the GFP gene into an organism occurred three decades later by Martin Chalfie and Roger Tsien.[122] Use of GFP as a marker became attractive because its gene encoded all information necessary to express the protein in an organism and to generate a fusion protein that included GFP as the fluorescent moiety. Modern recombinant DNA technologies allowed researchers to select a given protein, link its gene to that encoding green fluorescent protein, and express the resulting fusion protein. When appended to a protein specific to an organelle, GFP could be used to track specific organelles. GFP was first used to tag nuclei in mammalian cells by creating fusion proteins of two different nuclear glucocorticoid receptors in the 1980s.[123] GFP-tagged organelles appeared in plants in the 1990s, first in the chloroplasts,[124] then in the ER,[125] and the nucleus.[124] Since then, fluorescent protein research and development has focused on the creation of proteins with distinct excitation and emission maxima, optimized FRET pairs, and environmental sensitivity to pH and redox potential (see 3.2.). Several reviews have been published on the subject of GFPs and their applications alone.[31–35]

A new perspective on subcellular analysis began with the introduction of proteomics. In addition to assessing organelle function through visualization techniques such as microscopy, the ability to define an organelle's contents (e.g. proteins) could be helpful for probing function and physiological effects. The first application of proteomics was accomplished via gel electrophoresis. Patricia O'Farrell, Howard Goodman, and Patrick O'Farrell in 1977 used electrophoresis to analyze a wide range of proteins.[126] An issue of *Electrophoresis* in 1997 reported the first 2D gel electrophoretic s eparations of proteins specific to enriched organelle fractions.[127] These papers described the analysis of enriched fractions of endosomes,[128] Golgi,[129] late endosomes, e arly endosomes, E R-derived material,[130] plasma membrane,[131] and phagosomes.[132] In addition, bands were excised f or HPLC identification of enriched Golgi p roteins[133] and for nanoelectrospray tandem mass spectrometry identification of enriched phagosome proteins.[132]

The importance of mass spectrometry-based (MS-based) proteomics in subcellular profiling and quantification in the analysis of complex samples was realized soon after the development of electrospray ionization (ESI)[134] and matrix-assisted laser desorption/ionization (MALDI)[135] to volatilize and ionize large biomolecules. In 1997, the Yates lab analyzed soluble proteins in the periplasmic space of *E. Coli*.[136] Following concentration and collection of the proteins, SDS-PAGE fractionation identified 159 bands and electrospray ionization tandem mass spectrometry identified 80 proteins. In 2000, the Klaas J. van Wijk lab reported the use of MALDI-TOF mass spectrometry and ESI-tandem mass spectrometry to analyze the proteome of the chloroplast.[137] Proteins in enriched organelle fractions were separated by 2D gel electrophoresis (isoelectric focusing followed by SDS-PAGE), select protein spots were digested, and analyzed by peptide mass fingerprinting. Of the 400 spots analyzed with MALDI-TOF MS, 20 were also analyzed with ESI-MS/MS and 55 were analyzed via N-terminal Edman degradation-based sequencing. A total of 61 proteins were identified and 58 of those were classified by function (e.g. growth,

transcription, etc.). In 2001, the Ferdinand Hucho lab reported the nuclear envelope proteome analyzed by MALDI-TOF mass spectrometry.[138] Shortly after, Taylor *et al.* extensively characterized the human heart mitochondrial proteome utilizing metrizamide and sucrose gradients for purification prior to MALDI-mass spectrometry analysis.[139]

The concepts of metabolomics and lipidomics were coined in 1998 and 2003, respectively, in response to the appearance of large data sets of either metabolites or lipids defining changes associated with a given genotype or phenotype.[57,140] However, investigation of the metabolomic composition of organelles was actually performed prior to the emergence of the "metabolomics" terminology. R.R. Bensley and N.L. Hoerr investigated the total composition of "fatty substances" in enriched mitochondria fraction from guinea pig and rabbit liver mitochondria in 1934.[141] The authors found 43.6% of fatty substances, primarily glycerides, i n the enriched m itochondria and investigated the presence of lecithin and cephalin. C laude in vestigated the phospholipid composition of subcellular f ractions of rat lymphoid cells in 1944 and found the phospholipid composition of lipids from mitochondria to be 75–80% using elemental analysis.[142] In 1956, George Palade and Phillip Siekevitz studied the composition of microsomes and described their RNA and phospholipid phosphorous contents.[143] In the 1964, the George Rouser laboratory analyzed multiple lipids from bovine heart mitochondria using column chromatography coupled with thin layered chromatography.[144] In 1970, Grunwald determined the composition of sterols (such as glycosides, esters, cholesterol and campesterol) in organelle fractions from tobacco leaves using gas chromatography.[145] Excellent reviews were written by Fleischer and Rouser who focused on lipidomics studies from the 1960s[146] and W.C. McMurray on metabolomic and lipidomics studies from the late 1960s and early 1970s.[147]

The first reports of mass spectrometry being used for subcellular lipidomics appeared in 1984 and 1985 by Richard W. Gross who analyzed mitochondria and plasma membrane lipids from canine cardiac cells with HPLC separation and gas chromatography coupled to mass spectrometry.[148] Samples were enriched and analyzed with xenon fast atom bombardment. In the early 1990s, mass spectrometric methods utilizing ESI were introduced for the study of lipids. The Lowell Ericsson lab demonstrated that positive and negative electrospray ionization could be used with tandem mass spectrometry to analyze glycerophospholipids and ceramides.[149] These studies showed ESI could be used for biological lipids. This was followed shortly thereafter, if not concurrently, by Xianlin Han and Richard Gross who studied the plasma membrane phospholipids of human erythrocyte cells using ESI mass spectrometry with a triple quadrupole instrument.[150]

The development of subcellular organelle analysis techniques has continued in the late 1990s and 2000s with a focus on the study of individual organelles and b iological heterogeneity. In 1998, the Richard Zare laboratory examined single dense core vesicles from the gastropod mollusk *A. californica.*[151] Using optical trapping, individual organelles were introduced into a capillary where they were labeled and separated using capillary electrophoresis. While taurine was identified as a major component of the organelles, the organelles manifested a high level of heterogeneity. Single organelle analysis was continued by Jonathan Sweedler and coworkers who, in 2000, analyzed the same sample but with MALDI-TOF-mass spectrometry in order to identify bioactive peptides.[152] The Edgar Arriaga group developed single organelle detection techniques to separate and study tens to thousands of organelles.[153] The first of those papers was published in 2001 which featured the detection of mitochondria with capillary electrophoresis coupled to laser induced fluorescence detection (CE-LIF).[153a] Since then, that technique has been applied to monitor organelle properties such as pH of acidic organelles,[154] xenobiotic content,[155] and accumulation of reactive oxygen species (ROS) in mitochondria.[156]

The literature reviewed in the following sections focuses on labeling and imaging of organelles (3.), the "omics" of organelles (4.), the interactions of organelles (5.), the physiological effects of organelles (6.), and organelle heterogeneity (7.). The vast majority of the work described below builds upon the key discoveries outlined in this section. Needless to say, these discoveries will continue gaining historical importance and relevance as the interest in organelle analysis expands, new roles of organelles in biological function are elucidated and the classification of organelle into types and subpopulations continues to evolve.

3. Identification of subcellular compartments

Important advances in subcellular analysis include improvements in the specific id entification and classification of organelle types either by microscopy or biochemical assays that rely on specific markers for various organelle types.

3.1. Recently developed organelle-specific enzymatic assays

Enzyme assays have been used for characterization of organelle types in enriched fractions, both qualitatively and quantitatively. In general, these assays are performed following prior fractionation of whole cell homogenate and then the enzymatic assay is applied to each of the fractions. Common enzymatic assays include: succinate dehydrogenase assay for mitochondria,[157] acid phosphatase assay for lysosomes,[158] and the catalase assay for peroxisomes.[159] Table 3 provides a more detailed list of enzymatic assays specific for various organelle types.

The reader is directed to two reviews recently published for the correct use and interpretation of macroautophagy assays involving autophagosomes. These reviews discuss western blotting-based assays, fluorescence detection-based assays such as flow-activated cell sorting, and enzyme assays. Recent development of new organelle-specific enzyme assays used to characterize organelle activity has been sparse. Recently there have been two reports that focus on chloroplast and lysosome specific enzyme assays.

The lysosome-specific dipeptidyl peptidase 1 (DPP1) has been associated with normal cell growth and tissue differentiation. Because increased DPP1 expression has been associated with pulmonary disease, inhibitors for DPP1 are attractive therapeutic agents. A new assay that can be used for identification of lysosomes in fractions via DPP1 and to investigate the potential inhibitors of normal lysosomal DPP1 activity was recently reported.[169] This assay is based on the ability of DPP1 to cleave either amino-methyl-coumarin or amino-fluoro-coumarin dipeptide conjugates. Upon cleavage, these fluorophores are no longer quenched and their fluorescence increases. The optimal conditions for the assay (100μM per 30,000 cells with a 1h treatment time) were determined in the human acute monocytic leukemia cells, which have high DPP1 activity. As expected, the assay did not show an increase in f luorescence w hen analyzing DPP1 knockdown mouse bone marrow cells. The assay was also suitable for the identification of DPP1 inhibitors.

An improved high throughput assay focused on the activity of the chloroplast specific enzyme chlorophyllase was developed.[163] Previously used both chlorophyllase substrate and reaction product formed had similar UV-Vis absorption profiles, which required extraction of the product. The new assay does not require any extraction procedure because the new substrate, chlorophyll para-nitrophenyl ester is not colored, making it possible to monitor directly the enzymatic activity through the formation of the yellow-colored product para-nitrophenoxide in the reaction mixture. The results of the new assay were equivalent to those obtained with the extraction-based enzyme assay and had similar responses to changes in pH and the presence of metal ions such as $Mg+2$ and $Fe+2$. Without a need for an extraction

step, the new assay has much higher throughput and the potential to measure changes in photosynthesis of chloroplasts in response to stress.

3.2. Molecular Markers

3.2.1. Antibodies—The use of antibodies is not a new technology for subcellular analysis. Antibodies are largely used to visualize the localization of subcellular components. They can also be applied to studies in which changes in localization, quantity, or protein expression are being tracked. Their continued development and tuning for more sensitive analyses is important for the advancement of the field. However, limitations exist: (i) Many antibodies for subcellular proteins of organelles are not currently commercially available. (ii) The development of sensitive and specific antibodies, especially monoclonal antibodies, which are suitable for subcellular analysis, can be lengthy. (iii) It can be difficult to confirm an antibody's specificity to its desired target. (iv) Antibody labeling protocols are often time consuming. With these problems in mind, any advances in techniques that save time, allow for the use of smaller quantities of the antibody, or help verify antibody binding location or specificity are important for subcellular analysis.

Significant strides have been made in the creation of a human subcellular atlas of antibody location.[175] Using 466 proteins, three human cell lines and confocal microscopy, it was possible to accurately assign subcellular locations to 80% of the proteins studied. This method marks the first time that confocal microscopy was applied to a large-scale antibody-based protein localization study.

Quantum dots (QD) are nanoparticles made of semiconductor materials like cadmium or zinc that can be tuned to emit fluorescence light after their excitation. Quantum dots are excellent means of visualization because they have narrower fluorescence excitation and emission profiles allowing for less spectral cross-talk and low photobleaching.[176] In the past, their use as intracellular delivery markers has been limited. Because of their size, which is often less than 50 nm in diameter, their limited surface area does not leave sufficient room for their derivatization with either cell penetrating tags or intracellular target tags. A new method to overcome this limitation has been developed. Quantum dots were conjugated to antibodies and encapsulated within a biodegradable polymer delivery vehicle.[177] The encapsulating polymers can be engineered with cell-or organelle-penetrating moieties that cannot be directly connected to the quantum dots. In this study, the polymers were targeted to the late endosome and made use of the acidic nature of this compartment. Here, the cell-penetrating tags were protonated, rendering them uncharged and unable to exit the vacuoles. After protonation, the quantum dots accumulated at the periphery of the acidic vesicle, destabilized the membrane, and broke free inside the cell. This delivered its contents to the subcellular space of the human glioblastoma cell line used in these experiments. From there, the antibody-quantum dot conjugates could proceed to their targeted subcellular location. The pH sensitivity of the polymer capsule could be tuned to control the release of the QD-antibody conjugates, and the biodegradable poly(D,L-lactide-*co*-glycolide) polymers did not interfere with subcellular labeling.

Also in the category of multifunctional immunolabeling, an orange light emitting polymer dot has been developed for subcellular imaging.[178] Semiconducting polymer dots are highly applicable to intracellular studies due to their high quantum yields and narrow spectral e mission range allowing for simultaneous detection of multiple signals. To demonstrate the utility of this probe for subcellular analysis, dots were conjugated to streptavidin and used as reporters of biotinylated primary anti-α-tubulin antibodies. The streptavidin biotin binding resulted in the labeling of α-tubulin in the microtubules. Using other biotinylated primary antibodies, the polymer dot could be targeted anywhere within the cell.

As mentioned earlier, a significant limitation to wider application of antibodies is their cost. Therefore, any advances that can make more efficient use of small quantities of antibodies are essential. Related to this, a microarray capable of transferring 360 primary antibodies to permeabilized cells was used to monitor in parallel the presence of antibody targets (proteins) in the nucleus of nine different human breast cancer cell lines.[179] Each spot in the microarray possessed a unique antibody. Nine different permeabilized breast cancer cell lines were compared. When brought into contact with the cells, the primary antibodies dissociated from their microarray membranes and tagged a corresponding patch of cells. This resulted in a grid-like series of labeled spots o n the layer of cells. Each antibody bound to its antigen was visualized with a fluorescent secondary antibody. In addition, each cell was abeled with 4',6-diamidino-2-phenylindole, (DAPI), which defined the nuclear region. Because the positions of each antibody spot on the original antibody delivery membrane was known and correspond to a cell patch, overlap of immunofluorescence and the DAPI stain was used to identify protein targets localized to the nucleus. In this study, only one protein, Cyclin B1, showed different subcellular localization in different cell lines (nuclear-localized, non-nuclear-localized, and both). While this strategy was employed to examine breast cancer cell lines, this method should be applicable to any cell line as well as any organelles for which there exist known fluorescent markers. The ability to use a single sample of cells and just 50ng of each antibody per microarray is an advantage over other techniques.

Also related to cost-effectiveness, a chip-based method was developed to generate a higher throughput immunofluorescence assay to study lysosomal storage disorders.[180] The new method used a microfluidic device with normal rat kidney cells cultured on-chip to monitor changes in expression and distribution of LAMP1 and LC3 proteins and fifteen different lysosomal storage disorder-induced cell lines with confocal microscopy. The method used only a few hundred cells and 100 times less antibody than other methods. The method allows for much faster parameter optimization for assays and could be applied in other subcellular antibody studies.

Another recent publication describes a method for antibody localization and binding verification to 65 specific human proteins that localize to a wide range of organelles including mitochondria and the nucleus.[181] While current methods rely heavily on Western blots and immunofluorescence techniques, such as confocal fluorescence microscopy, to identify reliable antibodies for subcellular targets, this study verified that siRNA technology could also be used with automated microscopy to verify protein localization and verify antibody binding. Human osteosarcoma cells were treated with siRNA specific to the genes that corresponded to the antibody's suspected protein target. When the gene was silenced by the siRNA, fluorescence from antibody binding was reduced, but only if the antibody was specific to the down-regulated protein of interest. Different antibodies exhibiting similar subcellular localization patterns could be distinguished by down regulation of their specific protein target. As studies of the human genome atlas progresses, it is likely that there will be increasing focus on using molecular biology techniques such as the one described here to verify antibody binding. Verifying localization is particularly useful in the absence of pre-existing information on binding and localization.

3.2.2. Synthetic probes—Synthetic probes include small molecule structures or nanometer size species, that, when applied *in vitro* or *in vivo*, can be targeted almost anywhere in the cell. Reports in this category include probes designed to trace endocytic organelles,[182] label the c ytoskeleton,[183] measure pH in specific subcellular environments,[184] or detect divalent cations in a subcellular selective fashion.[185] Table 4 provides the structures and excitation and emission wavelengths for fluorescent dyes described in this section.

Advantages specific to synthetic probes over other probes are numerous. Because of their synthetic nature, they are often more cost effective and available in higher quantities than antibodies. Their usage in cells does not require transformation or other genetic manipulation unlike the fluorescent proteins, which allows for their application in studies where genetic techniques are not possible or practical. Synthetic probes can also have a wide range of reporting and targeting features built into them, making them versatile research tools. The development of probes, however, can be a difficult process and they can lack the specificity of antibody or GFP methods.

One significant area of advancement has been the creation of probes that exhibit increased photostability. A hyperbranched conjugated polyelectrolyte-phalloidin dye conjugate (HPCE phalloidin) has been developed and applied to the visualization of F-actin filaments in the cytoskeleton of a human cervical cancer cell line (Figure 2).[183] Using HPCE phalloidin required only a short incubation time for intracellular visualization and was not susceptible to p hotobleaching due to its reliance on the in herent fluorescent properties of the conjugated polyelectrolyte. Compared to a traditional non-GFP method for actin visualization, cell permeabilization and incubation with the organic probe Alexa Flour 488-phalloidin, the HPCE-phalloidin showed better cellular uptake without cell permeabilization as well as increased photostability. As the first study to look at functionalized hyperbranched polymers as intracellular delivery v ehicles, this work opens the f ield for further development of conjugated polyelectrolytes as subcellular tools.

Also related to increased photostability, nerve growth factor-quantum dot bioconjugates were developed. The nerve growth factor probes were tested for their ability to image and track receptor mediated endocytosis in the nerve growth factor sensitive rat adrenal medulla cell line.[176] The report further showed that bioconjugates were suitable to observe small-scale kinetics such as those of single-cell endocytic events.

In the report of another photostable probe, a new intracellular staining calixarene macrocycle capable of targeting to any organelle was developed (Figure 3).[182] In a follow up paper, the fluorescently labeled probe, a cationic calixarene (NBDCalAm), was used for subcellular analysis.[186] In Chinese hamster ovary and human cervical cancer cells, it showed uniform distribution across acidic vesicles and eventual localization in lysosomes with little to no nonspecific intracellular s taining. Acidic vesicle localization was accomplished thanks to the aniline moieties present in the calixarene. Molecules possessing weakly basic amines such as anilines were regularly shown to uptake into acidic vesicles. Fluorescence was passed onto daughter cells after division, and was more stable compared to other commercial lysosome dyes in two ways. First, fluorescence did not decrease when cells were transferred from the staining solution to dye-free medium, and secondly, fluorescence intensity showed very little decrease even after stained cells were stored for 72 hours in dye-free media. Both of these details demonstrate significant advances and they offer exciting possibilities for fluorescence studies over longer periods of time that are not possible with LysoTracker Red, the most commonly used probe for endocytic organelles.

Detection of ion concentrations in subcellular compartments is important to the understanding of subcellular dynamics. Inorganic ions like Mg^{+2}, Ca^{+2}, Fe^{+2}, and Fe^{+3} are integral to cellular functions such as membrane transport. A particularly bothersome problem in assessing subcellular ion concentrations is their ubiquitous presence throughout the subcellular location. In these situations, selectivity of the probes is critical to their successful application. The selective detection of Mg^{+2} in mitochondria based on the novel fluorescent probe, KMG-301, is a key advance in understanding mitochondrial Mg^{+2} dynamics.[185a] While a positively charged rhodamine backbone was used both as the fluorophore and to target these probes to the mitochondria, a charged beta diketone moiety

was used to selectively chelate the Mg^{+2}. This structure demonstrated a photoinduced electron transfer response in the presence of Mg^{+2}. Unlike other commercially available Mg^{+2} probes that also detect Ca^{+2}, KMG-301 was 100% Mg^{+2} selective in rat adrenal medulla and hippocampal neurons. This offers a tremendous advantage because calcium concentrations vary widely throughout the cytosol and are known to be higher and more variable within mitochondria. This probe may also find applicability in understanding the role of Mg^{+2} in altered mitochondrial function (e.g. ATP production and membrane potential) in neuronal diseases such as Alzheimer's and Parkinson's disease.

Iron is another ion that is im portant to cellular function. For example, free or "labile" iron in endosomes and lysosomes is of high biological interest because of their potential role in the generation of reactive oxygen species (ROS) and their associated potential for subcellular oxidative damage and toxicity.[187] While most methods of iron detection in cells are known to disrupt the existing levels of labile iron, a new, less-invasive method for its quantification in the endosomes and lysosomes has been developed.[185b] Two probes, both containing the moiety fluorescein labeled 3-hydroxypyridin-4-one, were developed along the lines of previous compounds used to measure cytosolic iron concentrations and delivered to bone marrow derived macrophage cells excised from the fibula and tibula of immature mice. Because the lysosomes and endosomes have an acidic interior, basic moieties were protonated, thereby trapping and enriching the resulting positively charged probes within these organelles. These probes showed high sensitivity towards changes in the concentrations of labile iron in the lysosomes and responded as expected to changes induced by the addition of clinically relevant lysosomal iron chelators. Non-specific subcellular localization was not observed. Sensitivity to other metals was not tested. The further development of these probes will likely be useful for examining cellular iron trafficking mechanisms in a wide variety of cellular disease states and in specific organelle environments.

The ability to accurately determine pH in subcellular spaces is another critical analysis that can be accomplished with the use of fluorescent probes. A near IR-excitable probe for pH determination in the vicinity of breast cancer tumors has been developed.[184] The probe was developed by conjugating a pH-sensitive cyanine dye to a cyclic arginine-glycine-aspartic acid peptide targeting Rvβ3 integrin, a protein involved in angiogenesis that is highly expressed in endothelial tumors. This probe was fluorescent at a pH of below 5, with a pK_a of 4.7 and was demonstrated as ideal for use in pH determination of tumor lysosomes and endosomes in a human melanoma cell line and a human breast cancer cell line. The fact that this probe is excited by near IR light makes it applicable for subcutaneous or even deep tissue detection or investigation of tumors. Additionally, it fluoresces better with decreasing pH, a feature not observed in other probes designed for similar purposes. With these factors in mind, this molecule would not only be a powerful tool for basic research but also a potential diagnostic tool for primary and metastatic tumors.

3.2.3. Bioengineered proteins—The GFP gene and its homologues encoding proteins of multiple fluorescent colors are commonly appended to the genes of natural proteins. Expression of this concatenated gene results in expression of protein constructs that are fluorescent and that typically retain the subcellular localization properties of the original protein. Because most of the subcellular localization signals are found at the N-terminus, the original protein and the fluorescent protein genes are fused so that the fluorescent protein moiety is located at the C-terminus of the original protein. These genes are delivered encoded in plasmids or viral vectors into the cells under study. Fluorescent proteins can be expressed in cell culture as fusion proteins that target specific organelles. Organelles containing such fluorescent proteins are distinguished as discrete, fluorescent punctuates. These punctuates can be detected to study properties of organelles using techniques such as

fluorescence confocal microscopy. Because GFP and GFP-related fusion proteins are relatively stable, and because recently developed proteins have minimal cytotoxicity, observation of fluorescent proteins has provided tremendous insight into the dynamics of subcellular regions that cannot be easily obtained with antibodies or other synthetic probes. There are potential problems with this technique, however, that do not exist when using other fluorescent techniques. One major issue is the potential for GFP-protein conjugates to exhibit altered subcellular localization or function. Expressing the GFP-protein conjugate may alter the original localization or function of the unlabeled protein. Fortunately, bioengineering of the genetic codes usually provides alternatives to avoid such detrimental effects. On the other hand, one major limitation that cannot be easily overcome is the labeling of n on-transformable tissues with GFP-protein conjugates.

Multiple fluorescent proteins constructs with unique spectral emission profiles continue to appear and are being applied for the purpose of sub-cellular co-localization studies.[188] Table 5 lists the currently available fluorescent proteins along with their excitation and emission wavelengths.[188]

Figure 4 depicts the different colors that have been developed with fluorescent fusion proteins.[188] Fine-tuning the molecular architecture of these proteins allows for large stokes shifts and reduced tendency to oligomerization, which may affect subcellular localization.

A common fluorescent protein, DsRed, has an excitation maximum of 558 nm and an emission maximum of 583 nm, with stokes shift of 25 nm. This protein tends to aggregate and oligomerize. Introduction of a point mutation within the monomer interface of a recently discovered tetrameric red-emitting protein eqFP611 similar to DsRed resulted in the formation of a dimeric version of eqFP611.[189] With an excitation maximum of 559 nm and an emission maximum of 611 nm, this protein exhibits a larger Stokes shift (52 nm). Compared to DsRed, eqFP611 exhibits reduced tendency to aggregate and oligomerize.

Ca^{+2} signaling in the Golgi is critical for maintaining protein traffic and the organelle's architecture. However, monitoring Ca^{+2} in the various regions of the Golgi has been a major challenge to date. A new genetically encoded FRET-based Ca^{+2} probe that is more specific for the *trans*-Golgi than other Golgi regions, Go-D1cpv, has been developed.[190] The probe was designed to have two GFP variants, CFP and YFP, joined through a linker to a calmodulin-binding domain. It was then expressed as a fusion protein in human cervical cancer cells bound to a known *trans*-Golgi protein sialyl-transferase I. Ca^{+2} concentrations were monitored by the analysis of the ratio of CFP/YRP fluorescence. While expressing this probe, researchers used a combination of RNAi and gene knockout animals to investigate four important calcium-related channels and receptors known to be unique to the Golgi: sarco-endoplasmic reticulum Ca^{+2} ATPase (SERCA) and secretory pathway Ca^{+2} ATPase1 (SPCA1) channels, ryanodine receptors (RyRs), and inositol 1,4,5-trisphosphate receptors. Using this probe, it was determined that the *trans*-Golgi relies entirely on SPCA1 channels for Ca^{+2} uptake and it showed no evidence of the involvement of inositol 1,4,5-trisphosphate receptors. However, RyRs receptors were observed instead of the inositol 1,4,5-trisphosphate receptors in cardiac myocytes. The use of this probe in future studies may provide detailed information about the calcium traffic through the Golgi in various disease states.

A tandem fusion protein, mRFP-GFP-LC3 targeting autophagosomes and autolysosomes was also recently described.[191] Both RFP and GFP have been used separately in LC3 constructs to track LC3 localization from the autophagosome to the autolysosome. While RFP retained its fluorescence in both organelles, GFP lost its fluorescence in the environment of the mature autolysosome. Thus, mRFP-GFP-LC3 allowed for a more

efficient screening of vesicle fusion of mouse embryonic fibroblast and human cervical cancer cells during autophagosome maturation than earlier visualization techniques such as transmission electron microscopy. In mRFP-GFP-LC3, the attenuation of the GFP fluorescence marked the end of the maturation process, while RFP tracked the autophagosome as it matured into an autolysosome.

Uses of redox sensitive green-fluorescent proteins (roGFPs) have recently exploded as a source of information on the redox status of various intracellular compartments by their conjugation with proteins of known subcellular localization. These proteins were first developed in 2004.[192] Since then, their application as intracellular compartment redox indicators had been widely applied to many facets of intracellular investigation. A defining characteristic of roGFPs is the inclusion of two cysteine residues on the exposed surface of the expressed protein that modulated the fluorescence of the protein based on whether or not a disulfide bridge has formed between them.

A significant application for these roGFPs was developed by coupling known roGFPs to glutaredoxin, a glutathione redox state sensor, and peroxidase 1, an intracellular peroxide sensor, both known to be expressed exclusively in the mitochondria.[193] Previous intra-organelle redox studies relied on indirect evidence to quantify redox species and effects. Many relied on disruptive methods to collect measurements that could alter the end result of an experiment. The roGFPs developed in this report provided a solution by not requiring invasive methods for detection and offering a direct readout of the redox state within the organelle. This was due to their conjugation to the very enzymes, in this case glutaredoxin, which process the redox species in question. Coupling of the roGFPs in this manner allowed for a more specific quantification of the redox effector by giving instantaneous measurements on the redox state of the mitochondrial compartment as the conjugated enzymes broke down the redox effector in question. Initial studies were conducted in human cervical cancer cells, but the approach was used successfully to examine differing redox potentials at subcellular resolutions across *D. melanogaster*. This probe allowed simultaneous monitoring of the cytosol and the mitochondria in various tissues over time and under varying conditions, including age and drug treatment.

A new way of monitoring protein release from mitochondria during apoptosis using modified bioluminescent proteins has also been developed.[194] The bioluminescent protein *R. reniformis* luciferase emits light when its substrate coelenterazine is converted into coelenteramide. For the purpose of this study, luciferase was split into two domains, the C-terminus and the N-terminus. Each half of the complete protein was engineered to contain half of a split intein sequence. This strategy is depicted in Figure 5.[194] One of the domains was expressed in the cytosol (C-Rluc) and the other (N-Rluc) was fused to the N-terminus of Smac/DIABLO, a mitochondrial protein. The fusion protein did not affect Smac/DIABLO subcellular localization to the mitochondria in human breast cancer cells. Upon treatment with staurosporine to induce apoptosis, the intein-N-Rluc-Smac/DIABLO construct was released from the mitochondria, which resulted in association with the C-Rluc-intein construct present in the cytosol. The association of the two halves of the split intein pieces resulted in the assembly of an intact functional intein that in turn caused excision of the intein and ligation of the two Rluc fragments to produce catalytically activated luciferase. The subsequent conversion of coelenterazine to coelenteramide produced light that can be easily and quickly measured with a photodetector in which the intensity is indicative of the amount of Smac/Diablo protein released from mitochondria.

3.3. Morphology

3.3.1. Fluorescence microscopy—Confocal microscopy has become a routine tool for investigating subcellular organization, organelle networks, and organelle dynamics in

cellular and tissue samples.[195] Confocal microscopy can also provide spatial 3D information by optical sectioning the specimen. The limitation of using confocal microscopy to characterize organelle properties is its resolution. The resolution along the Z-axis is ~500 nm and decreases with the increasing thickness of the observed specimen due to the necessity of using objectives with longer working distances. This typically limits the 3D observations to mostly flat, single layer specimens.[196] The lateral resolution of conventional confocal microscopes is restricted by the diffraction limit defined by the point-spread function. This value is ~200 nm and is above the size of many subcellular organelles. This prevents its use in the analysis of subcellular features, dynamics, and intra-organelle localization.

Resolution limitations have been overcome by the recent development of a variety of super-resolution fluorescence imaging techniques that break the diffraction barrier. Use of these techniques has uncovered new insights of subcellular organization of cells and tissue with subdiffraction resolution.[197] Relevant techniques are stimulated emission depletion (STED) microscopy,[198] photoactivation localization microscopy (PALM),[199] fluorescence photoactivation localization microscopy (FPALM),[200] and stochastic optical reconstruction microscopy (STORM).[201] Table 6 summarizes recent papers using STED and PALM.

STED microscopy uses co-illumination of the sample with two overlapping laser beams: an excitation beam and a red-shifted doughnut-shaped de-excitation beam (STED beam).[203] Figure 6 depicts the strategy involved. While the excitation beam excites the target fluorophores in the center, the STED beam de-excites all molecules on the outside edge of the excitation spot through the process of stimulated emission. As a result, only molecules that appear directly inside the clipped, excitation spot are excited. Using the STED approach, spatial resolution approaching ~50 nm can be achieved, allowing clear visualization of small organelle features. A comparison with a standard confocal microscopy is shown in Figure 7 depicting the clear intracellular network of citrine-labeled microtubules.

FPALM and STORM are based on repetitive activation, individual detection, and deactivation of a sparse subset of fluorescence molecules of interest. Figure 8 shows the schematic involved in FPALM. When individually visualized molecules are separated by a distance that exceeds the Abbe diffraction limit (~250 nm), their positions can be determined after deconvoluting their point spread functions with nanometer resolution (~ 20 nm).[215] This process of localization is repeated many times with different subsets of molecules in stochastic manner to create a super-resolution image. The dramatic improvement in the resolution obtained with FPALM over TIRF microscopy c an be s een in Figure 9.[199] The fluorophores used vary according to the techniques. PALM and FPALM typically use genetically encoded, photoactive fluorescence proteins.[216] STORM utilizes pairs of photoswitchable organic fluorophores, which are usually bound to antibodies to a specific target of interest.[217]

Since the super-resolution techniques permit observations of suborganellar details, they have been extensively used for studying organelle morphology, e.g. mitochondria. [197b,206,212] Heterogeneity in mitochondria cristae morphology was visualized w ith STED microscopy.[207] The focal volume was decreased by 3 orders of magnitude when compared to confocal microscopy. This decrease was sufficient to image details of the distribution of F1F0ATPase in the mitochondrial inner membrane. The same approach was used to resolve and observe 28-nm cytochrome c clusters and VDAC 1 clusters ranging from 33 to 88 nm in size in isolated c ardiac mitochondria.[205] A similar approach was used to investigate distributions of mtDNA nucleoids.[218] Using STED microscopy, 60% more nucleoids per cell were detected compared to the confocal microscopy, suggesting that the nucleoid

contained on average ~1.4 mtDNA copies. These findings confirm previous theories that many nucleoids must contain only a single mtDNA copy.[218] On the contrary, larger variation in nucleoids size and shape, high packing density, close association with inner membrane, and wrapping around cristae was found by PALM imaging in 3T3 Switch mouse fibroblasts.[209] Super-resolution techniques were used for imaging dynamic processes in living cells including real-time tracking and localization (TALM) of single TOM20 and ATP synthase complexes in mitochondria[210] and ER-network dynamics using STED microscopy.[203]

Most organelles have a dynamic, three-dimensional (3D) organization inside the cell, which is tightly connected to their physiological functions. Due to this, a single 2D image inherently limits the information acquired about the distribution of a particular property within the organelle. The concept of super-resolution imaging has been extended to 3D observations achieving 50–150 nm z-axis resolution. 3D STORM was used to observe mitochondrial network in green monkey epithelial cells,[197b] microtubule network,[219] clathrin-coated pits in live cells[220] and mapping neural connectivity in brain.[221]

Interferometric PALM was applied to visualize 3D opography of both orsal and ventral plasma membranes with the same precision as atomic force microscopy and other endomembrane systems such as integrin receptors within ER.[204] A temporal focusing PALM, which utilizes two-photon activation and one-photon excitation approach, was used to produce 3D images of mitochondrial network with 50 nm lateral resolution over an z-range up to 10 μm.[211]

3.3.2. Electron microscopy—Transmission electron microscopy has become a routine analytical tool complementary to light microscopy, particularly in studies concerning organelle morphology and structure.[222] The modern transmission electron microscopes produce a 2D image of a thin sample section with resolution of about ~1–2 nm. Transmission electron microscopy is fundamentally limited from capturing the n atural 3D organization of a cellular structure.[223] Thin sectioning of the sample and observing each slice one by one thus producing a 3D image has been the only method of choice. The drawback of this approach is limiting the resolution along the Z-axis to twice the thickness of the sample slice, approx. to 60–150 nm.

Transmission electron tomography (ET) is overcoming this limitation. ET uses a similar principle as other tomographic imaging methods commonly used in medical imaging, such as magnetic resonance imaging (MRI) or X-ray computed axial tomography (CAT).[224] In ET, multiple 2D projections of the same specimen are collected from different angles during a constant tilting of the sample around the axis, which is perpendicular to the imaged plane. The acquired projections are then computationally reconstructed to produce 3D tomograms of the sample with the Z-axis resolution up to 5–10 nm.[225] This results in a more than a 30 – 60 fold improvement in the resolution compared to the traditional serial thin sectioning and more than 500 fold improvement than that of confocal fluorescence microscopy.[223]

ET was used for the first time to study the mitochondria ultrastructure and organization in the calyx of Held, which is the largest nerve terminal in the central nervous system.[226] The ET observations revealed new features of mitochondrial cristae in the calyx-cytoskeletal anchoring suggesting new aspects of nerve terminal organization. This is shown in Figure 10.[226] A 3D topological complexity of membrane systems in mouse myocardium was investigated using ET providing new insights in the linkage b etween mitochondrial outer membranes, sarcoplasmic reticulum and their role in controlling cardiac calcium dynamics.[227]

Focused ion beam/scanning electron microscopy (FIB/SEM), sometimes called dual beam or ion abrasion electron microscopy, is another approach for providing 3D structural details of cells and tissue.[228] This technique integrates a scanning electron beam and a second, focused ion beam (FIB) in the same microscope. The ion beam, typically using accelerated, ion scan, performs site-specific removal (or milling) of thin layers of resin-embedded or cryo-prepared samples. By serial imaging of the abraded surfaces with SEM, one can produce a 3D map of the particular region of the sample. The subcellular architecture of membrane bound organelles in melanoma cells was imaged using FIB/SEM.[229] The quantitative 3D imaging indicated that mitochondria occupied about 5% of the volume in human melanoma cells with a mean width of individual mitochondrion equal to 450 nm. The images showed tethers between mitochondria and ER.

Similarly, FIB/SEM was used to study 3D morphology of ER and nuclei connectivity in frozen epithelial cells.[230] The study showed that ER morphology varies with its distance to the nucleus (ER was tubular at the cell periphery and sheet-like close to the nucleus). Another 3D map showed a continuous lipid path from the ER to the plasma membrane and to the nucleus bringing new insights into the ER trafficking routes. FIB/SEM analysis revealed heterogeneity in mitochondrial size and morphology in liver of mouse with methylmalonic acidemia.[231] Volumetric reconstruction of 2D slices found that mitochondria in mutated tissue had higher surface-to-area volume ratio and more hyperbolic curvature compared to the mitochondria observed in normal tissue. FIB/SEM has been also routinely used for the preparation of TEM lamellas thinner than 100 nm with the ability to target specific areas for the analysis.[232] It is likely that in the future, electron tomographies and reconstruction t echniques will be invaluable tools to describe three dimensional in tracellular organization, organelle morphology, and function.

3.3.3. Atomic force microscopy—Atomic force microscopy (AFM) uses a nanometer-sized probe (typically a silicon or silicon-nitride cantilever tip with a radius of 2 – 20 nm), which scans across the imaged area of the specimen. The intensity profile of interactions between the AFM tip with the sample surface is recorded and provides a three-dimensional image of the sample topography with a sub-nanometer resolution. In addition to topography, the AFM probe can also measure mechanical properties of the surface (e.g. rigidity). These features have made AFM an important method in the studies of cell adhesion, endocytosis, cell-to-cell interactions and cytoskeletal organization. New advances of AFM in these applications have been recently reviewed.[38–41] AFM can also be used to study behavior of organelles inside the cells.

One example is a mapping of fluid-filled vacuolar organelles inside the human umbilical vein endothelial cells.[233] In this approach, cells were fixed with f ormaldehyde and scanned with A FM. The vacuolar structures were localized as membrane areas with reduced stiffness, since these areas were depleted of otherwise formaldehyde hardened cytoskeletal and c ytosolic proteins.

Another application used an AFM tip as a nano-mechanical tool to study the response of the mitochondrial network in the cell when an external mechanical force was applied.[234] Mitochondria were fluorescently labeled and continuously observed using a fluorescence microscope. After the indentation of the outer membrane with the AFM tip, the changes of mitochondrial morphology were observed in real-time. The perturbations of mitochondrial morphology were detected as far as 26 μm from the point source, stressing the complexity of cytoskeleton interaction with mitochondria inside the cell.

AFM can be used to analyze isolated organelles without the need of any sample preparation. As an example, the process of mitochondrial swelling during the myocardial infarction was

studied by AFM.[235] Compared to normal mitochondria, the ischemic mitochondria were much larger in size, were stiffer, and had significantly decreased adhesion force. These results suggest that ischemic stress plays an important role in the induction of mitochondrial swelling.

Similarly, morphology, mechanical properties, and aggregation kinetics of synaptic vesicles were analyzed with AFM.[236] Two types of synaptic vesicles isolated from rat forebrains were used in the study: native synaptic vesicles associated with synapsin I (USVs) and synapsin-depleted vesicles (SSVs). USVs were found to be highly monodisperse with a spherical shape and sizes ranging between 25–45 nm. On the contrary, USVs were generally larger (between 40 to 70 nm) and more heterogeneous, indicating that synapsin acts as an important stabilizing agent that prevents clustering of synaptic vesicles.

The potential of characterization of mechanical properties of the organelle surface was also demonstrated by studying the age-related surface changes of isolated human retinal pigment epithelium (RPE) melanosomes.[237] Force-indentation measurements r evealed that older melanosomes had stronger tip-surface adhesion than the young ones. This adhesion was attributed to the age-related increase of lipofuscin content o n the melanosome surface.

AFM imaging was also applied as a complementary technique to TEM to obtain high-resolution ultrastructural images of various organelles in resin embedded tissue cross-sections[238] and cryo-sectioned biological specimens.[239]

4. Organelle Composition

The combination of subcellular fractionation with 'omic' technologies has become powerful resource to characterize and catalogue the various subcellular environments in a cell. This section focuses on the capabilities of proteomics, metabolomics and lipidomics, which currently p rovide the most comprehensive descriptions of molecular compositions of subcellular environments to date. The power of these 'omic' studies is clearly dependent on advances in the separation of complex molecular mixtures using various HPLC formats, suitable interfaces for volatilization and ionization of biomolecules, and the sensitivity, speed, and resolution of modern mass spectrometry systems. Combined with powerful bioinformatics resources and comprehensive databases, this hardware sets the stage for biomolecular discovery or 'omics' studies.

4.1. Organelle Proteomics

Successful proteomics requires suitable strategies for subcellular fractionation, separation and purification of peptides and proteins, high-sensitivity, high-resolution, high accuracy mass spectrometers, and a robust bioinformatics pipeline. Powerful mass spectrometers typically used in proteomic studies have included triple quadrupoles,[240] Orbitrap instrumentation,[241] and triple quadrupole time-of-flight (TOF)[242] instrumentation.[172,243] This section will review advances on various aspects of proteomic strategies and methodologies that are relevant to organelle proteomics, beginning with a general overview of bioinformatics and sample preparation.

Developments in bioinformatics and databases have been essential to the success of MS-based proteomic studies. Search algorithms such as Mascot,[244] SEQUEST,[245] X! Tandem,[246] OMSSA (open mass spectrometry search algorithm),[247] and ProteinPilot,[248] and databases such as the International Protein Index (IPI)[249] and UniProt[250] were all developed for the searching of proteomic data. Scaffold was developed to filter and process these search results.[251] ExPASy (the Expert Protein Analysis System),[252] is a service that provides access to a variety of databases and tools for proteomic analysis. MaxQuant[253] and

the more recent Andromeda[254] software were developed and made publicly available specifically to take advantage of high mass accuracy data of SILAC samples obtained from Orbitrap mass spectrometers.[241,255] Another tool developed for quantitation of proteomic data is Census[256] (based on the previously developed RelEx program),[257] which is capable of analyzing both high-and low-resolution spectra from single MS and tandem mass spectrometry (MS/MS) data.

Because subcellular proteomics requires association of proteomes with a specific organelle type, organelles must be isolated with high purity, acquired in the presence of other organelles, or distributed through continuous density gradients. As described in the sections below, selection of one of these preparation procedures depends on the goals of the study. Proteomic studies using high purity organelles provide a reliable catalogue of their proteome and subcellular information on specific target proteins. If obtaining a high-purity sample of organelles is impractical, the desired organelle may be analyzed in the presence of other organelles. Proteomic profiling addresses this issue as it includes the analysis of multiple subcellular proteomic profiles in organelle mixtures.

4.1.1. Technology and bioinformatics advances—Selection of spectrometers as well as pre-fractionation strategies best suited for proteomic studies is not always straightforward. One recent study utilizing mass spectrometers with differing scan rates compared affinity purified samples with bait proteins known to be from different subcellular components (cytosol, cytoplasm, mitochondrion, and nucleus) to study the benefit of a multidimensional s eparation of these affinity purified samples coupled to liquid-chromatography (LC)-MS/MS.[258] It was found that although t his multidimensional approach d id result in an in crease in spectral counts with the LTQ-Orbitrap XL (Thermo Scientific) (very important when spectral counting is used for quantitation), the slight increase in protein identifications did not outweigh practical considerations such as the drawback of increased sample preparation and mass spectrometer time. The authors also compared these results with 1-D and various 2-D results obtained from an even older generation mass spectrometer, the LTQ (Thermo Scientific). Acquisition of 1 high-resolution MS scan followed by 3 data-dependent MS/MS scans of the most abundant ions with a mass accuracy of <2 ppm was used for the LTQ-Orbitrap. The TripleTOF 5600 (AB Sciex) was used with a faster scan rate of 20 data-dependent MS/MS scans per one MS (1.3 second duty cycle). The TripleTOF 5600 operates via information-dependent acquisition (IDA) with high resolution (>30,000) and high mass accuracy (<3 ppm), and the speed in which it can acquire MS/MS spectra allows for the development of a LC-MS/MS platform capable of identifying approximately twice the number of peptides and proteins over a currently optimized LC-MS/MS method (FTMS).[242] The high duty cycle of the TripleTOF allowed for the analysis of the affinity purified samples (without the multidimensional separation step) with similar benefits but without the drawbacks of increased sample preparation and MS time. More specifically, the authors found that the increased scan rate of new mass spectrometers allowed for similar results to be obtained as on older mass spectrometers (i.e. LTQ-Orbitrap XL) using a multidimensional separation. Therefore, in the case of these affinity-purified samples, a faster scan rate allows for more identification in the absence of a multidimensional separation used w ith more complex samples.

Venable *et al.* specifically evaluated the LTQ-Orbitrap in regards to high mass accuracy data from both standards and complex tissue samples.[259] The authors searched the tandem mass spectra using SEQUEST[245] and Census[256] for quantitative analysis of N15-labeled rat synaptosomes. The quality of the spectra obtained from this study was compared to spectra obtained from an LTQ, and were of consistently higher quality. Using this data, the authors were able to determine that 149 synaptic proteins change in abundance (82 upregulated and 67 downregulated) during development.

Advances in preparation of proteomic samples have also allowed for high-sensitivity detection of proteins at the subcellular level. Zhou *et al.* simplified and employed a previously developed proteomic reactor[260] to characterize the ER and Golgi microsomal membrane proteomes of rat hepatic cells (McA-RH7777).[261] The reactor itself consists of a 1.5-mL Eppendorf tube in which strong cation exchange beads are added to a lysed, acidified, and delipidated membrane pellet. It is then able to preconcentrate, derivatize, and support enzymatic digestion of the proteins. Because of its format, it is compatible with benchtop centrifuges, making its utility much more widely applicable (i.e. "centrifugal proteomic reactor"). Using this reactor, it was possible to identify 945 plasma membrane proteins and 955 microsomal membrane proteins (which consist of the ER nd Golgi), of which >800 of these proteins could not be detected by the standard in-gel digestion technique.

Significant bioinformatics and database advances have improved the analysis of subcellular proteomic data. Databases that include previously reported subcellular localization of proteins and software that predicts subcellular location is of great value when it is not feasible to perform a comprehensive subcellular proteomic study. Table 7 lists other databases and predictors that include information such as gene ontology (GO) classifiers and subcellular p redictions based o n amino acid sequences. For example, iLoc-Euk can predict single or multiple subcellular locations of eukaryotic proteins.[263] It would be in error to ssign a single organelle location to these proteins. The GO formulations included incorporate hit probabilities and an accumulation-layer scale was included (which is helpful for proteins with multiple subcellular locations). If there is no GO information a vailable for a specific protein, the formulations are used for a higher-level subcellular localization p rediction. Similarly, Scott *et al.* claim that they can predict the fluidity of the nucleolar membrane by allowing for different classes of nucleolar proteins (i.e. nucleolar-enriched, nucleolar-nucleoplasmic, nucleolar-cytoplasmic, or non-nucleolar).[266] In developing this model, the authors took into consideration the frequency of specific amino acids, the predicted presence of signal peptides, mitochondrial targeting peptides, nucleolar localization sequences, e xpression data, GO annotations, and subcellular localization annotations of other protein interactors. This predictor was evaluated and demonstrated accuracy of 0.85 on an independent literature-based test set and demonstrated accuracy of 0.74 with a large independent quantitative proteomics dataset.

4.1.2. Purification strategies—The importance of high-purity organelles in subcellular proteomic analyses cannot be understated. Cross-contamination between organelle fractions can lead to incorrect protein localization assignments and therefore, mistaken biological conclusions or hypotheses.[267] In addition, it is vital to see protein translocations in response to treatments/stressors or in signaling pathways. Biological insight can be acquired by quantitative determination of protein translocation and abundance changes in many organelles and membrane fractions simultaneously.[268]

Complex, tissue-specific differential centrifugation methods (size-based) have been extensively developed to obtain pure organelle fractions (based on Western blot confirmation) for MS-based analyses.[269] Developments in density gradient centrifugation have also improved organelle purity for MS analysis, which can separate organelles based on differing densities.[270] Use of fluorescence-assisted organelle sorting (FAOS) to enrich dense-core secretory granules has recently been reported.[271] Frit-inlet asymmetrical flow field-flow fractionation (FI-AFlFFF) has also been used to size-fractionate and purify a specific type of organelle (i.e. mitochondria) from rat liver for MS/MS analysis.[272] This differs from traditional flow field-flow fractionation in that sample elaxation (equilibrium conditions before the sample components are separated) is achieved hydrodynamically via the frit inlet so that there is no momentary stop of the migration flow. More specifically, the

sample is able to quickly reach equilibrium via compression of the frit inlet flow so that there is no stop in the migration flow of the sample while it reaches equilibrium. Stopping the sample flow, as is the case FlFFF applications, can be problematic as the sample can become stuck. There have also been studies using free flow electrophoresis (FFE) for subcellular fractionation and isolation, which eliminates the need for tedious and time-consuming centrifugation steps.[273] These reports even demonstrate that subpopulations within heterogeneous populations of organelles may be resolved. More specifically, Islinger *et al.* used free flow-isotachophoresis (FF-ITP) followed by z onal FFE to pre-enrich mitochondria at the anodic side of the instrument and subsequently enrich the s ynaptosome fraction from brain tissue.[273b] This is an improvement over isotachophoresis (ITP), which is a focusing t echnique that separates organelles according to their different electrophoretic mobilities, but results in high mitochondria cross-contamination in the synaptosome fraction.

Of the organelles studied in subcellular proteomic analyses, the purification and isolation of lysosomes is of special interest to many groups because of their k nown role in disease (lysosomal storage diseases, or LSDs).[274] Unfortunately, the discovery and identification of lysosomal proteins has been difficult due to the presence of other contaminating organelles (such as mitochondria) in the lysosomal fraction when using conventional s ubcellular fractionation techniques. Using lysosomal density shifting techniques (treatment with either Triton WR-1339[275] or progesterone[276]), investigators have been able to assign proteins to the lysosome in Wistar rat livers and human hepatocellular carcinoma (HepG2) cells, respectively, that were n ot previously assigned to that organelle. In addition, they were able to identify proteins associated with other organelles in the same fraction that were previously assigned to the lysosome using a quadratic discriminant analysis.[275] More specifically, if levels of a given protein change in parallel with the organelle marker(s) (e.g. Lamp2 is a marker for lysosomes), it strongly suggests that the protein is localized with that particular o rganelle. Therefore, proteins that are density-shifted with the lysosomal organelle markers can be assigned lysosomal residence.

The ability to obtain relatively pure fractions of organelles allows for extension of proteomics analyses to identification and mapping of post-translational modifications (PTMs). In a study done by Tweedie-Cullen *et al.*, a comprehensive dataset of PTMs of the mitochondrial and h istone-containing subcellular fractions in the brain was generated.[277] The authors used an iminodiacetic acid-coupled (IMAC)/TiO$_2$ phospho-peptide enrichment strategy to identify 1062 phosphoproteins in the nuclear, histone, and synaptic subcellular fractions of the mouse brain. They were also able to clearly demonstrate that the phosphoproteins identified in each fraction are enriched in different gene ontology (GO) groups. Acetylation, methylation, and ubiquitination modifications were found on histone proteins. In addition, the authors identified PTMs on key synaptic, histone, and nuclear proteins with high confidence. More specifically, the authors reported high levels of histone PTMs in the brain.

Other studies have relied on various types of affinity purification step in order to isolate pure fractions of organelles. A cAMP capture compound (CC) developed by Luo *et al.* covalently links to target proteins using a photoactivatable reactive group and reversible binding of these target proteins by a selectivity group.[278] The bound complexes can be purified via streptavidin-coated magnetic beads since the CC contains a biotin moiety. The success of this strategy was demonstrated in *E. coli* cell lysate and human hepatocarcinoma (HepG2) cells. More specifically, the authors were able to capture ion channel (hyperpolarization-activated cyclic nucleotide-gated, HCN) proteins from rat synaptosomes, organelle-like structures c onsisting of the axon terminals of a pre-and post-synaptic neuron that are readily formed when neuronal tissue is gently homogenized. In another study, ER membranes were

enriched to analyze integral membrane proteins from canine pancreas.[279] The proteins within the ER are responsible for signaling and protein trafficking but many of their identities have not been established. Thus, rough microsomes were treated with Triton-X100 and with SM-2 beads to interact and capture the membranes, followed by centrifugation was used to enrich the membrane-collected fraction. The fraction containing ER luminal proteins and ER membrane proteins was subsequently extracted and analyzed.

Mass spectrometry for subcellular analysis can also be used to ensure that a class of contaminant proteins is not in the sample to be analyzed. A method was developed by Adam *et al.* to reduce contamination of nuclear proteins by 50% in lipid enrichments.[280] Cholesterol rich membrane microdomains, known as lipid rafts, are important in signal transduction, trafficking, and lipid transport. It has been recently found in proteomic s tudies that preparations of microdomains are often contaminated with nuclear proteins, which skews the composition of the microdomains. To address this problem, nuclei were centrifuged and depleted from the remaining cellular homogenate prior to detergent solubilization. The post nuclear fraction from Atk1 and LNCaP/LacZ yeast cells were treated with Triton X-100 and differential centrifugation was applied to collect the microdomains. The modified procedure only contained only 15% of the contaminating nuclear proteins found using the previous method. This correlated with an increase in non-nuclear proteins detected from 195 to 258 as determine via western blotting and their subsequent identification via proteomic analysis.

4.1.3. Subcellular profiling—Subcellular proteomic profiling refers to untargeted characterization of the protein sets found in multiple organelle types mixed in the same sample. Accurate subcellular proteomic profiling can give much biological insight into pathways, processes, and disease initiation and progression because it describes a global proteomic composition classified according to subcellular milieu.

A fast, new subcellular isolation technique used by Png *et al.* and Lan *et al.*, called centricollation, applies uniform centrifugal force across a sample and separates proteins and organelles based on a stepwise density gradient.[270,281] Because the samples undergo brisk acceleration (Edge™ instrumentation), a single extraction can be a ccomplished in a matter of minutes as opposed to several hours as with ultracentrifugation. The system uses extraction media of different densities that results in intact, non-denatured organelles in a reproducible manner for subsequent analyses (i.e. gel electrophoresis, Western blots, etc.) as shown in Figure 11. Using this technique coupled to mass spectrometry, the distribution and subcellular translocation of potential binding partners of transglutaminase-2 (TGM-2) were studied in the presence of short hairpin RNA (shRNA) in human SV-40 immortalized orneal epithelial cells (HCE-T).[281] The TGM-2 protein is important in the regulation of apoptosis, rearrangement of the cytoskeleton, is involved in protein cross-linking, and appears to be associated with multiple subcellular locations. Western blotting using organelle markers for early, late, and recycling endosomes, secretory vesicles, lysosomes, Golgi, ER, and mitochondria revealed the subcellular makeup of the centricollated fractions. These organelle markers helped to confirm the subcellular location of proteins (partners) interacting with TGM-2.

Subcellular proteomic profiling can also be accomplished by critically analyzing existing datasets.[282] Employing a systematic bioinformatics analysis, Hu *et al.* compared the mitochondrial proteomes from several different tissues and found that large numbers of "known" mitochondrial proteins were missing from many samples. In addition, it was found that ~70% of the mitochondrial proteome and ~52% of the ER proteome are unique to their respective proteomes, which makes sense as they are relatively easy to isolate from cell lysates. Special consideration was given to the analysis of organelle proteomes in which one

organelle originates from another (i.e. endosomes and lysosomes), because many of the proteins are colocalized. The authors were then able to demonstrate the dynamic nature of LROs, or lysosome-related organelles, which include the lysosomes themselves, as well as melanosomes, synaptosomes, exosomes, platelet dense granules, and neuromelanin granules.

The effect of thyroid hormones on sialylation of intracellular proteins of rabbit liver was investigated through the proteomic a nalysis of nriched nuclear, cytosolic, ER, and mitochondrial fractions.[283] While it is known that the role of sialylation of proteins on the surfaces of cells plays a role in cell-cell interactions, the role of sialic acid inside the cell is not understood, or how it specifically relates to hypo-and hyperthyroidism. Both rabbit models of hypothyroidism and hyperthyroidism were compared against untreated rabbits. Each subcellular fraction was separated with SDS-PAGE and sialyated proteins in each band were identified through detection of digioxogenin-labeled lectins. The authors were able to determine that the overall presence of sialic acids was lower in the mitochondria fraction of the hyperthyroid liver.

Subcellular proteomic analysis was also applied to the profiling of PTMs in mitochondrial and histone-containing fractions prepared from *Arabidopsis thaliana*.[284] More specifically, this report used immobilized metal a ffinity p urification IM AC enrichment of p hosphorylated peptides from cytoplasmic-and nuclear-enriched fractions to identify 303 in vivo phosphorylation sites. The phosphorylation PTM catalyzed by protein kinases is important in cellular signaling events, and the authors used a peptide chip analysis platform (kinome profiling of subcellular fractions) to form hypotheses associated with possible phosphorylation networks. The authors conclude that a large number of the identified phosphoproteins in *Arabidopsis* are targets of different protein kinases and serve as stages for multiple signal pathways.

4.1.4. Quantitative proteomics—Relative or absolute quantification of abundances of individual proteins detected in proteomic experiments is invaluable in subcellular proteomic analyses. Identification of up-regulated or down-regulated proteins as well as translocation events in cell or animal systems allows for the formation of biological hypotheses. Quantitative proteomics relies on associating the abundance of chemical or metabolic labels detected in a proteomics experiment with a given sample or treatment. It may also be based on label-free approaches that rely on using counts of protein-specific mass spectrum features when analyzing a given proteomic sample by mass spectrometry. Both strategies are briefly discussed below.

Chemical labeling techniques include isotope-coded affinity tagging (ICAT),[285] isobaric tag for relative and absolute quantification (iTRAQ),[286] tandem mass tags (TMTs).[287] All of these chemical labeling strategies involve the in troduction of an isotopically stable tag a t the peptide or protein level. Recent reports on the use of quantitative proteomics for subcellular analysis used mainly iTRAQ labeling. In the iTRAQ and TMT approaches, the lysine residues or N-termini of proteins or peptides are labeled with amine reactive tags. These tags are isobaric, or of the same initial mass, but yield reporter ions of different masses when the tags are fragmented during tandem mass spectrometry analysis. The intensities of these reporter io ns, detected in the second stage of tandem mass spectrometry analysis, are used for quantitation. Chemical labeling approaches are often chosen when metabolic labeling is not feasible (e.g. in tissue) or if a large number of groups or parameters are to be analyzed (i.e. iTRAQ 4-plex can quantify up to 4 different groups of proteins and TMT 6-plex can quantify up to 6 different groups of proteins while SILAC can quantify, at most, 3 groups of proteins). The utility of multiplexing these labeling schemes (that is, labeling proteins both metabolically and chemically) is beginning to be exploited. Recently, SILAC labeling was combined with TMTs to provide up to 18 different conditions (3

SILAC X 6 TMTs) that could be simultaneously analyzed.[288] While this multiplexing study was done in yeast, this labeling scheme could be expanded for use in eukaryotic subcellular analysis.

Labeling of proteins for quantitative analysis can also be done metabolically, as with stable isotope labeling with amino acids in cell culture (SILAC)[289] or stable isotope labeling of mammals (SILAM)[290]. In both cases, labeling takes place via metabolic in corporation of heavy or light isotopically stable essential amino acids. In SILAC, cells are cultured in media with either the heavy or light amino acids. In SILAM, animals are fed a diet of either the heavy or light label-containing food.

McClatchy et al. used SILAM to quantify changes in the subcellular neuronal compartments of rat brains during development in the study of neurodevelopmental disease.[291] Looking specifically at the synapses (or synaptosomes) and mitochondria, the authors were able to identify 1753 and 1328 significant changes, respectively, within a specific brain region over 45 days of postnatal development. Furthermore, the authors discovered that each brain region consists of differentially expressed proteins that act as a sort of signature for that region. It was concluded that a spatiotemporal understanding (brain regions as well as subcellular compartments) is necessary to fully understand the proteome changes that occur during development and neurodevelopmental disease.

Frequently, subcellular fractionation leads to impure fractions of organelles making it impossible to assign proteins present in a given fraction to a specific organelle type. When fractionations are accomplished by density gradient centrifugation, this inconvenience can be circumvented in some cases through the use of protein correlation profiling (PCP).[292] PCP works by correlating proteins with known organelle locations (marker proteins) with those of unknown subcellular locations in the same fraction as shown in Figure 12.[292a] More recently, Harner et al. combined quantitative proteomics (a SILAC spike-in standard)[289] with PCP to identify a novel protein complex, the mitochondrial contact site (MICOS) complex in W303 yeast strains. This complex is crucial in the formation of cristae junctions (CJ), which create the structure of the inner membrane of the mitochondria.[293]

In recent years, there has been substantial interest in p rofiling the subcellular proteome changes in response to viral or bacterial infection.[294] Those studies demonstrate the value of subcellular profiling in regards to research of infectious diseases. Quantitative proteomic analysis can also be used to profile changes in protein abundance in response to viral infection as well as virus-host protein interactions.[295] Emmott et al. identified and quantified 1830 proteins in control and coronavirus infectious bronchitis v irus (IBV)-infected Vero cells utilizing subcellular fractionation and S ILAC labeling. Coronaviruses can cause respiratory as well as gastrointestinal infections in humans and animals. The authors found changes in abundance of proteins involved in maintenance of cellular structure. Because most of the cellular proteome does not change in abundance in IBV-infected cells (in agreement with previous reports), the authors believe that the virus infection stimulates very specific changes in the nuclear, nucleolar, and cytoplasmic fractions studied. This is the first study of proteome changes using SILAC in response to this type of virus. It demonstrates the applicability of this method to study other host proteome changes in response to viral infection.

A recent study used iTRAQ labeling to quantitate proteome changes in host subcellular proteomes in response to viral or bacterial infection.[294a] The authors found dramatic changes in the nuclear and mitochondrial proteomes of human primary macrophages after the influenza A viral infection and less striking proteome changes in their cytoplasm and secretome. In total, more than 1000 host proteins changed in early phases of infection.

The Lilley lab developed a method to profile and quantify proteins in their subcellular locations using iTRAQ.[296] This method, called LOPIT, or Localization of Organelle Proteins by Isotope Tagging, was first developed using ICAT to label integral membrane proteins in *Arabidopsis thaliana*.[296a] LOPIT was further developed to profile proteins and protein complexes using iTRAQ in *Drosophila melanogaster* embryos.[296b] After homogenization, an iodixanol gradient was used to fractionate the embryo membranes. The different organelle fractions resulting from the gradient were iTRAQ labeled so that the peak of each organelle distribution was labeled with a different reagent. The iTRAQ labeling of the different organelle distributions allowed for both profiling as well as quantitation of the proteins within each fraction. PCA (principle component analysis) was then used to assign "co-resident" proteins to particular organelles (in this analysis, the mitochondria, ER/Golgi, and plasma membrane).

One of the drawbacks of quantitative subcellular proteomics is the large number of samples that must be processed through the proteomic pipeline. A new quantitative subcellular proteomic strategy, termed spatial proteomics, has begun to address this issue.[265,297] Spatial proteomics involves SILAC labeling of cells with light, m edium, or heavy isotopic labels, completing subcellular fractionation in to nucleolar, nucleoplasmic, and cytoplasmic fractions, and then recombining the 3 fractions with different labels. The schematic is s hown as a f low chart in Figure 13. This technique is useful because fewer samples may be analyzed while still obtaining subcellular information (as opposed to analyzing each fraction independently).

Spatial proteomics was used to quantify changes in protein abundance as well as subcellular localization in human colon carcinoma cells (HCT116) in response to DNA damage caused by treatment with etoposide.[297a] Spatial proteomics resulted in correct subcellular location (e.g. nuclear, nucleolar, and cytoplasmic) assignment for most of the proteins detected. They also found a general increase in abundance of nucleolar proteins due to etoposide treatment, but few proteins had changes in expected subcellular localization. Among the proteins that translocated, most of them were categorized as "proteolysis" proteins and were being shuttled out of the cytoplasm and into the nucleus. This work also offers evidence that DNA damage may alter the properties of the minichromosome maintenance (MCM) complex, which concentrates in the nucleus in response to DNA damage.[297a]

Spatial proteomics methods were also applied to study the effects of DNA damage in p53 knockout HCT116 cells on the subcellular proteome.[297b] Under normal growth conditions, p53 makes little contribution to subcellular lo calization of proteins. Few proteins relocalized in the p53 knockout cells in the absence of DNA damage. In the presence of DNA damage caused by etoposide treatment, shuttling of proteins between the cytosolic and nuclear components is similar between wild-type and knockout cells. However, p53 appears to halt nucleolar activity, causing proteins to stay put (i.e. ribosomal proteins) in wild-type cells. This effect was observed to a much lesser extent in the knockout cells, as the ribosomal proteins do not accumulate in the nucleolus in response to etoposide treatment. This may suggest that p53 is needed for the release of ribosomal proteins from the nucleolus following DNA damage.

In order to accomplish a comprehensive quantitative spatial proteomics analysis, or distribution between the nuclear, nucleolar, and cytoplasmic fractions, in the HeLa cell line,[265] Boisvert et. al. (Lamond lab) relied on an array of bioinformatics tools. One of these tools, PepTracker, was used to visualize the differing turnover rates in different subcellular compartments for the same protein. This is shown in Figure 14.[265] Although the results are limited by the impurities present in each fraction, the authors concluded that protein subunits from multiprotein complexes actually turnover more rapidly prior to complex assembly (i.e.

ribosomal proteins in the nucleus as opposed to in the cytoplasm where they form ribosomal units). Therefore, the subcellular location of a set of proteins dictates their turnover rates. They hypothesized that the turnover rates differ based on the specific function of the protein in each compartment.

An alternative to labeling schemes in quantitative proteomics is to adopt a label-free approach. Area under the curve (AUC)/signal intensity measurement (chromatographic peaks) and spectral counting (number of peptides assigned to a protein) are the two main label-free approaches used. The former assumes that the AUC of the chromatographic peak of a peptide corresponds with its concentration in the sample. Spectral counting asserts that if a peptide is more abundant, it will be selected for fragmentation more often than less abundant peptides and result in more MS/MS spectra.[298]

Label-free quantitation was the approach of choice in a proteomic study on the ER of murine liver.[299] There, the authors developed and demonstrated a 3D profiling strategy that combined SDS-PAGE with gas phase fractionation (GPF) just prior to MS/MS analysis. A spectral counting label-free approach was used for semi quantitation using cluster or co-cluster analyses [300] with known proteins associated with various organelles (i.e. cytosol, smooth ER, rough ER). The authors were able to identify 4 cytosolic proteins that clustered with ER proteins with high probability. More specifically, they suggested that they identified N-myc interactor (Nmi) as a new candidate in the ER associated degradation (ERAD) pathway.

4.1.5. Targeted proteomics—Subcellular targeted proteomics requires the ability to track or quantitate a set of proteins under various pathological or biological conditions as they occupy or translocate between various subcellular regions. Three examples include the subcellular analysis of proteins involved in chemotherapy resistance, the cAMP-Protein kinase A (PKA) pathway, and mitochondrial D-loop binding proteins.

Through the use of 2D liquid chromatography fractionation to create proteome maps of chemosensitive and chemoresistant cell lines, Skalnikova *et al.* were able to identify differentially expressed proteins. The authors found that Rho GDP-dissociation inhibitor 2 (Rho GDI2) and Y-box binding protein 1 (YB-1) increase and decrease, respectively, in resistant cells relative to sensitive cells. The Rho GDI2 increase observed in resistant cells may have an anti-apoptotic effect, and it may be a good marker for cancer resistance. In addition, the truncation of YB-1 may serve as a marker for multi-drug resistance. Moreover, this truncation is associated with nuclei in human cancer cells. The authors were also able to observe translocation of the protein Hop, an Hsp70/90 organizing protein, from the nuclei to the cytoplasm in chemosensitive cells using immunohistochemistry. This translocation may alter a cell's response to spreading cancer and drug resistance.

Targeted proteomics aided in defining the subcellular location of PKA isoforms thereby improving knowledge of the cAMP-PKA pathway. [301] This pathway is necessary to control growth and metabolism in response to stress and nutrients. PKA was identified in P-bodies, nuclei, and the cytosol of whole cells. The expression pattern of PKA changed based upon carbon and oxygen availability and demonstrated the specificity of PKA signaling.

Through the use of D-loop DNA-linked chromatography and peptide sequencing via mass spectrometry, Choi *et al.* were able to demonstrate that 152 mitochondrial proteins showed some binding affinity to the D-loop of mitochondrial DNA in human kidney cells and human hepatoma cells.[302] It was found that 114 of these proteins likely form complexes via protein-protein interactions (PPI). D-loop binding proteins were purified by D-loop affinity chromatography, and these proteins were analyzed via a shotgun proteomic approach. These

D-loop binding mitochondrial proteins may form various protein complexes via PPIs during different cellular processes. Network analysis of these identified proteins in selected cellular processes g ave further insight a s to possible PPIs involved in the formation of protein complexes and binding with the D-loop.

4.2. Endogenous metabolites and metabolomics

Subcellular metabolite analysis (subcellular metabolomics) generally focuses on identification of a set of metabolites associated with each other through biological cell functions such as the production of energy or the processing of ROS. Metabolite studies can also compare relative changes in metabolite concentrations or abundance. These variations could be associated with disease, developmental status, or response to xenobiotic treatments. Lastly, metabolite studies can determine how metabolites are transported among the various subcellular regions or how they are transformed within a subcellular environment. Endogenous metabolites comprise a highly heterogeneous set of chemical species that naturally occur in biological systems. The most commonly studied metabolite types are involved cellular energetics such as carbohydrates and glycogens,[303] cofactors (e.g. NAD^+),[304] vitamins (e.g. riboflavins),[305] and ROS. In some instances, metabolomic studies survey multiple classes of metabolites.[306]

Despite their different uses, subcellular metabolite analyses usually have similar experimental procedures: subcellular fractionation, metabolite extraction, separation of metabolite species with techniques such as gas chromatography and HPLC, and structural characterization using NMR or mass spectrometry. Libraries of either experimental mass spectra or predicted mass spectra can help expedite the identification of compounds when the structural characterization is based on mass spectrometry techniques. Table 8 lists relevant metabolomic databases useful for the analysis and identification of metabolites. These databases contain either experimentally observed or predicted data. It should be noted none of these databases associate metabolites with subcellular localization.

Several relevant techniques do not rely on structural characterization as shown in the studies reviewed in this section. Scintillation counting can be used to track radioactivity of known isotopes in enriched subcellular fractions.[324] Confocal fluorescence microscopy and transmission electron microscopy have been used to determine the subcellular location of known metabolites. This can be done with fluorescent probes such as MitoSox Red for detecting the subcellular locations of superoxide. Immunodetection, such as immunogold labeling of glutathione, can be used with transmission electron microscopy. Paper chromatography has also been utilized to separate metabolites.[324] Similar to thin layer chromatography, analytes interact with both the paper solid phase and a mobile phase. The degree of interaction determines their overall travel on the paper phase. Lastly, CE-LIF has been used to separate fluorescent or fluorescently tagged metabolites such as superoxide that are tracked by monitoring a unique fluorescent product that fractionates differently from non-specific fluorescent products.[325] The excellent sensitivity of CE-LIF allows for detection of zeptomolar amounts of certain fluorophores and is highly suitable for subcellular metabolite analysis. This section describes salient examples of subcellular metabolite analysis including selections from energy metabolism, ROS, oxidative damage, and metal ion analysis.

4.2.1. Small molecule metabolism and transport—Subcellular organization plays a critical role in the compartmentalization of carbohydrates and small molecules that participate in cellular metabolism. When carbohydrate metabolism is impaired, alteration in the subcellular localization of metabolites is likely altered, which is then associated with disease.[326] Similarly, carbohydrates are critical sources of energy and serve as growth

regulators in plants. However, carbohydrates comprise are only a small component of the metabolome. Other metabolites such as amino acids also play pivotal roles and define metabolic networks that are responsible for maintaining homeostatic control within the cell. This subsection describes relevant examples of recent reports in which small molecule metabolism and transport are described within the frame of the subcellular organization of the cell.

The subcellular description of glucose transport is critical to investigate the impact of glucose accumulation in coronary endothelial cells. Fluorescent glucose analogues were used to track glucose subcellular colocalization by confocal fluorescent microscopy in the presence of cytochalasin B and D-glucose (inhibitors of glucose transporter p roteins 1–5) and in the presence of insulin (an activator).[327] Stimulators and inhibitors of the transporters caused changes in the subcellular distribution of the fluorescent analogues. Thus, the authors demonstrated for the first time that endothelial cells could compartmentalize glucose near the plasma membrane and, specifically, at cell-to-cell junctions. This finding led them to suggest glucose forms a c oncentration gradient at the cell membrane, which is eliminated, with glucose transporter impairment.

The rate of carbon flux during photosynthesis in barley leaf cytosol, chloroplasts, and mitochondria was studied with $^{14}CO_2$-incubated protoplasts at different incubation times.[324] Three enriched subcellular fractions were prepared with a combination of pressure and filtration. The three fractions consisted of: (1) mitochondria, chloroplasts, cytosol; (2) mitochondria, cytosol; and (3) cytosol markers. Compounds of interest were separated with two-dimensional paper chromatography, extracted, and detected with liquid scintillation counting. The differences in radioactivity between fractions were quantified. The cytosolic fraction contained the largest pool of photosynthetic metabolites. A small, constant amount of the metabolites was found in chloroplasts-enriched (fraction 1) and to a lesser extent in the mitochondrial-enriched (fraction 2) fraction. Examples of the photosynthetic metabolites identified were 3-phosphoglyceric acid, triose phosphate, hexose monophosphate, fructose 1,6-bisphosphate, and ribulose 1,6-bisphosphate. Table 9 describes the localization of all a ccumulated carbon compounds.[324]

Changes in the colocalization of invertases in potato tubers led to changes in carbohydrate subcellular localization.[328] Invertases are enzymes responsible for the h ydrolytic degradation of sucrose. By changing the subcellular localization of invertases, their role in carbohydrate subcellular compartmentalization can be studied. The subcellular location of invertases changed when the peptide targeting sequence was changed. Plastid, cytosol, and vacuole fractions were isolated via non-aqueous fractionation (NAQF). Gas chromatography coupled to mass spectrometry was used to determine subcellular concentrations of 50 confirmed metabolites. Isomaltose and sucrose accumulated in vacuoles and trehalose, maltose, and malitol (a sugar alcohol) were found primarily in the cytosol. Cell lines with modified subcellular distributions of invertases had decreased levels of cytosolic glucose, fructose, and sucrose in the enriched plastid, cytosol, and vacuole subcellular fractions. While carbohydrate subcellular localization was affected by invertases, carbohydrate metabolites (glucose-6-phosphate, fructose-6-phoshphate, and 3-phospho-glycerate) were only slightly increased in concentration in the cytosol. Increases in amino acids in both invertase-modified cells lines were observed, which may represent a regulatory system to maintain amino acid biosynthesis.

NAD^+ has distinct roles in different subcellular compartments. Monitoring the activity of poly-ADP-ribose polymerase (PARP), which uses NAD^+ as a substrate, allows for the first visualization of free NAD^+.[304] PARP was used as an organelle-specific fusion protein for NAD^+ visualization. Hence, PARP was fused to glutamate dehydrogenase specific for

mitochondria NAD^+ visualization. When free NAD^+ was available, NAD^+ was polymerized onto PARP. The polymerized NAD^+ could then be immunodetected. Figure 15 shows a schematic description of NAD^+ visualization.[304] Free NAD^+ was found in mitochondria, peroxisomes, ER, and the Golgi of HeLa cells. Because many processes such as poly-ADP-ribose protein degradation use NAD^+ as signaling molecule, the indirect detection of NAD^+ has significant potential for future investigations of subcellular signaling.

Riboflavin is an intracellular regulator of cAMP. The subcellular distribution of riboflavin and how cAMP affects its distribution also was investigated.[305] Liquid scintillation counting was employed to track $[^3H]$-riboflavin in various subcellular fractions prepared from human choriocarcinoma and human epithelial colorectal adenocarcinoma cells. $[^{125}I]$-transferrin, a known endocytic marker was used as an experimental control. Riboflavin was more abundant in clathrin-coated vacuoles than endocytosed transferrin implying riboflavin endocytosis was receptor mediated. Riboflavin was also more abundant in the Golgi and mitochondria than transferrin suggesting that receptor-mediated endocytosis can deliver endocytosed contents to these organelles. Furthermore, the increased concentration of cAMP caused decreased internalized riboflavin and decreased association of riboflavin with clathrin-coated vacuoles.

Subcellular localization and dynamics of glycogen are important for the proper supply of energy during muscle exertion. Transmission electron microscopy was used to determine the subcellular location of glycogen g ranules during post-exercise restoration in human muscle.[303b] Changes in glycogen concentration in muscle-derived tissue sections were tracked over time via a glycogen-specific staining technique. This method utilized osmium tetroxide and $K_4Fe(CN)_6$ to quantify the subcellular glycogen volume with transmission electron microscopy. Glyocogen was observed in the nucleus, between the sarcolemma and nucleus, between nucleus and myofibrils, and in the sarcolemma both away and adjacent to subsarcolemmal mitochondria. However, the highest density of particulates and the highest rate of glycogen replenishment were in the subsarcolemmal mitochondria.

Carbohydrate concentrations in various subcellular compartments may play a role in rose flower blooming. A recent study examined carbohydrate profiles in the apoplastic, cytoplasmic, and vacuolar subcellular fractions of *R. hybrid*.[303a] NAQF was used to enrich subcellular fractions and cation exchange HPLC was used to separate and identify carbohydrates. Enzymatic assays were used to quantitate carbohydrates using sorbitol as an internal standard. Markers for the cytoplasm (NAD^+-glyceraldehyde-3-phosphate dehydrogenase) and vacuole (α-mannosidase) in the NAQF fractions were used to calculate the amount of carbohydrates in the respective subcellular location. Transmission electron microscopy was used for visualization of organelles and to calculate organelle volumes. The determination of carbohydrate content in the apoplasts required the infiltration method, a technique optimized for the enrichment of apoplastic fluids. While in a HEPES buffer, pedals were set onto an upper filter in a disposable tube and centrifuged. Soluble apoplastic carbohydrates were released from the pedals into the solution. Carbohydrates in solution were analyzed with HPLC. Glucose and fructose were present in the apoplasts in early petal development and were present in the vacuoles during f lower d evelopment and flower opening. Sucrose was present in the vacuole and cytoplasm in the early developing flower and in the vacuoles as the flower aged through development stages. The concentrations of glucose, fructose, sucrose, methyl glucoside, xylose, and myo-inositol were varied in the apoplast, cytoplasm, and vacuole at different flower development stages. A mechanism was proposed for flower opening involving increased fructose and glucose c oncentrations in the vacuole, which would cause an increased osmotic pressure in the vacuoles.

Another non-targeted metabolomic study investigating the subcellular distribution of metabolites in *G. max* soybean leaves was recently performed.[329] Non-aqueous extractions from cytosolic and vacuoles were analyzed with gas chromatography coupled to mass spectrometry. Over 92 different metabolites in enriched stroma, cytosol, and vacuole enriched subcellular fractions were identified when using the NIST02 Mass Spectral L ibrary (Table 8) as the reference database. A major finding from this study was vacuoles have high levels of carbohydrates, organic acids, and fatty acids. This supports the hypothesis that vacuoles are important reservoirs for starch metabolism. While there have been many metabolomics papers on plants, this was the first r eport f ocused on the subcellular distribution of metabolites in plants.

Thymidine-derived sugars (TdR) are potential angiogenesis markers because they are transformed by thymidine phosphorylase, an enzyme often overexpressed in cancer cells. A recent study determined the subcellular localization of TdR in human colon carcinoma cells.[330] Cells were treated with [5-^{3}H]-TdR for different periods of time. Figure 16 shows the distribution of TdRs in enriched subcellular fractions.[330] Tritium label signal decreased over time and was hardly detectable after 24 hours. The plasma membrane concentration of TdR increased up to 6 hours and was not detectable at 24 hours. Tritium was increased in the nucleus to 55% of the total radioactivity and 45% in the cytoskeletal protein fraction after 24 h. In RT112/TP cells, that have a lower rate of T dR degradation compared to Colo320 cells, the nuclear storage was decreased 25% compared to the nuclear fraction from Colo320 cells. This suggests thymidine sugars are primarily used in the cytosol and plasma membrane fractions but not primarily in the nuclei.

A global plant metabolomics study determined the subcellular distribution of known metabolites (e.g., starches, GAPDH, UGPase, nitrates, triacylglycerides, and flavonoids) and unknown metabolites in *A. thaliana* leaves.[306] Six fractions separated by differential centrifugation were characterized using organelle markers (e.g. citrate synthase for mitochondria) and extracted with a non-aqueous solvent before analysis by gas chromatography coupled to TOF-mass spectrometry or reverse phase UPLC-MS. UPLC-MS reported 726 and 461 lipophilic and semipolar metabolites and gas chromatography coupled to TOF-mass spectrometry reported 88 metabolites. Identifications were made by comparison with previously detected compounds from the KNApSAcK database (Table 8), fragmentation patterns, and mass shifts of ^{13}C, ^{15}N, and ^{34}S. Of the metabolites detected, 81.5% of the metabolites could be associated to a single non-aqueous fraction (Figure 17).[306] The findings of this subcellular metabolomic study are relevant for investigating signaling and trafficking pathways.

Single vacuoles from the algae *C. australis* were selected for metabolic analysis.[331] Due to their large size, single organelle metabolomics was possible using microscopy to visualize vacuoles and nanospray ionization tips as micropipettes to select specific vacuoles for analysis. The metabolites in single vacuoles were analyzed using capillary electrophoresis coupled to mass spectrometry. After vacuole collection, the remainder of the cell was also analyzed. Marker enzymes for the vacuole (α-mannosidase) and the remaining whole cell h omogenate (malate dehydrogenase) were analyzed from selected vacuoles using specific enzymatic assays. The vacuole fraction contained 99.9% of the α-mannosidase activity and the remaining whole cell homogenate contained 93.1% malate dehydrogenase activity indicating the importance of these organelles in maintaining mannosidase and malate dehydrogenase activity. Intermediates of the glycolytic and pentose phosphate pathway were observed in the remaining whole cell h omogenate but the pathway's products were found enriched in vacuoles.

4.2.2. Reactive oxygen species metabolism—ROS causes oxidative damage in biological systems and plays a critical role in signaling pathways. Both oxidative damage and signaling are regulated by antioxidant systems (e.g. glutathione). When antioxidant systems are insufficient to maintain homeostasis, oxidative damage ensues. Such damage is critical to the etiology and understanding of neurological disorders, age-related diseases, and cellular insults caused by hypoxia. ROS levels may also result from drug treatments or pathogenic invasion. ROS metabolism has recently been reviewed in the literature.[55] This section provides salient examples in the analysis of ROS and oxidative damage from a subcellular perspective.

Mitochondrial ROS have been associated with dysfunctional mitochondria in sperm and, in turn, may be associated with oxidative stress and male infertility. The subcellular accumulation of ROS and lipid peroxidation in sperm mitochondria was d etermined by confocal fluorescence microscopy.[332] Superoxide levels were indirectly determined using dihydroethidium or MitoSox Red. Lipid peroxidation was assessed using the probe BODIPY C_{11}. Confocal fluorescent imaging was sufficiently sensitive to detect basal rates of ROS in untreated mitochondria. Sperm incubation with antimycin A and myxothiazol (Complex III inhibitors) caused an expected increase in ROS. A positive correlation was observed between treatment of polyunsaturated fatty acids and ROS production. Decreased sperm mobility was suggested to be a result of increased polyunsaturated fatty acids and an increase in ROS. Although superoxide determination based on imaging was affected by non-specific responses of the probe, the insights gained here suggest a role for mitochondria in ROS production and a link to sperm mobility.

Superoxide dismutase 1 (SOD1) and cytochrome c oxidase (CCO) localize in mitochondria and are believed to play an important role in regulating mitochondrial ROS. In a recent study, mitochondria were treated with different reagents that increase ROS production.[333] The probe LO1 was used to monitor ROS generation in the mitochondrial-enriched fractions by measuring chemiluminescence. Valinomycin, calcium, iron, arachidonate, and palmitate long chain fatty acids all caused increased mitochondria respiration and produced increased ROS. Carbonyl cyanide *m*-chlorophenyl hydrazone (CCCP) used to depolarize mitochondria, also caused increased oxygen metabolism but inhibited ROS production. Table 10 summarizes the effects of treatment with these different reagents.[333] Overall, the study demonstrated that both SOD1 and CCO mitochondrial levels were greatly affected by increased mitochondrial ROS.

Cells respond to hypoxia with increased subcellular-specific ROS generation and non-esterified free fatty acid production. A recent study evaluated relationships between ROS and free fatty acid levels in a hypoxic cell m odel.[334] Superoxide levels in mitochondria were estimated using MitoSox Red in whole cells by confocal fluorescence microscopy and in enriched mitochondrial fractions using a fluorescence plate reader. Hydrogen peroxide levels were estimated in enriched mitochondrial fractions using the Amplex red/horseradish peroxidase assay in a plate reader. Hypoxia did not cause any changes in mitochondrial ROS production. This result was different from that observed in whole cell homogenate, where there was an increase in ROS. This suggested that hypoxia affects other parts of the cell more so than it does mitochondria. Surprisingly, treatment with free fatty acids caused increased hydrogen peroxide release from the mitochondrial fraction. Furthermore, mitochondria treated with free fatty acids under hypoxic conditions resulted in higher release of hydrogen peroxide and superoxide compared to similar treatment under normoxic (normal oxygen levels) conditions. Although the findings should be interpreted with caution because of the methodology used to evaluate superoxide levels, this study suggests free fatty acids play a role in elevating mitochondria ROS in concert with hypoxia.

ROS levels increase in response to pathogenic invasion in some plants. After infection of *P. sativum* peas leaves with Plum Plox virus, the levels of hydrogen peroxide, superoxide, lipid peroxidation and protein oxidation were determined in enriched chloroplasts.[335] Chloroplasts displayed increased levels of hydrogen p eroxide in the initiation phase of the p athogen infection. During the disease development phase, there was an additional increase in superoxide, lipid peroxidation, and protein oxidation. These metabolite changes were accompanied with changes in the levels of antioxidant enzyme levels. Oxidative pentose phosphate pathway and glucose-6-phosphate dehydrogenase activities were both increased in chloroplasts suggesting increased carbohydrate metabolism and ribonucleotide synthesis. Photosynthesis-associated peptides, such as the oxygen evolution enhancer protein/complex, were decreased in chloroplasts. These results suggest Plum Plox viral infection directly causes an oxidative stress response in cells and chloroplasts.

Immunoelectron microscopy was used to analyze the subcellular distribution of glutathione in the yeast *S. cerevisiae*.[336] Immunogold labeling of glutathione cannot distinguish b etween the oxidized or reduced forms of the enzyme, but does exclude detection of glutathione-conjugated proteins. Mitochondria had the highest glutathione content followed by the cytosol, nuclei, cell walls, and vacuoles. To test the response of the microscopy method to changes in glutathione, a hydrogen peroxide treatment that stimulated apoptosis caused an 87% decrease in glutathione in yeast mitochondria and the appearance of morphologically enlarged vacuoles and mitochondria. These results suggest that subcellular re-distribution of glutathione occurs in the yeast defense mechanisms against oxidative stress.

The mitochondrial redox status, indicated by ratio of glutathione (GSH)/glutathione disulfide (GSSG), is a potential indicator of o xidative damage. The mitochondrial GSH/GSSG ratios of seizure-induced and c ontrol rats were recently c ompared.[337] Mitochondrial enriched fractions from mouse hypocampus were analyzed by HPLC coupled to electrochemical detection. The mitochondrial GSH/GSSG ratio decreased following seizure induction suggesting the mitochondria had a more oxidizing environment following seizures. This highlights the importance of mitochondrial redox status in seizures and suggests mitochondria could be damaged following seizures.

It has been suggested that the production of ROS in mitochondria f ollowing doxorubicin treatments is associated with cardiotoxicity. Individual organelle analysis was utilized to investigate the genesis of superoxide in enriched mitochondria fractions from human leukemia cells treated with doxorubicin.[325] The mitochondria enriched fraction, containing other organelle types, was prepared by differential centrifugation and analyzed with CE-LIF. ROS levels were based on the fluorescence of 2'7'-dichlorofluorescein that forms upon oxidation of 2'7'-dichlorodihydrofluorescein diacetate. The presence of doxorubicin in an organelle was investigated by monitoring the native fluorescence of doxorubicin in a different spectral range. CE-LIF analysis could not specifically identify mitochondria but indicated that 9.3% of organelles contained doxorubicin, 66.6% had 2'7'-dichlorofluorescein, and only 2% of organelles included both. Organelles that contained doxorubicin had a large increase in ROS as determined by 2'7'-dichlorofluorescein fluorescence suggesting that doxorubicin induced the formation of ROS in this small fraction of detected organelles.

A second study utilized CE-LIF to estimate the levels of superoxide in individual mitochondria.[338] Prior to subcellular fractionation, human osteosarcoma cells were dually treated with hydroethidine (HE) to react with superoxide and with MitoTracker Green to fluorescently label mitochondria. Hydroethidine, which diffuses across the mitochondrial inner membrane is oxidized to hydroxyl-ethidium (superoxide specific) and ethidium (non-specific oxidation). Both products are positively charged and are unable to cross the

mitochondrial inner membrane. Although it was not possible to ascertain separately the contribution of the two hydroethidine oxidation products to the overall fluorescence, treatment with inhibitors of the electron transport chain (antimycin A and rotenone) that induced superoxide production c onfirmed that c hanges in fluorescence intensity could be a ssociated with increased superoxide production. The method was suitable for observation of superoxide production at the individual mitochondrion level.

Superoxide is released asymmetrically to both sides of the mitochondrial inner membrane by complexes I and III. Micellar electrokinetic chromatography, a form of capillary electrophoresis, was used to assess the relative levels of superoxide released into the mitochondrial matrix or outside the mitochondrial inner membrane.[156] Enriched mitochondrial fractions from human osteosarcoma cells, BALB/c mouse liver tissue, and Fischer 344 rat skeletal muscle were treated with the probe MitoSox Red. After treatment, an organelle-enriched fraction was separated into a pellet and a supernatant by differential centrifugation. The pellet contained the MitoSox Red products formed within mitochondria. The supernatant contained the MitoSox Red products released outside the inner membrane. The pellet and supernatant were analyzed separately by micellar electrokinetic chromatography with laser-induced fluorescence detection to clearly distinguish the superoxide-specific product triphenylphosphonium hydroxyethidium from the non-specific triphenylphosphonium ethidium. An application of this method consisted of evaluating the direction of superoxide release caused by various electron transport chain inhibitors including rotenone, antimycin A, and menadione. Figure 18 shows how these inhibitors affected superoxide accumulation outside and inside the mitochondria.[156] A subsequent report used this method to demonstrate that mitochondrial superoxide released outside mitochondria increases with inactivity in rat fast-twitch skeletal muscle.[339]

4.2.3. Subcellular metabolic modeling—Some metabolic models have begun utilizing subcellular organization and dynamics to predict metabolic pathways. Recently, a model of human heart mitochondria, based on the proteomics database Mitominer, was developed to improve knowledge of mitochondria metabolic dysfunction.[340] Previous mitochondria models were restricted by the limited amount of information on the mitochondrial proteome and biochemical pathways. Mitominer allowed for integration of an increased number of metabolic reactions and additional proteomic information. The new model accounts for the most recent stoichiometric information available for ROS production, maximum ATP production, citric acid cycle flux, and glycolysis. As an application, the new model was used to investigate disorders associated with deficiencies in fumarase, succinate dehydrogenase, and α-ketoglutarate dehydrogenase activities. Several simulations were performed to determine affected mitochondria function in response to decreases in substrates. When fumarase activity was deficient, maximum ATP production was reduced to 95%. Deficiency of succinate dehydrogenase activity led to a similar reduction in ATP to fumarase activity. A deficiency of α-ketoglutarate activity reduced ATP production by only 5% but an 80% increase in fatty acid synthesis due to an alternative enzymatic route being necessary for maintaining ATP production.

4.2.4. Lipid composition and metabolism—Lipids are important components of organelle composition and have been identified in both the membrane and lumen of organelles. Lipids included in this section are phosphatidylserines, phosphatidylethanolamines, phosphatidylcholines, cardiolipins, phosphatidylinositols, phosphatidylglycerol, sphingomyelins, and ceramides. Their molecular diversity and high biological significance has been a catalyst for the establishment of lipidomics as a new technological paradigm. Lipid MAPS has captured such diversity as shown in Figure 19.[322] Because of such diversity, the subcellular analysis of lipids requires an extensive ensemble of subcellular fractionation, lipid extraction, biomolecular separation and detection

techniques. This diversity also poses major challenges when the goal is to characterize or quantify the complete set of lipids and their function in a subcellular fraction (i.e. subcellular lipidomics).[57] It is not surprising that complete lipidomic surveys rely on separations accomplished by gas chromatography, reverse phase HPLC, and hydrophilic interaction chromatography (HILIC) to separate volatile, hydrophobic, and polar lipids, respectively. At the same time, structural characterization and quantification uses ^{1}H, ^{13}C, ^{17}O, and ^{31}P nuclear magnetic resonance (NMR) (for simple mixtures) or high mass accuracy mass spectrometry with the caveat that the latter usually requires an internal isotopically labeled standard for quantification. However, the availability and ongoing proliferation of databases with detailed listings of *m/z* values of lipids make mass spectrometry the method of choice for comprehensive lipid identifications in lipidomics studies.

Recent reviews on the biological roles of lipids have covered p eroxisome membrane lipids,[60] mitochondrial lipids,[61] the biological roles of lipids in lipid droplets,[62] lipids in plants cells and organelles,[58] cardiolipins in mitochondria,[63] and lipids and fatty acids in the brain.[59] The status of lipidomics techniques has a lso b een recently reviewed.[64–66] However, none of those reviews focused on subcellular analysis of lipids. In this section, we discuss reports focusing on membrane isolation, identification of lipids in different subcellular compartments, and how subcellular lipid findings contribute to the understanding of lipid metabolism and their effect on biological function. Lipid extraction, analytical separations, and structural characterization techniques will not be explicitly discussed unless they present unique aspects of subcellular analysis.

4.2.5. Membrane isolation for lipid analysis—Enrichment of membranes from a specific organelle type is essential to identify lipids specific to membranes and compare membrane compositions among different subcellular regions. While there were reports on the isolation of plasma membranes,[341] these will not be covered here because this review focuses primarily on intracellular organelles.

One such study was on the isolation of membranes of early and late endosomes accomplished in less than one hour and w ithout using any centrifugation.[342] Macrophages were allowed to endocytose iron-oxide magnetic particles and endocytic organelles were recovered by electromagnetic chromatography from the whole cell homogenate. In this technique, the cell homogenate was passed through a column, packed with a stainless s teel wire mesh and held between two magnets. Endosomes containing the magnetic particles were retained while other subcellular compartments were washed away. The magnetically retained endosome fraction contained no detectable ER contamination, but had some lysosomal and mitochondrial contaminants. Lipids from the endosome-enriched fraction were extracted with chloroform/methanol mixtures. High performance thin layer chromatography revealed that cholesterol was the most abundant lipid in endosomes consisting of 28%–30% of total lipid contents. Analysis of enriched early endosomes and late endosomes showed increases in phosphatidylcholine and phosphatidylglycerol in late endosomes and an increase in oleic acids in early endosomes. Relative to early endosomes, late endosomes had higher levels of phosphatidylcholine, phosphatidylethanolamine, phosphatidylglycerol, and sphingomyelin. Late endosomes also had lower levels of oleic acid and s tearic acid.

4.2.6. Lipidomics including multiple organelle types—An excellent subcellular lipidomic study investigated lipid composition in nuclear, plasmalemma, ER, mitochondria, and heavy microsome enriched fractions prepared from RAW264.6 macrophages.[343] Because of lipid diversity, separate extraction procedures were used to extract sterols, glycerophospholipids, cardiolipin, sphingolipids, and prenols. The analytical methods were tailored to each lipid class and used reverse phase HPLC and multiple reaction monitoring

performed via a Q-TOF mass spectrometer. In total, 163 glycerophospholipids, 48 sphingolipids, 13 sterols, and 5 prenols were observed containing different distributions in e ach organelle. Figure 20 describes the various lipid types found in each subcellular fraction, with the ER having the majority of the observed lipids.[343]

An *in vitro* approach to investigate subcellular transformations of pregnenolone, progesterone, dehydroepiandrosterone, and dehydroepiandrosterone in subcellular fractions prepared from chicken brain was recently reported.[344] This tissue was selected because of the role of steroids in memory formation. The nuclear, cytosolic, organelle and microsome fractions were treated with [^{3}H]-progesterone, [^{3}H]-pregnenolone, and [^{3}H]-dehydroepiandrosterone and supplemented with NADPH as a cofactor. Comparison of R_f values of radioactive spots in thin layer chromatography plates was adequate to identify lipid metabolites. Pregnenolone was metabolized to 20β-dihydropregnenolone and 5β-dihydropregnenolone in the cytosolic fraction and to 11-deoxycorticosterone and 3α,5β-tetrahydroprogesterone in the nuclear fraction. Interestingly, none of the steroids tested here were metabolized in the fraction containing other organelles. This suggests that steroids metabolism is mainly localized to nuclear and cytosolic regions.

Another recent study used thin layer chromatography to isolate phosphatiylethanolamine, phosphatidylcholine, and phosphatidylinositols in fractions enriched from plasma membrane, ER, nuclear, plastids, and clathrin-coated vesicles prepared from *A. thaliana*.[345] After thin layer chromatography isolation, compounds were identified by mass s pectrometry. Salt induced stress of *A. thaliana* leaves showed increases in phosphatidylinositols in enriched plasma membrane and clathrin-coated vesicles. ER, nuclei, and plastids had either no change or a decrease in phosphatidylinositol content or other phospholipids. These data are shown in Figure 21.[345] To confirm the role of clathrin with the plasma membrane's increase in lipids, YFP-clathrin was found to localize with the plasma membrane marked with RedStar-PLCδ1-PH, a protein with a specific binding site for phosphatidylinositol 4,5-bisphosphate. *A. thaliana's* response to hyperosmotic stress requires changes in membrane dynamics and lipid composition, which may be directly associated with the changes in phosphatidylinositols that were observed in this report.

The subcellular localization of metabolites of α-tocopherol, a c ommon ingredient in dietary supplements, was recently investigated in Sprague-Dewey rat liver.[346] Enriched subcellular fractions of microsomes, mitochondria, and peroxisomes were analyzed with HPLC equipped with a triple quadrupole mass spectrometry detector. α-Tocopherol and its metabolites α-2,5,7,8-tetramethyl-2-(2'-carboxyethyl)-6-hydroxychroman (α-CEHC; final metabolism product) and 13'-OH-α-tocopherol (intermediate from β-oxidation metabolism) were monitored. α-Tocopherol was enriched in the microsome and peroxisome fractions with each fraction containing ~40% of the total detected α-tocopherol. The mitochondria fraction had the lowest level (~20%). When rats were injected with additional α-tocopherol, greater accumulation of the parent compound occurred in the microsome fraction. These findings suggest that microsomes play an important role in α-tocopherol metabolism, while peroxisomes and mitochondria are less relevant. In relation to α-tocopherol metabolites, the abundance of 13'-OH-α-tocopherol was highest in the microsomal fraction followed by the mitochondrial fraction, and was lowest in the peroxisomal fraction either when α-tocopherol was dietary only or injected. α-CEHC was found largely enriched in the mitochondrial fraction and was not detectable in either the microsomal or peroxisomal fractions. However, α-Tocopherol injection caused a slight increase in α-CEHC microsome localization (~10% of the amount found in the mitochondrial fraction). Overall, these results show α-tocopherol metabolism products localize to different subcellular locations.

The role of mitochondria and cytosol in the metabolism of 17-α-hydroxyprogesterone, a steroid essential in inhibiting preterm delivery, was investigated in human placentas.[347] Mitochondria and cytosol possess hydrolases, cytochrome P450s, and other phase two metabolic enzymes conducive for the conversion of 17-α-hydroxyprogesterone into other metabolites. The analysis of mitochondrial and microsomal fractions enriched from placentas was performed by reverse phase HPLC with either liquid scintillation detection or a single-quadrupole mass spectrometer. Scintillation counting was used for quantification while mass spectrometry was used for structural characterization. Six metabolites were observed in the mitochondrial fraction and four metabolites in the microsomal fraction. The four metabolites in the microsomal fraction were also found in the mitochondrial fraction but in a higher concentration. These results demonstrate that in addition to the cytosol, the mitochondria are a key player in the metabolism of 17-α-hydroxyprogesterone.

A second paper investigated the metabolism of 17-α-hydroxyprogesterone in *D. labrax* male gonads.[348] Alteration in the metabolism of 17-α-hydroxyprogesterone may be used as an indicator of the presence of endocrine disruptors that lead to changes in reproductive behavior and sexual characteristics of this fish. Tritium labeled 17-α-hydroxyprogesterone and β-androsteredione were incubated with subcellular fractions prepared f rom the male gonads. The mitochondrial and microsomal fractions were analyzed by reverse phase HPLC with a radioactivity detector for quantitation and gas chromatography coupled to mass spectrometry for identification. In mitochondria, the main metabolite formed from 17-α-hydroxyprogesterone was β-androsteredione (39%), which was further metabolized to 11β-hydroxyandrostenedione (7%), and an unknown metabolite (28%). The microsomal fraction converted 17-α-hydroxyprogesterone into β-androsteredione (60%) and a different, uncharacterized metabolite (5%). The cytosol produced 41% β-androsteredione, 30% of second unknown metabolite, and 14% of a third unknown species. When fish were exposed to nonylphenol or ketoconazole, 17-α-hydroxyprogesterone metabolism to β-androsteredione in the mitochondrial fractions decreased to 50% and 26% relative to the metabolism of non-exposed fish, respectively. Overall, this data suggests the metabolism of 17α-hydroxyprogesterone may be monitored to investigate mitochondrial-related endocrine disruption.

A less conventional approach to investigate the subcellular localization of lipids is confocal fluorescence microscopy. In a recent report, 3T3 cells were treated with cholines modified with an alkyne moiety to form propargylcholine, which then was fluorescently labeled via click chemistry to visualize cholines within the cell.[349] The choline analogues were found at high levels in the plasma membrane, Golgi, mitochondria, and the ER. Because mitochondria and the plasma membrane do not synthesize choline phospholipids, these findings demonstrate that choline analogues were incorporated and synthesized into phospholipids in the ER and Golgi and trafficked successfully to other organelle types. This method cannot be used with detergents, which removes the choline derivatives from membranes, and is incompatible with phospholipase C b ecause i t cleaves the choline head groups and eliminates fluorescence. This method may provide applications in future lipid trafficking studies.

Treatment with palmitate in cells leads to incorporation of this phospholipid in the ER membrane causing morphological and functional alterations. In order to investigate the chemical fate of [^{3}H]-palmitate, Chinese hamster ovary cells were treated with of [^{3}H]-palmitate and subcellular fractions were analyzed by scintillation counting.[350] Palmitate-treated Chinese hamster ovary cells had 58% of the palmitate in the crude mitochondrial fraction and 23% in the rough microsomal fraction, which mainly contains ER. Treatment with the AMP-activated protein kinase activator 5-aminoimidazole-4-carboxamide-1-β-4-ribofuranoside, which stimulates β-oxidation of lipids, decreased palmitate incorporation in

the rough microsomal fraction (which contains ER) by 50% and in the mitochondria-enriched fraction by 30%. The reduced incorporation into the mitochondrial fraction was attributed to two factors: increased mitochondrial oxidation of palmitate and organelle fraction contamination. In the rough microsomal fraction, palmitate was incorporated mainly into phosphatidylcholine (50%), free fatty acids (27%), and triacylglycerol (5%) as determined with ESI mass spectrometry. ER calcium concentrations were found to decrease up to 25% following palmitate treatment. Palmitate treatment also caused morphological disruption of the ER as determined by transmission electron microscopy. In addition to 5-aminoimidazole-4-carboxamide-1-β-4-ribofuranoside sensitivity, palmitate was shown to cause mitochondrial loss of cytochrome c and loss of mitochondrial membrane potential. Mitochondrial toxicity could be a result of decreased ER calcium concentration. It is likely that the accumulation of palmitate in the membranes of these subcellular compartments is intimately associated with ER stress.

4.2.7. Golgi lipidomics—The membranes of organelles involved in the secretory pathway (i.e. endoplasmic reticulum, Golgi, vesicles, vacuoles, and plasma membrane) have unique lipid profiles.[351] A recent report assessed the lipid composition of Golgi-derived vesicles in the yeast strain KSY302 that overexpresses FusMidGFP, which is the fusion construct of FusMid and GFP. FusMid is a protein involved in vesicular transport from the Golgi to the plasma membrane.[352] In this study, Golgi-derived vesicles and Golgi were separated by density gradient centrifugation and immunoenriched with antibodies against FusMidGFP. Lipid standards were mixed with the vesicle fractions prior to lipid extraction and analyzed by direct infusion (without HPLC) into either an LTQ Orbitrap or a Q-TOF mass spectrometer. Instrumental parameters were adjusted to allow the investigators to focus on specific lipids (e.g. diacylglycerol, phosphatidylcholine, and ceramide) using precursor ion scanning and multiple reaction monitoring. In the vesicles, the lipids consisted of ergosterols (22.8 mol %) and mannosyl-di-inositolphosphoceramides (11.1%). In the Golgi fraction, the lipids detected were phosphoinositols (8.5%) and ergosterols (9.8%). Relative to the Golgi fraction, vesicles displayed a 3.2-fold phosphatidic acid, 2.3-fold ergosterol, 2.6-fold mannosyl-di-inositolphosphoceramide, 2.2-fold inositolphosphoceramide, and 2.4-fold mannosyl-inositolphosphoceramide enrichments. R elative to vesicles, the Golgi f raction showed ~3-fold phosphatidylserine, ~2.5-fold phosphatidylethanolamine, ~2-fold diacylglycerol, and ~1.5-fold phosphatidylcholine enrichments. The difference in lipid profiles between the vesicles and Golgi could not have been accomplished without the subcellular purification strategy that was introduced in this report.

Cells receive cholesterol mainly as low-density lipoprotein through endocytosis and hydrolysis of low-density lipoprotein. The role of the Golgi in cholesterol transport is unknown even though it has been identified in the ER and plasma membrane. The involvement of the Golgi in low-density lipoprotein and cholesterol transportation was evaluated in C hinese hamster ovary cells.[353] After a short treatment with [^{3}H]-cholesteryl linoleate, the preparation was diluted with label-free cell culture medium. Subcellular fractions were prepared at 0, one, and two hours later to monitor ^{3}H-cholesterol traffic. The Golgi-enriched subcellular fraction was further purified using an immunoaffinity column having a nti-Syntaxin 6 antibody as the affinity reagent. Treatment with tritium labeled linoleate allowed for tracking of cholesterol in the organelle fractions. Tritium-radioactivity was detected in Golgi-enriched fractions prior to detection in the ER and plasma m embrane. This report suggests new routes of cholesterol transport in the cell.

4.2.8. Lipid droplets lipidomics—Understanding the trafficking and lipid composition of lipid droplets is essential to cellular energetics, lipid metabolism, membrane trafficking, and intracellular signaling. A recent study investigated lipid composition of lipid droplets is olated from *G. hirsutum* (cotton) embryos and *A. thaliana* seeds and leaves.[354] Individual

lipid droplets observed by microscopy were selected for extraction via ammonium acetate and 1:1 v/v chloroform:methanol. Their lipids were directly infused into a nanospray source for mass spectrometry analysis. The analysis included both lipids in lipid droplets of wild type *G. hirsutum* and the genetically modified variety Bn*fad2*, which has lipid droplets larger than the wild type. The same eight lipids were detected in both varieties of *G. hirsutum but with different compositions*. The Bn*fad2* lipid droplets had higher concentrations of triacylglycerides. These compositions and triacylglyceride contents are shown in Figure 22.[354] Comparing the lipid droplets of *A. thaliana* seeds and leaves, the seeds had more eicosenoic fatty acid-containing triacyl glyceride. Also, *A. thaliana* leaves had 16:3, and 18:3 fatty acids-containing triacyl glycerides that were absent in the seeds. This methodology can be easily applied to other tissues and other species. Furthermore, since lipid droplets can be visualized prior to analysis, lipid droplets in similar spatial arrangement or similar morphology can be independently analyzed.

Another study on lipid droplets investigated whether prostaglandins were present in lipid droplets of cancer cells.[355] Because prostaglandins are produced via the cyclooxygenase pathway they also monitored cyclooxygenase-2 expression. Confocal immunofluorescence microscopy was used to determine the localization lipid droplets with either prostaglandin or both prostaglandin and cyclooxygenase-2. Cancerous colon tissue showed increased lipid droplet and prostaglandin production when compared to healthy tissue from the same individual. Because prostaglandin colocalized with lipid droplets, the authors suggested that lipid droplets of cancer cells play an important role in the synthesis of prostaglandins and possibly other eicosanoids.

4.2.9. Mitochondria lipidomics—The abundance of cardiolipins and the oxidation status of their fatty acids are both active participants in the apoptosis pathway and have been associated with release of pro-apoptotic factors from the mitochondria. Developing therapies to prevent oxidation of the fatty acids in cardiolipin could prevent excessive apoptosis. Some of the protection may be based on administration of oxidation resistant fatty acids such as octadecanoic acid. In a recent study, mouse embryonic and ASCL cells were treated with the modified fatty acid triphenylphosphonium-linked octadecanoic acid and studied under conditions leading to apoptosis.[356] Actinomycin D was used to stimulate apoptosis. Cardiolipin and triphenylphosphonium-linked octadecanoic acid were analyzed w ith liquid chromatography coupled to a linear ion t rap mass spectrometer. Triphenylphosphonium-linked octadecanoic acid and triphenylphosphonium were both observed in the mitochondria-enriched fraction. Cardiolipins contained an increased amount of octadecanoic acid when cells have been treated with triphenylphosphonium-linked octadecanoic acid. Treatment with this modified fatty acid also conferred the cells with more resistance to apoptosis relative to untreated cells and cells treated with unmodified octadecanoic acid.

Although it is accepted that ceramide synthesis occurs in the ER,[357] a recent study suggested that this process may occur in the plasma membrane and mitochondria as well.[358] After treatment of Jurkat E6.1 cells with ^{3}H-palmitic acid and ^{3}H-dihydrosphingosin, cells were γ-ray irradiated to induce ceramide and sphingolmyelin syntheses. The levels of ceramide in subcellular-enriched fractions were quantified by 2D thin layer chromatography and scintillation counting. In plasma membrane rafts, ceramide was detected 15 minutes following irradiation. In mitochondria, ceramide synthesis began immediately and remained steady 4–8 hours after irradiation. Sphingomyelin was also found in mitochondria 4 hours following irradiation. Consistent with these findings, immunogold transmission electron microscopy of sphingomyelinase, an enzyme that produces ceramide from sphingomyelin, confirmed that ceramide could be synthesized in the mitochondria.

The inner and outer mitochondrial membranes have different function and composition. The effect of growth conditions on the lipid composition of the mitochondrial inner and outer membranes from the yeast *P. pastoris* was recently investigated.[359] Carbon sources used for growth included glycerol, glucose, sorbitol, methanol, and fatty acids. After isolating mitochondria, they were treated with hypo-and hyperosmolar buffers followed by sonication to rupture the mitochondrial membranes. Sucrose gradient centrifugation was adequate to separate the outer and inner mitochondrial membrane because they have different densities. Lipids from each membrane type were extracted and then separated by two-dimension thin layer chromatography. Fatty acid lipid analysis was conducted via gas chromatography. Changes in the carbon source for yeast growth modified the mitochondrial levels of fatty acids, phosphatidic acid, phosphatidylinositol, phosphatidylserine, phosphatidylcholine, phosphatidylethanolamine, cardiolipin, dimethyl phosphatidylethanolamine, zymosterol, ergosterol, fecosterol, episterol, lanosterol, and lysophospholipids. When compared to the inner mitochondrial membrane, the outer membrane had higher phospholipid and phosphotidylinositol levels but lower ergosterol levels. As expected, the inner membrane did contain more cardiolipin. Lastly, the study showed that the inner mitochondrial membrane has a lower phospholipid to protein ratio than the outer mitochondrial membrane.

Three reports by the same group focused on comparing the lipidome of non-synaptic and synaptic mitochondria.[360] In the first study, the strategy to separate the two mitochondria types is based on Ficoll density gradient centrifugation that separates non-synaptic mitochondria from synaptosomes. The synaptosomes were subsequently disrupted and the released mitochondria were further purified by sucrose gradient centrifugation. In contrast, the non-synaptic mitochondria were directly purified by sucrose gradient centrifugation. Lipids in each mitochondria type were then extracted and analyzed by ESI-triple quadrupole mass spectrometry. In the second study,[360b] the lipid profiles of the two mitochondria types were similar, except for increased phosphatidylserine and ceramide in synaptic mitochondria and increased cardiolipin in non-synaptic mitochondria. Phosphatidylethanolamine, phosphatidylcholines, cholesterol, cardiolipin, phosphatidylinositol, phosphatidylglycerol, sphingomyelin, phosphatidylserine, and ceramide were all detected. The second study focused on the analysis of lipids extracted from non-synaptic mitochondria isolated from VM and B6 mice; the former has a 210-fold increase in incidence of brain tumors.[360a] Relative to B6, the VM mouse model showed higher levels of ethanolamine glycerophospholipid, plasmenylethanolamine, phosphatidylinositol, phosphatidylserine, and ceramide. However, the VM mouse model manifested lower levels of choline glycerophospholipid and phosphatidylcholine. These results suggest an association of mitochondria lipid composition with brain cancer incidence. The third study compared the lipidomes of mouse mitochondria isolated from cancerous and non cancerous tissue and non-synaptic mouse mitochondria isolated from cultured astrocytes and mouse tumor cells.[360c] This allowed for comparisons between both *in vivo* and *in vitro* models. Mitochondria were enriched as previously described.[360b] A comparison of the lipid profiles is shown in Table 11.[360c] While there were expected differences in lipid profiles between cancerous and non-cancerous tissue, surprising findings of this study were that the *in vitro* cell culture environments and the tissue had marked differences in the mitochondrial lipid profiles, which challenges the significance of in vitro lipidomic studies.

A streamlined method to characterize the lipidome of mitochondria used MALDI-TOF mass spectrometry.[361] Using this method, lipid extraction and separation technologies were not needed as the mitochondria fraction was directly analyzed after mixing with the MALDI matrix 9-aminoacridine. The method was applied to the analysis of lipids in mitochondria from various sources including bovine heart and *S. cerevisiae.* The lipids detected included cardiolipin, phosphatidic acids, phosphatidylethanolamines, phosphatidylglycerols, phosphatidylserines, and phosphatodylinositols. A typical mass spectrum showing these

chemical signatures is shown in Figure 23.[361] The method was capable of detecting cardiolipin modifications in the null-*S. cerevisiae* CRD1 gene (cardiolipin synthase) and null-TAZ1 (remodeling of acyl groups in mitochondria). In CRD1 mitochondria, the lipids detected were different from the wild type and, as anticipated, cardiolipin was not detected. The TAZ1 mitochondria contained different cardiolipin species with modified acyl compositions. This is a promising method to quickly survey the lipid composition of enriched mitochondrial fractions.

A separate survey of the mitochondrial lipidome was based on shotgun LC-MS.[362] A HPLC instrument hyphenated to an E xactive ESI-orbitrap mass spectrometer, operated at high energy collision-induced dissociation for extensive M S/MS analysis, was used to analyze the lipids extracted from rat mitochondria. The cardiolipin limit of detection was 5 picomoles and with a mass a ccuracy of less than 1.5 ppm. The lipid classes d etected included prenolipids, sterols, sphingolipids, fatty acyls, cardiolipins, phosphocholines, lysophosphocholine, phosphoethanolamine, and phosphoserines. Usually cardiolipins subclasses are not identified when using other shotgun techniques. Impressively, this report identified and quantified 28 u nique cardiolipin containing species.

A separate study reported the effect of tacrine and tacrine analogue treatments on the lipid profile of non-synaptic rat brain mitochondria.[363] Tacrine and its analogues are cholinesterase inhibitors used as a treatment for Alzheimer's disease. Lipids extracted from mitochondria were separated into classes by thin layer chromatography and then f urther characterized with ESI-linear io n trap-tandem mass spectrometry or quantified with a phosphorous assay. Lipid classes present included sphingomyelin, phosphatidylcholine, phosphatidylinositol, phosphatidylserine, phosphatidylethanolamine, cardiolipin, and ceramide-1-phosphate. Following treatment with tacrine analogues, phosphatdiylethanolamine and phosphatidylcholine were the most abundant lipids in mitochondria. On the other hand, tacrine treatment resulted in Increased phosphatidylserine levels in mitochondria. In addition, tacrine and tacrine analogues treatments caused the appearance of four new types of phosphatidylserines. Integrating this data with other functional data on cholinesterase activity is a promising avenue to elucidate the potency and therapeutic window of tacrine and tacrine related compounds.

4.2.10. Nucleus lipidomics—The nucleus contains a pool of lipids known as endonuclear lipids. The key lipid forms in this environment are diacylglycerols, generated from phosphatidylinositols and phosphatidylcholines, and has been suggested to play a key role in the nuclear biosynthetic pathway of nuclear phosphatidylcholine.[364] A recent report evaluated the phospholipid composition of the endonuclear environment and developed a method to monitor the synthesis of endonuclear phosphatidylcholine using ESI-MS/MS.[365] Mouse embryonic fibroblasts were treated with choline-d_9 to accumulate intracellular pools of deuterium la beled lipids. Cells were then homogenized in the presence of Triton X-100, which removes the nuclear envelope and contaminating phosphatidylcholine upon fractionation by differential centrifugation. After isolation of the nuclear pellet, lipids were extracted and analyzed with an ESI-triple quadrupole mass spectrometer. Endonuclear pools of phosphatidylcholine (deuterium-labeled and wild-type), sphingomyelin, phosphatidylethanolamine, and phosphatidylinositol (labeled and wild-type) were all detected. Phosphatidylcholines, phosphatidylethanolamines, and phosphatidylserines contained more saturated species in the nuclei-enriched fractions than in the whole cell homogenate.

4.3. Subcellular metabolism and distribution of xenobiotics

Xenobiotics are compounds or objects that are not native to the cell but are found intracellularly after they enter the cell by passive diffusion or active transport. Once inside, such compounds can distribute to one or several subcellular regions where they may either interact with biomolecules, altering their molecular function, or experience biotransformations catalyzed by endogenous enzymes such as cytochrome P450s. Intracellular localization of xenobiotics may result from medical treatments or from voluntary or involuntary exposure to such compounds. Analysis of the organelle contents of xenobiotics and their metabolic products is essential to assess their toxicological, therapeutic, agonistic, or antagonistic effects. Subcellular xenobiotic analysis is similar to the analysis of endogenous metabolites. The study of xenobiotics usually involves subcellular fractionation followed by compound extraction, and analysis with CE-LIF, HPLC-MS, flow cytometry, scintillation counting, inductively coupled plasma-atomic emission spectrometry (ICP-AES) or inductively coupled plasma – mass spectrometry (ICP-MS). The last two are well suited for elemental analysis without complications from matrix interferences. Fluorescence microscopy is also a dequate to monitor fluorescent xenobiotics and/or their fluorescent metabolites.

There have been several recent reviews that focus on xenobiotics.[67–70] Specialized topics have included the advancements in technology and animal models for the analysis of xenobiotics, mammalian enzymes that metabolize carbonyl xenobiotics,[366] the effect of drugs, pollutants, cosmetics, and diet on endogenous or xenobiotic metabolism.[367] This review focuses on select examples of the subcellular analysis of various kinds of xenobiotics. It includes contaminants such as polyaromatic hydrocarbons,[368] anti-cancer compounds such as *p*-boronphenylalanine,[369] ruthenium drugs,[370] and triphenylphosphine compound derivatives.[371]

4.3.1. Therapeutic compounds—To be effective, therapeutic compounds exert their effects by acting extracellularly on cell receptors (such as Gefinib that targets and epidermal growth hormone receptor for treatment of malignant glioma)[372] or by entering the cell. To be effective, a compound that penetrates the cell must also reach the organelle that contains the compound's molecular target. In some instances, compound precursors (such as pro-drugs) may need activation in a given subcellular environment before they exert their influence on the corresponding molecular target in the same or other subcellular environment. In contrast, localization of therapeutic compounds in non-target subcellular locations (or in non-target tissues) or biotransformations of the compound into other metabolic products may lead to unwanted side effects, cytotoxicity, or reduced potency. Subcellular analysis of xenobiotics helps establish whether a compound is potentially effective or if it may lead to secondary cytotoxic effects.

The relevance of subcellular anti-cancer agent accumulation and metabolism has drawn significant attention. *N*-L-leucyldoxorubicin is an approved doxorubicin p rodrug that upon activation to doxorubicin causes cardiotoxicity. The subcellular distribution and metabolic transformations of *N*-L-leucyldoxorubicin in cultured c ancer cells were recently investigated.[373] Four subcellular fractions prepared from wild type and doxorubicin-resistant human uterine sarcoma cells were treated with *N*-L-leucyldoxorubicin and analyzed by m icellar electrokinetic chromatography. This technique separates doxorubicin from *N*-L-leucyldoxorubicin making their quantification possible. The accumulation of doxorubicin relative to *N*-L-leucyldoxorubicin was highest in the nuclear fraction, followed by the lysosome-containing fraction. These findings suggest that the pro-drug *N*-L-leucyldoxorubicin is effective at delivering its product doxorubicin to the nucleus, which

hosts one of the primary doxorubicin targets. It also suggests that accumulation in the lysosome may modulate the overall efficacy of this anti-cancer treatment.

Mitoxantrone is a fluorescent anthracenedione whose anti-cancer properties resemble those of doxorubicin. The subcellular distributions of mitoxantrone in human MDB-MB-231 cells and MCF-7 breast cancer cell lines were determined by confocal fluorescence microscopy.[374] Although mitoxantrone was found in the nucleus in both cell types, the compound was also co-localized in the cytosol, which is an indicator of trafficking by this compound in each cell line. MCF-7 cells manifested a diffuse cytosolic localization of mitoxantrone, while MDB-MB-231 cells displayed a more punctuate pattern. Fluoresence intensity was 2.5-fold higher in MCF-7 suggesting a higher intracellular concentration, which is in agreement with the higher cytotoxicity of this compound in the latter cell line. Surprisingly, the ER of the MCF-7 cells displayed fluorescence with a different emission spectrum, which may be caused by either a different subcellular environment or biotransformation of mitoxantrone into a different compound.

Ruthenium drugs and the platinum drug cisplatin bind to DNA in the nucleus halting DNA replication, which is vital for cancer cell proliferation. Unfortunately, platinum drugs are also very toxic to non-cancer cells. Such toxicity may be associated with drug accumulation in other subcellular environments. A recent study investigated the uptake and subcellular distribution of cisplatin and two ruthenium drugs, KP1019 and NAMI-A (Figure 24), in wild type human ovarian carcinoma cells and cisplatin-resistant cells.[370] The subcellular enriched fractions were analyzed by size exclusion chromatography equipped with an ICP-MS detector. This detector can easily monitor platinum and ruthenium with high sensitivity. The analysis showed cisplatin and the ruthenium drugs are present in the nuclear, organellar, and cytosolic fractions in both cell types. Ruthenium drugs were most localized in the organelle fraction while cisplatin distributed equally between the nuclear and organelle fraction in the wild type cell line. Further analysis indicated that all three drugs were present in the mitochondrial fractions. In the cisplatin-resistant cell line, all t hree drugs were still observed in the nuclear, organelle, and cytosolic fractions; however, their subcellular distributions were different. A majority of cisplatin was observed in the organelle fraction and most of the ruthenium-compounds were found in the nuclear and organelle fractions. Cisplatin was not detected in the mitochondrial fraction of resistant cells and KP1019 was decreased 3.7-fold in the mitochondria fraction. Determining the subcellular localization of the cisplatin and ruthenium drugs is relevant to define their intracellular trafficking and their possible cytotoxicity mechanisms.

Compounds with triphenylphosphine moieties, which are positively charged and hydrophobic, accumulate in mitochondria due to the negative membrane potential of these organelles. A series of triphenylphosphine moiety-containing compounds were screened for anti-cancer effects in numerous cancer cell lines.[371] Three novel triphenylphosphine-containing compounds (Figure 25) showed mitochondrial colocalization and contained anti-cancer properties as determined from submicromolar IC_{50}, arrested cell cycle, and inhibited tumor growth i n mice. These compounds caused decreased oxygen consumption, increased superoxide production, and changes in abundance or phosphorylation of 103 proteins. The latter is critical to cancer studies because phosphorylation regulates cell cycle progression, growth factor signaling, and DNA transcription. Subcellular localization was investigated by confocal fluorescence microscopy. These findings imply that mitochondria may play a prominent role in the anti-cancer properties of these compounds.

A promising compound for brain cancer therapy is *para*-boronphenylalanine whose subcellular distribution in T98 glioblastoma cells was recently investigated.[369] Secondary ion mass spectrometry of glioblastoma cells treated with ^{10}B-boronphenylalanine revealed

boron accumulation in mitochondrial, nuclear, and the cytosolic regions with levels that increased with treatment length. The mitochondrial region had lower ^{10}B levels than either the nuclear or the cytosolic regions. Boron accumulation in the nucleus increased in cells after 1 hour, was unchanged at 2 hours, but nearly doubled after 6 hours. Dual labeled ^{13}C and ^{15}N-phenylalanine uptake had a similar profile to ^{10}B-boronphenylalanine. The authors suggest that intracellular processing of boronphenylalanine and phenylalanine was different due to their different subcellular distributions.

Nilutamide is an anti-androgenic drug used for metastatic prostate cancer that has interstitial pneumonitis as a side effect, o r inflammation of lung tissue. Biotransformations of nilutamide in three subcellular fractions revealed that the cytosolic and not other subcellular fractions (microsomal, mitochondrial, or nuclear) had the highest metabolic activity in rat lung.[375] Reverse phase HPLC-ESI mass spectrometry revealed that the main metabolites were hydroxylamino-and amino-derivatives of nilutamide when the subcellular fractions were incubated with nilutamide and FMN, NADPH, and NADH as cofactors. These findings may imply that the cytosolic accumulation of metabolites contribute to the etiology of the observed side effect.

A new type of noncationic myocardial imaging agent that exhibits wide-range bio-distribution in tissues is ^{99m}Tc(N)-bis-(*N*-ethoxyethyl)dithiocarbamato-bis-(dimethoxy-propylphosphinoethyl)ethoxyethalamine (^{99m}Tc(N)-(DBOC)(5)) (Figure 26). A recent report described the subcellular localization and metabolism of ^{99m}Tc(N)-DBODC(5) in subcellular fractions from rat myocardial tissue.[376] To calculate the levels of this agent in each subcellular fraction, the ^{99m}Tc(N)-(DBOC)(5), detected with a gamma counter, was normalized to the mitochondria-specific malate dehydrogenase activity of the corresponding fraction. The mitochondrial fraction contained ^{99m}Tc(N)(DBODC)(5), but its levels decreased dramatically when mitochondria were depolarized with carbonylcyanide-*m*-chlorophenylhydrazone. This suggested localization to mitochondria is membrane potential dependent. One drawback of this study was that mitochondria ruptured during the sample preparation procedure and released ^{99m}Tc(N)-(DBOC)(5) into other subcellular fractions, which implies higher than reported accumulation of these compounds in mitochondria.

4.3.2. Toxic compounds—With the increase of nanoparticle use for drug delivery systems, it is important to ensure that the nanoparticles themselves do not cause non-target toxicity or decrease the efficacy of the delivered drug. Subcellular analysis of medulloblastoma cells exposed to rhodamine B isothiocyanate poly (glycerol-adipate) nanoparticles demonstrated that the particles were degraded effectively in endosomes and lysosomes.[377] Transmission electron microscopy, flow cytometry, and confocal fluorescence microscopy all indicated the nanoparticles entered endosomes and localized to lysosomes where they were rapidly degraded. None of the nanoparticles were observed in the nucleus or other subcellular regions where they may contribute to cytotoxicity.

Polycyclic aromatic hydrocarbons are a potential hazard because of their mutagenic and carcinogenic properties. As soil contaminants, they may enter organisms, particularly plants, thereby entering the food chain. The first step in this process is the accumulation of polycyclic aromatic hydrocarbons in the subcellular locations of plants. In a recent study, the accumulation of acenaphthene was determined in subcellular fractions of *G. mosseae* and *G. etunicatum* roots by HPLC with UV detection.[368] Acenaphthelene accumulation in organelles was higher than in the cell walls for both examined species. This report is the first in shifting the focus of polycyclic aromatic hydrocarbon distribution to studies at the subcellular level.

Alcohol intake is associated with deleterious effects in the uterus. Because alcohol metabolites that accumulate in different subcellular regions may be implicated, the subcellular metabolism of alcohol to acetylaldehyde in rat uterine horn tissue was recently analyzed.[378] Ethanol metabolites were analyzed with gas chromatography coupled to flame ionization detection in cytosolic, microsomal, and mitochondrial enriched fractions. Microsomal analysis was performed with and without a NADPH regeneration system (NADPH, *d,l*-isocitric acid, and isocitric dehydrogenase) under aerobic conditions. Cytosolic analysis was carried out with hypoxanthine, NAD$^+$, and ethanol under aerobic c onditions. The microsomal fraction displayed higher metabolism than the cytosolic fraction and did not require NADPH. The cytosolic fraction was also capable of metabolizing ethanol to acetaldehyde in the presence of NAD$^+$ but to a lesser extent. Nearly negligible aldehyde dehydrogenase levels existed in both fractions suggesting that acetaldehyde is synthesized and not further metabolized in the microsome and cytosol subcellular fractions.

Mining and contamination introduces increased arsenic le vels into water and sediment. This makes sediment-feeding polychaetes, such as marine worms, at risk for increased toxicity resulting from exposure to arsenite that forms from arsenate in sea water.[379] The association of arsenic exposure with accumulation, distribution, and speciation of arsenic in *A. marina* worm and its surroundings were examined in a recent study.[380] Arsenate was measured with either scintillation counting for seawater treatments or ICP-AES for sediment treatments. Subcellular fractionation of frozen-thawed *A. marina* produced three fractions containing: metal rich granules and cellular debris, organelles, and cytosolic components. The latter was further fractionated to produce a heat-sensitive protein fraction containing enzymes and a heat-stable protein fraction containing metalloproteins. Metalloproteins and metal-rich granules contained biologically detoxified arsenic, while organelles, enzymes, and cellular debris contained active arsenic species (likely arsenate and arsenite). The environments *of A. marina* had a dramatic effect on the subcellular distribution of total arsenic. Polychelates exposed to sediment with low levels of naturally occurring arsenic had 50% of the total arsenic detected in the cell homogenate (control) was in the metalloprotein fraction and 25% in the cellular debris. When worms were exposed to arsenic in the seawater, the metalloprotein and cellular debris levels remained similar to the basal levels, but arsenic appeared at 15% in the metal rich granules, 10% in the enzymes, and 5% in the organelles. With increasing arsenic levels, the cellular debris had 50% of the total arsenic and the relative arsenic levels in organelles and enzymes were lo wer. In the presence of high levels of arsenic in the sediment, arsenic levels reached 50% in the metalloproteins, 25% in the cellular debris, and 10% in the metal rich granules. These results suggest the cytosol is the main arsenic reservoir at basal-levels, but increased exposure leads to arsenic accumulation in the cellular debris, organelles, and enzyme fractions. While storage in the cellular debris is likely temporary, the transient storage of arsenic in both the organelle and enzyme fractions is significant when considering their association with arsenic toxicity.

4.4. Elemental analysis

The subcellular distribution of different transition metals using X-ray fluorescence microscopy has recently been reviewed.[56] Both labile and metalloprotein-bound iron were found to play critical roles as reaction centers in many subcellular compartments including the nucleus, mitochondrion, lysosome, and chloroplast.[381] The subcellular distribution of iron in *P. sativum, L. esculentum* and *A. thaliana* was investigated by transmission electron microscopy, confocal fluorescence microscopy, micro X-ray fluorescence (μXRF), and micro particle-induced x-ray emission (μPIXRE). μXRF and μPIXRE detected x-ray fluorescence specific to elements such as iron. The nucleus of *P. sativum* embryos and *A. thaliana* and *L. esculentum* embryos and leaves were iron-rich. As determined from overlapping images obtained with different techniques used in this report, iron was observed

in the cell periphery and in vacuoles. The increased concentration of iron in the nucleus is an interesting discovery when considering its possible interactions with nucleic acids.

5. Organelle dynamics, interactions, and maturation

Organelles display a dynamic morphology and movement within the cell. Dynamic morphologies result from maturation and growth, fusion and fission, and from interactions with other organelles. The subset of interactions in this complex network that is discussed in this section, as shown in Figure 27, occur among organelles of the same type (homotypic interactions) or different types (heterotypic interactions). Homotypic interactions will be reviewed in 5.1. –5.5. and heterotypic interactions will be reviewed in 5.6. –5.10.

Organelle movement within the cell changes with cellular function as the cell undergoes processes like cell division, stress, or cytokinesis. Not surprisingly, one of the critical areas of subcellular analysis has included monitoring the dynamics of m ovement and morphological changes of organelles both in whole cells and after organelle isolation. A recent review has focused on the most common techniques used to monitor and investigate organelle dynamics.[71] The reader may consult this review to explore such techniques in more detail.

Most observations of organelle dynamics have been obtained by imaging cultured cells and not tissues. Subcellular images are difficult at deep tissue regions due to field penetration issues. However, when tissues such as plant roots have microscopic features such as root hairs, organelle dynamics could be monitored in vivo.[382] Therefore most of the studies included in this section investigate dynamics in cell culture systems. One alternative to investigate dynamics in whole tissue is to utilize indirect methods such as those based on the morphology of mitochondrial networks in the heart determined by electron microscopy.[72] Some reports mentioned in this section make use of this technique.

Another essential component to investigate subcellular interactions has been the ever increasing knowledge of the proteins involved. Despite the multiple types of possible organelle interactions (c.f. Figure 27), the majority of these interactions rely on three types of proteins: Soluble *N*-ethylmaleimide-sensitive factor activating protein receptors (SNARE), Rab, and proteins that are part of large complexes such as the homotypic fusion and vacuole p rotein-sorting (HOPS) complex. Understanding the role of these proteins in subcellular interactions generally requires genetic alteration of their levels using knockouts, knockdowns or overexpression and the use of techniques such as confocal fluorescence microscopy or transmission electron microscopy. Because of the importance of the function of these proteins in multiple reports included in this section, we explain salient features of these proteins in the next three paragraphs.

SNARE proteins are responsible for trafficking, docking and fusion.[383] When SNARE proteins interact with each other they coil, b ringing membranes in different organelles in d irect contact with each other.[383] SNAREs are typically classified into subgroups such as v-SNARE (SNARE present on an interacting *vesicle*) and t-SNARE (the SNARE residing on the interacting vesicle's *targeted* membrane). Another common classification is R-SNARE (v-SNARE) and Q-SNARE (t-SNARE). The R and Q designation indicates the presence of either a glutamine or arginine amino acid in the SNARE.[383] When organelles begin to interact and SNARE proteins interact, SNAREs can be classified as *trans*-SNARE complexes. Once tethering occurs, the two organelle membranes begin to interact with each other and eventually form a single membrane. At this point, the SNARES are classified as *cis*-SNARE complexes. Interacting organelles will then complete fusion and the individual SNAREs used to form the SNARE complexes can be recycled or degraded. Some of the essential tSNARE proteins that are part of recent reports involving subcellular analysis are

synaptosome-associated proteins (SNAP) and syntaxin. Similarly, among the vSNAREs that are relevant to recent reports involving subcellular analysis is the vesicle-associated membrane protein (VAMP).[383]

Rab proteins are GTPases that cycle between GTP-bound and GDP-bound states and are believed to regulate SNARE activity.[384] Rabs are able to recruit multiple cytosolic proteins to the membranes. These proteins are capable of regulating SNAREs either directly or indirectly through Rab effector proteins.[385] An excellent review of Rab proteins has been recently published.[384]

In addition to Rabs and SNAREs, protein complexes can have either a direct involvement in the formation of the *trans*-SNARE complex or promote organelle interactions indirectly. One of these complexes is the HOPS complex that is a tethering factor capable of inducing vacuole-vacuole and endosome-vacuole interactions through t-SNARE formation.[386] HOPS can function independent of Rab proteins or in association with Rab proteins that facilitate organelle interaction.[386] Another important player in organelle interactions is the CORVET complex (class C core vacuole/endosome tethering), which is similar in protein composition to the HOPS complex, but involved in interactions between endosomes and the Golgi.[387] A third important complex is the ESCORT complex (endosomal sorting complex required for transport), which is utilized for endosomal interactions.[388]

5.1. Mitochondrial dynamics and morphology

Mitochondrial fusion, fission, and movement along the cytoskeleton are essential processes in cell function. Mitochondrial movement along the cytoskeleton is highly coordinated with their morphology. Two mitochondria moving towards each other may fuse and exchange their contents after contact. Similarly, fission of mitochondria has to involve adjacent mitochondrial regions pulling apart with opposite directionality. The balance between these two processes defines morphology and is influenced by factors such as Ca^{2+}, nitric oxide, and protein aggregates.[389] While many proteins involved in these processes have been identified,[390] one of the remaining challenges is to understand how such proteins contribute to the plasticity and dynamics of mitochondria. Most of the recent advances in mitochondrial fusion and fission have involved the use of fluorescent proteins in combination with live track fluorescence microscopy. Salient examples of advances in the field of mitochondrial dynamics include studies comparing the dynamics of mitochondria and cytoskeleton,[391] description of mitochondria that are unable to exchange contents,[392] the exchange of respiration complexes due to mitochondria fusion and fission,[393] and the discovery that mitochondria on different cytoskeletal tracks can still interact.[394]

Because cytoskeletal polymerization and depolymerization dynamics occur at rates of microns per minute and are ten-fold faster than mitochondrial movement, the interactions between cytoskeleton and mitochondria require speed-matching molecular adaptors. Subcellular imaging facilitated the identification of a new molecular adaptor mmb1p in yeast.[391] The approach to define the role of this adaptor protein required using the proteins atb2p and cox4, which are in the cytoskeleton and mitochondria, respectively, as trackers. Colocalization of the green fluorescent protein (GFP) and red fluorescent protein (RFP) constructs of mmb1p and cox4, respectively, demonstrated that mmb1p interacts with the mitochondrial network. Similarly, colocalization of the fluorescent protein mCherry construct of atb2p with the mmb1p-GFP demonstrated that mmb1p also interacts with cytoskeletal microtubules. Live imaging using these protein constructs demonstrated that mmb1p slows down depolymerization of the cytoskeleton confirming that this protein works as a speed-matching molecular adaptor.

Mitochondrial fusion enables the mixing of mitochondrial contents and may help compensate for damage in mitochondrial regions. Fission of a mitochondrion leads to two daughter mitochondria: one polarized and one depolarized, with the depolarized mitochondrion commonly destined for mitophagic degradation. Live track imaging has shown that mitochondria show concerted fusion/fission events as shown in Figure 28.[395] These events appear in a "kiss and run" pattern with fusion lasting for 1 to 2 minutes. However, not all mitochondria appear to fuse or to experience fission.[395–396] Live track imaging of mitochondria labeled with MTPA-GFP, a photoactivable (PA) fluorescent protein that localizes to the mitochondrial matrix, has shown that the activated GFP redistributes among some but not all mitochondria. In fact, some mitochondria retained their fluorescent load instead of distributing it to other mitochondria. The use of live track imaging of mitochondria with photoactivation of fluorescent proteins has also been applied to other biological systems as shown by a recent report that used this approach to monitor the movement of mitochondria on the cytoskeletal tracks of live BY-2 tobacco cells.[397]

Live tracking microscopy has been adapted to monitor exchange of membrane proteins after mitochondrial fusion. A study focused on the distribution of Complex I, tagged with RFP or GFP after fusion of cells induced by polyethylene glycol.[398] After one hour, Complex I in mitochondria from both cells have mixed and Complex I showed a patchy appearance. Similarly, other complexes of the electron transport chain, labeled with either GFP or DsRed, showed mixing and patchy appearance in 10–24h after fusion as seen in Figure 29.[393]

An important discovery based on live track imaging was the transient fusion of mitochondria from adjacent microtubule scaffolds.[394] Using various matrix targeted fluorescent proteins, such as PA-GFP, kindling fluorescent protein (KFP), GFP, yellow fluorescent protein (YFP), and RFP, high resolution confocal imaging showed extremely short exchanges (4 seconds) between two mitochondria, that upon separation preserved their original morphology. Monitoring membrane potential with the dye $DiIC_1(5)$ and controlling temporal resolution using photoctivable KFP suggested that having a high membrane potential is not required for transient fusion/complete fusion. This report strongly suggests that mitochondrial dynamics are indeed more complex than initially anticipated. In may not be simply a fusion-fission process that uses the cytoskeleton as scaffold. In fact, other forms of communication between mitochondria and peroxisomes that appear budding of 100-nm diameter vesicles from mammalian mitochondria have been recently suggested.[399]

5.2. Peroxisome dynamics and morphology

Peroxisomes form de novo from the ER or via growth and division. Both mechanisms appear to operate simultaneously in mammalian cells and only by growth and division in yeast. Therefore, subcellular analysis of yeast is a suitable model to explore the process of peroxisome fission.

The yeast species *Hansenula polymorpha* has only one peroxisome that experiences fission during vegetative reproduction, which results in the transfer of a new peroxisome to the daughter yeast cell. The dnm1 mutant of *H. polymorpha* has its peroxisome arrested in a late step of fission. In order to monitor the process of fission, GFP constructs of proteins involved in this process, including Pex8, Pex10, Pex 14 and Pex25, observed by fluorescence microscopy showed the spatio-temporal distribution of these peroxisome membrane proteins in budding cells.[400] The stages of peroxisome division were controlled using different media containing methanol/methilamine to induce peroxisome biogenesis and then methanol/ammonium sulfate to repress Pex25-GFP synthesis. Two distinct regions were apparent: a single large organelle in the mother cell and a long tubular extension protruding into the developing bud. These regions are shown in Figure 30. Because

biogenesis of peroxisomes by fusion is conserved, the findings of these subcellular studies are of high relevance to investigating peroxisome biogenesis in other species.

Similar subcellular studies of peroxisomes using confocal microscopy showed the role of Pex11p in segmentation and d ivision in peroxisomes of mammalian COS-7 cells.[401] The fluorescent protein DsRed fused to the peroxisomal targeting signal 1 was used to localize peroxisomes and their tubular extensions. The protein fusion Pex11p beta-YFP(m) was used as scaffold and then truncated versions of this scaffold were used to identify the key molecular features in this protein that are responsible for its distribution during peroxisomal fusion.

5.3. ER and Golgi apparatus dynamics

The ER and the Golgi apparatus display one of the most complex and dynamic subcellular structures. The ER has a series of tubules and sheets that are thought to be interconnected, defining a continuous luminal space. Dynamic processes of the ER include budding (secretory pathway), vesicle incorporation (secretory pathway), new tubule formation (cytoskeleton association), tubule retraction (cytoskeleton association), transitions between tubules and sheets, fusion of tubules, and tubule breakage.[402] The interactions of the Golgi have also recently been reviewed.[73]

The morphological changes of the ER that occur during mitosis have been recently investigated.[403] Using confocal microscopy to monitor the ER-specific fluorescently tagged protein Hsp47-GFP, this report shows that during mitosis the ER is mostly tubular and remains continuous. It also demonstrated that stripping the rough ER of ribosomes during the interphase made the ER mostly tubular. The images were processed to quantify subcellular features including branch points, total profiles and tubule lengths. ET confirmed the morphological details determined from the confocal microscopy images.

One of the challenges in subcellular studies of the Golgi is that the same molecular markers are also found in the ER from which they shuttle to the Golgi. A clever approach to investigate Golgi dynamics in response to treatments used confocal microscopy imaging to determine the subcellular localization of β-1,4-galactosyltransferase-cyan fluorescent protein (GalT-CFP) as either Golgi (condensed structure) or the ER (diffuse structure).[404] Treatment with Brefeldin A (BFA), which fully collapses the Golgi complex toward the ER was used to illustrate this technique and its automation. After application of Brefeldin A the Golgi disappeared. After washing off BFA, the Golgi began reassembling as reported by tracking GalT-CFP. The procedure took advantage of subcellular features (i.e. nuclear envelope) to automatically localize the Golgi in many cells in parallel. Although the dynamics of subtle processes are not revealed in this system due to speed of image acquisition and resolution, this is a promising technique to elucidate morphological changes of the Golgi resulting from other drug treatments or cellular states.

5.4. Lipid droplet dynamics

Lipid droplets have been reported to experience fusion (See Table 1). Time lapse microscopy was used to monitor fusion of lipid droplets in Drosophila S2 cells expressing LSD1-mCherry and BODIPY 493/503.[405] LSD1-mCherry is on the surface of the droplet, while the BODIPY stain accumulates within the entire droplet. This subcellular assay was used as a reporter to identify genes that are associated with lipid droplet fusion that leads to their enlargement.

5.5. Dynamics of isolated organelles and organelle models

Fusion and fission studies carried out in cell-free assays facilitate control of the experimental conditions used for subcellular analysis. On the other hand, many previous reports carried out on isolated organelles had been unable to mimic the *in vivo* dynamics of organelles. Recent reports demonstrated the use of isolated organelle preparations to investigate mitochondria fusion and fusion, fission of vacuoles in yeast, antegrade and retrograde transport between the Golgi and ER, and fusion of artificial vesicles. Salient examples on these topics are reported below.

A chemiluminescence assay to monitor fusion of isolated mitochondria was recently reported.[406] The assay is based on two separate cell lines expressing only venus-zipper-luciferase or luciferase-zipper-venus localized to mitochondria. Chemiluminescence is only emitted if the venus-zipper luciferase and luciferase-zipper-venus combine to form an active renilla luciferase. In this study, mitochondria were isolated and mixed that resulted in detection of chemiluminescence under conditions resembling those of the cytosol in whole cells. Investigation of how cytosolic factors such as those involved in apoptosis or involved in organelle fusion confirmed the validity of the method.

In yeast, vacuoles are the t erminal compartment in the endocytic pathway. Fusion of vacuoles is an essential process of this pathway. In order to elucidate the molecular basis of this process, a previously used in vitro technique combined isolated vacuoles isolated from two separate yeast strands.[407] Each strand has the components needed for activation of alkaline phosphatase upon vacuolar fusion. One strand had Prb1p, a vacuolar serine protease; the second strand had pro-alkaline phosphatase that was activated by Prb1p upon fusion. Fusion was reported as activity of alkaline phosphatase that transforms para-nitrophenol phosphate into *p*-nitrophenol. This assay is widely applicable as demonstrated by extending its use to investigate how novel factors that control fusion and fission of yeast vacuoles[408] and the role of osmolarity on yeast vacuole fusion.[409]

Fission of yeast vacuoles has been also investigated *in vitro*.[410] The studies revealed that the vacuole-associated target-of-rapamycin complex 1 (TORC1) stimulates vacuole fragmentation. Although salt concentration and temperature also play a role in fission, these factors cannot explain the level of fission caused by TORC1. On the other hand, ATP and GTP hydrolysis were essential for in vitro fission. Because TORC1 is inactivated during nutrient restriction (autophagy) during which vacuole volume increases, the *in vitro* observations of the TORC1 reported here are in agreement with physiological aspects of vacuole fission.

Another study on fission used unillamellar liposomes immobilized onto silica beads as organelle models. An excess of liposomes were deposited onto the silica beads in the presence of a high ionic strength buffer. Addition of dynamin and GTP led to formation of tubules, formation of vesicles and their fission in the form of budding vesicles. Although the dynamics are much slower than those observed in cells, this subcellular model provides evidence that dynamin is a key player in fusion and that it is not removal of GTP that causes fusion. Similar studies on fission using artificial organelle models could be done with other proteins that are involved in the fission of the ER (Sar1 GTPase) or the Golgi (Arf1 GTPase).[411]

Fission is also a key feature of transport between the Golgi and the ER, because it is involved in the formation of vesicles where budding begins. Transport from the ER to the Golgi requires GTP hydrolysis and a coating defined as COPII, which includes Sar1p, Sec23/24p, and Sec 13/31p proteins. Using giant unilammelar liposomes that mimic the composition of the ER and that are observable by confocal microscopy, a recent report

described that the coat is essential for formation of a tubular structure (bead-on-a-string morphology) that is prominent in the reconstituted liposomes when GTP is replaced by a non-hydrolysable analog. These observations also suggest that other proteins must be participating to regulate the degree of fission and that transport may include structures other than single vesicles such as a fused train of partially joined vesicles.[412]

A related study used giant unilammelar liposomes with compositions resembling that of the Golgi to investigate the retrograde transport from the Golgi to the ER.[413] Because of the enlarged size of the liposomes, the resolution of fluorescence microscopy was adequate to observe membrane deformation and track fluorescently labeled species. Resembling conditions in the Golgi (e.g., low membrane tension) the protein Arf1 interacted with the coatamer (complex mixture of coat-related proteins) in the Golgi membrane system inducing regions of extensive membrane deformations with lipid compositions, which are believed to b e different from the parental membrane. In contrast to fission observed in the liposome model of ER to Golgi transport, the retrograde transport model from the Golgi to the ER did not show vesiculation. On the other hand, the clearly defined membrane deformations that were observed suggested that such deformations are critical to the tubovesicular transport between the Golgi and other intracellular compartments.

5.6. Endocytic organelles and endocytosis

While the autophagy pathway is responsible for the degradation of cargos already present in the cell, the endocytic pathway is responsible for the internalization and degradation of extracellular material. Endocytosed cargo can be recycled for usage at the plasma membrane or degraded to serve as cellular fuel. Internalization may take different forms: phagocytosis, macro-pinocytosis, clathrin-coated, and caveolae based endocytosis. A schematic of endocytosis is shown in Figure 32.[414] After internalization, the first intracellular organelles formed are the early endosomes. In addition to their maturation to late endosomes, early endosomes may interact with recycling endosomes to return endocytosed material back to the extracellular space. Early endosomes may also interact with the Golgi to deliver endocytosed materials.[415] Despite their multiple interactions, the most common fate of early endosomes is their maturation into late endosomes. Late endosomes are more acidic than their precursors, the early endosomes. Due to their structure, they are also known as multivesicular bodies (Table 1). In addition to maturation to lysosomes, late endosomes are also able to interact with autophagosomes to form amphiosomes (See 5.7.2).

Some of the key molecular players in the maturation of endocytic organelles and their interactions with other subcellular compartments have been identified as described in the Introduction of 5. For example, Rab7 is recruited and activated to mature early endosomes into late endosomes.[416] The importance of subcellular analysis in defining the roles of such molecules cannot be underestimated. On the other hand, describing all the studies in which subcellular analysis has contributed to examine the roles of such molecules would be repetitive. For this reason, we have tabulated most of these recent studies in Table 12. Below, we discuss salient reports related to maturation (5.6.1) and other interactions (5.).

5.6.1. Maturation, from early endosome to lysosome—The first interactions in the endocytic organelle pathway are those of the early endosomes. The SNARE protein sorting nexin 27 (SNX27) mediates early endosome maturation to late endosomes through Phox-containing domains.[417] Recruitment of these protein domains to endosomes is regulated by phosphatidylinositol 3-phosphate. A recent study used confocal fluorescence microscopy to show that SNX27 is present in early endosomes, clathrin coated vacuoles, and endocytic trafficking vacuoles of rat neurons. This study also used a yeast two-hybrid screen, which is a valuable tool to identify protein binding partners and to assist in determining the specific

function of proteins. This screening revealed that SNX27 interacts with *N*-methyl-D-aspartate receptor 2C, which was reflected by an increase in this protein level when SNX27 was knocked down. Lastly, the SNX27 knockdown had an 85% reduction in N-methyl-D-aspartate receptor 2C localized to endocytic vesicles, which confirms the importance of the role of SNX27 in endocytic maturation.

Vps45 is a SNARE protein essential for organelle fusion. The effects of Vps45 and its interacting protein rabenosyn-5 on early endosome maturation were studied in *C. elegans*.[418] Texas Red-labeled BSA was endocytosed to monitor endocytosis flux and GFP-Rme8 fluorescence was used as a marker for endosomes. Confocal fluorescence microscopy was performed at multiple time points to determine changes associated with modified Vps45 and rabenosyn-5 functionality. An increase in the number of small endosomes and a decrease in late endosome-lysosome interaction were observed in V ps45 mutated cells. The yeast two-hybrid assay confirmed rabenosyn-5 interacted with Vps45. Expression of a mutated form of rabenosyn-5 gave a similar phenotype observed with mutated Vps45. Lysosome morphology was not affected by mutations in either Vps45 or radenosyn-5 suggesting Vps45 and rabenosyn-5 mainly exerted their effects on endosomes. This data suggests Vps45 and rabenosyn-5 are able to regulate interactions between endosomes and lysosomes.

Early endosomes collect vacuoles from the plasma membrane containing endocytosed materials, such as transferrin, cholera toxin B, low-density lipoprotien, and dextran. Materials such as transferrin and cholera toxin B are then delivered to the Golgi and ER for reuse in the cell and low density lipoprotein and dextran are delivered to the late endosome and lysosome for degradation. Synthetic fluorescent analogues of transferrin, acetylated-low density lipoprotein, cholera toxin subunit, and dextran were used to investigate *in vitro* fission of early endosomes in rat adrenal medulla cells.[419] The *in vitro* assay developed is based on confocal fluorescence microscopy imaging of organelles isolated from cells loaded with he fluorescent analogues m entioned above. After endocytosis of transferrin or low-density lipoprotein for five minutes, cells were diluted into cargo-free medium for 30 minutes. After the chase, the cells were homogenized and the post-nuclear fraction was imaged. To increase fission of early endosomes, the supernatant was incubated at 37°C in the presence of ATP and rat brain cytosol. Confocal fluorescent microscopy showed fission of early endosomes characterized by the segregation of cargo consisting of two fluorescent species originally colocalized within the early endosome. Such segregation reflects mechanisms by which the fission process separates cargo trafficking to the Golgi and ER (e.g., AlexaFluor488-transferrin) or to late endosomes and lysosomes (e.g., AlexaFluor594-acetylated low density lipoprotein). Initially early endosomes will contain both fluorophores, but as they segregate into vesicles, the fluorophores are no longer colocalized. The assay was used to identify key proteins involved in early endosome fission. Inhibiting the function of early endosomal auto antigen 1 (EEA1), which is used in binding vesicles, by treatment with anti-EEA1 antibody inhibited the fission of early endosomes (i.e. the fluorescent transferrin and low density lipoprotein cargo remained colocalized). Cells possessing a mutated form of the protein *N*-ethylmaleimide-sensitive factor, which participates in recycling of *cis*-SNARE complexes, also inhibited early endosome fission. This suggests both EEA1 and *N*-ethylmaleimide-sensitive factor are important for early endosome interactions with other organelles.

A recent study investigated diphtheria toxin processing through endocytosis and showed the importance of Rab5 in this process in H eLa cells.[423] Confocal fluorescence microscopy was used to determine colocalization and fusion of early endosomes and late endosomes by tracking either YFP-labeled or GFP-Rab5. After cellular exposure to diphtheria toxin, YFP-Rab5-containing organelles increased in size. Increasing the pH of these organelles with the lysosomotropic agent ammonium chloride prevented the increase in size and suggested the

organelles were early endosomes. YFP-Rab5-labeled organelles also had E EA1, a marker for early endosomes, confirming their identity as early endosomes. When Rab5 was mutated, the increase in the size of early endosomes after diphtheria toxin exposure was also no longer observed. Since Rab5 is known to regulate endosome interactions, this also suggests endosome-endosome interactions are involved in the mechanism that causes the diphtheria toxin effects.

Another experiment in the report above used photoactivatable GFP-Rab5 to determine how fusion and fission of early endosome change with diphtheria toxin processing.[423] Rab5-containing early endosomes had an increase in size with diphtheria toxin treatment but had no effect with Rab7 containing late endosomes suggesting that diphtheria toxin was not able to interact with late endosomes. Untreated early endosomes manifested a significant decrease in fluorescence after 5 minutes, likely due to organelle fission that decreases the levels of GFP-Rab5 below the detection limits of the imaging system. In contrast, diphtheria toxin treatment resulted in GFP fluorescent intensities that were 40% higher compared to organelles from untreated cells. The higher GFP-Rab5 fluorescence intensity suggests Rab5 had decreased fission. Overall t his experiment also suggests decreased interactions between other organelles and late e ndosomes due to diphtheria toxin incubation.

The epidermal growth factor (EGF) and its receptor (EGFR) are quite different from Influenza A virus as endocytic cargos and in their final subcellular location. EGF and EGFR are targeted to early endosomes, transferred to the late endosomes, and finally degraded in lysosomes, while the influenza A virus is endocytosed, transferred to the early endosome, then retained in the late endosome, and then finally released into the nucleus and cytosol. A recent study investigated the role of the ubiquitin-complex scaffolding protein Cullin-3 (Cul3) in the endocytosis of three very different cargos in adenocarcinomic human alveolar basal epithelial cells and HeLa cells.[425] Confocal fluorescence microscopy was used to monitor EGFR, EGF, and influenza A virus in organelles and Western blotting was used to track EGFR degradation. Transmission electron microscopy of Cul3 knockdown cells showed an increased size and increase number of vacuoles. These vacuoles were likely late endosomes because LysoTracker staining showed that they were acidic and because immunolabeling revealed that they contained Rab7. In addition, confocal fluorescence microscopy of knockdowns of Cul3 showed an increased colocalization of Influenza A virus with both LAMP1 and cation-independent mannose-6-phosphate receptor positive organelles. This suggests that they were retained in the late endosomes. In the case of EGF and EGFR, knockdowns of Cul3 had twice as many EGF-positive vesicles, which were seemingly late endosomes or lysosomes b ecause they were also immunolabeled with L AMP1 antibodies. Western blotting indicated a 9-fold increase in EGFR signal in the Cul3 knockdown cell suggesting that Cul3 is essential for EGFR degradation after EGF binding. Interestingly, when EGF was bound to EGFR for degradation, the complex was ubiquitinated even in Cul3 knockdown cells. This suggests the EGFR complex was marked for degradation by an ubiquitin ligase (not activity from Cul3) but the absence of Cul3 caused changes in endocytic flux.

5.6.1. Heterotypic interactions not involved in maturation of endocytic organelles—Endocytic organelles do not just interact with each other as shown in Figure 32 but also with other non-endocytic organelles as shown in Figure 27. An example of this is an indirect interaction with autophagosomes. The ability of ubiquilin to be degraded in chaperone-mediated autophagy (CMA) was recently investigated.[431] Ubiquilin is known to regulate ER-mediated protein degradation but its role it macroautophagy and CMA have not been determined. CMA was examined by treating enriched lysosomes with ubiquilin and assessing CMA-based lysosome internalization with an *in vitro* assay. This assay used media optimized for CMA either with or without the presence of protease inhibitors. To determine

the rate of lysosome internalization, Western blotting of ubiquilin, glyceraldehyde-3-phosphate dehydrogenase (known to be internalized by CMA), and ovalbumin (not internalized by CMA) was used. The assay indicated that 10% of ubiquilin was internalized into lysosomes by CMA. When ubiquilin had to compete for CMA internalization with simultaneous treatment with glyceraldehyde-3-phosphate dehydrogenase, ubiquilin internalization was decreased 50%. This competition was not observed with ovalbumin. When antibodies that bind either hsc70 or LAMP2A were added, both known CMA protein mediators, ubiquilin internalization was eliminated providing further evidence that ubiquilin is internalized into lysosomes with CMA. Enriched autophagosome fractions also contained ubiquilin. The authors proposed that depletion of ubiquilin with CMA could decrease the formation of autophagosomes. Accordingly, the decrease of CMA could increase the formation of autophagosomes.

Nine different Rab proteins have been identified in lipid droplets. A recent study investigated the role of some of these Rab proteins as mediators of interactions between lipid droplets and early endosomes.[432] Immunolabeling of enriched fractions analyzed by transmission electron microscopy showed high abundance of Rab5, Rab11, and Rab18 on the surface of lipid droplets suggesting that these Rabs could be the most relevant. When Rabs were inactivated via treatment with a Rab GDP dissociation inhibitor, the amount of interaction between early endosomes and lipid droplets was significantly decreased as determined by Western blotting of lipid droplets after removal of other components. To further strengthen the argument that Rabs were critical to interactions with lipid droplets and early endosomes, lipid droplets were treated with GTPγS and early endosomes. Due to their GTPase activity, presence of GTPγS locks Rabs in their active form. When droplets were treated with early endosomes and GTPγS, there was a significant increase in EEA1 and transferrin (both early endosome markers), which colocalized with Rab5 and Rab11 (lipid droplet markers). Overall, these results confirmed that Rab proteins are needed for lipid droplet-early endosome interaction. To confirm the role of Rab5, a protein known to interact with EEA1, the interaction between immunolabeled EEA1 and either wild type or mutated Myc-tagged-Rab5 was monitored *in vivo* by confocal fluorescent microscopy. Unlike the wild type, mutated Rab5 was unable to colocalize with EEA1. This suggests Rab5 is indeed needed for interactions between lipid droplets and early endosomes.

A recent report analyzed the role of endosomes in the recycling of synaptic vesicles in rat adrenal medulla cells and hamster kidney fibroblast cells.[433] Confocal fluorescence microscopy of immunolabeled early endosome SNARE proteins enabled their detection in synaptic vesicles, suggesting interactions between these two types of organelles. An *in vitro* assay was used to determine the homotypic interactions of enriched synaptic vesicles and the heterotypic interaction with endocytic organelles. Confocal fluorescence microscopy was used to track interactions with two different fluorescent treatments. Synaptic vesicles could be incubated with dextran-labeled AlexaFluor488 and dextran-labeled AlexaFluor 568 to assess colocalization of fluorophores as a result of homotypic fusion. Styryl-labeled early synaptic vesicles could also be used for confocal fluorescence microscopy analysis *in vivo*. Upon interaction and fusion with other organelles, styryl will diffuse and create increased numbers of fluorescent organelles. Homotypic fusion of synaptic vesicles and heterotypic fusion of synaptic vesicles and endosomes were both low (4%) as determined from colocalization of two different dextran labels. Styryl labeling showed extensive organelle interaction to much higher levels than with the *in vitro* assay. Nearly 50% of synaptic vesicles possessed the early endosome marker Rab5 suggesting that recycling vesicles and early endosomes had interacted and suggests synaptic vesicle interactions could extend to other endosomes e.g. late endosomes.

SNAP proteins are a type of SNARE protein with two SNARE motifs in their protein sequence. A recent report showed that the GFP-SNAP-29 protein in *C. elegans* localized to recycling endosomes.[434] Confocal fluorescence microscopy revealed the knockdown of GFP-SNAP-29 caused modified morphology of recycling endosomes, which were identified by the presence of recycling endosome specific proteins GFP-RME1, GFPRab11, and GFP-Rab10. In comparison, Golgi markers RFP-mannosidase-II, RFP-Rab6, and RFP-Rab2 and ER markers GFP-Sp-12 indicated Golgi and ER morphology were not affected by SNAP29 knockdown. As expected, knockdown of SNAP-29 also caused a decrease in secretory pathways that deliver the contents of recycling e ndosomes to the plasma membrane. This was determined by monitoring GFP labeled caveolin1 and RME2. Instead of localizing in the plasma membrane, both were located in punctates near the nucleus. The compromised secretory pathway and the altered morphology of the recycling endosomes suggest an interaction between the ER/Golgi complex and recycling endosomes.

A recent study investigated how VAMP7 and VAMP3 (both SNAREs) affected late endosome interactions with autophagosomes and the plasma membrane (through exosomes), respectively.[435] VAMP7 regulated plasma membrane-late endosome interactions in human bone marrow lymphoblast cells. Confocal fluorescence microscopy showed that a GFP-VAMP7 construct (with GPF at the N-terminus) caused VAMP7 containing exosomes to traffic but not interact with the plasma membrane. GFP-containing exosomes were larger in size as compared to exosomes possessing VAMP7-GFP (with GFP at the C-terminus). This suggests exosomes originating from late endosome interactions were unable to interact with the plasma membrane when VAMP7 was not f unctional. V AMP3 was also shown to regulate autophagosome-late endosome interactions.[435] Transmission electron microscopy revealed that VAMP3 colocalized with LC3. Starvation, which induces autophagy, caused an increase in the colocalization of Rab11, a late endosome protein, and LC3 indicating increased interaction between late endosomes and autophagosomes. Accordingly, the expression of the light chain of the tetanus protein, a protein that cleaves VAMP-3 rendering it non-functional, caused decreased interaction between autophagosomes and late endosomes. The interactions of late endosomes were further assessed to determine if VAMP7 and VAMP3 are able to regulate each other. When VAMP7 function was decreased, autophagosome-late endosome in teractions also decreased. This suggests the VAMP7 in late endosomes is able to regulate autophagosome interactions indirectly.

The unique morphology of late endosomes may originate from a subcellular network defined by the Golgi and early endosomes.[436] V-ATPase inhibition with concanamycin A caused a decrease in vesicle genesis from the Golgi. Concanamycin A treatment caused both a reduction in the number of late endosomes and protein export from the Golgi. Transmission electron microscopy of late endosomes following concanamycin A treatment displayed modified, tubular morphology. Overall, this suggests V-ATPase function is required to maintain the morphology of late endosomes. A separate experiment using confocal fluorescent microscopy and transmission electron microscopy indicated the ESCRT proteins Vps28, Vps22, and Vps2 were also distributed between both late endosomes and Golgi in wild-type *A. thaliana* protoplasts. The shared distribution of the ESCRT proteins between the two organelles suggested that the organelles had interactions. In wild type Vps2, the Golgi and late endosomes markers Syp61 and Vps2 gradually delocalized over time. The expression of mutated-Vps2 resulted in sustained colocalization of the Golgi and late endosome markers. This suggests late endosomes originated from the Golgi and that the protein Vps2 is responsible for the interaction of the two organelles.

Plants recycle plasma membrane proteins in response to environmental stress and developmental signals. A recent report provided evidence that the Golgi network and early endosomes are important in the recycling of plasma membrane proteins in *A. thaliana*

root.[437] Comparisons of Golgi and early endosome morphologies and their localization of plasma membrane markers under conditions of stress were made by transmission electron microscopy and confocal fluorescence microscopy. Stress resulted in the formation of a *trans*-Golgi network-early endosome fused organelle that contains the brassinosteroid insensitive receptor 1, which is a known plasma membrane protein.

5.7. Autophagosome maturation and interactions

Autophagosome membranes appear to originate from multiple source organelles including the ER and plasma membrane. Autophagosome interactions are shown in Figure 31. Additionally, as autophagosomes form, they must be able to interact with organelles tagged for degradation (e.g. peroxisomes, mitochondria, and ER). Once autophagosomes are formed and organelles destined for degradation have been incorporated into their double-membrane lumen, autophagosomes fuse with lysosomes to facilitate the d egradation of their cargo. Autophagosomes may also fuse with endosomes. Recent reviews have described the stages of autophagosome maturation[74–75] as well as the role of key biomolecules.[76–78] There have also been many excellent reviews published on specialized forms of autophagy such as peroxisomes (pexophagy),[79–81] mitochondria (mitophagy),[82–83] and the ER (reticulophagy).[74] These reviews have not focused on subcellular analysis.

Several reports in which subcellular analysis was essential to investigate the roles of various proteins in autophagy are summarized in Table 13. These reports have utilized confocal fluorescence microscopy of cell systems expressing fluorescent proteins or stained with chemical probes, flow cytometry, Western blotting, or transmission electron microscopy. Among these, some salient reports are further discussed below. They cover topics on the origin of autophagosome membrane,[438] the role of the protein Atg8,[439] and a new method to monitor autophagosome maturation.[440] We also review reports on autophagosome-lysosome interactions,[441] autophagosome-late endosome interactions,[442] and insights into autophagosome-mitochondria interactions.[443]

5.7.1. Autophagosome formation—The origin of the autophagosome membrane has been extensively investigated because multiple organelles have been associated with the autophagosome membrane. In particular, the ER region termed the omegasome, rich in phosphatidylinositol-3-phosphate, h as been associated with autophagosome genesis (Figure 33).[438a] Confocal fluorescence microscopy revealed that in human embryonic kidney cell the autophagosomal membrane originated from the omegasome.[438] A GFP fusion protein of double FYVE domain-containing protein 1 (DFCP1), which binds to phosphatidylinositol-3-phosphate was used to localize this phospholipid. DFCP1-fluorescent areas (punctates) were present in both ER and autophagosomes and were colocalized with LC3 in autophagosomes. Although other organelles, such as mitochondria and the plasma membrane, may contribute to the contents of autophagosome membranes, these findings provide convincing evidence for the role of ER regions in autophagosome formation and interactions between ER and autophagosomes.

A key process in autophagosome formation is membrane fusion. A recent study investigated the involvement of Atg8 in membrane f usion of liposomes and a utophagosome formation in yeast.[439] Atg8 formed a complex with phosphatidylethanolamine-containing liposomes and Atg8 mediated the tethering of membranes. Atg8 was essential for the expansion of autophagosomal membranes as determined with confocal fluorescence microscopy and Western blotting. The level of fusion between autophagosomes and liposomes increased with increasing concentrations of Atg8. Similarly, the extent of fusion was based upon the presence of Atg8 as indicated by the mutated Atg8-containing yeast. In these cells, mutations of Atg8 were identified to impair tethering and membrane fusion by decreases of

50%. Transmission electron microscopy also indicated an increase of autophagic bodies in mutated Atg8 cells.

A flow cytometry assay for monitoring autophagosome formation in human osteosarcoma cells was recently reported.[440] The cells expressed GFP-LC3, which shows the same localization properties of native LC3. GFP-LC3-I is cytosolic and GFP-LC3-II is lipidated and localized to a utophagosomes. To remove GFP-LC3-I, cells were treated with saponin that p ermeabilized the cell m embrane and solubilized LC3-I. On the other hand, GFP-LC3-II r emains within the cell. Flow cytometry measurements after saponin treatment demonstrated that very low GFP fluorescence levels remained following permeabilization, suggesting that only small amounts of GFP-LC3 were in the LC3-II f orm. Not surprisingly, when cells were treated with chloquinine, which prevents processing of LC3-II in the autolysosome, flow cytometry revealed that the levels of detectable LC3-II p rotein increased dramatically (Figure 34).[440] While cells expressing GFP-LC3 constructs were necessary, the assay was able to report how LC3-II levels during maturation of autophagosomes.

5.7.2. Autophagosome-lysosome and autophagosome-endosome interactions

—The final stage of the autophagy pathway is the interaction and fusion of lysosomes and autophagosomes to form autolysosomes. This fusion facilitates degradation of cargo internalized inside autophagosomes. Subcellular analysis has been critical to investigate the roles of proteins involved in autophagosome-lysosome interactions. Some examples of these s tudies include the identification of new proteins involved in the process such as TECPR1[444] and the Rab protein OTAL1,[447] the characterization of the interaction between UVRAG with either beclin1 or C-Vps [449] and the role of histone deacetylase 6.[446] The effect of cellular conditions, such as ER stress,[450] lipid levels, cofactor presence, pH, and temperature,[448] on autophagosome-lysosome interactions have also been investigated.

On this topic, a recent study monitored the dynamics of the interactions between autophagosomes and lysosomes in real time.[441] Rat kidney cells were used for this study. Live-cell imaging was used to monitor lysosomes labeled with Oregon Green 488 dextran and autophagosomes labeled with mCherrry LC3. Both interactions between the lysosomes and autophagosomes, kiss-and-run and complete fusion, were observed. Autolysosomes formed by complete fusion had a much longer lifetime than autophagosomes.

Besides their terminal interaction with lysosomes, autophagosomes have also been shown to fuse with endosomes to form amphiosomes. Subcellular analysis has helped explore the role of proteins involved in the process of amphiosome formation including endosomal sorting complex required for transport (ESCRT) proteins: Vps4, Fab1,[388a] β-COP, and α-COP.[388b] These and other recent reports on autophagosome-endosome interactions are included in Table 13.

Besides proteins, other species such as calcium also regulate interactions between autophagy and late endosomes to form amphiosomes.[442] In human bone marrow lymphoblast cells, autophagy induction caused amphiosome formation in a calcium-dependent manner as assessed by fluorescence confocal microscopy. Amphiosomes were identified because they displayed colocalization of the autophagosome marker LC3 and the late endosome marker protein Rab11. The interaction was confirmed by knocking down Rab11, which prevented the interaction from occurring. This study also demonstrated that the formation of amphiosomes is independent from the formation of autolysosomes, because inhibition of the interaction of the autophagosomes and lysosomes had no effect on the fusion of late endosomes and autophagosomes.

Autophagosomes containing pathogenic bacteria can be defined as xenophagosomes that are able to degrade bacteria as part of the immune response in non-phagocytic cells. A recent study investigated whether specific SNARE proteins such as VAMP7, VAMP8, and Vti1b were involved in xenophagosome-lysosome interactions in human breast adenocarcinoma cells, lung adenocarcinoma epithelial cells, and HeLa cells infected with Group A *Streptococcus.*[339] Confocal fluorescence microscopy was used to assess the localization SNARE proteins in the lysosome (colocalization with LAMP1), the autophagosome (colocalization with LC3-II) or the autolysosome (both markers). Vti1b-GFP was localized with xenophagosomes independently of lysosome interaction. VAMP7 and VAMP8 localized to xenophagosomes only when these organelles interacted with lysosome. Knock down of the SNARE proteins suggested only Vti1b and VAMP8 mediated the interaction of autoxenophagosomes and lysosomes. Proteins required for t raditional autophagosome-lysosome interactions such a s the q-SNAREs syntaxin 7 and syntaxin 8 were not needed for fusion of the xenophagosome and the lysosome. This suggests that VAMP8 and Vti1b are involved in a different route for autophagic degradation that does not involve syntaxins 7 and 8.

5.7.3. Mitophagy—There have been several recent reports in which subcellular analysis has advanced understanding of autophagy that specifically targets mitochondria, which is termed mitophagy. We review here studies that provide insights on the proteins required for proper mitophagy activity.

One study investigated the role of the protein Parkin in the recruitment of dysfunctional mitochondria to autophagosomes in HeLa cells.[443a] The loss of function of Parkin2, which is commonly associated with the early onset of Parkinson's disease, has been linked to autophagy deficiency. Because mitochondria depolarization is involved in Parkin recruitment to mitochondria, CCCP treatment was used to cause mitochondrial depolarization. Small, depolarized mitochondria labeled with mCherry-Parkin were colocalized with GFP-LC3-II in autophagosomes pointing to mitophagy of depolarized mitochondria. To further investigate the role of Parkin, either wild-type or knocked-down Parkin HeLa cells were treated with CCCP. In the wild-type, no mitochondria were detectable after 48 hours. In the Parkin knock-downs, fragmented mitochondria were still present after 48 hours. This work points to the critical role of Parkin in mitophagy of HeLa cells.

Similar to Parkin, extracellular signal-regulated protein kinase 1/2 (ERK1/2) is responsible for the regulation of several neuronal functions. A recent study reported that increased activation (through phosphorylation from MAPK/ERK kinase 2 or 6-hydroxyldopamine treatment) of ERK1/2 caused increased mitophagy in neuronal cells similar to the phenotype observed w ith treatment with 6-hydroxydopamine, a known neurotoxin.[443b] In agreement, mutation of ERK1/2's kinase decreased mitophagy. Similar activation of ERK1/2 has resulted from acute and chronic treatments with the neurotoxin 1-methyl-4-phenylpyridinium.[443c,d] After treatment with this neurotoxin, autophagy increased as reported by increased in the relative level of LC3-II v ersus LC3-I, detected by Western blotting, and by higher number of autolysosomes labeled with monodansylcadaverine, detected by fluorescence confocal microscopy. Increased mitochondria degradation and fragmentation was also observed by fluorescence confocal microscopy, which was consistent with reduced levels of mitochondria proteins (pyruvate dehydrogenase and p110[54]), detected by Western blotting. Overall, the authors suggested that the neurotoxin treatment activated the ERK signaling pathway and induced mitophagy because knockdown of LC3, ATG5, or ATG7 prevented degradation of mitochondrial proteins and decreased levels of LC3-II following neurotoxin treatment.

Microtubule-associated protein 1S (MAP1S) is implicated in microtubule dynamics, mitotic abnormalities, and cell death. MAP1S association with mitochondria has been known but its role in mitochondrial removal through mitophagy was only explored recently.[443e] This study focused on the interactions between MAP1S and autophagosome biogenesis and degradation in mice embryo cells and mouse embryonic fibroblasts. MAP1S associated with LC3 and regulated autophagosome trafficking as determined by transmission electron microscopy. When MAP1S was knocked-out, autophagosomal biogenesis and autophagy flux became defective and led to accumulation of autophagosomes and dysfunctional mitochondria as detected by fluorescence confocal microscopy, Western blotting of LC3-II, and sustained mitochondrial enzymatic activity (citrate synthase activity). These findings suggested that MAP1S is necessary for the interactions of mitochondria and autophagosomes.

5.8. Phagocytosis

Another cellular internalization pathway in the cell is phagocytosis. Phagosomes entrap foreign objects after introduction into the cell by phagocytosis. Phagosomes will typically fuse with either lysosomes or autophagosomes in order to degrade the phagocytosed materials (Figures 27, 32). Many pathogenic bacteria, such as *M. tuberculosis, L. monocytogenes*, and *L. pneumophilia*, are able to enter cells through phagocytosis and are able to escape degradation by preventing fusion of phagosomes and lysosomes. As a result, these pathogens have been used to study phagosome interactions with lysosomes because they halt the phagosome-lysosome interaction at a critical step of phagosomal maturation.

Phagocytosis can also be triggered with antibody coated latex beads (opsonized beads) and with pathogenic bacteria such as those mentioned previously. As with autophagosomes and endocytic organelles, confocal fluorescence microscopy and transmission electron microscopy are the main methods of subcellular analysis to study phagosomal interactions. Studying phagosomal interactions has benefited from overexpressing, mutating, or knocking down proteins with potential roles in phagosomal interactions.

The first portion of this section describes non-pathogen based studies used to investigate phagosome maturation and some essential features of phagosome maturation.[451] Next, phagosome-lysosome interactions with pathogen-based models[452] and phagosome-autophagosome interactions are discussed.[453] Finally we discuss recent insights into phagosome interactions with other membrane systems such as the plasma membrane[454], ER,[455] and Golgi.[456] For interested readers, Table 14 summarizes proteins of interest involved in phagosome interactions.

5.8.1. Phagosome-endocytic organelle interactions—The formation of phagosomes can be induced by exposure to latex beads after their opsonization with antibodies. This is a common procedure that takes advantage of accelerated phagocytosis of objects destined to generate an immune response from the cell. Opsonization is often utilized to elicit an immune response in cells. The interaction of phagosomes and lysosomes is critical to this pathway. The roles of LAMP1 and LAMP2 proteins in phagosome interactions with endocytic organelles were determined in mice peritoneal macrophages.[451a] LysoTracker served as an acidotropic probe. Phagosomes interacting with lysosomes should appear as morphologically large organelles stained with LysoTracker when observed by confocal fluorescence microscopy. Knockdowns of LAMP1, LAMP2, or double knockdowns were all able to phagocytose opsonized beads, however, the double knockdown had a nearly complete loss of lysosome-phagosome interactions as confirmed by transmission electron microscopy. In addition, live cell microscopy showed that lysosomes and phagosomes had decreased mobilities in the double knockdowns relative to wild type microphages. Lastly, the effect was lysosomal specific because the double knockdown had no effect on early

endosome-phagosome interactions (tracked with the early endosome marker Rab5-GFP) and had very little effect on the interactions b etween late endosomes and phagosomes (tracked with Rab7-GFP or CD63-GFP).

Opsonization of latex beads with antibodies was found to increase phagocytosis in mouse macrophage cells, human histiocytic lymphoma cells, and primary mouse peritoneal m acrophages.[451b] This study investigated whether opsonization accelerated the rate of lysosome-phagosome interactions as well. Cells were treated with either BSA or IgG labeled, 1-μm diameter, latex beads. Phagosomes were monitored with the dye filipin and lysosomes were monitored with tetramethylrhodamine-labeled dextran. When observed by confocal fluorescence microscopy, cells treated with IgG-coated beads had an increased and faster colocalization with the late endosome/lysosome protein marker CD63 than the BSA coated beads. A novel *in vitro* assay involving enriched cytosol, lysosomes containing [^{3}H]-cholesteryl ether, and phagosomes containing beads was used to further study the interaction between lysosomes and phagosomes. S cintillation from the latex beads in the phagosomes require immediate contact of tritium-derived β-particles found in lysosomes.[470] Scintillation decreases exponentially with distance between tritium and the beads thereby providing exquisite selectivity and selectivity to detect phagosomes interacting with lysosomes.

This study also investigated the role of the Fcγ receptor and protein kinase C in autophagosome-lysosome interaction in a Chinese hamster ovary cells.[451b] After treatment with antibody-opsonized beads, cells overexpressing both Fcγ receptor and protein kinase C (or control cells transfected with an empty plasmid) were used to prepare cytosolic fractions. When the cytosolic fraction was mixed with isolated phagosomes and lysosomes, those overexpressing both Fc-γ receptor and protein kinase C showed an increase of 37% in the number of interactions with the tritium-based scintillation assay described above.[470] To further investigate the origin of the increased interaction between phagosomes and lysosomes, the *in vitro* assay was performed in the presence of latrunculin A, cytochalasin D (both of which are inhibitors of actin polymerization), or alkaline carbonate (which prevents tethering). These three agents blocked the observed increase of phagosome-lysosome interactions suggesting that opsonization increases actin dynamics between organelles and increases tethering of SNAREs between phagosomes and lysosomes.

Flashing is the process of F-actin polymerization around a phagosome. A recent study utilized latex beads labeled with either antibody, mannan, or avidin to investigate how the F-actin flashing regulates phagosome-lysosome interactions in mouse macrophages.[471] Confocal fluorescent microscopy and transmission electron microscopy revealed that flashing only occurred in phagosomes before they interacted with ly sosomes. Phagosomes containing a ctin coats from flashing could not interact with lysosomes. This suggests flashing down regulates phagosome-lysosome interactions. Furthermore, when both lysosomes were overloaded with non-degradable materials, such as BSA-colloidal gold, and phagosomes were overloaded with antibody-labeled latex beads, the number of flash-activated actin-coated phagosomes increased. These results suggest that actin is an important regulator of phagosome-lysosome interactions.

5.8.2. Interactions of endocytic organelles with pathogen-containing phagosomes—As mentioned above, pathogenic bacteria often cause decreased interactions between endocytic organelles and phagosomes to survive inside cells and maximize infection. Understanding of such interactions could help design strategies to slow down bacterial infections. One study investigated the role of the sodium ion channel NaV1.5 on phagosome maturation in human peripheral blood monocytes, which were differentiated to macrophages and treated with dead bacillus Camille-Guerin, a model for mycobacterial infection.[452a] Confocal immunofluorescence microscopy showed that NaV1.5 was localized

in the endosomes near the periphagosome region. Knockdown of NaV1.5 caused about a 9-fold decrease in phagocytosis of the dead bacillus. Furthermore, NaV1.5 knockdown cells did not have mitochondria in the phagosome periphery (which was observed in the wild-type macrophages). Because mitochondria are an important site for calcium storage, calcium levels were also monitored. When NaV1.5 was knocked down, the cytosol had lower calcium levels as reported by Fluo-4, a fluorescent calcium indicator. The importance of NaV1.5 in the interplay between Na^+/Ca^{+2} needed for successful phagocytosis was further confirmed by inactivated mitochondria Na^+/Ca^{+2} mitochondrial voltage-gated pumps with the inhibitor CGP-37157. This suggests that NaV1.5 activity in the endocytic organelles and mitochondria in proximity to the phagosome is critical for sustained phagocytosis.

M. tuberculosis stops phagosome maturation in infected macrophages. The role of Rab14 in phagosome maturation was studied with *M. tuberculosis*-infected mouse macrophage cells and human embryonic kidney cells.[452b] Although Rab14 is known to participate in early endosome-Golgi trafficking, confocal fluorescence microscopy revealed that Rab 14 was colocalized with phagosomes containing *M. tuberculosis*. Decreased expression of Rab14 with siRNA knockdown caused increased interaction of lysosomes and phagosomes containing *M. tuberculosis*. On the other hand, an increase in Rab14 expression caused decreased phagosome-phagosome and phagosome-lysosome interactions. However, this decrease may have been a consequence of a competitive preferred interaction between phagosomes and early endosomes.

L. monocytogenes is a microbe that evades cellular degradation by escaping delivery to the degradative environment of the lysosome. This event is dependent upon production of the enzyme listeriolysin O, which causes poration of the phagosome membrane and facilitates the scape of this pathogen. A recent study investigated the role of phagosome membrane permeability on the fusion of the phagosome with lysosomes in *L. monocytogenes*-infected mouse macrophages.[452c] Confocal fluorescence microscopy was used to monitor the pH and calcium concentrations in phagosomes using ratiometric fluorescent probes. In cells expressing listeriolysin O, phagosomes were permeabilized, and the pH and calcium concentration of the *L. monocytogenes*-containing vacuoles remained close to cytosolic pH, i ndicating compromised membrane permeability. In contrast, Listerolysin O-deficient phagosomes became more acidic and had increased calcium concentration. These results suggest that an increase in membrane permeability allows escape of *L. monocytogenes* into the cytosol, but also compromises the fusion between infected phagosomes and lysosomes.

Given that a large number of Rabs are key regulators of phagosome interactions, an excellent study addressed this issue by surveying 48 Rab proteins for their ability to associate with maturing phagosomes in HeLa and mouse macrophage cells infected with in *S. Typhimurium*.[452d] The Rab proteins were tagged with GFP or CFP and their subcellular location was determined by colocalization with organelle markers using confocal fluorescent microscopy. Eighteen Rab proteins showed association with maturing phagosomes in pathogen containing phagosomes. Mutants with knocked out Rab23 and Rab35 inhibited phagosome-lysosome fusion. Rab5A, Rab5B, Rab5C, Rab7, Rab11A, Rab11B, Rab7, and Rab9 appeared associated with invasion of *S. Typhimurium*.

Another study done on mouse macrophages investigated the role of Rab proteins in the maturation of phagosomes after infection with *M. tuberculosis* and *S. aureus*.[452e] Confocal fluorescent microscopy and transmission electron microscopy were used to monitor the localization of 42 different GFP-Rab proteins and to describe phagosomal morphology. Western blotting of phagosome enriched fractions 'floated' in sucrose density gradient centrifugation revealed 22 and 17 Rab proteins present in phagosomes when cells were infected with *S. aureus* and *M. tuberculosis*, respectively. Only Rab8, Rab8b, Rab9, Rab22b,

and Rab43 were common in phagosomes after infection with either bacterium. Mutated forms of each Rab made it possible to single out those involved in phagosome-lysosome interactions. Rab7, Rab20, and Rab39 favored phagosome-lysosome interaction in *M. tuberculosis*-containing phagosomes. Furthermore, Rab7, Rab20, Rab22b, Rab32, Rab34, Rab38, and Rab43 recruited lysosomal cathepsin D to phagosomes indicating that *M. tuberculosis*-containing phagosomes were able to interact with lysosomes. Further confirmation showed that mutated forms of Rab7, Rab20, Rab22b, Rab32, Rab34, Rab38, and Rab43 prevented phagosome acidification and cathepsin D recruitment. Since both this study[452e] and the study mentioned in the previous paragraph[452d] used the same cell line, but different pathogens, it is feasible to compare the role of Rab proteins that were studied. Surprisingly, Rab7 was the only protein with equivalent roles in the pathogenic systems that were investigated. Rab32 had several roles: it was involved in the degradation of *S. Typhimurium* and was used to internalize *S. aureus* and *M. tuberculosis*.

The subcellular localization of the *M. avium* subspecies *Paratuberculosis* in mouse macrophage cells and polymorphonuclear cells from Crohn's disease was part of a study aiming at understanding the effects of this pathogen on the interaction of the phagosome with endocytic organelles.[452f] Fluorescence confocal microscopy revealed that *Paratuberculosis* was present in early endosomes as determined by colocalization with the transferrin receptor, which is an early endosome marker. In contrast, dead *Paratuberculosis* was internalized in mouse macrophage cells, but was primarily found in lysosomes. This suggests functional *Paratuberculosis* inhibits interaction of phagosomes w ith late endosomes and lysosomes. By preventing phagosome-late endosome and phagosome-lysosome interactions, *Paratuberculosis* increases its odds for survival.

The phagocytic entry of bacteria into cells requires cholesterol in the plasma membrane, which results in accumulation of bacteria in phagosomes, but not in autolysosomes. A recent study investigated the effect of cholesterol d epletion on the phagosome-lysosome interactions after infection of mice bone marrow cells with *M. avium*.[452g] Cholesterol depletion was triggered by treatment with methyl-β-cyclodextran. The phagosome-lysosome fusion, i nduced by cholesterol depletion, was observed through transmission electron microscopy. Although *M. avium*-containing phagosomes fused with lysosomes, the lytic environment of the phagolysosomes was not sufficient to degrade this pathogen.

Some protozoa parasites have an amastigotes (intracellular stage of cell cycle) and a promastigotes (extracellular stage of cell cycle). In *L. chagasi* both parasitic stages display unique interactions with membrane c omponents to maximize their survival. In a recent study the parasitic *L. chagasi* parasitic cell line was used to investigate the interactions of phagosomes in mouse bone marrow macrophages, containing one of the two stages of *L. chagasi*, and endocytic organelles.[452h] Confocal fluorescence microscopy revealed that disrupting the cholesterol-containing lipid rafts on the plasma membrane decreased promastigote phagocytosis. Despite this decrease, promastigotes transferred to organelles with LAMP1 (late endosomes, lysosomes) earlier than amastigotes; this transfer continued over 24 hours. On the other hand, an entirely different intracellular route was observed for amastigotes. Amastigotes localized longer than promastigotes in vacuoles that displayed early endosome markers Rab5 and EA1 (early endosome-antigen 1). This colocalization was persisted for up to 2 hours and was not affected by disruption in lipid rafts. Overall, these two parasitic forms seem to use two different intracellular routes to avoid degradation: amastigotes extend their survival by retaining early endosome markers. Promastigotes extend their survival by delaying their interaction with late endosomes and lysosomes.

5.8.3. Phagosome-autophagosome interactions—Autophagy is an indirect route for pathogenic bacteria degradation. After phagocytosis of a pathogen, phagosomes may fuse

with autophagosomes, which would subsequently lead to degradation of the pathogen when the autophagosome fuse with lysosomes to form autolysosomes (Figure 31). The participation of the proteins CD40 and CD154 in autophagosome-phagosome interactions in human monocyte-derived macrophages, mouse resident peritoneal macrophages, and mouse bone marrow macrophages was recently investigated.[453] Macrophages were infected with *T. gondii*. Immunofluorescence and f luorescence confocal microscopy demonstrated that, upon overexpression of CD40, phagosomes containing *T. gondii* fused with late endosomes and lysosomes. Binding of CD40 with an anti-CD40 antibody resulted in detection of phagosome-autophagosome fusion, suggesting that phagosome-lysosome interactions occur via autophagosomes. Similarly, when CD154 was inactivated through binding with an anti-CD154 antibody, phagosome-lysosome fusion did not occur. This suggests that CD40 and CD154 protein play critical roles in regulating in autophagosome-phagosome interactions in . *T. gondii*.

5.8.4. Interactions of the phagosome with other membrane systems—In addition to their interactions with the endocytic pathway, phagosomes interact with other membrane structures as well. The analysis of interactions between the plasma membrane and phagosome for recycling cellular components gave new insights into the role of Rab11 in mouse macrophage cells.[454] A unique aspect of this study was the introduction of proteins such as Rab 11 and antibodies after permeabilization of the plasma membrane with streptolysin O. To monitor the recycling of phagosomal components to the plasma membrane, *S. aureus* was opsonized with ^{125}I-mouse anti-DNP IgG and the radioactivity of ^{125}I-mouse anti-DNP IgG was measured in the extracellular media, which is indicative of phagosome-plasma membrane interactions. Rab11 was required for phagosome-plasma membrane interactions. Mutations of Rab11 reduced ^{125}I-mouse anti-DNP IgG recycling to the extracellular space by ~50%. Incubation with non-hydrolyzable GTPγS increased ^{125}I-mouse anti-DNP IgG scintillation and confirmed the role of a Rab protein that requires GTP for plasma membrane-phagosome interactions. Prenylated Rab11 increased ^{125}I-mouse anti-DNP IgG scintillation in the extra cellular locale suggesting the anchoring of Rab11 to membranes through prenyl groups enhanced the recycling of phagosomal components. Lastly, treatment of macrophages with latex beads that had been opsonized with fluorescently-labeled antibodies made it possible to visualize interactions between either wild-type or mutated Rab11-GFP with phagosomes.

The interaction between phagosome membranes and the ER was investigated in mouse macrophages treated with latex beads coated with IgGs.[455] It was already known that phagosomes have membrane components from the ER, which would imply that SNAREs from the ER could also impact interactions in phagosomes. Phagosomes were isolated by 'floating' in sucrose density gradient centrifugation after phagocytosis of latex beads. Confocal fluorescent microscopy of whole cells and Western blotting of enriched fractions showed the ER's SNARE proteins syntaxin 18, D12, and sec22b were all also localized in phagosomes. M utation and siRNA knockdown of D12 and s yntaxin 18 decreased phagosome formation. In addition, a binding assay and Western blotting showed syntaxin 18 interacted with the plasma membrane syntaxins 1–4. This suggests the ER's SNAREs proteins become incorporated into phagosomal membranes where they facilitate interactions with plasma membrane syntaxins, which would imply that SNAREs from the ER indirectly regulate exocytosis.

Sortilin is a neurotensin receptor responsible for mediating signaling through chemical compounds, growth factors, and lysosomal proteins. Sortilin is known for its traffic from the Golgi to lysosomes. It is upregulated in response to infection of macrophages by pathogenic mycobacteria. A recent report explored the role of sortilin in Golgi-phagosome interactions in mouse and rat macrophages.[456] Confocal fluorescence microscopy and transmission

electron microscopy indicated sortilin localized to both the Golgi and phagosomes. Live cell fluorescence imaging showed sortilin-GFP trafficked from the Golgi to phagosomes through Golgi-derived vesicles. Brefeldin A treatment, which inhibits Golgi transport of proteins to other organelles e xcept the ER, decreased the delivery of sortilin-GFP to phagosomes. In addition, sortilin knockdown caused decreased delivery of acid sphingomyelinase and prosaposin, a sphingolipids catabolism enzyme, to the phagosome. This suggests sortilin traffics proteins from the Golgi to the phagosome in addition to the lysosome.

5.9. Secretory organelles interactions with other organelle types

There are multiple routes for secretion of cellular components into the extracellular medium involving organelles such as exosomes, secretory granules, secretory lysosomes and enlargeosomes. For a brief description of the function of these organelles see Table 1. Exosomes interact with the plasma membrane as part of exocytosis. An excellent review on the topic appeared recently.[472] While many details of this interaction are known, some of the aspects such as the role of the protein complex munc-13-4-Rab27 in tethering,[473] and identifying additional SNARE proteins used in the interaction[474] await elucidation.

Intracellular organelle interactions that precede secretion include exosome-plasma membrane,[472] secretory lysosome-plasma membrane,[473] immature secretory granule-mature secretory granule,[475] and enlargeosome-plasma membrane interactions.[476] These interactions are commonly investigated using the subcellular analysis techniques d escribed in 5.6. The rest of this section focuses on salient examples of recent reports that utilize subcellular analysis to understand the mechanisms of these interactions. A general description of key proteins involved in these interactions appears in the Introduction of 5.

Syt proteins are believed to participate in membrane fusion. A report focused on the role of SytIV on the maturation of secretory granules in rat adrenal medulla cells.[475b] Western blotting revealed that SytIV was present in an immature secretory granule enriched fraction. When SytIV was knocked down, homotypic fusion of immature secretory granules decreased and compromised maturation. Autoradiography was used to monitor the abundance of $[^{35}S]$-sulfate-labeled secretogranin 2 (Sg2) in enriched fractions of immature and mature secretory granules. This is an important marker of secretory granule maturation. After a 5-minute pulse and 15-minute chase with Sg2 in rat adrenal medulla cells, Sg2 was present only in the immature secretory granules. In contrast, a one-hour pulse followed by an overnight chase resulted in Sg2 accumulation in the mature secretory granules. These results suggest that the protein SytIV was needed for processing of Sg2 from the immature to mature secretory granules.

Golgi-associated, γ-ear-containing, ADP-ribosylation factor binding proteins (GAs) are a family of clathrin-protein adaptors that facilitate cargo sorting in clathrin coated vesicles, an organelle used to internalize materials during endocytosis and a lso in cellular trafficking. A recent study used mutated GAs to investigate the involvement of clathrin-coated vesicles in the maturation of immature secretory granules in rat adrenal medulla cells.[475c] Confocal fluorescence microscopy showed mutated GAs inhibited membrane remodeling in immature secretory granules. Although the mutation did not cause changes in homotypic fusion of immature secretory granules, it impaired maturation as observed by accumulation of sSg2 in the immature secretory granules in flow cytometry experiments. Another experiment was based on the transfection of rat adrenal medulla cells with prohormone convertase 2, an enzyme that processes Sg2 to the protein p18, present in mature secretory granules. Mutated GAs inhibited the activity of prohormone convertase 2, which is responsible for processing Sg2 to p18, which resulted in accumulation of Sg2 and decrease in p18 levels. The study also investigated the role of the SNARE protein VAMP4. During maturation VAMP4 from the immature secretory granules appeared in the mature secretory granules. Knockdown of

GAs caused the accumulation of VAMP4-Flag protein in secretory granules suggesting degranulation was not occurring. Overall, these results suggest that interactions between secretory granules and clathrin-coated vesicles are necessary for maturation and degranulation of secretory granules.

Tethering of secretory lysosomes to the plasma membrane is a key process prior to secretion. A recent report showed the Munc13-4/Rab27 complex was required for secretory lysosome tethering to the plasma membrane in rat fibroblast cells and cytotoxic T lymphocytes isolated from whole blood.[473] Prior to this report, the mechanism regulating secretory lysosome degranulation through interaction with the plasma membrane was uncertain. Protein interaction assays aided in identifying Munc-13-4 as one of the proteins interacting with GTPγ^{35}S--Rab27a. Total internal reflectance fluorescence (TIRF) microscopy, which provides an observation window that is localized within tens of nanometers from the surface of the cell, was used to visualize interactions between secretory lysosomes and the plasma membrane. Munc-13-4 point mutations prevented binding between Munc-13-4 with Rab27 and resulted in impaired CD-107 localization to the plasma membrane. CD-107 is associated with the secretory lysosomes. This suggests that Rab27 and Munc-13-4 must bind to allow interactions between the secretory lysosome and plasma membrane.

Instead of using S NARE proteins to investigate secretory vesicle t rafficking to the plasma membrane in plants, a recent study used SNARE protein fragments called Sp2 fragments.[474] Sp2 fragments can be used as a dominant negative form, or mutation, of specific SNARE proteins, which prevent normal SNARE function. Confocal fluorescence microscopy of *N. tabacum* and *A. tumerfaciens* cells was performed to monitor the accumulation of GFP used as secretory marker. This marker accumulated in secretory lysosomes when plasma membrane interactions were blocked. Sp2 fragments of the plasma membrane SNAREs AtSYP121, AtSYP122, and AtSYP71 blocked the interaction between the plasma membrane and secretory vesicles resulting in cargo retention in secretory vacuoles. On the other hand, the Sp2 fragments of AtSYP111 and AtSUP21 did not inhibit secretion (i.e. plasma membrane-secretory vesicle interaction). In addition to the interaction with the plasma membrane, the report also demonstrated the use of Sp2 fragments to investigate interactions between the ER and secretory vesicles. Vesicles were labeled with tonoplast intrinsic factor-yellow fluorescent protein (TIF-YFP). The Sp2 fragment AtSYP21 prevented accumulation of YFP-TIF to the ER and had a significant loss in fluorescence. This suggests that Sp2 methodology can be generalized to study other secretory compartment-organelle interactions.

Enlargeosomes are small vesicles that have rapid exocytosis in response to increases in cytosolic calcium levels. Confocal fluorescence microscopy showed how enlargeosomes in rat adrenal gland cells and human neuroblastoma cells respond to changes in SNARE protein expression.[476] This technique showed that SNARE proteins Stx6 and VAMP4 were in the membrane of enlargeosomes. Knocking down either one of these proteins with siRNA inhibited enlargeosome exocytosis. This was the case even when calcium levels were kept high through use ionomycin, which is a calcium ionophore. This is the first time a SNARE had been implicated in enlargeosome-mediated exocytosis.

5.10. ER interactions with the Golgi and nucleus

The ER maintains multiple interactions with endocytic organelles, exocytic organelles, the autophagy system, mitochondria, the Golgi, and the nucleus (Figure 27). Recent reports describing interactions with the Golgi, liposomes, autophagosomes, endocytic organelles and phagophores were presented earlier (5.3., 5.5., 5.6.1., 5.7.2., 5.8.4.). In this section we focus on interactions of the ER with the Golgi and the nucleus. The subcellular analysis

techniques used to investigate these interactions have been described in other subsections of 5.

The association of the ER with the Golgi is essential because proteins and lipids are sent from the ER to the Golgi via anterograde transport, where proteins are modified, sorted, and packed into vesicles. In addition, other material returns to the ER from the Golgi via retrograde transport. Studies included here have used subcellular analysis to investigate ER-Golgi interactions at the molecular level.[477] Another paper reviewed here focuses on the description of the ER-nuclear envelope interaction.[478] Lastly, a report demonstrating the use of artificial liposomes to deliver material to the ER illustrates a strategy to investigate subcellular interactions[479]

Sec22 is a highly conserved SNARE protein that mediates fusion of vesicles shuttling between the ER and Golgi. This role was supported in a recent study that investigated the subcellular localization and effects of altering Sec22 levels on the morphology of the ER and the Golgi.[477a] Confocal fluorescence microscopy and transmission electron microscopy indicated Myc-Sec22 fusion protein localized to the ER membrane (colocalized with the marker calreticulin) and not in the Golgi in *A. thaliana* seedlings. Similar results were observed for mouse Sec22 and human Sec22 homologue proteins. Knockdown of Sec22 resulted in changed (narrower) morphology of Golgi stacks. Another effect of knocking down Sec22 was the formation of vesicle aggregates derived from the Golgi as determined from transmission electron microscopy colocalization experiments using the Golgi marker γ-COP immuno-gold.

Another study identified Rab GTPase activating proteins (GAP) necessary to support the role of Rab proteins in ER-Golgi interactions.[477b] Thirty-eight GAPs with known effects on 60 Golgi Rabs were investigated in HeLa and telomerase-immortalized human retinal epithelial cells. Two GAPs were of relevance: TBC1D20 and RN-tre. When RN-tre was knocked down, it had a minimal effect on the appearance ER-Golgi associated vesicles, suggesting that its role may be associated with the interactions of the Golgi with a different organelle. Rab1 was the main TBC1D20 interactor discovered via a yeast two-hybrid screen. There were high rates of GTP hydrolysis when both proteins were present and complete fragmentation of the Golgi when Rab1 was knocked down. On the other hand, Rab1 inactivation through knockdown of TBC1D20 caused an accumulation of ER-derived vesicles containing COPII. The COPII-labeled vesicles in the ER could not be tethered to the Golgi and c argo could not be delivered to the Golgi. This suggests Rab1 regulates tethering of vesicles from the ER to the Golgi.

The nuclear envelope and endoplasmic reticulum are continuous membrane systems. A recent study investigated the indirect effect of ER tubule formation inhibitors on the nuclear envelope morphology.[478] Morphological changes in the ER and the nuclear envelope of HeLa cells were imaged with live cell and confocal fluorescence microscopy. GTPγS and ATPγS treatment, both of which inhibit ER tubule formation, caused alterations in nuclear envelope morphology and protein expression. By altering the ER tubular network, the nuclear envelope could not grow. Inhibitors appeared to act by inhibiting ER membrane fusion. This suggests ER tubules provide topology for assembly of the nuclear envelope.

Targeting liposomes to the ER may be a suitable strategy for improved intracellular delivery of hydrophilic and hydrophobic materials to this subcellular compartment. In a related report, human hepatoma cells were treated with liposomes and analyzed with standard and live-cell confocal fluorescent microscopies.[479] Liposomes, made of phosphotidylinositol, phosphatidylcholine, phosphoinositide, and phosphotisylserine, fused with ER membranes. Docking and cargo delivery were confirmed with the self-quenching of R18 and calcein.

When docking occurs, diffusion of either dye results in dilution and fluorescence increase. Based on such dequenching experiments, the liposome cargo was released into the ER lumen within 30 minutes of endocytosis. This is the first report demonstrating that artificial vesicles directly interact with the ER.

6. Organelle function

Each organelle type has unique biochemical activities and physiological function. Biochemical activities involve molecular transformations such as formation or disappearance of compounds, the regulation of multiple molecules (e.g. ROS, carbohydrates, and histones), and metabolism of lipids and other small molecules. Physiological functions refer to processes such as cellular growth, protein fixation, membrane potentials, oxidative phosphorylation, and molecular and ionic transport. This portion of the review describes studies related to organelle-specific function and activities.

Monitoring biochemical and physiological activities in an organelle-specific manner has been accomplished, directly or indirectly, using multiple techniques including confocal fluorescence microscopy, transmission electron microscopy, enzymatic and spectrometric assays and Western blotting. Other techniques include gel electrophoresis, respirometry, spectrofluorometry, gas chromatography, liquid chromatography, and mass spectrometry. These techniques allow for monitoring the appearance of products, disappearance of substrates, activity of reporters, presence of enzymes, or the subcellular localization in whole cells. These techniques will not be described in detail here. Below, each subsection is dedicated to a specific organelle type, organized alphabetically. It should be noted that this section includes only salient examples. For those readers interested in the topic Table 15 provides a more comprehensive list of studies focused on organelle function.

6.1. Chloroplast function

Glutathione peroxidase (GPX) is an important regulator of reactive oxygen species levels in plants. The role of the GPX1 and GPX7 isoforms of glutathione peroxidase as antioxidants in enriched chloroplasts from *A. thaliana* leaves under light stress was recently investigated.[526] Chloroplasts with either GPX1 or GPX7 knockouts were isolated and assayed for glutathione peroxidase activity. Glutathione peroxidase activity was determined from the ratio of hydrogen peroxide degradation to NADPH oxidation using spectrophotometry. Increased ROS production and cell death were observed in both knockdowns. When knockdowns and wild type were exposed to high intensity light, the glutathione peroxidase activity was reduced more dramatically in the knockdowns. Furthermore, knockdowns had increased foliar ascorbate, glutathione, and salicylic acid levels as determined with HPLC. These molecular changes are indicators of an increase in the phenylpropanoid defense mechanism. Together, these studies describe the importance of GPX 1 and GPX7 as defense agents against photo-oxidative stress in the chloroplast.

The subcellular distribution and activity of glucose-6-phosphate dehydrogenase in peach fruit *P. persica* was recently investigated.[527] This enzyme oxidizes glucose-6-phosphate to 6-phosphogluconate. Enzymatic activity was assessed with a spectrophotometric enzymatic assay of $NADP^+$ reduction in enriched subcellular fractions (nuclei, organelles, cytosol). Immunogold transmission electron microscopy indicated that glucose-6-phosphate dehydrogenase was found in chloroplasts and cytosol. Glucose-6-phosphate dehydrogenase activity increased in aged fruit chloroplasts and cytosol and with decreased fruit firmness. This increase, however, was mainly associated with the cytosol.

Flavin adenine dinucleotide and flavin mononucleotide are essential cofactors for many enzyme activities, many of which remain unexplored. Two new flavin adenine dinucleotide

synthetases (AtRibF1 and AtRibF2) in leaves from *A. thaliana* were recently described and their subcellular roles were determined.[528] Confocal fluorescence microscopy revealed that the GFP-AtRibF1 and GFP-AtRibF2 enzymes were localized to chloroplasts. Scintillation counting of fractions enriched in chloroplasts and mitochondria isolated from *C. bohatyr* peas incubated with [^{3}H]-riboflavin indicated that chloroplasts contained [^{3}H]-flavin mononucleotide and [^{3}H]-flavin adenine dinucleotide. This suggests chloroplasts were able to synthesize and hydrolyze flavin nucleotides in plants.

Alkaline/neutral invertase is an enzyme that hydrolyzes sucrose into hexose. Functional studies of the alkaline/neutral invertase isoforms were performed in chloroplasts isolated from leaves of *S. oleracea* and *A. thaliana*.[529] *A. thaliana* and *S. oleracea* chloroplasts had 13% and 20% of the total alkaline/neutral invertase of the lysate, respectively. Confocal fluorescence microscopy of GFP-alkaline/neutral invertase and Western blotting confirmed the presence of the enzyme in chloroplasts. Furthermore, chloroplasts of alkaline/neutral invertase knockdowns contained a 33% loss in starch contents in whole cell homogenate when compared to whole cell homogenate of wild type. There was no significant change in sucrose concentration when comparing the whole cell homogenate. Overall, this report suggested that chloroplasts can regulate carbon storage.

Both NADPH thioredoxin reductase C and plastidial thioredoxins are essential for the function of 2-Cys peroxiredoxins, which metabolize ROS in the photosynthetic pathway. The relationships between these enzymes were investigated by monitoring ROS and oxidative damage in enriched chloroplasts from leaves of *A. thaliana*.[530] Knockdowns for all three enzymes caused increased oxidative stress as indicated by increased protein carbonylation. S imilarly, knockdowns of N ADPH thioredoxin reductase C and 2-Cys peroxiredoxins showed higher production of hydrogen peroxide by chloroplasts. Furthermore, monitoring the redox status by Western blotting of 2-Cys peroxiredoxins indicated 2-Cys was oxidized only when NADPH thioredoxin reductase C was knocked down. Together, the analysis of these enzymes established a functional relationship between 2-Cys peroxiredoxins and NADPH thioredoxin reductase C, which is essential for regulation of ROS.

6.2. Endocytic organelle function

Deficiency in acetyl-CoA:α-glucosaminide *N*-acetyltransferase (NAT), a known lysosomal membrane enzyme that acetylates membrane proteins, has been implicated in the etiology of mucopolysaccharidosis IIIC, an autosomal disorder. Purification and characterization of the protein were performed in tissues and cells.[531] NAT was enriched from human placenta through a series of purifications (ammonium sulfate fractionation, affinity, ion-exchange, gel-focusing, and chromatofocusing chromatography). Despite the purification procedure, the final preparation contained multiple proteins. To identify NAT, the fraction was treated with acetyl-[^{14}C]-coenzyme A to label NAT. Two protein fragments (120 kDa and 145 kDa) were identified via SDS-PAGE and audioradiography. Only the 120 kDa molecular weight band was irreversibly bound to N-bromosuccinimide suggesting that such species was NAT. Human skin fibroblasts were collected from healthy individuals and individuals afflicted with mucopolysaccharidosis IIIC. Lysosome membranes were enriched and incubated with acetyl-[^{14}C]-coenzyme A to determine the presence of NAT. The 120k Da band corresponding to NAT was not present in cells from afflicted patients indirectly suggesting that NAT could be an important protein relevant to the phenotype of mucopolysaccharidosis IIIC.

6.3. Endoplasmic reticulum and Golgi functions

Phosphatidylinositols have essential functions in eukaryotic cells, where they are converted to multiple metabolites by phosphatidylsynthases. A recent study investigated the subcellular localization of phosphatidylsynthase 1 and phosphatidylsynthase 2 in *A. thaliana*.[532] Fluorescent phosphatidylsynthases were expressed in C43 cells. Confocal fluorescent microscopy revealed that both fluorescent proteins localized to the ER. In addition, the activities of these enzymes were monitored through the analysis of phosphatidylinositols and phospholipids in subcellular fractions by gas chromatography with flame ionization detection. Overexpression of phosphatidylsynthase 1 increased the levels of saturated and unsaturated phosphatidylinositols and phospholipids. Similarly, overexpression of phosphatidylsynthase 2 increased in phosphatidylinositol 4-phosphate and phosphatidylinositol 4,5-bisphosphate. The authors suggest that phosphatidylsynthases acts in different metabolic contexts for similar pathways and supplies different types of inositol-containing lipids.

Protein tyrosine phosphatase 1B resides in the ER and is believed to play a role in ER stress response. An important step in this process is the deactivation of this phosphatase via covalent modification of the cysteine at its active site with hydrogen peroxide and nitric oxide. A recent study investigated the hypothesis that hydrogen sulfide is also an important regulator of protein tyrosine phosphatase 1B associated with ER stress.[533] Human embryonic kidney cells were treated with tunicamycin to causes ER stress. Western blotting of the ER protein BiP, which is upregulated in response to ER stress, was used as an indicator of ER stress. Because, ER stress induced by tunicamycin generates hydrogen sulfide, such stress decreased tyrosine phosphatase 1B activity. This effect was reversible as confirmed by treatment with reducing agents. Liquid chromatography coupled to tandem mass spectrometry indicated the active site cysteine residue was reduced following deactivation with hydrogen sulfide. When cystathionine-γ-lyase, an enzyme that produces hydrogen sulfide, was knocked down and ER stress was triggered with tunicamycin, hydrogen sulfide production was reduced. There was no decrease in protein tyrosine phosphatase 1B activity relative to the wild type enzyme, and protein tyrosine phosphatase 1B inhibition via hydrogen sulfide was reduced. This suggests that cystathionine-γ-lyase is needed to regulate protein tyrosine phosphate 1B.

The roles of X-box binding protein 1 (XBP1) and choline cytidylyl-transferase (CCT) in the ER were determined in mouse fibroblast cells.[534] XBP1 is stimulated in response to activation of the unfolded protein response pathway, which compensates for excessive demands on protein folding. XBP1 causes extension of ER size and increased levels of phosphatidylcholine, the most abundant lipid in the ER. Phosphatidylcholine is synthesized through the Kennedy pathway and the rate-limiting enzyme is CCT, which converts phosphocholine to cytidine diphosphocholine. This suggests that XBP1 regulates CCT and CCT could regulate growth of the ER. Increased expression of XBP1 caused increased CCT expression as determined by Western blotting. In agreement, there was an increase in CCT enzymatic activity and increased production of cytidine diphosphocholine and phosphatidylcholine, which were determined from methyl-[^{3}-H]-choline chloride incorporation, detected with scintillation spectroscopy. When CCT expression was increased independently of XBP1, a similar increase in production of cytidine diphosphocholine and phosphatidylcholine was observed. To determine the ability of CCT to regulate ER extension, the surface area of the E R in cells expressing XBP1, CCT, or simply an empty vector were compared by transmission electron microscopy. XBP1 caused a 3-fold increase in surface area and volume, however, CCT expressing cells caused only a modest increase over the empty vector. This suggests that even though CCT does significantly alter phosphatidylcholine concentration in the ER, CCT was not sufficient to account for the significant ER size changes observed.

Identifying ER stress-inducing compounds could be the basis to screen potentially toxic compounds. Along this concept, a new subcellular assay was recently developed to determine nuclear proteins activated by ER induced stress.[535] A molecular construct termed XBP1-HA-PL-C3 was designed and expressed in human osteosarcoma cells. Upon ER stress, IRE1 endoribonuclease activity was stimulated. IRE1 was able to splice an intron from the inactive XBP1 molecule rendering it active and able to traffic to the nucleus. Two enzymatic fragments of β-galactosidase were present in the cell. One fragment (PL) was bound to active XBP1. The other fragment (EA) was bound to the unfolded protein response element (UPRE) in the nucleus. Upon XBP1-PL arrival to the nucleus, it interacted with the UPRE recombining the two enzyme fragments and rescuing galactosidase activity. Treatment with a chemiluminescent substrate for galactosidase was used to detect expression of galactosidase. When there was no ER stress, the XBP1 component was localized to the cytosol and did not have the correct binding domain to interact in the nucleus. Known ER-stress inducing compounds such as colchicines and podophyllotoxin were confirmed to produce chemiluminescence.

6.4. Mitochondria function

UMP-CMP kinases are involved in the nucleotide synthesis pathway that has been previously observed in *D. melanogaster*. A recent study described the subcellular localization and phosphorylation activity of UMP-CMP kinase 2 in HeLa cells.[536] Confocal fluorescence microscopy revealed GFP-UMP-CMP kinase 2 colocalized with MitoTracker Red in mitochondria. Scintillation counting revealed that UMP-CMP kinase 2 uses $[\gamma\text{-}^{32}P]$-ATP to phosphorylate cytidine monophosphate, uridine monophosphate, deoxycytidine monophosphate, and deoxyuridine monophosphate. These results suggest UMP-CMP could have multiple roles in mitochondria including DNA regulation.

Rosiglitazone is an anti-diabetic drug that localizes to mitochondria and that has been subject to conflicting reports on its effect on lipid metabolism and possibly fatty acid metabolism. A recent study investigated the role and mechanism of rosiglitazone in skeletal muscle.[537] The study evaluated mRNA and protein expression levels of fatty acid translocase (FAT), plasmalemmal and mitochondrial contents of FAT, the rates of fatty acid transport in sarcolemmal vesicles, and fatty acid oxidation in subsarcolemmal and intermyofibrillar mitochondria.[537] Radioactively labeled $[^{14}C]$-palmitate was used to monitor the metabolism of fatty acids in mitochondrial-enriched fractions. Although there were no effects on FAT mRNA or protein expression levels, the overall fatty acid levels were reduced in sarcolemmal vesicles of rosiglitazone-treated rats. In addition, rosiglitazone caused an increase of palmitate oxidation and increased FAT activity in both subsarcolemmal and intermyofibrillar mitochondria. These results suggest that rosiglitazone act exclusively at the metabolic level and not at the genomic or transcriptomic level.

A recent study investigated the function and subcellular localization of malate dehydrogenase isoforms in *T. brucei*.[538] Confocal fluorescence microscopy of immuno-labeled malate dehydrogenase confirmed that malate dehydrogenases were localized in the cytosolic, glycosomal or mitochondrial regions. In the cytosol, this enzyme was responsible for reducing oxaloacetate to malate in the glycolysis pathway. In the mitochondria, malate dehydrogenases were active in the Krebs cycle. In the glycosome, a peroxisome-like o rganelle present in *T. brucei*, the malate dehydrogenase appeared to have similar roles to the cytosolic form and be involved in malate oxidation and oxaloacetate reduction.

The relationships between metabolism in kidney cells, chronic kidney disease, and obesity are still poorly understood. A recent comprehensive study investigated the effect of high fat, low carbohydrate diet on respiration, lipid levels, and ROS production in mouse kidney mitochondria.[539] Mouse embryonic stem cells were fed a high-fat, low-carbohydrate diet.

This diet increased levels of hydrogen peroxide in mitochondria-enriched fractions that were linked to Complex 1 function because, upon Complex 1 inhibition, the hydrogen peroxide levels decreased. However, this diet did not alter mitochondrial respiration and had only a modest increase on lipid levels of mitochondrial-enriched fractions. These findings suggest that high-fat low-carbohydrate diets do not dramatically affect kidney mitochondrial function.

Sphingolipids are important lipids in cells for growth and apoptosis. In *S. cerevisiae* the enzyme inositol sphingolipid phospholipase C (Isc1p) synthesizes ceramide from non-fermentable carbon sources. A recent study demonstrated a direct link between Isc1p activity and phytoceramide synthesis in mitochondria.[540] The Isc1p and lipid levels were assessed by Western blotting and HPLC-ESI-tandem mass spectrometry, respectively. As expected, Isc1p knockdowns and wild-types had different mitochondrial lipid profiles. Relative to wild-type, knockdown of Isc1p caused a reduction in the levels of α-hydroxylated C_{26}-phytoceramide, non-hydroxylated C_{26}-phytoceramide, α-hydroxylated C_{14}-phytoceramide, and α-hydroxylated $C_{24:1}$-phytoceramide, in mitochondrial enriched fractions. Confirming the role of Isc1p, expression of FLAG-Isc1p protein in the Isc1p knocked-down cells caused an increase in the levels of ceramide molecules.

Another related study investigated the role of sphingomyelinase in mitochondrial ceramide synthesis in zebrafish cell cultures.[541] Confocal immunofluorescence microscopy and Western blotting of subcellular fractions revealed that sphingomyelinase localized to mitochondria. Thin layer chromatography of the mitochondrial fraction, followed by ammonium molybdate/ascorbic acid detection confirmed ceramide synthesis in this fraction.

Acid sphingomyelinase (ASM) causes ceramide release, which in turn results in apoptosis. In a recent study ASM was activated with gemcitabine which resulted in ceramide production in mouse glioma cells, which in turn increased the levels of apoptotic markers.[542] Western blot analysis of mitochondrial fractions showed an increase in Bax, a Bcl-2 family member and an apoptosis mediator. On the other hand, the activation did not seem to be uniquely regulated through mitochondria. Fluorescence microscopy revealed that upon treatment with gemcitabine, lysosomes accumulated ceramides that in turn activated pro-apoptotic cathepsin D, which was detected by Western blotting. This result suggests that the chemotherapeutic agent gemcitabine induces apoptosis through the ceramide pathway that cross-talks between mitochondria and the lysosome.

Aluminum limits plant growth and is a neurotoxin in animals. The effects of aluminum exposure on mitochondrial activity was determined in *R. glutinis* aluminum-sensitive and aluminum-insensitive cells.[543] Aluminum insensitive cells were developed with constant aluminum treatment. Transmission electron microscopy demonstrated that aluminum-insensitivity was associated w ith increased the number of mitochondria, which were smaller and had simplified cristae. PCR revealed that aluminum-insensitive cells had also 2.5 to 3 fold increase in mitochondrial DNA relative to their sensitive counterparts. Furthermore, aluminum toxicity was manifested as increased ROS and increased membrane potential in mitochondrial fractions from aluminium-insensitive cells. Aluminum-sensitive cells also had reduced cytochrome *C* oxidase findings imply that aluminum toxicity is associated with increased ROS production and that mitochondria genesis could play an important role preventing aluminum toxicity.

Soluble hydrocarbons accumulate following exposure in membranes and other lipid stores of cells of shrimp (*M. Borelli)* affecting the composition and dynamics of phospholipids and triacylglycerides. A recent study investigated mitochondrial and cytosolic enzymatic activities associated with activation of triacylglyceride and fatty acid mobilization and

degradation in response to crude oil exposure.[544] Scintillation counting monitored long-chain fatty acyl-CoA synthetase and β-oxidation activities using [1-^{14}C]-palmitic acid as a substrate and triacylglycerol lipase activity using carboxyl-[^{14}C]-triolein as substrate. The mitochondrial fractions from both adults and eggs exposed to water-soluble hydrocarbons had statistically significant increased triacylglyceride lipase activity relative to unexposed controls. Water-soluble hydrocarbon exposure also caused increased fatty acid β-oxidation in the mitochondria of adult and stage 5 eggs.

6.5. Nucleus function

The subcellular localization and function of human biliverdin reductase A (BRA) protein was studied in HeLa cells.[545] BRA is a transcription factor and a kinase and has been suggested to be a heme moiety transporter. Fluorescence correlation spectroscopy revealed that GFP-BRA localized to both the cytosol and the nucleus. When treated with hematin, BRA had increased nuclear colocalization. Its binding was confirmed by observing a changed absorption spectrum for hematin in the presence of BRA. Furthermore, incubation of BRA with hematin and double-stranded DNA fragments caused a 2-fold increase in its kinase activity and an increase in the expression of heme oxygenase s uggesting BRA kinase activity is nucleus specific.

Nuclear specific detection of oxidative stress has been challenged because most probes specific for oxidative stress are not specific for a subcellular location. A new electron spin resonance probe, F-DisT, that targets the nucleus for the detection of nuclear oxidative stress has been recently developed.[546] The probe uses a 2,2,6,6-tetramethylpiperidin-1-oxyl (TEMPO) derivative that employs a pyrrole polyamide, a known DNA minor-groove binding moiety. TEMPO is a paramagnetic compound that is routinely used for nitroxide detection. Under oxidative or reductive conditions, the probe is reversibly transformed into its diamagnetic species (under reducing conditions, to its hydroxylamine form and under oxidizing conditions, its oxo-ammonium form). When in diamagnetic form, the probe's electron spin resonance (ESR) signal is decreased. Using the ESR signal decay rate, it is possible to detect the reducing or oxidizing environments inside cellular compartments. This probe detects oxidative stress caused by NO, as confirmed by the r eduction of its response upon t reatment with nitric oxide synthase. These studies revealed that NO, which is not a significant player in mitochondrial or cell membrane oxidative stress, plays a larger role in oxidative stress in the nucleus.

Sal1 is a nucleotidase/phosphatase that provides retrograde signaling from the chloroplast to the nucleus in response to light or draught. A recent study investigated the activity of Sal1 in the subcellular environments of *A. thaliana* under different light conditions.[547] Confocal fluorescence microscopy revealed Sal1-GFP localized to both the chloroplast and the nucleus and that it increased in abundance upon increased light exposure. The activity of Sal1 was indicated by the formation of 3'phosphoadenosine-5'-phosphate, which was monitored by HPLC analysis of cytosolic, nuclear, chloroplast, and mitochondrial fractions. As expected, the Sal1 knockdown caused decreased formation of this metabolite.

Stat5 and PDC-E2 are involved in gene transcription involving both nuclear and mitochondrial localizations. A r ecent study found b oth proteins in the nucleus of mouse pro-B cell line BaF3, while only PDC-E2 was found in mitochondria.[548] Immunoprecipitation suggested PDC-E2 is a co-activator of Stat5. This interaction causes translocation of PDC-E2 the nucleus, which was observed by confocal fluorescence microscopy. Once localized in the nucleus, PDC-E2 is able to regulate STAT5 to activate transcription suppressor of cytokine signaling 3 (SOCS3) as determined from SOCS3 mRNA levels.

6.6. Peroxisome function

Xanthine oxidoreductase (XOR) catalyzes the formation of uric acid and had two forms: oxygen-dependent xanthine oxidase (XOD) and NAD dependent xanthine dehydrogenase (XDH). A recent study investigated the distributions and a ctivities of XDH and XOD in peroxisomes of *P. sativum* under different stress conditions.[549] An enzymatic assay for uric acid synthesis in the presence of either oxygen or NAD was used to determine the relative distributions of XDH and XOD, respectively. Wild type peroxisome fractions from *P. sativum* had 62% XDH and 38% XOD (normalized to total XOR activity). An anti-XOR antibody was used with transmission electron microscopy to show that XOR proteins were present in both peroxisomes and chloroplasts. Cadmium-induced oxidative stress reduced the overall activity of both XOD and XDH relative to the basal levels but maintained the relative activity of XOD and XDH.

7. Organelle heterogeneity

Heterogeneity is an intrinsic property of all living systems. Similar to cell-to-cell variations, heterogeneity exists at the organelle level in almost every organelle type as a result of normal processes, disease and aging.[392] The identification and characterization of organelle subpopulations, that can be hidden within the whole population, is of great importance for providing a more complete understanding of many biological processes (e.g. autophagy).[550] Organelle heterogeneity can be characterized either directly inside the cellular environment or after the organelle isolation and purification.

7.1. Heterogeneity of organelles within the cell

Microscopic techniques are typically the methods of choice for *in vivo* identification of inter-organelle differences within cells.[84] Observing cells by confocal microscopy has revealed a variety of mitochondrial subpopulations, which differ in their size and morphology, energy status and the abundance of characteristic proteins.

Imaging of the autofluorescence of mitochondrial flavoproteins, which reflect electron transport through the electron transport chain and its relation to mitochondrial metabolic activity, revealed large, perinuclear clusters of mitochondria in cardiomyocytes suggesting their important role in nuclear import and ATP metabolism.[551] Similar clusters were observed in subsarcolemmal mitochondria in mouse skeletal muscle tissue. The intensity of flavoprotein autofluorescence was more than four times higher in subsarcolemmal compared to interfibrillar mitochondria, pointing to higher oxidative stress in the vicinity of the cell membrane.

Accumulation of a subgroup of enlarged mitochondria, identified by c onfocal microscopy, was observed in long term-cultured and autophagy-compromised cells.[552] This group of so-called "giant mitochondria" characterized by a width larger than 1 μm (approx. 3 times larger than normal mitochondria) had lower membrane potential, the inability to fuse with other mitochondria and decreased abundance of the OPA1 fusion protein, suggesting that they are relevant to aging and disease.[553]

7.2. Heterogeneity of populations of isolated organelles

Although microscopic techniques provide high-resolution information about organelle properties in the natural cellular environment, their major drawback is their low throughput. The number of organelles and cells that can be analyzed is usually limited to a maximum of t ens of organelles, which limits the available sample size for subsequent data analysis. Isolation, purification and the subsequent analysis of intact organelles have been the method of choice for analyzing organelle function. The benefit is usually a high number of

organelles that are analyzed, while the drawback is that the function of organelles may change after their release from the cellular environment.[554] Similarly, flow cytometry is a well-established technique for a high throughput, detection of cell-to-cell heterogeneity. However, its use for the analysis of intact organelles has been quite limited due to its rather poor sensitivity.[555]

Capillary electrophoresis with laser induced fluorescence detection (CE-LIF) has been shown to be a powerful method for the analysis of individual organelles.[556] CE separates individual organelles based on the differences in their surface charge density, thus providing information about the surface properties of each organelle. The separation takes place in a narrow bore fused silica capillary attached to an ultra-sensitive laser-induced fluorescence d etector with a zeptomolar limit of detection. In this arrangement, CE-LIF can measure multiple fluorescence parameters of each organelle with a higher sensitivity compared to flow cytometry and provide additional information about the surface properties of each particular organelle. CE-LIF was used to investigate distributions of mtDNA in individual mitochondria released from 143B cells.[396] This method enabled the detection of a single copy of mtDNA in a single mitochondrion. The same approach was used to d etermine the pH heterogeneity within acidic organelles in two human leukemia cell lines.[154] The drug-resistant human lymphoblast cell line CEM/C2 contained acidic organelles with a mean pH of 5.1. This was 1 pH unit lower than the mean pH of acidic organelles found in the drug resistant human lymphoblast cell line C CRF-CEM. Cytoskeletal binding to mitochondria was also investigated by CE-LIF.[557] By simultaneous fluorescence labeling of mitochondria and F-actin, it was found that 21% of mitochondria isolated by a standard isolation technique contained cytoskeletal remnants on their surface. The electropherogram showing cytoskeleton binding to mitochondria is shown in Figure 35.[557] Another major benefit of the narrow capillary of a CE instrument is that it can also be easily u sed as a precise injection device, which allows investigators to sample and characterize properties of mitochondria from single cells[558] and muscle tissue cross-sections.[559]

8. Future directions

This section provides an opinion on developments that are needed in the field of organelle analysis. It also describes emerging strategies that are relatively new or that may not have been applied previously that, in the long-term, could help advance this field.

8.1 Organelle imaging

Continued emphasis on the direct visualization of subcellular organization, both under static and dynamic conditions will further assist refining our understanding of the subcellular environment. Super resolution fluorescence imaging and new p owerful electron microscopy techniques w ill likely continue to evolve and become more common in subcellular imaging.

The challenge of subcellular imaging of tissue has been only partially met by multi-photon excitation imaging. Developments in subcellular tissue imaging continue to be a major obstacle. On the other hand, the development of infrared multi-photon excitation may soon provide opportunities to observe subcellular environments in tissue.[560] This technique uses wavelengths above 1080 nm, which enables the use of red fluorophores and fluorescent proteins, doubles imaging depth, improves second harmonic generation of tissue structures, and strongly reduces phototoxicity and photobleaching, compared with conventional multi-photon excitation techniques. Furthermore, it still provides subcellular resolution at depths of several hundred micrometers and will enhance long-term live cell and deep tissue microscopy.

The use of the near infrared light may also provide new possibilities for probe development that could be used in subcutaneous and even deeper tissue systems. As an example, a near-infrared excitable probe for pH determination in the vicinity of breast cancer tumors has recently been developed.[184] The molecular structure of this probe consists of a pH-sensitive cyanine dye conjugated to a cyclic arginine-glycine-aspartic acid peptide that targets Rvβ3 integrin, a protein involved in angiogenesis that is highly expressed in endothelial tumors. This probe is fluorescent when the pH is below 5 and would be ideal for use in pH determination of tumor lysosomes and endosomes.

Multiparametric imaging such hyperspectral imaging,[561] quadriwave lateral shearing interferometry,[562] coherent anti-stokes Raman spectroscopy,[563] and mass spectrometry imaging[564] have potential in the subcellular analysis field. However, issues of spatial resolution and insufficient sensitivity to obtain sufficient signal-to-noise ratio measurements are still major limitations that must be addressed.

Lastly, fluorescence imaging will likely continue being a commonly used technique in subcellular analysis for many more years. The current arsenal of subcellular-specific fluorescent probes will continue to expand to include new synthetic probes, affinity reagents, and molecularly engineered proteins.

An example of a recently developed engineered protein is the RFP variant, mNectarine, which may become the preferred probe for biological pH measurements.[565] This fluorescent protein displays a dramatic change in fluorescence intensity within the range of biologically significant pH with an excitation maximum of 558 nm and an emission maximum of 578 nm. While most fluorescent proteins exhibit pH-dependent changes in their fluorescence intensity, excitation wavelengths or emission wavelengths, not all of them experience changes in a pH range that is biologically relevant.

Another intriguing approach for subcellular fluorescent labeling would be the use of targeted antibody-tagged nanoparticles in which the orientation of binding of the antibody to nanoparticles is tightly controlled. A recent report has elegantly demonstrated such technology in the immobilization of glycosylated antibodies.[566] Controlled orientation resulted in a more efficient use of nanoparticle surface area, which enhances the sensitivity of the detection scheme. This methodology would offer a great advantage when the antibody targets have low abundance in the subcellular regions of interest.

It is also envisioned that labeling of samples for subcellular analysis will also progress with the introduction of microfluidic devices. A preview of such a future is a recent publication on the use of microfludic devices to immunolabel and image multiple cell lines, in parallel, to analyze the properties of endocytic organelles.[180] These technologies will certainly have a positive impact on reducing sample size requirements, providing reproducible sample preparation procedures, and enabling high-throughput comparisons of the subcellular properties of multiple cells lines or cell treatments.

8.2. Analysis of isolated organelles

For many decades, the determination of organellar functions and molecular composition has been based on the analysis of isolated organelles. The process of organelle isolation has many drawbacks because it causes destruction, dramatic structural reorganization of the original organellar morphology, loss of function, and loss of the spatial surroundings of the organelle. On the other hand, it possesses powerful advantages as it provides access to an extensive array of bioanalytical technologies that rely on specialized sample preparation procedures.

It is likely that isolated organelles will continue being a critical resource in organelle analysis. Indeed, developments in sample preparation m ay help decrease lo ss-of-function detrimental morphological rearrangements, which are currently a significant limitation of this approach.[554] Other initiatives may simply h elp emulate the interactions between o rganelles that occur naturally in the intracellular milieu. Ultimately a deeper understanding of how an organelle is transformed when it is removed from its cellular context will facilitate more judicious selection of conditions that minimize perturbation of the properties being monitored or measured.

Current limitations are also imposed by the purification techniques used to prepare organelle fractions. The investigator is constantly faced with the dilemma that higher organelle purity is associated with lower yield and lower biochemical activity or function. While it is not anticipated that centrifugation-based organelle purifications will be displaced by newer techniques in the near future, it is anticipated that f aster purification procedures such as t hose provided by immunoaffinity reagents[567] or other separation techniques that are compatible with functional organelles, such as electrophoretic techniques[273a,273c,568] will provide a greater range of options to conduct subcellular-specific analyses.

Indeed, the need for subcellular purification strategies is dictated by the instrumentation utilized in the subcellular analysis. Regarding molecular characterization techniques, ultrafast separations (UPLC) and advanced mass spectrometers will likely enhance the depth and coverage in studies focusing on the subcellular cosmos. Two examples of recent developments in mass spectrometry are the Q Exactive and the TripleTOF 5600 mass spectrometers. The "Exactive" was developed earlier for small molecule applications, but contains only the Orbitrap analyzer.[569] The Q Exactive is an Exactive mass spectrometer coupled to a quadrupole.[570] This mass spectrometer employs only HCD (higher energy collision dissociation), which tremendously simplifies the hardware associated with the Orbitrap Velos that has been used extensively for proteomic analysis of complex peptide mixtures. On the other hand, proteomic analysis of complex peptide mixtures using the Q Exactive instrument produces results that are, in fact, very comparable to those obtained with the Orbitrap Velos. Yet the Q Exactive machine is truly a benchtop mass s pectrometer and is capable of extremely fast switching time of the quadrupoles, which allows it to select ions for HCD fragmentation almost instantaneously. While the Q Exactive device has not yet been used for subcellular proteomics, its use exemplified by the sensitive detection of peginesatide, a performance-enhancing pegylated peptide in dried blood spots clearly suggests it should be useful for subcellular proteomic analysis.[571]

8.3. Organelle dynamics, interactions and heterogeneity

Improvements in monitoring dynamic processes in the subcellular environment are intimately linked to developments in time-lapse microscopy, stable, non-toxic organelle markers such as fluorescent proteins, fast response probes, and image analysis software capable of extracting kinetic parameters from image frames. It is anticipated that there are ample opportunities to expand this area as resources supporting live cell imaging, probes, and software become more standardized and relatively easy to use.

The interactions between organelles may also be considered from the point of view of the thermodynamic equilibrium between molecular species. These interactions may involve various membrane components including lipids, carbohydrates, and proteins and span K_D values over nine orders of magnitude, having as their ceiling, the classical interaction between biotin and streptavidin ($K_D \sim 10^{-15}$).

Some of these interactions may be studied by adapting techniques that are based on the direct determination of binding and dissociation rates, such as those based on surface

plasmon resonance[572] or non-equilibrium capillary electrophoresis of mixtures at equilibrium.[573] On the other hand, when the interactions have slow dissociation rates, which are usually associated with low KD values, the involved molecular species remain bound even upon isolation of subcellular environments. Indeed, techniques to investigate subcellular in teractions characterized by low KD values and that withstand extensive sample handling have included immunoprecipitation, western blotting, and affinity chromatography. Other techniques capable of reporting interactions between organelles, such as the analysis of binding between mitochondria and cytoskeleton by capillary electrophoresis with laser-induced fluorescence detection, have also begun to appear. [557] Lastly, other future developments in this area will likely involve adaptations of existing methodologies (e.g. development of aptamers for cells) to characterize or purify organelles with high selectivity.[574]

Another possibility to investigate transient interactions between organelles (i.e. involving interacting molecules that dissociate at high rate) is to use clickable crosslinkers. For instance, clickable reagents that penetrate cells and crosslink proteins within the cell efficiently 'freeze' transient subcellular interactions. An example of development in this field used ubiquitin as their model system.[575] The cross-linked peptides were purified and their m ass spectrometric analysis made possible to identify intra-and inter-protein interactions. It is anticipated that the use of cross-linking technologies to analyze molecular interactions occurring between two organelles b oth *in vivo* and in *in vitro* systems will likely enable a variety of new types of subcellular analyses to be performed.

High throughput analysis of strong subcellular interactions is also a critically emerging area. An example of such development is the analysis of interactomes by Parallel Affinity Capture (iPAC) in a *D. melanogaster* model system.[576] iPAC is a triple-tagged system in which yellow fluorescent protein is used for screening and expression profiling, and StrepII and FLAG tags are used for parallel affinity capture. A tagless control identifies proteins common to both StrepII and FLAG purifications. The method appears to generate a "catalogue" of high-confidence interactions as well as a library of proteins that nonspecifically bind to many resins (termed "BEADomes").

One of unexplored areas of subcellular analysis is that of the sources of organelle heterogeneity in terms of organelle morphology, biophysical properties, or composition. In many instances such heterogeneity simply represents the stochastic nature of the property under investigation. Modeling of such properties may be an approach to predict such heterogeneity. However, heterogeneity may also have a component associated with the existence of subpopulations of organelles. Some subpopulations are difficult to observe because they are defined morphologically (e.g. giant and normal mitochondria),[553] while identification and definition of other subpopulations will likely need unbiased data analysis systems and experimental models that can be directed to define such subpopulations.

8.4. Subcellular analysis-Large datasets and models

One of the greatest challenges in the subcellular analysis field is the integration of powerful biostatistical and bioinformatics resources to analyze imaging data, 'omics' data, or large data sets of multiparametric measurements such as those obtained through individual organelles. This collection of disparate data sets usually requires development or adaptation of resources existing in other data intensive disciplines. Such adaptations require the additional spatial and temporal dimensions provided by the subcellular architecture.

An example of subcellular focused database is a recent resource on plant organelle dynamics.[577] In its current form, it includes static images, procedures for isolation of organelles and movies. These resources aid at identifying position, movement, division and

behavior, particularly in response to a stimuli. Efforts to make large datasets downloadable and to develop quantitative tools are in progress. In addition, there are efforts in predicting subcellular f unction, such as the seminal work of Smith et al. on mitochondrial dysfunction (reviewed in 6.4.)[340] and cataloguing information on the distributions of biomolecules in various subcellular environments, such as the initiatives described by Murphy et al.[88]

8.5. Future areas enabled by organelle analysis

Areas that will continue benefiting from the development of organelle analysis methodologies are the fields of drug and gene delivery in which both cellular uptake and subcellular targets require extensive subcellular experimentation. This is particularly relevant when the drug target is localized in an intracellular organelle. Recent reviews describe m ethods of subcellular drug targeting based on molecular designs.[578] These developments clearly rely on our understanding on how membrane proteins, lipids, nutrients and some pathogens are internalized into the cell to be targeted to distinct subcellular compartments via membrane trafficking (reviewed in 5.). A more specialized drug delivery system is gene therapy that aims to regulate gene expression.

Gene delivery faces similar challenges for delivery to its molecular targets. A recent review covered efforts to use polymers, peptides, liposomes and nanoparticles to enhance cellular uptake of genetic material, including organelle-targeted systems. Among these carriers, cationic polymers and peptides have been further developed as intracellular organelle-targeted delivery systems. The cytoplasm, nucleus, and mitochondria have been considered primary targets for gene delivery using targeting moieties or environment-responsive materials.[579]

The importance of biomedical nanotechnology in modern society is having unprecedented impact on research addressing gene therapies, m olecular imaging devices, and treatments for organelle-specific diseases. A recent review clearly highlights the importance of subcellular targeting,[580] in which the authors describe the present and predict the future in which engineered nanoparticles take into consideration intracellular interactions, processing, and trafficking. Clearly, the development and performance of these technologies ultimately relies on the existence of subcellular analysis.

An ambitious project is the mapping the subcellular distribution of all human proteins, which is the cornerstone for deciphering the complexities associated with the spatial distribution of proteins at all levels: from organelles to organs. While the more established mass spectrometry-based proteomics have reported unprecedented progress,[54] more recently antibody based approaches are reporting remarkable advances in cataloguing the human proteome providing a first glimpse of the subcellular framework.[49]

Acknowledgments

Biographies

Chad P. Satori is a Ph.D. candidate in the Department of Chemistry at the University of Minnesota, Twin Cities, USA. He was a recipient of a 2011 Baxter Young Investigator Award, was a trainee of the University of Minnesota Biotechnology Training Grant, and was a member the Center for Analysis of Biomolecular Signaling. His research focuses on the development of methods to acquire highly enriched organelle fractions and the development of methods to analyze and characterize organelles and their properties.
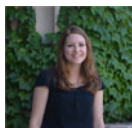
Michelle M. Henderson is a Ph.D. candidate in the Department of Chemistry at the University of Minnesota, Twin Cities, USA. Michelle was a trainee on the Chemistry-Biology Interface Training grant from 2010 to 2012. Her research focuses on quantifying the proteomes associated with normal and giant mitochondria, as well as quantifying protein carbonylation abundance changes with changing mitophagy flux. Before beginning her doctoral research at the University of Minnesota, she was a Research Associate at NewLink Genetics in Ames, Iowa, USA, from 2007 to 2009 working in small molecule development.

Elyse Krautkramer is a Ph.D. candidate in the Department of Chemistry at the University of Minnesota, Twin Cities, USA. Her project entails the development of intra-organelle probes for redox environment analysis.

Vratislav Kostal received his Ph.D. in Analytical chemistry in 2007 at the Palacky University in Olomouc, Czech Republic. During his studies he also spent four years at the Institute of Analytical Chemistry, Brno, Czech Republic developing fluorescence detectors for capillary separation methods. Between 2007 and 2011, Vratislav was a postdoctoral trainee in the laboratory of Professor Edgar A. Arriaga at the University of Minnesota, Twin Cities, MN, USA working on the analyses of mitochondrial subpopulations using capillary electrophoresis and fluorescence imaging. He is currently a Field Application Scientist at Tescan, located in Brno, Czech Republic. His main responsibility is developing new applications of state-of-the-art scanning electron microscopy for life sciences.

Mark Distefano was born in Baton Rouge, LA, USA, and grew up in California and Paris, France. He received his B.A. degree in Chemistry and Biochemistry from the University of California at Berkeley in 1985 and his Ph.D. degree from Massachusetts Institute of Technology in1989, where he worked with Professor Christopher T. Walsh. He was a postdoctoral fellow in the laboratory of Peter B. Dervan at California Institute of Technology. He is currently Distinguished McKnight Professor of Chemistry and Medicinal Chemistry at the University of Minnesota, Twin Cities, MN, USA. His research is focused on the use of organic chemistry to create synthetic probes that can provide insights into biological processes. Currently, his laboratory is focused on understanding protein lipid modification.

Edgar A. Arriaga was born in Guatemala. He received a Licenciatura in Chemistry from Universidad del Valle de Guatemala, a Ph.D. in Chemistry from Dalhousie University, Canada. His post-doctoral training included electrophysiological and photosensitization research at the University of Kansas Medical Center, USA, and bioanalytical chemistry research at the University of Alberta, Canada. Currently, he is a Professor of Chemistry at the University of Minnesota, Twin Cities, USA. He was the 2007–2008 Fesler–Lampert Chair in Aging Studies and is a member of the graduate faculties in Biomedical Engineering, Gerontology, Molecular Biology, Biochemistry and Biophysics programs at the University of Minnesota, Minneapolis, MN, USA. Over the last 10 years he has served as *ad hoc* and chartered member of the National Institutes of Health (NIH) in various Review Study Sections. His research program focuses on the development of bioanalytical methodologies to investigate tissue complexity, single cells and subcellular compartments.

Abbreviations

ANT	Adenine nucleotide translocase
AUC	Area under the curve
BRA	Human biliverdin reductase A protein
C-rluc	Carbon-terminal renilla luciferase protein fragment
CAT	X-Ray computed axial tomography
CCCP	Carbonyl cyanide *m*-chlorophenyl hydrazone
CCT	Choline cytidylyl-transferase
CE-LIF	Capillary electrophoresis coupled to laser induced fluorescence detection
CFP	Cyan fluorescent protein
CMA	Chaperone mediated autophagy

CORVET	Class C core vacuole/endosome tethering
Cul3	Cullin3
Cyt c	Cytochrome C oxidase
DAPI	4'6-diamidino-2-phenylindole
DFCP1	Double FYVE domain-containing protein 1
DPP1	Dipeptidyl peptidase 1
DOMS	Direct organelle mass spectrometry
EEA1	Early endosome antigen 1
EGF	Epidermal growth factor
EGFR	Epidermal growth factor receptor
ER	Endoplasmic reticulum
ERAD	ER associated degradation
ERK1/2	extracellular signal-regulated protein kinase 1/2
ESCRT	Endosomal sorting complex required for transport
ESI	Electrospray Ionization
ESR	Electron spin resonance
ET	Electron tomography
FAOS	Fluorescence-assisted organelle sorting
FAT	Fatty acid translocase
FIB	Focused ion beam
FIB/SEM	Focused ion beam/scanning electron microscopy
FFE	Free flow electrophoresis
FFF	Field-flow fractionation
FI-AFIFFF	Frit-inlet asymmetric flow field-flow fractionation
FPALM	Fluorescence photoactivation localization microscopy
FRET	Fluorescence resonance energy transfer
FTMS	Fourier transform mass spectrometry
GA	Golgi-associated, γ-ear-containing, ADP-ribosylation factor binding protein
GAP	GTPase activating protein
GFP	Green fluorescent protein
GPF	Gas phase fractionation
GTP	Guanosine triphosphate
GO	Gene ontology
GPX	Glutathione peroxidase
GSH	Glutathione

GSSG	Glutathione disulfide
HCD	Higher energy collision dissociation
HE	Hydroethidine
HILIC	Hydrophilic interaction chromatography
HOPS	Homotypic fusion and vacuole protein sorting
HPCE	phalloidin-hyperbranched polymer conjugated electrolyte
HPLC	High-performance liquid chromatography
ICP-AES	Inductively-coupled plasma - atomic emission spectrometry
ICP-MS	Inductively-coupled plasma - mass spectrometry
IMAC	Iminodiacetic acid
IP3	Inosine triphosphate
IPI	International Protein In dex
IR	Infrared
ISC1p	Inositol sphingolipid p hospholipase C
ITP	Isotachophoresis
iTRAQ	Isobaric tag for r elative and absolute quantification
KGDHC	α-ketoglutaric acid dehydrogenase complex
KFP	Kindling fluorescent protein
LOPIT	Localization of organelle proteins by isotope tagging
LRO	Lysosome-related organelle
LSD	Lysosomal storage disease
LTQ	Linear ion trap
MAC	Mitochondrion-associated adherens complex
MALDI	Matrix-assisted laser desorption/ionization
MAP1S	Microtubule-associated protein 1S
MCM	Minichromosome maintenance
MDH	Malate dehydrogenase
MemO	Membrane Protein Prediction
mRFP	Monomeric red fluorescent protein
MRI	Magnetic resonance imaging
MVB	Multivesicular bodies
N-rluc	Nitrogen-terminal renilla luciferase protein fragment
NAT	Acetyl-CoA:α-glucosaminide N-acetyltrasferase
NAQF	Non-aqueous fractionation
NMR	Nuclear magnetic resonance
NSF	N-ethylmaleimide-sensitive factor

PALM	Photoactivation localization microscopy
PARP	Poly-ADP-ribose polymerase
PCP	Protein correlation profiling
PI3P	Phosphatidylinositol-3-phosphate
μ-PIXRE	Micro particle-induced X-Ray emission
PKA	Protein kinase A
PPI	Protein-protein interaction
PSF	Point spread function
PTM	Post-translational modification
QD	Quantum dot
roGFP	Redox active green fluorescent protein
ROS	Reactive oxygen species
RPE	Retinal pigment epithelial
RyRs	Ryanondine receptors
SDH	Succinate dehydrogenase
SDS	Sodium dodecyl sulfate
SDS-PAGE	Sodium dodecyl sulfate-polyacrylamide gel electrophoresis
SEM	Scanning electron microscope
Sg2	Secretogranin 2
SILAC	Stable isotope labeling of amino acids in cell culture
SILAM	Stable isotope labeling of amino acids of mammals
siRNA	Small interfering RNA or silencing RNA
SNAP	Synaptosome-associated protein
SNARE	Soluble *N*-ethylmaleimide-sensitive factor activating protein
SNX	Sorting nexin
SOD1	Superoxide dismutase 1
STED	Stimulated emission depletion
STORM	Stochastic optical reconstruction microscopy
TALM	Real-time tracking and localization
TAP	Tandem affinity purification
TdR	Thymidine-derived sugars
TEM	Transmission electron microscopy
TEMPO	2,2,6,6-tetramethylpiperidin-1-oxyl
TGM-2	Transglutaminase-2
TIF-YFP	Tonoplast intrinsic factor-yellow fluorescent protein
TIRF	Total internal reflectance fluorescence microscopy

TOF	Time-of-flight
TORC1	vacuole associated target of rapamycin complex 1
μPIXRE	micro particle-induced x-ray emission
UPLC	Ultra performance liquid chromatography
UPRE	Unfolded protein response element
μXRF	micro X-ray fluorescence
VAMP	Vesicle-associated membrane protein
XBP1	X-box binding protein 1
XDH	Xanthine dehydrogenase
XOD	Xanthine oxidase
XOR	Xanthine oxidoreductase
YFP	Yellow fluorescent protein

References

1. (a) Guo Y, Cordes KR, Farese RV, Walther TC. J. Cell Sci. 2009; 122:749. [PubMed: 19261844] (b) Reue K. J. Lipid Res. 2011; 52:1865. [PubMed: 21921134]

2. Berg TO, Fengsrud M, Stromhaug PE, Berg T, Seglen PO. J. Biol. Chem. 1998; 273:21883. [PubMed: 9705327]

3. Maréchal E, Cesbron-Delauw M-F. Trends Plant Sci. 2001; 6:200. [PubMed: 11335172]

4. Takeshige K, Baba M, Tsuboi S, Noda T, Ohsumi Y. J. Cell. Biol. 1992; 119:301. [PubMed: 1400575]

5. Karp, G. Cell and molecular biology: concepts and experiments. John Wiley & Sons; 1996.

6. Cocucci E. Mol. Biol. Cell. 2004; 15:5356. [PubMed: 15469985]

7. Ganley IG, Carroll K, Bittova L, Pfeffer S. Mol. Biol. Cell. 2004; 15:5420. [PubMed: 15456905]

8. Kesimer M, Scull M, Brighton B, DeMaria G, Burns K, O'Neal W, Pickles RJ, Sheehan JK. The FASEB Journal. 2009; 23:1858.

9. Kühnel, W. Color Atlas of Cytology, Histology, and Microscopic Anatomy. Thieme; 2003.

10. Wasmeier C, Hume AN, Bolasco G, Seabra MC. J. Cell Sci. 2008; 121:3995. [PubMed: 19056669]

11. Van Gestel K, Verbelen JP. J. Exp. Bot. 2002; 53:1215. [PubMed: 11971932]

12. Dittmer TA, Stacey NJ, Sugimoto-Shirasu K, Richards EJ. The Plant Cell Online. 2007; 19:2793.

13. Voet, D.; Voet, JG. Biochemistry. John Wiley & Sons; 2004.

14. Toyohara A, Inaba K. J. Cell Sci. 1989; 94:143. [PubMed: 2693471]

15. Hammel I, Lagunoff D, Galli SJ. J. Cell. Mol. Med. 2010; 14:1904. [PubMed: 20406331]

16. Blott EJ, Griffiths GM. Nat Rev Mol Cell Biol. 2002; 3:122. [PubMed: 11836514]

17. Gonatas NK, Autilio-Gambetti L, Gambetti P, Shafer B. J. Cell. Biol. 1971; 51:484. [PubMed: 5112652]

18. Melnikov S, Ben-Shem A, de Loubresse NG, Jenner L, Yusupova G, Yusupov M. Nat. Struct. Mol. Biol. 2012; 19:560. [PubMed: 22664983]

19. Bornens M. Science. 2012; 335:422. [PubMed: 22282802]

20. Barenz F, Mayilo D, Gruss OJ. Eur. J. Cell Biol. 2011; 90:983. [PubMed: 21945726]

21. Mao YTS, Zhang B, Spector DL. Trends Genet. 2011; 27:295. [PubMed: 21680045]

22. Wei N, Serino G, Deng XW. Trends Biochem. Sci. 2008; 33:592. [PubMed: 18926707]

23. Kato JY, Yoneda-Kato N. Genes Cells. 2009; 14:1209. [PubMed: 19849719]

24. Murat D, Byrne M, Komeili A. Cold Spring Harbor Perspectives in Biology. 2010; 2

25. Cheng SQ, Liu Y, Crowley CS, Yeates TO, Bobik TA. Bioessays. 2008; 30:1084. [PubMed: 18937343]

26. Nevo-Dinur K, Govindarajan S, Amster-Choder O. Trends Genet. 2012; 28:314. [PubMed: 22521614]

27. Klionsky DJ, Abeliovich H, Agostinis P, Agrawal DK, Aliev G, Askew DS, Baba M, Baehrecke EH, Bahr BA, Ballabio A, Bamber BA, Bassham DC, Bergamini E, Bi XN, Biard-Piechaczyk M, Blum JS, Breclesen DE, Brodsky JL, Brumell JH, Brunk UT, Bursch W, Camougrand N, Cebollero E, Cecconi F, Chen YY, Chin LS, Choi A, Chu CT, Chung JK, Clarke PGH, Clark RSB, Clarke SG, Clave C, Cleveland JL, Codogno P, Colombo MI, Coto-Montes A, Cregg JM, Cuervo AM, Debnath J, Demarchi F, Dennis PB, Dennis PA, Deretic V, Devenish RJ, Di Sano F, Dice JF, DiFiglia M, Dinesh-Kumar S, Distelhorst CW, Djavaheri-Mergny M, Dorsey FC, Droge W, Dron M, Dunn WA, Duszenko M, Eissa NT, Elazar Z, Esclatine A, Eskelinen EL, Fesues L, Finley KD, Fuentes JM, Fueyo J, Fujisaki K, Galliot B, Gao FB, Gewirtz DA, Gibson SB, Gohla A, Goldberg AL, Gonzalez R, Gonzalez-Estevez C, Gorski S, Gottlieb RA, Haussinger D, He YW, Heidenreich K, Hill JA, Hoyer-Hansen M, Hu X, Huang WP, Iwasaki A, Jaattela M, Jackson WT, Jiang X, Jin SK, Johansen T, Jung JU, Kadowaki M, Kang C, Kelekar A, Kessel DH, Kiel J, Kim HP, Kimchi A, Kinsella TJ, Kiselyov K, Kitamoto K, Knecht E. Autophagy. 2008; 4:151. [PubMed: 18188003]

28. Barth S, Glick D, Macleod KF. The Journal of Pathology. 2010; 221:117. [PubMed: 20225337]

29. Hoffman RM. Curr. Pharm. Biotechnol. 2012; 13:537. [PubMed: 22214502]

30. Takeuchi M, Ozawa T. Anal. Sci. 2007; 23:25. [PubMed: 17213619]

31. Tsien RY. Annu. Rev. Biochem. 1998; 67:509. [PubMed: 9759496]

32. Waggoner A. Curr. Opin. Chem. Biol. 2006; 10:62. [PubMed: 16418012]

33. Chiesa A, Rapizzi E, Tosello V, Pinton P, de Virgilio M, Fogarty KE, Rizzuto R. Biochem. J. 2001; 355:1. [PubMed: 11256942]

34. Piston DW, Kremers G-J. Trends Biochem. Sci. 2007; 32:407. [PubMed: 17764955]

35. VanEngelenburg SB, Palmer AE. Curr. Opin. Chem. Biol. 2008; 12:60. [PubMed: 18282482]

36. Tse YC, Lam SK, Jiang LW. J. Plant. Biol. 2009; 52:1.

37. Wessels JT, Yamauchi K, Hoffman RM, Wouters FS. Cytometry Part A. 2010; 77A:667.

38. Muller DJ, Dufrene YF. Nature Nanotechnology. 2008; 3:261.

39. Muller DJ, Helenius J, Alsteens D, Dufrene YF. Nat. Chem. Biol. 2009; 5:383. [PubMed: 19448607]

40. Goksu EI, Vanegas JM, Blanchette CD, Lin WC, Longo ML. Biochim. Biophys. Acta. Biomembr. 2009; 1788:254.

41. Franz CM, Puech PH. Cellular and Molecular Bioengineering. 2008; 1:289.

42. Agrawal GK, Bourguignon J, Rolland N, Ephritikhine G, Ferro M, Jaquinod M, Alexiou KG, Chardot T, Chakraborty N, Jolivet P, Doonan JH, Rakwal R. Mass Spectrom. Rev. 2011; 30:772.

43. Gao QB, Jin ZC, Wu C, Sun YL, He J, He X. Curr. Bioinf. 2009; 4:120.

44. Gatto L, Vizcaino JA, Hermjako H, Huber W, Lilley KS. Proteomics. 2010; 10:3957. [PubMed: 21080489]

45. Gauthier DJ, Lazure C. Expert Rev. Proteomics. 2008; 5:603. [PubMed: 18761470]

46. Hossain Z, Nouri MZ, Komatsu S. J. Proteome Res. 2012; 11:37. [PubMed: 22029473]

47. Jung E, Heller M, Sanchez JC, Hochstrasser DF. Electrophoresis. 2000; 21:3369. [PubMed: 11079557]

48. Lee YH, Tan HT, Chung MCM. Proteomics. 2010; 10:3935. [PubMed: 21080488]

49. Lundberg E, Uhlen M. Proteomics. 2010; 10:3984. [PubMed: 20648481]

50. Sorek N, Bloch D, Yalovsky S. Curr. Opin. Plant Biol. 2009; 12:714. [PubMed: 19796984]

51. Yan W, Aebersold R, Raines EW. J. Proteomics. 2009; 72:4. [PubMed: 19110081]

52. Du PF, Li TT, Wang X. Expert Rev. Proteomics. 2011; 8:391. [PubMed: 21679119]

53. Imai K, Nakai K. Proteomics. 2010; 10:3970. [PubMed: 21080490]

54. Altelaar AFM, Heck AJR. Curr. Opin. Chem. Biol. 2012; 16:206. [PubMed: 22226769]

55. Liu J, Litt L, Segal MR, Kelly MJS, Pelton JG, Kim M. Int. J. Mol. Sci. 2011; 12:6469. [PubMed: 22072900]

56. Fahrni CJ. Curr. Opin. Chem. Biol. 2007; 11:121. [PubMed: 17353139]

57. Han X, Gross RW. J. Lipid Res. 2003; 44:1071. [PubMed: 12671038]

58. Horn PJ, Chapman KD. Plant J. 2012; 70:69. [PubMed: 22117762]

59. Hamilton JA, Hillard CJ, Spector AA, Watkins PA. J. Mol. Neurosci. 2007; 33:2. [PubMed: 17901539]

60. Boukh-Viner T, Titorenko VI. Biochim. Biophys. Acta, Mol. Cell Res. 2006; 1763:1688.

61. Huang HY, Frohman MA. Biochim. Biophys. Acta, Mol. Cell Biol. Lipids. 2009; 1791:839.

62. Murphy DJ. Protoplasma. 2012; 249:541. [PubMed: 22002710]

63. Paradies G, Petrosillo G, Paradies V, Ruggiero FM. Free Radical Biol. Med. 2010; 48:1286. [PubMed: 20176101]

64. Bou Khalil M, Hou W, Zhou H, Elisma F, Swayne LA, Blanchard AP, Yao Z, Bennett SAL, Figeys D. Mass Spectrom. Rev. 2010; 29:877. [PubMed: 20931646]

65. Zemski Berry KA, Hankin JA, Barkley RM, Spraggins JM, Caprioli RM, Murphy RC. Chem. Rev. 2011; 111:6491. [PubMed: 21942646]

66. Subramaniam S, Fahy E, Gupta S, Sud M, Byrnes RW, Cotter D, Dinasarapu AR, Maurya MR. Chem. Rev. 2011; 111:6452. [PubMed: 21939287]

67. Balaz S. Chem. Rev. 2009; 109:1793. [PubMed: 19265398]

68. Miyashiro KY, Bell TJ, Sul JY, Eberwine J. Trends Pharmacol. Sci. 2009; 30:203. [PubMed: 19285735]

69. Zheng N, Tsai HN, Zhang XY, Rosania GR. Mol. Pharm. 2011; 8:1619. [PubMed: 21805990]

70. D'Souza GGM, Weissig V. Expert Opin. Drug Delivery. 2009; 6:1135.

71. van Zutphen T, van der Klei IJ. Curr. Opin. Biotechnol. 2011; 22:127. [PubMed: 21106361]

72. Hoppel CL, Tandler B, Fujioka H, Riva A. Int. J. Biochem. Cell Biol. 2009; 41:1949. [PubMed: 19446651]

73. Egea G, Lazaro-Dieguez F, Vilella M. Curr. Opin. Cell Biol. 2006; 18:168. [PubMed: 16488588]

74. Tanida I. Antioxid. Redox Signaling. 2011; 14:2201.

75. Longatti A, Tooze SA. Cell Death Differ. 2009; 16:956. [PubMed: 19373247]

76. Chua CEL, Gan BQ, Tang BL. Cell. Mol. Life Sci. 2011; 68:3349. [PubMed: 21687989]

77. Wong ASL, Cheung ZH, Ip NY. Biochim. Biophys. Acta, Mol. Basis Dis. 2011; 1812:1490.

78. Mizushima N, Yoshimori T, Ohsumi Y. Annual Review of Cell and Developmental Biology, Vol 27. 2011; 27:107.

79. Sibirny AA. Biochemistry-Moscow. 2011; 76:1279. [PubMed: 22150273]

80. Oku M, Sakai Y. FEBS J. 2010; 277:3289. [PubMed: 20629742]

81. Manjithaya R, Nazarko TY, Farre JC, Subramani S. FEBS Lett. 2010; 584:1367. [PubMed: 20083110]

82. Youle RJ, Narendra DP. Nat. Rev. Mol. Cell Biol. 2011; 12:9. [PubMed: 21179058]

83. Tolkovsky AM. Biochim. Biophys. Acta, Mol. Cell Res. 2009; 1793:1508.

84. Navratil M, Mabbott GA, Arriaga EA. Anal. Chem. 2006; 78:4005. [PubMed: 16771538]

85. Storrie B, Madden EA. Methods Enzymol. 1990; 182:203. [PubMed: 2156127]

86. Olson KJ, Ahmadzadeh H, Arriaga EA. Analytical and Bioanalytical Chemistry. 2005; 382:906. [PubMed: 15928950]

87. Pasquali C, Fialka I, Huber LA. J. Chromatogr. B. 1999; 722:89.

88. Murphy RF. Cytometry Part A. 2010; 77A:686.

89. Murphy, RF. Laboratory Methods in Cell Biology. New York: Academic Press; 2012.

90. Satori CP, Kostal V, Arriaga EA. Analytica Chimica Acta. 2012; 753:8. [PubMed: 23107131]

91. Michelsen, U.; von Hagen, J. Guide to Protein Purification. New York: Academic Press; 2009.

92. Harris, H. The Birth of the the Cell. New Haven CT: Yale University Press; 2000.

93. Yang F, Moss LG, Phillips GN. Nat Biotech. 1996; 14:1246.

94. Chaffey N. Ann. Bot. 2010; 106:vi.

95. Ernster L, Schatz G. J. Cell. Biol. 1981; 91:227s. [PubMed: 7033239]

96. Fabene PF, Bentiboglio M. Brain Res. Bull. 1998; 47:195. [PubMed: 9865849]

97. Pringsheim, N.; Pfeffer, W.; Strasburger, E. Jahrbücher für wissenschaftliche Botanik. Berlin: August Hirschwald; 1885.

98. Porter KR, Claude A, Fullam EF. J. Exp. Med. 1945; 81:233. [PubMed: 19871454]

99. Frederick SE, Eldon HN. Science. 1969; 163:1353. [PubMed: 17807816]

100. Claude A. J. Exp. Med. 1946; 84:51.

101. Hogeboom GH, Schneider WC, Pallade GE. Proceedings of the Society for Experimental Biology and Medicine. Society for Experimental Biology and Medicine (New York, N.Y.). 1947; 65

102. Duve CD, Pressman BC, Gianetto R, Wattiaux R, Appelmans F. J. Biochem. 1955; 60:604.

103. Duve CD. Proceedings of the Royal Society of London. Series B. Biological Sciences. 1969; 173:71.

104. Steinman RM, Brodie SE, Cohn ZA. J. Cell. Biol. 1976; 68:665. [PubMed: 1030706]

105. Helenius A, Mellman I, Wall D, Hubbard A. Trends Biochem. Sci. 1983; 8:245.

106. Bohmer, F. Awerzil. Munich: Intelligenzb; 1865.

107. Michaelis L. Arch. Mikrosk. Anat. 1900; 55:558.

108. Lewis WH. Bull. Johns Hopkins Hosp. 1931; 49:17.

109. Rotman B, Papermaster BW. Proc. Natl. Acad. Sci. U.S.A. 1966; 55:134. [PubMed: 5220862]

110. Robbins E, Marcus PI. J. Cell. Biol. 1963; 18:237. [PubMed: 14079487]

111. V Marinetti G. J. Lipid Res. 1962; 3:1.

112. Lewis MR, Lewis WH. The American Journal of Anatomy. 1915; 17:339.

113. Porter KR. J. Exp. Med. 1953; 97:727. [PubMed: 13052830]

114. Dalton AJ, Felix MD. Am. J. Anat. 1954; 94:171. [PubMed: 13148119]

115. Novikoff AB, Beaufay H, Duve Cd. The Journal of Biophysical and Biochemical Cytology. 1956; 2:179. [PubMed: 13357540]

116. Palade GE. J. Histochem. Cytochem. 1953; 1:188. [PubMed: 13069686]

117. Wittekind D. J. R. Microsc. Soc. 1964; 83:83. [PubMed: 14322120]

118. Loken MR, Parks DR, Herzenberg LA. J. Histochem. Cytochem. 1977; 25:899. [PubMed: 330738]

119. Yang HY, Lieska N, Goldman AE, Goldman RD. J. Cell. Biol. 1985; 100:620. [PubMed: 3881459]

120. Schipper HM, Cisse S, Walton PA. Exp. Cell Res. 1993; 207:62. [PubMed: 8391468]

121. Shimomura O, Johnson F, Saiga Y. J. Cell Comp. Physiol. 1962; 59:223. [PubMed: 13911999]

122. (a) Chalfie M, Tu Y, Euskirchen G, Ward WW, Prasher DC. Science. 1994; 11:802. [PubMed: 8303295] (b) Okane DJ, Prasher DC. Mol. Microbiol. 1992; 6:443. [PubMed: 1560772]

123. Picard D, Yamamoto KR. EMBO J. 1987; 6:3333. [PubMed: 3123217]

124. Chiu, W-l; Niwa, Y.; Zeng, W.; Hirano, T.; Kobayashi, H.; Sheen, J. Curr. Biol. 1996; 6:325. [PubMed: 8805250]

125. Boevink P, Santa Cruz S, Hawes C, Harris N, Oparka KJ. The Plant Journal. 1996; 10:935.

126. O'Farrell PZ, Goodman HM, O'Farrell PH. Cell. 1977; 12:1133. [PubMed: 23215]

127. Huber LA. Circul. Res. 2003; 92:962.

128. Scianimanico S, Pasquali C, Lavoie J, Huber LA, Gorvel J-P, Desjardins M. 1997; 18:2566.

129. Taylor RS, Fialka I, Jones SM, Huber LA, Howell KE. 1997; 18:2601.

130. Fialka I, Pasquali C, Lottspeich F, Ahorn H, Huber LA. Electrophoresis. 1997; 18:2582. [PubMed: 9527488]

131. Pasquali C, Fialka I, Huber LA. Electrophoresis. 1997; 18:2581.

132. Sturgill-Koszycki S, Haddix PL, Russell DG. Electrophoresis. 1997; 18:2565.

133. Fiedler K, Kellner R, Simons K. Electrophoresis. 1997; 18:2619.

134. Fenn JB, Mann M, Meng CK, Wong SF, Whitehouse CM. Science. 1989; 246:64. [PubMed: 2675315]

135. Karas M, Hillenkamp F. Anal. Chem. 1988; 60:2299. [PubMed: 3239801]

136. Link AJ, Carmack E, Yates JR Iii. IJMSI. 1997; 160:303.

137. Peltier J-B, Friso G, Kalume DE, Roepstorff P, Nilsson F, Adamska I, van Wijka KJ. The Plant Cell Online. 2000; 12:319.

138. Dreger M. Proc. Natl. Acad. Sci. U.S.A. 2001; 98:11943. [PubMed: 11593002]

139. Taylor SW, Fahy E, Zhang B, Glenn GM, Warnock DE, Wiley S, Murphy AN, Gaucher SP, Capaldi RA, Gibson BW, Ghosh SS. Nat. Biotechnol. 2003; 21:281. [PubMed: 12592411]

140. Oliver SG, Winson MK, Kell DB, Baganz F. Trends Biotechnol. 1998; 16:373. [PubMed: 9744112]

141. Bensley RR, Hoerr NL. The Anatomical Record. 1934; 60:449.

142. Claude A. J. Exp. Med. 1944; 80:19. [PubMed: 19871395]

143. Palade GE, Siekevitz P. The Journal of Biophysical and Biochemical Cytology. 1956; 2:171. [PubMed: 13319380]

144. Rouser G, Galli C, Lieber E, Blank M, Privett O. J. Am. Oil Chem. Soc. 1964; 41:836.

145. Grunwald C. Plant Physiol. 1970; 45:663. [PubMed: 16657369]

146. Fleischer S, Rouser G. J. Am. Oil Chem. Soc. 1965; 42:588. [PubMed: 14328357]

147. McMurray, WC. Form and Function of Phospholipids. Ansell, GB.; H, JN.; Dawson, RMC., editors. Vol. Vol. 3. Amsterdam, Netherlands : Elsevier Scientific Pub Co; 1973.

148. (a) Gross RW. Biochemistry (Mosc). 1984; 23:158.(b) Gross RW. Biochemistry (Mosc). 1985; 24:1662.

149. Kerwin JL, Tuininga AR, Ericsson LH. J. Lipid Res. 1994; 35:1102. [PubMed: 8077849]

150. Han X, Gross RW. Proc. Natl. Acad. Sci. U.S.A. 1994; 91:10635. [PubMed: 7938005]

151. Chiu DT, Lillard SJ, Scheller RH, Zare RN, Rodriguez-Cruz SE, Williams ER, Orwar O, Sandberg M, Lundqvist JA. Science. 1998; 279:1190. [PubMed: 9469805]

152. Rubakhin SS, Garden RW, Fuller RR, Sweedler JV. Nat Biotech. 2000; 18:172.

153. (a) Strack A, Duffy CF, Malvey M, Arriaga EA. Anal. Biochem. 2001; 294:141. [PubMed: 11444809] (b) Duffy CF, Fuller KM, Malvey MW, O'Kennedy R, Arriaga EA. Anal. Chem. 2001; 74:171. [PubMed: 11795787]

154. Chen Y, Arriaga EA. Anal. Chem. 2006; 78:820. [PubMed: 16448056]

155. Chen Y, Walsh RJ, Arriaga EA. Anal. Chem. 2005; 77:2281. [PubMed: 15828758]

156. Xu X, Arriaga EA. Free Radical Biol. Med. 2009; 46:905. [PubMed: 19168125]

157. Alston TA, Mela L, Bright HJ. Proc. Natl. Acad. Sci. U.S.A. 1977; 74:3767. [PubMed: 269430]

158. Barret, AJ.; Heath, MF. Lysosomes: A Laboratory Handbook. Amsterdam: North-Holland Publishing Company; 1977.

159. Leighton F, Poole B, Beaufay H, Baudhuin P, Coffey JW, Fowler S, De Duve C. J. Cell. Biol. 1968; 37:482. [PubMed: 4297786]

160. Marzella L, Ahlberg J, Glaumann H. J. Cell Biol. 1982; 93:144. [PubMed: 7068752]

161. Kopitz J, Kisen GO, Gordon PB, Bohley P, Seglen PO. J. Cell Biol. 1990; 111:941. [PubMed: 2391370]

162. Uedan K, Sugiyama T. Plant Physiol. 1976; 57:906. [PubMed: 16659596]

163. Arkus KAJ, Jez JM. Anal. Biochem. 2006; 353:93. [PubMed: 16643837]

164. Claus V, Jahraus A, Tjelle T, Berg T, Kirschke H, Faulstich H, Griffiths G. J. Biol. Chem. 1998; 273:9842. [PubMed: 9545324]

165. Pool RRJ, Maurey KM, Storrie B. Cell Biol. Int. Rep. 1983; 7:361. [PubMed: 6850866]

166. Sottocasa GL, Kuylenstierna B, Ernster L, Bergstrand A. J. Cell. Biol. 1967; 32:415. [PubMed: 10976232]

167. Nordlie, RC.; Arion, WJ. Methods Enzymol. New York: Academic Press; 1966.

168. Cheetham RD, Morré DJ, Pannek C, Friend DS. J. Cell. Biol. 1971; 49:899. [PubMed: 5092211]

169. Thong B, Piling J, Ainscow E, Beri R, Unitt J. J. Biomol. Screen. 2011; 16:36. [PubMed: 21088147]

170. Pennington RJ. Biochem. J. 1961; 80:649. [PubMed: 13734134]

171. Fischle W. Methods. 2005; 36:362. [PubMed: 16085425]

172. Yates JR, Gilchrist A, Howell KE, Bergeron JJM. Nat. Rev. Mol. Cell Biol. 2005; 6:702. [PubMed: 16231421]

173. Howell KE, Palade GE. J. Cell. Biol. 1982; 92:822. [PubMed: 6282895]

174. Touster O, Aronson NN, Dulaney JT, Hendrickson H. J. Cell. Biol. 1970; 47:604. [PubMed: 5497542]

175. Barbe L, Lundberg E, Oksvold P, Stenius A, Lewin E, Bjorling E, Asplund A, Ponten F, Brismar H, Uhlen M, Andersson-Svahn H. Mol. Cell. Proteomics. 2008; 7:499. [PubMed: 18029348]

176. Rajan SS, Liu HY, Vu TQ. ACS Nano. 2008; 2:1153. [PubMed: 19206333]

177. Kim BYS, Jiang W, Oreopoulos J, Yip CM, Rutka JT, Chan WCW. Nano Lett. 2008; 8:3887. [PubMed: 18816147]

178. Ye F, Wu C, Jin Y, Wang M, Chan Y-H, Yu J, Sun W, Hayden S, Chiu DT. Chem. Commun. (Cambridge, UK.). 2012; 48:1778.

179. Fu GY, Song XC, Yang XF, Peng T, Wang YJ, Zhou GW. Proteomics. 2010; 10:1536. [PubMed: 20127686]

180. Shen J, Zhou Y, Lu T, Peng JY, Lin ZX, Huang L, Pang YH, Yu L, Huang YY. Lab Chip. 2012; 12:317. [PubMed: 22124660]

181. Stadler C, Hjelmare M, Neumann B, Jonasson K, Pepperkok R, Uhlen M, Lundberg E. J. Proteomics. 2012; 75:2236. [PubMed: 22361696]

182. Lalor R, Baillie-Johnson H, Redshaw C, Matthews SE, Mueller A. J. Am. Chem. Soc. 2008; 130:2892. [PubMed: 18278915]

183. Li K, Pu K-Y, Cai L, Liu B. Chem. Mater. 2011; 23:2113.

184. Lee H, Akers W, Bhushan K, Bloch S, Sudlow G, Tang R, Achilefu S. Bioconjugate Chem. 2011; 22:777.

185. (a) Shindo Y, Fujii T, Komatsu H, Citterio D, Hotta K, Suzuki K, Oka K. PLoS ONE. 2011; 6:1. (b) Fakih S, Podinovskaia M, Kong X, Collins HL, Schaible UE, Hider RC. J. Med. Chem. 2008; 51:4539. [PubMed: 18624421]

186. Duvvuri M, Gong Y, Chatterji D, Krise JP. J. Biol. Chem. 2004; 279:32367. [PubMed: 15181006]

187. Halliwell, B.; Gutteridge, JMC. Methods Enzymol. New York: Academic Press; 1990.

188. Shaner NC, Campbell RE, Steinbach PA, Giepmans BN, Palmer AE, Tsien RY. Nat. Biotechnol. 2004; 22:1567. [PubMed: 15558047]

189. (a) Wiedenmann J, Schenk A, Rocker C, Girod A, Spindler KD, Nienhaus GU. Proc. Natl. Acad. Sci. U.S.A. 2002; 99:11646. [PubMed: 12185250] (b) Wiedenmann J, Vallone B, Renzi F, Nienhaus K, Ivanchenko S, Rocker C, Nienhaus GU. J. Biomed. Opt. 2005; 10:14003. [PubMed: 15847584]

190. Lissandron V, Podini P, Pizzo P, Pozzan T. Proc. Natl. Acad. Sci. U.S.A. 2010; 107:9198. [PubMed: 20439740]

191. Kimura S, Noda T, Yoshimori T. Autophagy. 2007; 3:452. [PubMed: 17534139]

192. Hanson GT, Aggeler R, Oglesbee D, Cannon M, Capaldi RA, Tsien RY, Remington SJ. J. Biol. Chem. 2004; 279:13044. [PubMed: 14722062]

193. Albrecht SC, Barata AG, Grosshans J, Teleman AA, Dick TP. Cell Metabolism. 2011; 14:819. [PubMed: 22100409]

194. Kanno A, Ozawa T, Umezawa Y. Anal. Chem. 2006; 78:8076. [PubMed: 17134142]

195. Fricker M, Runions J, Moore I. Annu. Rev. Plant Biol; Annual Reviews: Palo Alto. 2006

196. Fischer RS, Wu YC, Kanchanawong P, Shroff H, Waterman CM. Trends Cell Biol. 2011; 21:682. [PubMed: 22047760]

197. (a) Hell SW. Science. 2007; 316:1153. [PubMed: 17525330] (b) Huang B, Jones SA, Brandenburg B, Zhuang XW. Nat. Methods. 2008; 5:1047. [PubMed: 19029906] (c) Schermelleh

L, Heintzmann R, Leonhardt H. J. Cell Biol. 2010; 190:165. [PubMed: 20643879] (d) Lippincott-Schwartz J, Manley S. Nat. Methods. 2009; 6:21. [PubMed: 19116610]

198. Willig KI, Rizzoli SO, Westphal V, Jahn R, Hell SW. Nature. 2006; 440:935. [PubMed: 16612384]

199. Betzig E, Patterson GH, Sougrat R, Lindwasser OW, Olenych S, Bonifacino JS, Davidson MW, Lippincott-Schwartz J, Hess HF. Science. 2006; 313:1642. [PubMed: 16902090]

200. Hess ST, Girirajan TPK, Mason MD. Biophys. J. 2006; 91:4258. [PubMed: 16980368]

201. Rust MJ, Bates M, Zhuang XW. Nat. Methods. 2006; 3:793. [PubMed: 16896339]

202. Donnert G, Keller J, Medda R, Andrei MA, Rizzoli SO, Lurmann R, Jahn R, Eggeling C, Hell SW. Proc. Natl. Acad. Sci. U.S.A. 2006; 103:11440. [PubMed: 16864773]

203. Hein B, Willig KI, Hell SW. Proc. Natl. Acad. Sci. U.S.A. 2008; 105:14271. [PubMed: 18796604]

204. Shtengel G, Galbraith JA, Galbraith CG, Lippincott-Schwartz J, Gillette JM, Manley S, Sougrat R, Waterman CM, Kanchanawong P, Davidson MW, Fetter RD, Hess HF. Proc. Natl. Acad. Sci. U.S.A. 2009; 106:3125. [PubMed: 19202073]

205. Singh H, Lu R, Rodriguez PFG, Wu Y, Bopassa JC, Stefani E, Toro L. Mitochondrion. 2012; 12:230. [PubMed: 21982778]

206. Wurm CA, Neumann D, Lauterbach MA, Harke B, Egner A, Hell SW, Jakobs S. Proc. Natl. Acad. Sci. U.S.A. 2011; 108:13546. [PubMed: 21799113]

207. Schmidt R, Wurm CA, Punge A, Egner A, Jakobs S, Hell SW. Nano Lett. 2009; 9:2508. [PubMed: 19459703]

208. He J, Scott JL, Heroux A, Roy S, Lenoir M, Overduin M, Stahelin RV, Kutateladze TG. J. Biol. Chem. 2011; 286:18650. [PubMed: 21454700]

209. Brown TA, Tkachuk AN, Shtengel G, Kopek BG, Bogenhagen DF, Hess HF, Clayton DA. Mol. Cell. Biol. 2011; 31:4994. [PubMed: 22006021]

210. Appelhans T, Richter CP, Wilkens V, Hess ST, Piehler J, Busch KB. Nano Lett. 2012; 12:610. [PubMed: 22201267]

211. Vaziri A, Tang JY, Shroff H, Shank CV. Proc. Natl. Acad. Sci. U.S.A. 2008; 105:20221. [PubMed: 19088193]

212. Brown TA, Fetter RD, Tkachuk AN, Clayton DA. Methods. 2010; 51:458. [PubMed: 20060907]

213. Watanabe S, Punge A, Hollopeter G, Willig KI, Hobson RJ, Davis MW, Hell SW, Jorgensen EM. Nat. Methods. 2011; 8:80. [PubMed: 21102453]

214. Cseresnyes Z, Schwarz U, Green CM. BMC Cell Biol. 2009; 10:12. [PubMed: 19228417]

215. Leung BO, Chou KC. Appl. Spectrosc. 2011; 65:967. [PubMed: 21929850]

216. (a) Lippincott-Schwartz J, Patterson GH. Trends Cell Biol. 2009; 19:555. [PubMed: 19836954] (b) McKinney SA, Murphy CS, Hazelwood KL, Davidson MW, Looger LL. Nat. Methods. 2009; 6:131. [PubMed: 19169260]

217. Fernandez-Suarez M, Ting AY. Nat. Rev. Mol. Cell Biol. 2008; 9:929. [PubMed: 19002208]

218. Kukat C, Wurm CA, Spahr H, Falkenberg M, Larsson NG, Jakobs S. Proc. Natl. Acad. Sci. U.S.A. 2011; 108:13534. [PubMed: 21808029]

219. Huang B, Wang WQ, Bates M, Zhuang XW. Science. 2008; 319:810. [PubMed: 18174397]

220. Jones SA, Shim S-H, He J, Zhuang X. Nat. Methods. 2011; 8:499. [PubMed: 21552254]

221. Lakadamyali M, Babcock H, Bates M, Zhuang XW, Lichtman J. PLoS ONE. 2012; 7:1.

222. Barcena M, Koster AJ. Semin. Cell Dev. Biol. 2009; 20:920. [PubMed: 19664718]

223. Donohoe BS, Mogelsvang S, Staehelin LA. Methods. 2006; 39:154. [PubMed: 16854591]

224. Koning RI, Koster AJ. Ann. Anat. 2009; 191:427. [PubMed: 19559584]

225. Jonic S, Sorzano COS, Boisset N. J. Microsc. 2008; 232:562. [PubMed: 19094041]

226. Perkins GA, Tjong J, Brown JM, Poquiz PH, Scott RT, Kolson DR, Ellisman MH, Spirou GA. J. Neurosci. 2010; 30:1015. [PubMed: 20089910]

227. Hayashi T, Martone ME, Yu ZY, Thor A, Doi M, Holst MJ, Ellisman MH, Hoshijima M. J. Cell Sci. 2009; 122:1005. [PubMed: 19295127]

228. Grandfield K, Engqvist H. Adv. Mater. Sci. Eng. 2012; 2012:1.

229. Heymann JAW, Shi D, Kim S, Bliss D, Milne JLS, Subramaniam S. J. Struct. Biol. 2009; 166:1. [PubMed: 19116171]

230. McGeoch JEM. J. Microsc. (Oxford, UK.). 2007; 227:172.

231. Murphy GE, Lowekamp BC, Zerfas PM, Chandler RJ, Narasimha R, Venditti CP, Subramaniam S. J. Struct. Biol. 2010; 171:125. [PubMed: 20399866]

232. Bassim ND, De Gregorio BT, Kilcoyne ALD, Scott K, Chou T, Wirick S, Cody G, Stroud RM. J. Microsc. 2012; 245:288.

233. Riethmüller C, Schäffer TE, Kienberger F, Stracke W, Oberleithner H. Ultmi. 2007; 107:895.

234. Silberberg YR, Pelling AE, Yakubov GE, Crum WR, Hawkes DJ, Horton MA. J. Mol. Recognit. 2008; 21:30. [PubMed: 18247356]

235. Lee GJ, Chae SJ, Jeong JH, Lee SR, Ha SJ, Pak YK, Kim W, Park HK. Micron. 2011; 42:299. [PubMed: 21050769]

236. Awizio AK, Onofri F, Benfenati F, Bonaccurso E. Biophys. J. 2007; 93:1051. [PubMed: 17483172]

237. Guo SL, Hong L, Akhremitchev BB, Simon JD. Photochem. Photobiol. 2008; 84:671. [PubMed: 18399921]

238. Matsko NB. Ultmi. 2007; 107:95.

239. Graham HK, Hodson NW, Hoyland JA, Millward-Sadler SJ, Garrod D, Scothern A, Griffiths CEM, Watson REB, Cox TR, Erler JT, Trafford AW, Sherratt MJ. Matrix Biol. 2010; 29:254. [PubMed: 20144712]

240. Yost RA, Enke CG. J. Am. Chem. Soc. 1978; 100:2274.

241. Makarov A. Anal. Chem. 2000; 72:1156. [PubMed: 10740853]

242. Andrews GL, Simons BL, Young JB, Hawkridge AM, Muddiman DC. Anal. Chem. 2011; 83:5442. [PubMed: 21619048]

243. Zhu H, Bilgin M, Snyder M. Annu. Rev. Biochem. 2003; 72:783. [PubMed: 14527327]

244. Perkins DN, Pappin DJC, Creasy DM, Cottrell JS. Electrophoresis. 1999; 20:3551. [PubMed: 10612281]

245. Eng JK, McCormack AL, Yates JR. J. Am. Soc. Mass Spectrom. 1994; 5:976.

246. (a) Fenyo D, Beavis RC. Anal. Chem. 2003; 75:768. [PubMed: 12622365] (b) Craig R, Beavis RC. Bioinformatics. 2004; 20:1466. [PubMed: 14976030]

247. Geer LY, Markey SP, Kowalak JA, Wagner L, Xu M, Maynard DM, Yang XY, Shi WY, Bryant SH. J. Proteome Res. 2004; 3:958. [PubMed: 15473683]

248. Shilov IV, Seymour SL, Patel AA, Loboda A, Tang WH, Keating SP, Hunter CL, Nuwaysir LM, Schaeffer DA. Mol. Cell. Proteomics. 2007; 6:1638. [PubMed: 17533153]

249. Kersey PJ, Duarte J, Williams A, Karavidopoulou Y, Birney E, Apweiler R. Proteomics. 2004; 4:1985. [PubMed: 15221759]

250. Apweiler R, Bairoch A, Wu CH, Barker WC, Boeckmann B, Ferro S, Gasteiger E, Huang HZ, Lopez R, Magrane M, Martin MJ, Natale DA, O'Donovan C, Redaschi N, Yeh LSL. Nucleic Acids Res. 2004; 32:D115. [PubMed: 14681372]

251. Searle BC. Proteomics. 2010; 10:1265. [PubMed: 20077414]

252. Gasteiger E, Gattiker A, Hoogland C, Ivanyi I, Appel RD, Bairoch A. Nucleic Acids Res. 2003; 31:3784. [PubMed: 12824418]

253. Cox J, Matic I, Hilger M, Nagaraj N, Selbach M, Olsen JV, Mann M. Nat. Protoc. 2009; 4:698. [PubMed: 19373234]

254. Cox J, Neuhauser N, Michalski A, Scheltema RA, Olsen JV, Mann M. J. Proteome Res. 2011; 10:1794. [PubMed: 21254760]

255. (a) Hardman M, Makarov AA. Anal. Chem. 2003; 75:1699. [PubMed: 12705605] (b) Hu QZ, Noll RJ, Li HY, Makarov A, Hardman M, Cooks RG. J. Mass Spectrom. 2005; 40:430. [PubMed: 15838939]

256. Park SK, Venable JD, Xu T, Yates JR. Nat. Methods. 2008; 5:319. [PubMed: 18345006]

257. MacCoss MJ, Wu CC, Liu HB, Sadygov R, Yates JR. Anal. Chem. 2003; 75:6912. [PubMed: 14670053]

258. Dunham WH, Larsen B, Tate S, Badillo BG, Goudreault M, Tehami Y, Kislinger T, Gingras AC. Proteomics. 2011; 11:2603. [PubMed: 21630450]

259. Bartz R, Li WH, Venables B, Zehmer JK, Roth MR, Welti R, Anderson RGW, Liu PS, Chapman KD. J. Lipid Res. 2007; 48:837. [PubMed: 17210984]

260. Ethier M, Hou WM, Duewel HS, Figeys D. J. Proteome Res. 2006; 5:2754. [PubMed: 17022646]

261. Zhou H, Wang FJ, Wang YW, Ning ZB, Hou WM, Wright TG, Sundaram M, Zhong SM, Yao ZM, Figeys D. Mol. Cell. Proteomics. 2011; 10:11.

262. Sprenger J, Fink JL, Karunaratne S, Hanson K, Hamilton NA, Teasdale RD. Nucleic Acids Res. 2008; 36:D230. [PubMed: 17986452]

263. Chou K-C, Wu Z-C, Xiao X. PLoS ONE. 2011; 6:e18258. [PubMed: 21483473]

264. Chou K-C, Shen H-B. PLoS ONE. 2010; 5

265. Boisvert F-M, Ahmad Y, Gierlinski M, Charriere F, Lamont D, Scott M, Barton G, Lamond AI. Mol. Cell. Proteomics. 2012; 11:1.

266. Scott MS, Boisvert F-M, Lamond AI, Barton GJ. BMC Genomics. 2011; 12:1.

267. Zheng YZ, Berg KB, Foster LJ. J. Lipid Res. 2009; 50:988. [PubMed: 19136664]

268. Inder KL, Zheng YZ, Davis MJ, Moon H, Loo D, Nguyen H, Clements JA, Parton RG, Foster LJ, Hill MM. Mol. Cell. Proteomics. 2011; 11:012245/1. [PubMed: 22030351]

269. Timmons MD, Bradley MA, Lovell MA, Lynn BC. J. Neurosci. Methods. 2011; 197:279. [PubMed: 21392528]

270. Lan, W.; Horn, MJ.; Urano, F.; Kopoyan, A.; Tam, SW. Sample Preparation in Biological Mass Spectrometry. New York: Springer Science+Business Media; 2011.

271. Gauthier DJ, Sobota JA, Ferraro F, Mains RE, Lazure C. Proteomics. 2008; 8:3848. [PubMed: 18704904]

272. Kang D, Oh S, Reschiglian P, Moon MH. Analyst. 2008; 133:505. [PubMed: 18365121]

273. (a) Islinger M, Li KW, Loos M, Liebler S, Angermueller S, Eckerskorn C, Weber G, Abdolzade A, Voelkl A. J. Proteome Res. 2010; 9:113. [PubMed: 19739631] (b) Islinger, M.; Kirsch, J.; Angermueller, S.; Rotaru, R.; Abdolzade-Bavil, A.; Weber, G. Neuroproteomics. New York: Humana Press; 2011. (c) Zischka H, Braun RJ, Marantidis EP, Buringer D, Bornhovd C, Hauck SM, Demmer O, Gloeckner CJ, Reichert AS, Madeo F, Ueffing M. Mol. Cell. Proteomics. 2006; 5:2185. [PubMed: 16917120]

274. Shachar T, Lo Bianco C, Recchia A, Wiessner C, Raas-Rothschild A, Futerman AH. Mov. Disord. 2011; 26:1593. [PubMed: 21618611]

275. Della Valle MC, Sleat DE, Zheng H, Moore DF, Jadot M, Lobel P. Mol. Cell. Proteomics. 2011; 10:1.

276. Gasingirwa MC, Thirion J, Costa C, Flamion B, Lobel P, Jadot M. Anal. Biochem. 2008; 374:31. [PubMed: 18082124]

277. Tweedie-Cullen RY, Reck JM, Mansuy IM. J. Proteome Res. 2009; 8:4966. [PubMed: 19737024]

278. Luo Y, Blex C, Baessler O, Glinski M, Dreger M, Sefkow M, Koester H. Mol. Cell. Proteomics. 2009; 8:2843. [PubMed: 19741253]

279. Sakai K, Hamanaka R, Yuki H, Watanabe M. Proteomics. 2009; 9:3036. [PubMed: 19526556]

280. Adam RM, Yang W, Di Vizio D, Mukhopadhyay NK, Steen H. BMC Cell Biol. 2008; 9:1. [PubMed: 18186933]

281. Png E, Lan W, Lazaroo M, Chen S, Zhou L, Tong L. Anal. Bioanal. Chem. 2011; 400:767. [PubMed: 21380751]

282. Hu Z-Z, Valencia JC, Huang H, Chi A, Shabanowitz J, Hearing VJ, Appella E, Wu C. Int. J. Mass spectrom. 2007; 259:147. [PubMed: 17375895]

283. Nowosadzka E, Szymonik-Lesiuk S, Kurzepa J. Folia Biol. (Praha). 2009; 55:7. [PubMed: 19445840]

284. van Bentem SD, Anrather D, Dohnal I, Roitinger E, Csaszar E, Joore J, Buijnink J, Carreri A, Forzani C, Lorkovic ZJ, Barta A, Lecourieux D, Verhounig A, Jonak C, Hirt H. J. Proteome Res. 2008; 7:2458. [PubMed: 18433157]

285. Gygi SP, Rist B, Gerber SA, Turecek F, Gelb MH, Aebersold R. Nat. Biotechnol. 1999; 17:994. [PubMed: 10504701]

286. Ross PL, Huang YLN, Marchese JN, Williamson B, Parker K, Hattan S, Khainovski N, Pillai S, Dey S, Daniels S, Purkayastha S, Juhasz P, Martin S, Bartlet-Jones M, He F, Jacobson A, Pappin DJ. Mol. Cell. Proteomics. 2004; 3:1154. [PubMed: 15385600]

287. Thompson A, Schafer J, Kuhn K, Kienle S, Schwarz J, Schmidt G, Neumann T, Hamon C. Anal. Chem. 2003; 75:1895. [PubMed: 12713048]

288. Dephoure N, Gygi SP. Sci. Signaling. 2012; 5:8.

289. Ong SE, Blagoev B, Kratchmarova I, Kristensen DB, Steen H, Pandey A, Mann M. Mol. Cell. Proteomics. 2002; 1:376. [PubMed: 12118079]

290. Wu CC, MacCoss MJ, Howell KE, Matthews DE, Yates JR. Anal. Chem. 2004; 76:4951. [PubMed: 15373428]

291. McClatchy DB, Liao L, Lee JH, Park SK, Yates JR. J. Proteome Res. 2012; 11:2467. [PubMed: 22397461]

292. (a) Andersen JS, Wilkinson CJ, Mayor T, Mortensen P, Nigg EA, Mann M. Nature. 2003; 426:570. [PubMed: 14654843] (b) Foster LJ, de Hoog CL, Zhang YL, Zhang Y, Xie XH, Mootha VK, Mann M. Cell. 2006; 125:187. [PubMed: 16615899]

293. Harner M, Korner C, Walther D, Mokranjac D, Kaesmacher J, Welsch U, Griffith J, Mann M, Reggiori F, Neupert W. EMBO J. 2011; 30:4356. [PubMed: 22009199]

294. (a) Lietzen N, Ohman T, Rintahaka J, Julkunen I, Aittokallio T, Matikainen S, Nyman TA. PLoS Pathog. 2011; 7:e1001340. [PubMed: 21589892] (b) Zhang HM, Zhao CQ, Li X, Zhu Y, Gan CS, Wang Y, Ravasi T, Qian PY, Wong SC, Sze SK. Proteomics. 2010; 10:2780. [PubMed: 20486119] (c) Skiba M, Glowinski F, Koczan D, Mettenleiter TC, Karger A. Vet. Microbiol. 2010; 143:14. [PubMed: 20233642] (d) Salsman J, Jagannathan M, Paladino P, Chan P-K, Dellaire G, Raught B, Frappier L. J. Virol. 2012; 86:806. [PubMed: 22072767]

295. Emmott E, Rodgers MA, Macdonald A, McCrory S, Ajuh P, Hiscox JA. Mol. Cell. Proteomics. 2010; 9:1920. [PubMed: 20467043]

296. (a) Dunkley TPJ, Watson R, Griffin JL, Dupree P, Lilley KS. Mol. Cell. Proteomics. 2004; 3:1128. [PubMed: 15295017] (b) Tan DJL, Dvinge H, Christoforou A, Bertone P, Arias AM, Lilley KS. J. Proteome Res. 2009; 8:2667. [PubMed: 19317464]

297. (a) Boisvert F-M, Lam YW, Lamont D, Lamond AI. Mol. Cell. Proteomics. 2010; 9:457. [PubMed: 20026476] (b) Boisvert F-M, Lamond AI. Proteomics. 2010; 10:4087. [PubMed: 21080495]

298. Neilson KA, Ali NA, Muralidharan S, Mirzaei M, Mariani M, Assadourian G, Lee A, van Sluyter SC, Haynes PA. Proteomics. 2011; 11:535. [PubMed: 21243637]

299. Song Y, Jiang Y, Ying W, Gong Y, Yan Y, Yang D, Ma J, Xue X, Zhong F, Wu S, Hao Y, Sun A, Li T, Sun W, Wei H, Zhu Y, Qian X, He F. J. Proteome Res. 2010; 9:1195. [PubMed: 20073521]

300. Eisen MB, Spellman PT, Brown PO, Botstein D. Proc. Natl. Acad. Sci. U.S.A. 1998; 95:14863. [PubMed: 9843981]

301. Tudisca V, Recouvreux V, Moreno S, Boy-Marcotte E, Jacquet M, Portela P. Eur. J. Cell Biol. 2010; 89:339. [PubMed: 19804918]

302. Choi YS, Jeong JH, Min HK, Jung HJ, Hwang D, Lee SW, Pak YK. Mol. BioSyst. 2011; 7:1523. [PubMed: 21359316]

303. (a) Yamada K, Norikoshi R, Suzuki K, Imanishi H, Ichimura K. Planta. 2009; 230:1115. [PubMed: 20183924] (b) Marchand I, Tarnopolsky M, Adamo KB, Bourgeois JM, Chorneyko K, Graham TE. J. Physiol. (Oxford, UK.). 2007; 580:617.

304. Dolle C, Niere M, Lohndal E, Ziegler M. Cell. Mol. Life Sci. 2010; 67:433. [PubMed: 19902144]

305. D'Souza VM, Foraker AB, Free RB, Ray A, Shapiro PS, Swaan PW. Biochemistry (Mosc). 2006; 45:6095.

306. Krueger S, Giavalisco P, Krall L, Steinhauser MC, Bussis D, Usadel B, Flugge UI, Fernie AR, Willmitzer L, Steinhauser D. PLoS ONE. 2011; 6:1.

307. Broecker S, Herre S, Wust B, Zweigenbaum J, Pragst F. Anal. Bioanal. Chem. 2011; 400:101. [PubMed: 21127842]

308. Brown M, Dunn WB, Dobson P, Patel Y, Winder CL, Francis-McIntyre S, Begley P, Carroll K, Broadhurst D, Tseng A, Swainston N, Spasic I, Goodacre R, Kell DB. Analyst. 2009; 134:1322. [PubMed: 19562197]

309. Kanehisa M, Goto S, Sato Y, Furumichi M, Tanabe M. Nucleic Acids Res. 2011; 40:D109. [PubMed: 22080510]

310. Kind T, Wohlgemuth G, Lee DY, Lu Y, Palazoglu M, Shahbaz S, Fiehn O. Anal. Chem. 2009; 81:10038. [PubMed: 19928838]

311. Kopka J, Schauer N, Krueger S, Birkemeyer C, Usadel B, Bergmuller E, Dormann P, Weckwerth W, Gibon Y, Stitt M, Willmitzer L, Fernie AR, Steinhauser D. Bioinformatics. 2004; 21:1635. [PubMed: 15613389]

312. Oikawa A, Nakamura Y, Ogura T, Kimura A, Suzuki H, Sakurai N, Shinbo Y, Shibata D, Kanaya S, Ohta D. Plant Physiol. 2006; 142:398. [PubMed: 16905671]

313. Skogerson K, Wohlgemuth G, Barupal DK, Fiehn O. BMC Bioinformatics. 2011; 12:1. [PubMed: 21199577]

314. Jewison T, Knox C, Neveu V, Djoumbou Y, Guo AC, Lee J, Liu P, Mandal R, Krishnamurthy R, Sinelnikov I, Wilson M, Wishart DS. Nucleic Acids Res. 2012; 40:D815. [PubMed: 22064855]

315. Udayakumar M, Prem Chandar D, Arun N, Mathangi J, Hemavathi K, Seenivasagam R. Med. Chem. Res. 2012; 21:47.

316. Degtyarenko K, de Matos P, Ennis M, Hastings J, Zbinden M, McNaught A, Alcantara R, Darsow M, Guedj M, Ashburner M. Nucleic Acids Res. 2007; 36:D344. [PubMed: 17932057]

317. Wishart DS, Knox C, Guo AC, Eisner R, Young N, Gautam B, Hau DD, Psychogios N, Dong E, Bouatra S, Mandal R, Sinelnikov I, Xia J, Jia L, Cruz JA, Lim E, Sobsey CA, Shrivastava S, Huang P, Liu P, Fang L, Peng J, Fradette R, Cheng D, Tzur D, Clements M, Lewis A, De Souza A, Zuniga A, Dawe M, Xiong Y, Clive D, Greiner R, Nazyrova A, Shaykhutdinov R, Li L, Vogel HJ, Forsythe I. Nucleic Acids Res. 2009; 37:D603. [PubMed: 18953024]

318. Wagner C, Sefkow M, Kopka J. Phytochemistry. 2003; 62:887. [PubMed: 12590116]

319. Smith CA, Maille GO, Want EJ, Qin C, Trauger SA, Brandon TR, Custodio DE, Abagyan R, Siuzdak G. Ther. Drug Monit. 2005; 27:747. [PubMed: 16404815]

320. Horai H, Arita M, Kanaya S, Nihei Y, Ikeda T, Suwa K, Ojima Y, Tanaka K, Tanaka S, Aoshima K, Oda Y, Kakazu Y, Kusano M, Tohge T, Matsuda F, Sawada Y, Hirai MY, Nakanishi H, Ikeda K, Akimoto N, Maoka T, Takahashi H, Ara T, Sakurai N, Suzuki H, Shibata D, Neumann S, Iida T, Funatsu K, Matsuura F, Soga T, Taguchi R, Saito K, Nishioka T. J. Mass Spectrom. 2010; 45:703. [PubMed: 20623627]

321. Babu MM, Priya ML, Selvan AT, Madera M, Gough J, Aravind L, Sankaran K. J. Bacteriol. 2006; 188:2761. [PubMed: 16585737]

322. Sud M, Fahy E, Cotter D, Brown A, Dennis EA, Glass CK, Merrill AH, Murphy RC, Raetz CRH, Russell DW, Subramaniam S. Nucleic Acids Res. 2007; 35:D527. [PubMed: 17098933]

323. Wishart DS. Nucleic Acids Res. 2006; 34:D668. [PubMed: 16381955]

324. Keerberg O, Ivanova H, Keerberg H, Parnik T, Talts P, Gardestrom P. BioSyst. 2011; 103:291.

325. Eder AR, Arriaga EA. Chem. Res. Toxicol. 2006; 19:1151. [PubMed: 16978019]

326. (a) Raddatz D, Ramadori G. Z. Gastroenterol. 2007; 45:51. [PubMed: 17236121] (b) Hartil K, Charron MJ. J. Mol. Cell. Cardiol. 2005; 39:581. [PubMed: 16140322] (c) Schugar RC, Crawford PA. Curr. Opin. Clin. Nutr. Metab. Care. 2012; 15:374. [PubMed: 22617564] (d) Potenza M, Via MA, Yanagisawa RT. Endocrine Practice. 2009; 15:254. [PubMed: 19364696]

327. Gaudreault N, Scriven DRL, Laher I, Moore EDW. Microvasc. Res. 2008; 75:73. [PubMed: 17531273]

328. Farre EM, Fernie AR, Willmitzer L. Metabolomics. 2008; 4:161. [PubMed: 19816536]

329. Benkeblia N, Shinano T, Osaki M. Metabolomics. 2007; 3:297.

330. Bijnsdorp IV, Azijli K, Jansen EE, Wamelink MM, Jakobs C, Struys EA, Fukushima M, Kruyt FAE, Peters GJ. Biochem. Pharmacol. 2010; 80:786. [PubMed: 20488166]

331. Oikawa A, Matsuda F, Kikuyama M, Mimura T, Saito K. Plant Physiol. 2011; 157:544. [PubMed: 21846815]

332. Koppers AJ, De Iuliis GN, Finnie JM, McLaughlin EA, Aitken RJ. J. Clin. Endocrinol. Metab. 2008; 93:3199. [PubMed: 18492763]

333. Li Q, Sato EF, Kira Y, Nishikawa M, Utsumi K, Inoue M. Free Radical Biol. Med. 2006; 40:173. [PubMed: 16337891]

334. Schonfeld P, Schluter T, Fischer KD, Reiser G. J. Neurochem. 2011; 118:69. [PubMed: 21517851]

335. Diaz-Vivancos P, Clemente-Moreno MJ, Rubio M, Olmos E, Garcia JA, Martinez-Gomez P, Hernandez JA. J. Exp. Bot. 2008; 59:2147. [PubMed: 18535298]

336. Zechmann B, Liou LC, Koffler BE, Horvat L, Tomasic A, Fulgosi H, Zhang ZJ. FEMS Yeast Res. 2011; 11:631. [PubMed: 22093747]

337. Liang LP, Patel M. Free Radical Biol. Med. 2006; 40:316. [PubMed: 16413413]

338. Meany DL, Poe BG, Navratil M, Moraes CT, Arriaga EA. Free Radical Biol. Med. 2006; 41:950. [PubMed: 16934678]

339. Xu X, Chen CN, Arriaga EA, Thompson LV. J. Appl. Physiol. 2010; 109:1133. [PubMed: 20689097]

340. Smith AC, Robinson AJ. BMC Systems Biology. 2011; 5:1. [PubMed: 21194489]

341. Fong-ngern K, Chiangjong W, Thongboonkerd V. Anal. Biochem. 2009; 395:25. [PubMed: 19679094]

342. Guha S, Rajani M, Padh H. Indian J. Biochem. Biophys. 2007; 44:443. [PubMed: 18320843]

343. Andreyev AY, Fahy E, Guan ZQ, Kelly S, Li XA, McDonald JG, Milne S, Myers D, Park H, Ryan A, Thompson BM, Wang E, Zhao YH, Brown HA, Merrill AH, Raetz CRH, Russell DW, Subramaniam S, Dennis EA. J. Lipid Res. 2010; 51:2785. [PubMed: 20574076]

344. Sujkovic E, Mileusnic R, Fry JP. J. Neurochem. 2009; 109:348. [PubMed: 19200338]

345. Konig S, Ischebeck T, Lerche J, Stenzel I, Heilmann I. Biochem. J. 2008; 415:387. [PubMed: 18721128]

346. Mustacich DJ, Leonard SW, Patel NK, Traber MG. Free Radical Biol. Med. 2010; 48:73. [PubMed: 19819327]

347. Fokina VM, Zharikova OL, Hankins GDV, Ahmed MS, Nanovskaya TN. Reprod. Sci. 2012; 19:290. [PubMed: 22138546]

348. Fernandes D, Bebianno MJ, Porte C. Aquat. Toxicol. 2007; 85:258. [PubMed: 17977610]

349. Jao CY, Roth M, Welti R, Salic A. Proc. Natl. Acad. Sci. U.S.A. 2009; 106:15332. [PubMed: 19706413]

350. Borradaile NM, Han X, Harp JD, Gale SE, Ory DS, Schaffer JE. J. Lipid Res. 2006; 47:2726. [PubMed: 16960261]

351. (a) Simons K, Vanmeer G. Biochemistry (Mosc). 1988; 27:6197.(b) Vanmeer G. Annu. Rev. Cell Biol. 1989; 5:247. [PubMed: 2688705] (c) Vanmeer G, Simons K. J. Cell. Biochem. 1988; 36:51. [PubMed: 3277985] (d) Zinser E, Daum G. Yeast. 1995; 11:493. [PubMed: 7645343]

352. Klemm RW, Ejsing CS, Surma MA, Kaiser HJ, Gerl MJ, Sampaio JL, de Robillard Q, Ferguson C, Proszynski TJ, Shevchenko A, Simons K. J. Cell Biol. 2009; 185:601. [PubMed: 19433450]

353. Urano Y, Watanabe H, Murphy SR, Shibuya Y, Geng Y, Peden AA, Chang CCY, Chang TY. Proc. Natl. Acad. Sci. U.S.A. 2008; 105:16513. [PubMed: 18946045]

354. Horn PJ, Ledbetter NR, James CN, Hoffman WD, Case CR, Verbeck GF, Chapman KD. J. Biol. Chem. 2010; 286:3298. [PubMed: 21118810]

355. Accioly MT, Pacheco P, Maya-Monteiro CM, Carrossini N, Robbs BK, Oliveira SS, Kaufmann C, Morgado-Diaz JA, Bozza PT, Viola JPB. Cancer Res. 2008; 68:1732. [PubMed: 18339853]

356. Tyurina YY, Tungekar MA, Jung MY, Tyurin VA, Greenberger JS, Stoyanovsky DA, Kagan VE. FEBS Lett. 2012; 586:235. [PubMed: 22210054]

357. Andrieu-Abadie N, Levade T. Biochim. Biophys. Acta, Mol. Cell Biol. Lipids. 2002; 1585:126.

358. Ardail D, Maalouf M, Boivin A, Chapet O, Bodennec J, Rousson R, Rodriguez-Lafrasse C. Int. J. Radiat. Oncol. Biol. Phys. 2009; 73:1211. [PubMed: 19251092]

359. Wriessnegger T, Leitner E, Belegratis MR, Ingolic E, Daum G. Biochim. Biophys. Acta, Mol. Cell Biol. Lipids. 2009; 1791:166.

360. (a) Kiebish MA, Han X, Cheng H, Chuang JH, Seyfried TN. Lipids. 2008; 43:951. [PubMed: 18560917] (b) Kiebish MA, Han X, Cheng H, Lunceford A, Clarke CF, Moon H, Chuang JH, Seyfried TN. J. Neurochem. 2008; 106:299. [PubMed: 18373617] (c) Kiebish MA, Han X, Cheng H, Seyfried TN. Asn Neuro. 2009; 1:125.

361. Angelini R, Vitale R, Patil VA, Cocco T, Ludwig B, Greenberg ML, Corcelli A. J. Lipid Res. 2012; 53:1417. [PubMed: 22556215]

362. Bird SS, Marur VR, Sniatynski MJ, Greenberg HK, Kristal BS. Anal. Chem. 2011; 83:940. [PubMed: 21192696]

363. Melo T, Videira RA, André S, Maciel E, Francisco CS, Oliveira-Campos AM, Rodrigues LM, Domingues MRM, Peixoto F, Oliveira MM. J. Neurochem. 2012; 120:998. [PubMed: 22192081]

364. Hunt AN. J. Biol. Chem. 2000; 276:8492. [PubMed: 11121419]

365. Hunt AN, Postle AD. Methods. 2006; 39:104. [PubMed: 16831558]

366. Matsunaga T, Shintani S, Hara A. Drug Metab. Pharmacokinet. 2006; 21:1. [PubMed: 16547389]

367. Johnson, CH.; Patterson, AD.; Idle, JR.; Gonzalez, FJ. Annual Review of Pharmacology and Toxicology, Vol 52. Insel, PA.; Amara, SG.; Blaschke, TF., editors. Vol. Vol. 52. Palo Alto: Annual Reviews; 2012.

368. Gao Y, Cao X, Kang F, Cheng Z. J. Environ. Qual. 2011; 40:653. [PubMed: 21520772]

369. Chandra S, Lorey DR. Int. J. Mass spectrom. 2007; 260:90.

370. Groessl M, Zava O, Dyson PJ. Metallomics. 2011; 3:591. [PubMed: 21399784]

371. Millard M, Pathania D, Shabaik Y, Taheri L, Deng JX, Neamati N. PLoS ONE. 2010; 5:1.

372. Gadji M, Crous AMT, Fortin D, Krcek J, Torchia M, Mai S, Drouin R, Klonisch T. Eur. J. Pharmacol. 2009; 625:23. [PubMed: 19836372]

373. Wang Y, Arriaga EA. Cancer Lett. 2008; 262:123. [PubMed: 18194838]

374. Vibet S, Maheo K, Gore J, Dubois P, Bougnoux P, Chourpa I. Drug Metab. Disposition. 2007; 35:822.

375. Ask K, Decologne N, Ginies C, Lag M, Boucher JL, Holme JA, Pelczar H, Camus P. Biochem. Pharmacol. 2006; 71:377. [PubMed: 16313887]

376. Bolzati C, Cavazza-Ceccato M, Agostini S, Tokunaga S, Casara D, Bandoli G. J. Nucl. Med. 2008; 49:1336. [PubMed: 18632814]

377. Meng W, Parker TL, Kallinteri P, Walker DA, Higgins S, Hutcheon GA, Garnett MC. J. Controlled Release. 2006; 116:314.

378. Buthet LR, Bietto FM, Castro JA, Castro GD. Hum. Exp. Toxicol. 2011; 30:1785. [PubMed: 21257642]

379. Maher W, Foster S, Krikowa F. Mar. Freshwater Res. 2009; 60:885.

380. Casado-Martinez MC, Duncan E, Smith BD, Maher WA, Rainbow PS. Ecotoxicology. 2012; 21:576. [PubMed: 22083342]

381. Roschzttardtz H, Grillet L, Isaure MP, Conejero G, Ortega R, Curie C, Mari S. J. Biol. Chem. 2011; 286:27863. [PubMed: 21719700]

382. Ovecka M, Baluska F, Lichtscheidl I. Cell Biol. Int. 2008; 32:549. [PubMed: 18158257]

383. Duman JG, Forte JG. Am. J. Physiol. 2003; 285:C237.

384. Hutagalung AH, Novick PJ. Physiol. Rev. 2011; 91:119. [PubMed: 21248164]

385. Seabra MC, Mules EH, Hume AN. Trends Mol. Med. 2002; 8:23. [PubMed: 11796263]

386. Hickey CM, Wickner W. Mol. Biol. Cell. 2010; 21:2297. [PubMed: 20462954]

387. Peplowska K, Markgraf DF, Ostrowicz CW, Bange G, Ungermann C. Dev. Cell. 2007; 12:739. [PubMed: 17488625]

388. (a) Rusten TE, Vaccari T, Lindmo K, Rodahl LMW, Nezis IP, Sem-Jacobsen C, Wendler F, Vincent JP, Brech A, Bilder D, Stenmark H. Curr. Biol. 2007; 17:1817. [PubMed: 17935992] (b) Razi M, Chan EYW, Tooze SA. J. Cell Biol. 2009; 185:305. [PubMed: 19364919]

389. Rintoul GL, Reynolds IJ. Biochim. Biophys. Acta, Mol. Basis Dis. 2010; 1802:143.

390. Palmer CS, Osellame LD, Stojanovski D, Ryan MT. Cell. Signal. 2011; 23:1534. [PubMed: 21683788]

391. Fu CH, Jain D, Costa J, Velve-Casquillas G, Tran PT. Curr. Biol. 2011; 21:1431. [PubMed: 21856157]

392. Wikstrom JD, Twig G, Shirihai OS. Int. J. Biochem. Cell Biol. 2009; 41:1914. [PubMed: 19549572]

393. Muster B, Kohl W, Wittig I, Strecker V, Joos F, Haase W, Bereiter-Hahn J, Busch K. PLoS ONE. 2010; 5:1.

394. Liu XG, Weaver D, Shirihai O, Hajnoczky G. EMBO J. 2009; 28:3074. [PubMed: 19745815]

395. Twig G, Elorza A, Molina AJA, Mohamed H, Wikstrom JD, Walzer G, Stiles L, Haigh SE, Katz S, Las G, Alroy J, Wu M, Py BF, Yuan J, Deeney JT, Corkey BE, Shirihai OS. EMBO J. 2008; 27:433. [PubMed: 18200046]

396. Navratil M, Poe BG, Arriaga EA. Anal. Chem. 2007; 79:7691. [PubMed: 17877423]

397. Watanabe W, Shimada T, Matsunaga S, Kurihara D, Fukui K, Arimura S, Tsutsumi N, Isobe K, Itoh K. Opt. Express. 2007; 15:2490. [PubMed: 19532486]

398. Busch KB, Bereiter-Hahn J, Wittig I, Schagger H, Jendrach M. Mol. Membr. Biol. 2006; 23:509. [PubMed: 17127623]

399. Neuspiel M, Schauss AC, Braschi E, Zunino R, Rippstein P, Rachubinski RA, Andrade-Navarro MA, McBride HM. Curr. Biol. 2008; 18:102. [PubMed: 18207745]

400. Cepinska MN, Veenhuis M, van der Klei IJ, Nagotu S. Traffic. 2011; 12:925. [PubMed: 21507161]

401. Delille HK, Agricola B, Guimaraes SC, Borta H, Luers GH, Fransen M, Schrader M. J. Cell Sci. 2010; 123:2750. [PubMed: 20647371]

402. Pendin D, McNew JA, Daga A. Curr. Opin. Cell Biol. 2011; 23:435. [PubMed: 21641197]

403. Puhka M, Vihinen H, Joensuu M, Jokitalo E. J. Cell Biol. 2007; 179:895. [PubMed: 18056408]

404. Lisauskas T, Matula P, Claas C, Reusing S, Wiemann S, Erfle H, Lehmann L, Fischer P, Eils R, Rohr K, Storrie B, Starkuviene V. Traffic. 2012; 13:416. [PubMed: 22132776]

405. Guo Y, Walther TC, Rao M, Stuurman N, Goshima G, Terayama K, Wong JS, Vale RD, Walter P, Farese RV. Nature. 2008; 453:657. [PubMed: 18408709]

406. Schauss AC, Huang HY, Choi SY, Xu LQ, Soubeyrand S, Bilodeau P, Zunino R, Rippstein P, Frohman MA, McBride HM. BMC Biol. 2010; 8:1. [PubMed: 20051105]

407. Merz AJ, Wickner WT. Proc. Natl. Acad. Sci. U.S.A. 2004; 101:11548. [PubMed: 15286284]

408. Baars TL, Petri S, Peters C, Mayer A. Mol. Biol. Cell. 2007; 18:3873. [PubMed: 17652457]

409. Brett CL, Merz AJ. Curr. Biol. 2008; 18:1072. [PubMed: 18619842]

410. Michaillat L, Baars TL, Mayer A. Mol. Biol. Cell. 2012; 23:881. [PubMed: 22238359]

411. Pucadyil TJ, Schmid SL. Cell. 2008; 135:1263. [PubMed: 19084268]

412. Bacia K, Futai E, Prinz S, Meister A, Daum S, Glatte D, Briggs JAG, Schekman R. Sci. Rep. 2011; 1:1. [PubMed: 22355520]

413. Manneville J-B, Casella J-F, Ambroggio E, Gounon P, Bertherat J, Bassereau P, Cartaud J, Antonny B, Goud B. Proc. Natl. Acad. Sci. U.S.A. 2008; 105:16946. [PubMed: 18974217]

414. Soldati T, Schliwa M. Nat. Rev. Mol. Cell Biol. 2006; 7:897. [PubMed: 17139330]

415. (a) Mayor S, Presley JF, Maxfield FR. J. Cell. Biol. 1993; 121:1257. [PubMed: 8509447] (b) Seaman M. Cell. Mol. Life Sci. 2008; 65:2842. [PubMed: 18726175]

416. (a) Rink J, Ghigo E, Kalaidzidis Y, Zerial M. Cell. 2005; 122:735. [PubMed: 16143105] (b) Lakadamyali M, Rust MJ, Zhuang X. Cell. 2006; 124:997. [PubMed: 16530046]

417. Cai L, Loo LS, Atlashkin V, Hanson BJ, Hong W. Mol. Cell. Biol. 2011; 31:1734. [PubMed: 21300787]

418. Gengyo-Ando K, Kuroyanagi H, Kobayashi T, Murate M, Fujimoto K, Okabe S, Mitani S. EMBO Rep. 2007; 8:152. [PubMed: 17235359]

419. Barysch SV, Aggarwal S, Jahn R, Rizzoli SO. Proc. Natl. Acad. Sci. U.S.A. 2009; 106:9697. [PubMed: 19487677]

420. Sun QM, Westphal W, Wong KN, Tan I, Zhong Q. Proc. Natl. Acad. Sci. U.S.A. 2010; 107:19338. [PubMed: 20974968]

421. Lelouvier B, Puertollano R. J. Biol. Chem. 2011; 286:9826. [PubMed: 21245134]

422. Hirota Y, Kuronita T, Fujita H, Tanaka Y. Biochem. Biophys. Res. Commun. 2007; 364:40. [PubMed: 17927960]

423. Antignani A, Youle RJ. Proc. Natl. Acad. Sci. U.S.A. 2008; 105:8020. [PubMed: 18539770]

424. Chotard L, Mishra AK, Sylvain MA, Tuck S, Lambright DG, Rocheleau CE. Mol. Biol. Cell. 2010; 21:2285. [PubMed: 20462958]

425. Huotari J, Meyer-Schaller N, Hubner M, Stauffer S, Katheder N, Horvath P, Mancini R, Helenius A, Peter M. Proc. Natl. Acad. Sci. U.S.A. 2012; 109:823. [PubMed: 22219362]

426. Nordmann M, Cabrera M, Perz A, Brocker C, Ostrowicz C, Engelbrecht-Vandre S, Ungermann C. Curr. Biol. 2010; 20:1654. [PubMed: 20797862]

427. Okumura AJ. J. Biol. Chem. 2006; 281:4495. [PubMed: 16354670]

428. Nakae I, Fujino T, Kobayashi T, Sasaki A, Kikko Y, Fukuyama M, Gengyo-Ando K, Mitani S, Kontani K, Katada T. Mol. Biol. Cell. 2010; 21:2434. [PubMed: 20484575]

429. Takahashi Y, Nada S, Mori S, Soma-Nagae T, Oneyama C, Okada M. Biochem. Biophys. Res. Commun. 2012; 417:1151. [PubMed: 22227194]

430. Garg S, Sharma M, Ung C, Tuli A, Barral DC, Hava DL, Veerapen N, Besra GS, Hacohen N, Brenner MB. Immunity. 2011; 35:182. [PubMed: 21802320]

431. Rothenberg C, Srinivasan D, Mah L, Kaushik S, Peterhoff CM, Ugolino J, Fang SY, Cuervo AM, Nixon RA, Monteiro MJ. Hum. Mol. Genet. 2010; 19:3219. [PubMed: 20529957]

432. Liu P, Bartz R, Zehmer JK, Ying Y-s, Zhu M, Serrero G, Anderson RGW. Biochim. Biophys. Acta, Mol. Cell Res. 2007; 1773:784.

433. Rizzoli SO, Bethani I, Zwilling D, Wenzel D, Siddiqui TJ, Brandhorst D, Jahn R. Traffic. 2006; 7:1163. [PubMed: 17004320]

434. Kang J, Bai ZY, Zegarek MH, Grant BD, Lee J. Dev. Biol. 2011; 355:77. [PubMed: 21545795]

435. Fader CM, Sanchez DG, Mestre MB, Colombo MI. Biochim. Biophys. Acta, Mol. Cell Res. 2009; 1793:1901.

436. Scheuring D, Viotti C, Kruger F, Kunzl F, Sturm S, Bubeck J, Hillmer S, Frigerio L, Robinson DG, Pimpl P, Schumacher K. Plant Cell. 2011; 23:3463. [PubMed: 21934143]

437. Viotti C, Bubeck J, Stierhof YD, Krebs M, Langhans M, van den Berg W, van Dongen W, Richter S, Geldner N, Takano J, Jurgens G, de Vries SC, Robinson DG, Schumacher K. Plant Cell. 2010; 22:1344. [PubMed: 20435907]

438. (a) Axe EL, Walker SA, Manifava M, Chandra P, Roderick HL, Habermann A, Griffiths G, Ktistakis NT. J. Cell Biol. 2008; 182:685. [PubMed: 18725538] (b) Walker S, Chandra P, Manifava M, Axe E, Ktistakis NT. Autophagy. 2008; 4:1093. [PubMed: 18927492]

439. Nakatogawa H, Ichimura Y, Ohsumi Y. Cell. 2007; 130:165. [PubMed: 17632063]

440. Eng KE, Panas MD, Hedestam GBK, McInerney GM. Autophagy. 2010; 6:634. [PubMed: 20458170]

441. Jahreiss L, Menzies FM, Rubinsztein DC. Traffic. 2008; 9:574. [PubMed: 18182013]

442. Fader CM, Sanchez D, Furlan M, Colombo MI. Traffic. 2008; 9:230. [PubMed: 17999726]

443. (a) Narendra D, Tanaka A, Suen DF, Youle RJ. J. Cell Biol. 2008; 183:795. [PubMed: 19029340] (b) Dagda RK, Zhu JH, Kulich SM, Chu CT. Autophagy. 2008; 4:770. [PubMed: 18594198] (c) Zhu, J-h; Horbinski, C.; Guo, F.; Watkins, S.; Uchiyama, Y.; Chu, CT. Am. J. Pathol. 2007; 170:75. [PubMed: 17200184] (d) Zhu JH, Gusdon AM, Cimen H, Van Houten B, Koc E, Chu CT. Cell Death Dis. 2012; 3:e312. [PubMed: 22622131] (e) Xie R, Nguyen S, McKeehan K, Wang F, McKeehan WL, Liu L. J. Biol. Chem. 2011; 286:10367. [PubMed: 21262964]

444. Chen DD, Fan WL, Lu YT, Ding XJ, Chen S, Zhong Q. Mol. Cell. 2012; 45:629. [PubMed: 22342342]

445. Liang C, Lee J-s, Inn K-S, Gack MU, Li Q, Roberts EA, Vergne I, Deretic V, Feng P, Akazawa C, Jung JU. Nat. Cell Biol. 2008; 10:776. [PubMed: 18552835]

446. Lee JY, Koga H, Kawaguchi Y, Tang WX, Wong E, Gao YS, Pandey UB, Kaushik S, Tresse E, Lu JR, Taylor JP, Cuervo AM, Yao TP. EMBO J. 2010; 29:969. [PubMed: 20075865]

447. Itoh T, Kanno E, Uemura T, Waguri S, Fukuda M. J. Cell Biol. 2011; 192:839. [PubMed: 21383079]

448. Koga H, Kaushik S, Cuervo AM. FASEB J. 2010; 24:3052. [PubMed: 20375270]

449. Liang CY, Lee JS, Inn KS, Gack MU, Li QL, Roberts EA, Vergne I, Deretic V, Feng PH, Akazawa C, Jung JU. Nat. Cell Biol. 2008; 10:776. [PubMed: 18552835]

450. Ganley IG, Wong PM, Gammoh N, Jiang XJ. Mol. Cell. 2011; 42:731. [PubMed: 21700220]

451. (a) Huynh KK, Eskelinen EL, Scott CC, Malevanets A, Saftig P, Grinstein S. EMBO J. 2007; 26:313. [PubMed: 17245426] (b) Trivedi V, Zhang SC, Castoreno AB, Stockinger W, Shieh EC, Vyas JM, Frickel EM, Nohturfft A. Proc. Natl. Acad. Sci. U.S.A. 2006; 103:18226. [PubMed: 17110435]

452. (a) Carrithers LM, Hulseberg P, Sandor M, Carrithers MD. FEMS Immunol. Med. Microbiol. 2011; 63:319. [PubMed: 22092558] (b) Kyei GB, Vergne I, Chua J, Roberts E, Harris J, Junutula JR, Deretic V. EMBO J. 2006; 25:5250. [PubMed: 17082769] (c) Shaughnessy LM, Hoppe AD, Christensen KA, Swanson JA. Cell. Microbiol. 2006; 8:781. [PubMed: 16611227] (d) Smith AC, Do Heo W, Braun V, Jiang XJ, Macrae C, Casanova JE, Scidmore MA, Grinstein S, Meyer T, Brumell JH. J. Cell Biol. 2007; 176:263. [PubMed: 17261845] (e) Seto S, Tsujimura K, Koide Y. Traffic. 2011; 12:407. [PubMed: 21255211] (f) Rumsey JW, Valentine JF, Naser SA. Medical Science Monitor. 2006; 12:BR130. [PubMed: 16572045] (g) de Chastellier C, Thilo L. Cell. Microbiol. 2006; 8:242. [PubMed: 16441435] (h) Rodriguez NE, Dixit UG, Allen LAH, Wilson ME. PLoS ONE. 2011; 6:1.

453. Andrade RM, Wessendarp M, Gubbels MJ, Striepen B, Subauste CS. J. Clin. Invest. 2006; 116:2366. [PubMed: 16955139]

454. Leiva N, Pavarotti M, Colombo MI, Damiani MT. Exp. Cell Res. 2006; 312:1843. [PubMed: 16563376]

455. Hatsuzawa K. Mol. Biol. Cell. 2006; 17:3964. [PubMed: 16790498]

456. Wahe A, Kasmapour B, Schmaderer C, Liebl D, Sandhoff K, Nykjaer A, Griffiths G, Gutierrez MG. J. Cell Sci. 2010; 123:2502. [PubMed: 20571055]

457. Marion S, Hoffmann E, Holzer D, Le Clainche C, Martin M, Sachse M, Ganeva I, Mangeat P, Griffiths G. Traffic. 2011; 12:421. [PubMed: 21210911]

458. Ferguson JS, Martin JL, Azad AK, McCarthy TR, Kang PB, Voelker DR, Crouch EC, Schlesinger LS. Infect. Immun. 2006; 74:7005. [PubMed: 17030585]

459. Balestrieri B, Maekawa A, Xing W, Gelb MH, Katz HR, Arm JP. J. Immunol. 2009; 182:4891. [PubMed: 19342668]

460. Wang QQ, Li H, Oliver T, Glogauer M, Guo J, He YW. Journal of Immunology. 2008; 180:2419.

461. Seto S, Matsumoto S, Tsujimura K, Koide Y. Microbiol. Immunol. 2010; 54:170. [PubMed: 20236428]

462. Sun J, Deghmane AE, Soualhine H, Hong T, Bucci C, Solodkin A, Hmama Z. J. Leukocyte Biol. 2007; 82:1437. [PubMed: 18040083]

463. Schramm M, Herz J, Haas A, Kronke M, Utermohlen O. Cell. Microbiol. 2008; 10:1839. [PubMed: 18485117]

464. Fang J, Brzostowski JA, Ou S, Isik N, Nair V, Jin T. J. Cell Biol. 2007; 178:411. [PubMed: 17664333]

465. Starr T, Ng TW, Wehrly TD, Knodler LA, Celli J. Traffic. 2008; 9:678. [PubMed: 18266913]

466. Parashuraman S, Madan R, Mukhopadhyay A. FEBS Lett. 2010; 584:1251. [PubMed: 20176016]

467. Carrasco-Marin E, Fernandez-Prieto L, Rodriguez-Del Rio E, Madrazo-Toca F, Reinheckel T, Saftig P, Alvarez-Dominguez C. J. Biol. Chem. 2011; 286:3332. [PubMed: 21123180]

468. Sanjuan MA, Dillon CP, Tait SWG, Moshiach S, Dorsey F, Connell S, Komatsu M, Tanaka K, Cleveland JL, Withoff S, Green DR. Nature. 2007; 450:1253. [PubMed: 18097414]

469. Robinson CG, Roy CR. Cell. Microbiol. 2006; 8:793. [PubMed: 16611228]

470. Trivedi V, Zhang SC, Stockinger W, Nohturfft A. Sci. STKE. 2007; 2007:pl3. [PubMed: 17595222]

471. Liebl D, Griffiths G. J. Cell Sci. 2009; 122:2935. [PubMed: 19638408]

472. Essid M, Gopaldass N, Yoshida K, Merrifield C, Soldati T. Mol. Biol. Cell. 2012; 23:1267. [PubMed: 22323285]

473. Elstak ED, Neeft M, Nehme NT, Voortman J, Cheung M, Goodarzifard M, Gerritsen HC, Henegouwen P, Callebaut I, de Saint Basile G, van der Sluijs P. Blood. 2011; 118:1570. [PubMed: 21693760]

474. Tyrrell M, Campanoni P, Sutter JU, Pratelli R, Paneque M, Sokolovski S, Blatt MR. Plant J. 2007; 51:1099. [PubMed: 17662029]

475. (a) Tyrrell M, Campanoni P, Sutter J-U, Pratelli R, Paneque M, Sokolovski S, Blatt MR. The Plant Journal. 2007; 51:1099. [PubMed: 17662029] (b) Ahras M. J. Cell. Biol. 2006; 173:241. [PubMed: 16618809] (c) Kakhlon O, Sakya P, Larijani B, Watson R, Tooze SA. EMBO J. 2006; 25:1590. [PubMed: 16601685]

476. Cocucci E, Racchetti G, Rupnik M, Meldolesi J. J. Cell Sci. 2008; 121:2983. [PubMed: 18713833]

477. (a) El-Kasmi F, Pacher T, Strompen G, Stierhof YD, Muller LM, Koncz C, Mayer U, Jurgens G. Plant J. 2011; 66:268. [PubMed: 21205036] (b) Haas AK, Yoshimura S, Stephens DJ, Preisinger C, Fuchs E, Barr FA. J. Cell Sci. 2007; 120:2997. [PubMed: 17684057]

478. Anderson DJ, Hetzer MW. Nat Cell Biol. 2007; 9:1160. [PubMed: 17828249]

479. Pollock S, Antrobus R, Newton L, Kampa B, Rossa J, Latham S, Nichita NB, Dwek RA, Zitzmann N. FASEB J. 2010; 24:1866. [PubMed: 20097877]

480. Caputo E, Ceglie V, Lippolis M, La Rocca N, De Tullio MC. Environ. Exp. Bot. 2010; 69:63.

481. Chen JY, Wen PF, Kong WF, Pan QH, Wan SB, Huang WD. J. Plant Physiol. 2006; 163:115. [PubMed: 16399002]

482. Chen G, Law K, Ho P, Zhang X, Li N. Mol. Biol. Rep. 2012; 39:2147. [PubMed: 21643750]

483. Kirchsteiger K, Pulido P, Gonzalez M, Cejudo FJ. Molecular Plant. 2009; 2:298. [PubMed: 19825615]

484. Granell S, Mohammad S, Ramanagoudr-Bhojappa R, Baldini G. Mol. Endocrinol. 2010; 24:1805. [PubMed: 20631012]

485. Kajiura H, Koiwa H, Nakazawa Y, Okazawa A, Kobayashi A, Seki T, Fujiyama K. Glycobiology. 2010; 20:235. [PubMed: 19914916]

486. Kim HJ, Ok SH, Bahn SC, Jang J, Oh SA, Park SK, Twell D, Ryu SB, Shin JS. Plant Cell. 2011; 23:94. [PubMed: 21278126]

487. Tahay G, Wiame E, Tyteca D, Courtoy PJ, Van Schaftingen E. Biochem. J. 2012; 441:105. [PubMed: 21936773]

488. Wang W. J. Biol. Chem. 2006; 281:19676. [PubMed: 16687406]

489. Dong HB, Dalton TP, Miller ML, Chen Y, Uno S, Shi Z, Shertzer HG, Bansal S, Avadhani NG, Nebert DW. Mol. Pharmacol. 2009; 75:555. [PubMed: 19047483]

490. Dutheil F, Dauchy S, Diry M, Sazdovitch V, Cloarec O, Mellottee L, Bieche I, Ingelman-Sundberg M, Flinois JP, de Waziers I, Beaune P, Decleves X, Duyckaerts C, Loriot MA. Drug Metab. Disposition. 2009; 37:1528.

491. Jia P, Zhang C, Jia Y, Webster KA, Huang X, Kochegarov AA, Lemanski SL, Lemanski LF. J. Biomed. Sci. 2011; 18:46. [PubMed: 21696616]

492. Leroux A, Fleming-Canepa X, Aranda A, Maugeri D, Cazzulo JJ, Sanchez MA, Nowicki C. Mol. Biochem. Parasitol. 2006; 149:74. [PubMed: 16750864]

493. Mastorodemos V, Kotzamani D, Zaganas I, Arianoglou G, Latsoudis H, Plaitakis A. Biochem. Cell Biol. 2009; 87:505. [PubMed: 19448744]

494. Pino P, Foth BJ, Kwok LY, Sheiner L, Schepers R, Soldati T, Soldati-Favre D. PLoS Path. 2007; 3:1092.

495. Sans CL, Satterwhite DJ, Stoltzman CA, Breen KT, Ayer DE. Mol. Cell. Biol. 2006; 26:4863. [PubMed: 16782875]

496. Wong JWY, Chan CL, Tang WK, Cheng CHK, Fong WP. J. Cell. Biochem. 2010; 109:74. [PubMed: 19885858]

497. Yoval-Sanchez B, Jasso-Chavez R, Lira-Silva E, Moreno-Sanchez R, Rodriguez-Zavala JS. J. Bioenerg. Biomembr. 2011; 43:519. [PubMed: 21833603]

498. Suozzi A, Malatesta M, Zancanaro C. J. Anat. 2009; 214:956. [PubMed: 19538638]

499. Wang XL, Xu YH, Peng CC, Fan RC, Gao XQ. J. Exp. Bot. 2009; 60:1025. [PubMed: 19174457]

500. Kowalik D, Haller F, Adamski J, Moeller G. J. Steroid Biochem. Mol. Biol. 2009; 117:117. [PubMed: 19703561]

501. Lee SJ, Park MH, Kim HJ, Koh JY. Glia. 2010; 58:1186. [PubMed: 20544854]

502. Cobbe N, Marshall KM, Rao SG, Chang CW, Di Cara F, Duca E, Vass S, Kassan A, Heck MMS. J. Cell Sci. 2009; 122:3414. [PubMed: 19706689]

503. Ondzighi CA, Christopher DA, Cho EJ, Chang SC, Staehelin LA. Plant Cell. 2008; 20:2205. [PubMed: 18676877]

504. Verhaar R, Drukarch B, Bol J, Jongenelen CAM, Musters RJP, Wilhelmus MMM. Neurobiol. Dis. 2012; 45:839. [PubMed: 22051113]

505. Bleve G, Di Sansebastiano GP, Grieco F. Biochim. Biophys. Acta, Biomembr. 2011; 1808:733.

506. Zhao C, Shono M, Sun A, Yi S, Li M, Liu J. J. Plant Physiol. 2007; 164:835. [PubMed: 16904232]

507. Granneman JG, Moore HPH, Mottillo EP, Zhu Z. J. Biol. Chem. 2008; 284:3049. [PubMed: 19064991]

508. Bubber P, Hartounian V, Gibson GE, Blass JP. Eur. Neuropsychopharmacol. 2011; 21:254. [PubMed: 21123035]

509. Garmier M, Carroll AJ, Delannoy E, Vallet C, Day DA, Small ID, Millar AH. Plant Physiol. 2008; 148:1324. [PubMed: 18784283]

510. Geng TY, Li P, Okutsu M, Yin XH, Kwek J, Zhang M, Yan Z. American Journal of Physiology-Cell Physiology. 2010; 298:C572. [PubMed: 20032509]

511. Lu ZB, Xu X, Hu XL, Fassett J, Zhu GS, Tao Y, Li JX, Huang YM, Zhang P, Zhao BL, Chen YJ. Antioxid. Redox Signaling. 2010; 13:1011.

512. Grunewald A, Gegg ME, Taanman JW, King RH, Kock N, Klein C, Schapira AHV. Exp. Neurol. 2009; 219:266. [PubMed: 19500570]

513. Lapaille M, Thiry M, Perez E, Gonzalez-Halphen D, Remacle C, Cardol P. Biochim. Biophys. Acta, Bioenerg. 2010; 1797:1533.

514. Lenglet S, Antigny F, Vetterli L, Dufour JF, Rossier MF. Endocrinology. 2008; 149:5461. [PubMed: 18653718]

515. Marti MC, Florez-Sarasa I, Camejo D, Ribas-Carbo M, Lazaro JJ, Sevilla F, Jimenez A. J. Exp. Bot. 2011; 62:3863. [PubMed: 21460385]

516. Sun F, Suen PK, Zhang Y, Liang C, Carrie C, Whelan J, Ward JL, Hawkins ND, Jiang L, Lim BL. New Phytol. 2012; 194:206. [PubMed: 22269069]

517. Wu R, Smeele KM, Wyatt E, Ichikawa Y, Eerbeek O, Sun L, Chawla K, Hollmann MW, Nagpal V, Heikkinen S, Laakso M, Jujo K, Wasserstrom JA, Zuurbier CJ, Ardehali H. Circul. Res. 2010; 108:60.

518. Mancuso DJ, Sims HF, Han X, Jenkins CM, Guan SP, Yang K, Moon SH, Pietka T, Abumrad NA, Schlesinger PH, Gross RW. J. Biol. Chem. 2007; 282:34611. [PubMed: 17923475]

519. Dickinson BC, Tang Y, Chang Z, Chang CJ. Chem. Biol. (Cambridge, MA, U.S.). 2011; 18:943.

520. Reina CP, Zhong XY, Pittman RN. Hum. Mol. Genet. 2010; 19:235. [PubMed: 19843543]

521. Han C, Lim K, Xu L, Li G, Wu T. J. Cell. Biochem. 2008; 105:534. [PubMed: 18636547]

522. Khan Z, Michalopoulos GK, Stolz DB. Am. J. Pathol. 2006; 169:1251. [PubMed: 17003483]

523. Woudenberg J, Rembacz KP, van den Heuvel FAJ, Woudenberg-Vrenken TE, Buist-Homan M, Geuken M, Hoekstra M, Deelman LE, Enrich C, Henning RH, Moshage H, Faber KN. Hepatology. 2010; 51:1744. [PubMed: 20146263]

524. Maissel A, Marom M, Shtutman M, Shahaf G, Livneh E. Cell. Signal. 2006; 18:1127. [PubMed: 16242915]

525. Ebine K, Okatani Y, Uemura T, Goh T, Shoda K, Niihama M, Morita MT, Spitzer C, Otegui MS, Nakano A, Ueda T. Plant Cell. 2008; 20:3006. [PubMed: 18984676]

526. Chang CCC, Slesak I, Jorda L, Sotnikov A, Melzer M, Miszalski Z, Mullineaux PM, Parker JE, Karpinska B, Karpinski S. Plant Physiol. 2009; 150:670. [PubMed: 19363092]

527. Kong WF, Chen JY, Hou ZX, Wen PF, Zhan JC, Pan QH, Huang WD. J. Plant Physiol. 2007; 164:934. [PubMed: 16884825]

528. Sandoval FJ, Zhang Y, Roje S. J. Biol. Chem. 2008; 283:30890. [PubMed: 18713732]

529. Vargas WA, Pontis HG, Salerno GL. Planta. 2008; 227:795. [PubMed: 18034262]

530. Pulido P, Spinola MC, Kirchsteiger K, Guinea M, Pascual MB, Sahrawy M, Sandalio LM, Dietz KJ, Gonzalez M, Cejudo FJ. J. Exp. Bot. 2010; 61:4043. [PubMed: 20616155]

531. Ausseil J, Landry K, Seyrantepe V, Trudel S, Mazur A, Lapointe F, Pshezhetsky AV. Mol. Genet. Metab. 2006; 87:22. [PubMed: 16293432]

532. Lofke C, Ischebeck T, Konig S, Freitag S, Heiliviann I. Biochem. J. 2008; 413:115. [PubMed: 18402553]

533. Krishnan N, Fu C, Pappin DJ, Tonks NK. Sci. Signaling. 2011; 4:ra86.

534. Sriburi R, Bommiasamy H, Buldak GL, Robbins GR, Frank M, Jackowski S, Brewer JW. J. Biol. Chem. 2007; 282:7024. [PubMed: 17213183]

535. Hahmann C, Weiser A, Duckett D, Schroeter T. Assay Drug Dev. Technol. 2011; 9:79. [PubMed: 20858054]

536. Xu Y, Johansson M, Karlsson A. J. Biol. Chem. 2007; 283:1563. [PubMed: 17999954]

537. Benton CR, Holloway GP, Campbell SE, Yoshida Y, Tandon NN, Glatz JFC, Luiken J, Spriet LL, Bonen A. J. Physiol. (Oxford, U.K.). 2008; 586:1755.

538. Aranda A, Maugeri D, Uttaro AD, Opperdoes F, Cazzulo JJ, Nowicki C. Int. J. Parasitol. 2006; 36:295. [PubMed: 16321390]

539. Ruggiero C, Ehrenshaft M, Cleland E, Stadler K. Am. J. Physiol.: Endocrinol. Metab. 2011; 300:E1047. [PubMed: 21386058]

540. Kitagaki H, Cowart LA, Matmati N, de Avalos SV, Novgorodov SA, Zeidan YH, Bielawski J, Obeid LM, Hannun YA. Biochim. Biophys. Acta, Biomembr. 2007; 1768:2849.

541. Yabu T, Shimuzu A, Yamashita M. J. Biol. Chem. 2009; 284:20349. [PubMed: 19429680]

542. Dumitru CA, Sandalcioglu IE, Wagner M, Weller M, Gulbins E. J. Mol. Med. (Heidelberg, Ger.). 2009; 87:1123.

543. Tani A, Inoue C, Tanaka Y, Yamamoto Y, Kondo H, Hiradate S, Kimbara K, Kawai F. Microbiology. 2008; 154:3437. [PubMed: 18957597]

544. Lavarias S, Pollero R, Heras H. Aquat. Toxicol. 2006; 77:190. [PubMed: 16413620]

545. Tudor C, Lerner-Marmarosh N, Engelborghs Y, Gibbs PEM, Maines MD. Biochem. J. 2008; 413:405. [PubMed: 18412543]

546. Ikeda M, Nakagawa H, Ban S, Tsumoto H, Suzuki T, Miyata N. Free Radical Biol. Med. 2010; 49:1792. [PubMed: 20854901]

547. Estavillo GM, Crisp PA, Pornsiriwong W, Wirtz M, Collinge D, Carrie C, Giraud E, Whelan J, David P, Javot H, Brearley C, Hell R, Marin E, Pogson BJ. Plant Cell. 2011; 23:3992. [PubMed: 22128124]

548. Chueh FY, Leong KF, Cronk RJ, Venkitachalam S, Pabich S, Yu CL. Cell. Signal. 2011; 23:1170. [PubMed: 21397011]

549. Corpas FJ, Palma JM, Sandalio LM, Valderrama R, Barroso JB, del Rio LA. J. Plant Physiol. 2008; 165:1319. [PubMed: 18538891]

550. Shevyakova NI, Bakulina EA, Kuznetsov VV. Russ. J. Plant Physiol. 2009; 56:663.

551. Kuznetsov AV, Troppmair J, Sucher R, Hermann M, Saks V, Margreiter R. Biochim. Biophys. Acta, Bioenerg. 2006; 1757:686.

552. Terman A, Kurz T, Navratil M, Arriaga EA, Brunk UT. Antioxid. Redox Signaling. 2010; 12:503.

553. Nauratil M, Terman A, Arriaga EA. Exp. Cell Res. 2008; 314:164. [PubMed: 17964571]

554. Picard M, Taivassalo T, Gouspillou G, Hepple RT. J. Physiol. (Oxford, U.K.). 2011; 589:4413.

555. (a) Hu CF, Sun QP, Peng XJ, Huang Q, Wang MF, Li SQ, Zhu YG. Protoplasma. 2010; 241:91. [PubMed: 20157834] (b) Poe BG, Navratil M, Arriaga EA. J. Chromatogr. 2006; 1137:249.

556. Kostal V, Arriaga EA. Electrophoresis. 2008; 29:2578. [PubMed: 18576409]

557. Kostal V, Arriaga EA. Anal. Chem. 2011; 83:1822. [PubMed: 21309532]

558. (a) Johnson RD, Navratil M, Poe BG, Xiong GH, Olson KJ, Ahmadzadeh H, Andreyev D, Duffy CF, Arriaga EA. Anal. Bioanal. Chem. 2007; 387:107. [PubMed: 16937092] (b) Chen DH, Zhang XY, Shi YG. Biochem. J. 2006; 398:169. [PubMed: 16716149]

559. Ahmadzadeh H, Thompson LV, Arriaga EA. Anal. Bioanal. Chem. 2006; 384:169. [PubMed: 16320040]

560. Andresen V, Alexander S, Heupel WM, Hirschberg M, Hoffman RM, Friedl P. Curr. Opin. Biotechnol. 2009; 20:54. [PubMed: 19324541]

561. Studer V, Bobin J, Chahid M, Mousavi HS, Candes E, Dahan M. Proc. Natl. Acad. Sci. U.S.A. 2012; 109:E1679. [PubMed: 22689950]

562. Bon P, Maucort G, Wattellier B, Monneret S. Opt. Express. 2009; 17:13080. [PubMed: 19654713]

563. Krafft C, Dietzek B, Schmitt M, Popp J. J. Biomed. Opt. 2012; 17

564. Matusch A, Fenn LS, Depboylu C, Klietz M, Strohmer S, McLean JA, Becker JS. Anal. Chem. 2012; 84:3170. [PubMed: 22413784]

565. Johnson DE, Ai HW, Wong P, Young JD, Campbell RE, Casey JR. J. Biol. Chem. 2009; 284:20499. [PubMed: 19494110]

566. Kumar S, Aaron J, Sokolov K. Nat. Protoc. 2008; 3:314. [PubMed: 18274533]

567. (a) Lawson EL, Clifton JG, Huang FL, Li XS, Hixson DC, Josic D. Electrophoresis. 2006; 27:2747. [PubMed: 16739230] (b) Burre J, Zimmermann H, Volknandt W. Anal. Biochem. 2007; 362:172. [PubMed: 17266918] (c) Truernit E, Hibberd JM. Plant J. 2007; 50:926. [PubMed: 17461787] (d) Hornig-Do HT, Gunther G, Bust M, Lehnartz P, Bosio A, Wiesner RJ. Anal. Biochem. 2009; 389:1. [PubMed: 19285029] (e) Wang Y, Taylor TH, Arriaga EA. Anal. Bioanal. Chem. 2011; 402:41. [PubMed: 22065344] (f) Nylandsted J, Becker AC, Bunkenborg J, Andersen JS, Dengjel J, Jaattela M. Proteomics. 2011; 11:2830. [PubMed: 21674799]

568. Moschallski M, Hausmann M, Posch A, Paulus A, Kunz N, Duong TT, Angres B, Fuchsberger K, Steuer H, Stoll D, Werner S, Hagmeyer B, Stelzle M. Electrophoresis. 2010; 31:2655. [PubMed: 20665923]

569. Suhre K, Meisinger C, Doring A, Altmaier E, Belcredi P, Gieger C, Chang D, Milburn MV, Gall WE, Weinberger KM, Mewes HW, de Angelis MH, Wichmann HE, Kronenberg F, Adamski J, Illig T. PLoS ONE. 2010; 5:1.

570. Michalski A, Damoc E, Hauschild JP, Lange O, Wieghaus A, Makarov A, Nagaraj N, Cox J, Mann M, Horning S. Mol. Cell. Proteomics. 2011; 10:11.

571. Moller I, Thomas A, Geyer H, Schanzer W, Thevis M. Anal. Bioanal. Chem. 2012; 403:2715. [PubMed: 22592927]

572. (a) Yashunsky V, Shimron S, Lirtsman V, Weiss AM, Melamed-Book N, Golosovsky M, Davidov D, Aroeti B. Biophys. J. 2009; 97:1003. [PubMed: 19686647] (b) Ferracci G, Seagar M, Joel C, Miquelis R, Leveque C. Anal. Biochem. 2004; 334:367. [PubMed: 15494144]

573. (a) Ostergaard J, Moeller EH. Electrophoresis. 2010; 31:339. [PubMed: 20024925] (b) Krylov SN. J. Biomol. Screen. 2006; 11:115. [PubMed: 16418314]

574. Ye M, Hu J, Peng M, Liu J, Liu J, Liu H, Zhao X, Tan W. Int. J. Mol. Sci. 2012; 13:3341. [PubMed: 22489154]

575. Sohn CH, Agnew HD, Lee JE, Sweredoski MJ, Graham RLJ, Smith GT, Hess S, Czerwieniec G, Loo JA, Heath JR, Deshaies RJ, Beauchamp JL. Anal. Chem. 2012; 84:2662. [PubMed: 22339618]

576. Rees JS, Lowe N, Armean IM, Roote J, Johnson G, Drummond E, Spriggs H, Ryder E, Russell S, St Johnston D, Lilley KS. Mol. Cell. Proteomics. 2011; 10:1.

577. Mano S, Miwa T, Nishikawa S, Mimura T, Nishimura M. Plant Cell Physiol. 2011; 52:244. [PubMed: 21115470]

578. (a) Rajendran L, Udayar V, Goodger ZV. Trends Pharmacol. Sci. 2012; 33:215. [PubMed: 22385603] (b) Roodbeen R, van Hest JCM. Bioessays. 2009; 31:1299. [PubMed: 19877005]

579. Won YW, Lim KS, Kim YH. J. Controlled Release. 2011; 152:99.

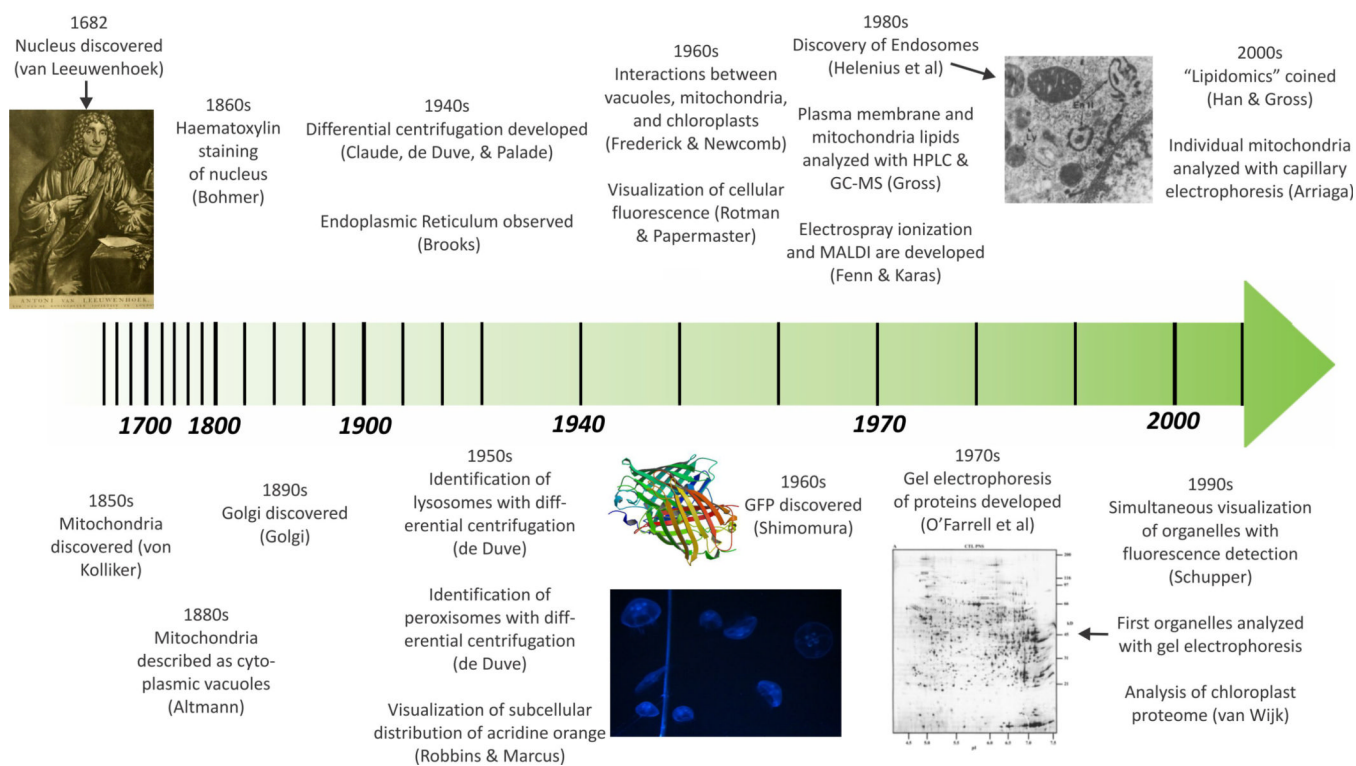580. Huang JG, Leshuk T, Gu FX. Nano Today. 2011; 6:478.

Figure 1. History of subcellular analysis
2D-gel electrophoresis image of reprinted from reference 129. Copyright 1997 John Wiley and Sons. Transmission electron microscopy image reprinted from reference 105. Copyright 1983 Elsevier. GFP structure reprinted from the protein data bank and reference 93.[93]
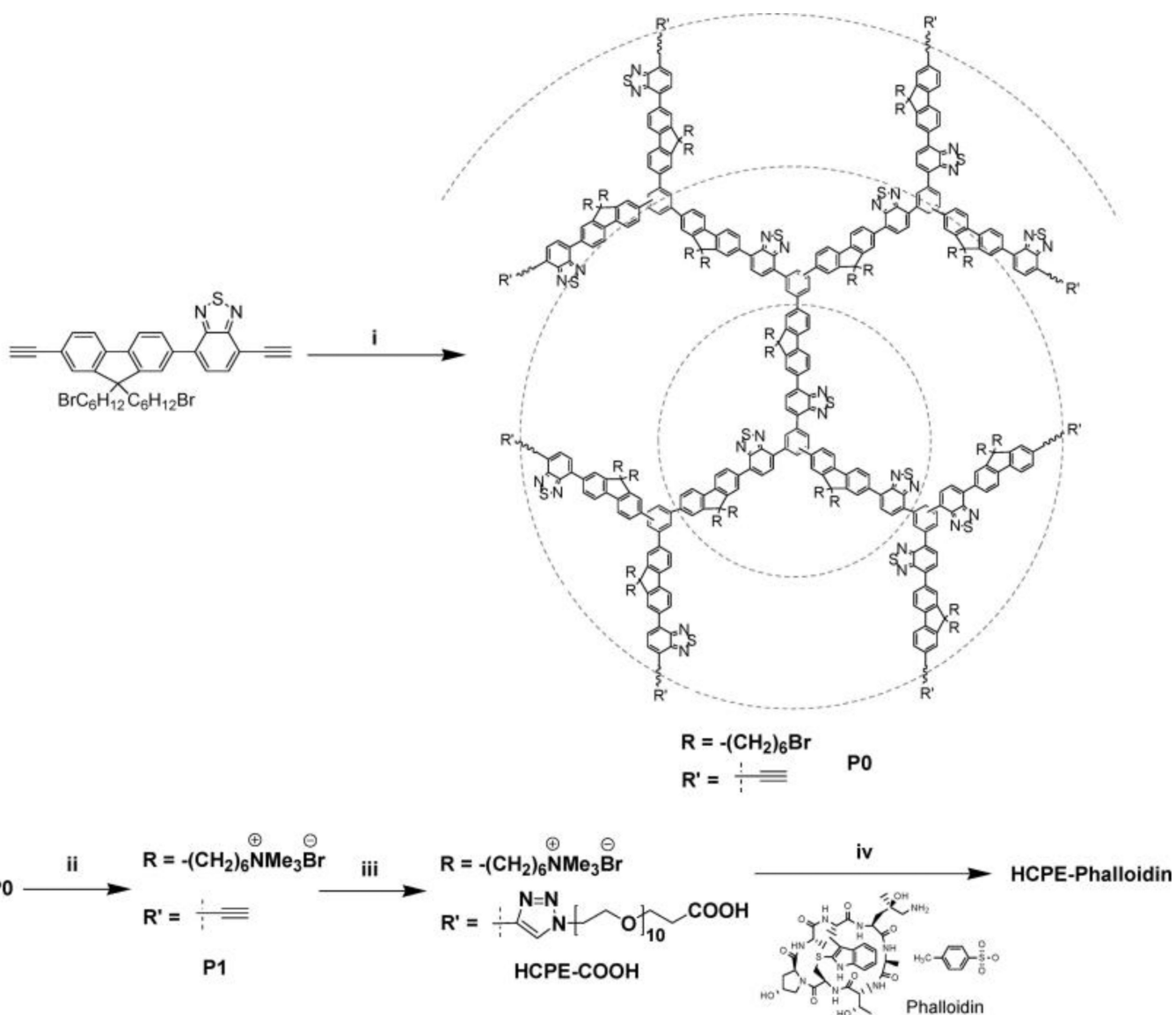
Figure 2. Synthesis of phalloidin-hyperbranched polymer conjugated electrolyte (Phalloidin-HPCE)

Additional information reported in Scheme 1 from reference 183. Reprinted with permission from reference 183. Li, K.; Pu, K.Y.; Cai, L.; Liu, B. *Chem. Mater.* **2011**, *23*, 2113 Copyright 2011. American Chemical Society.
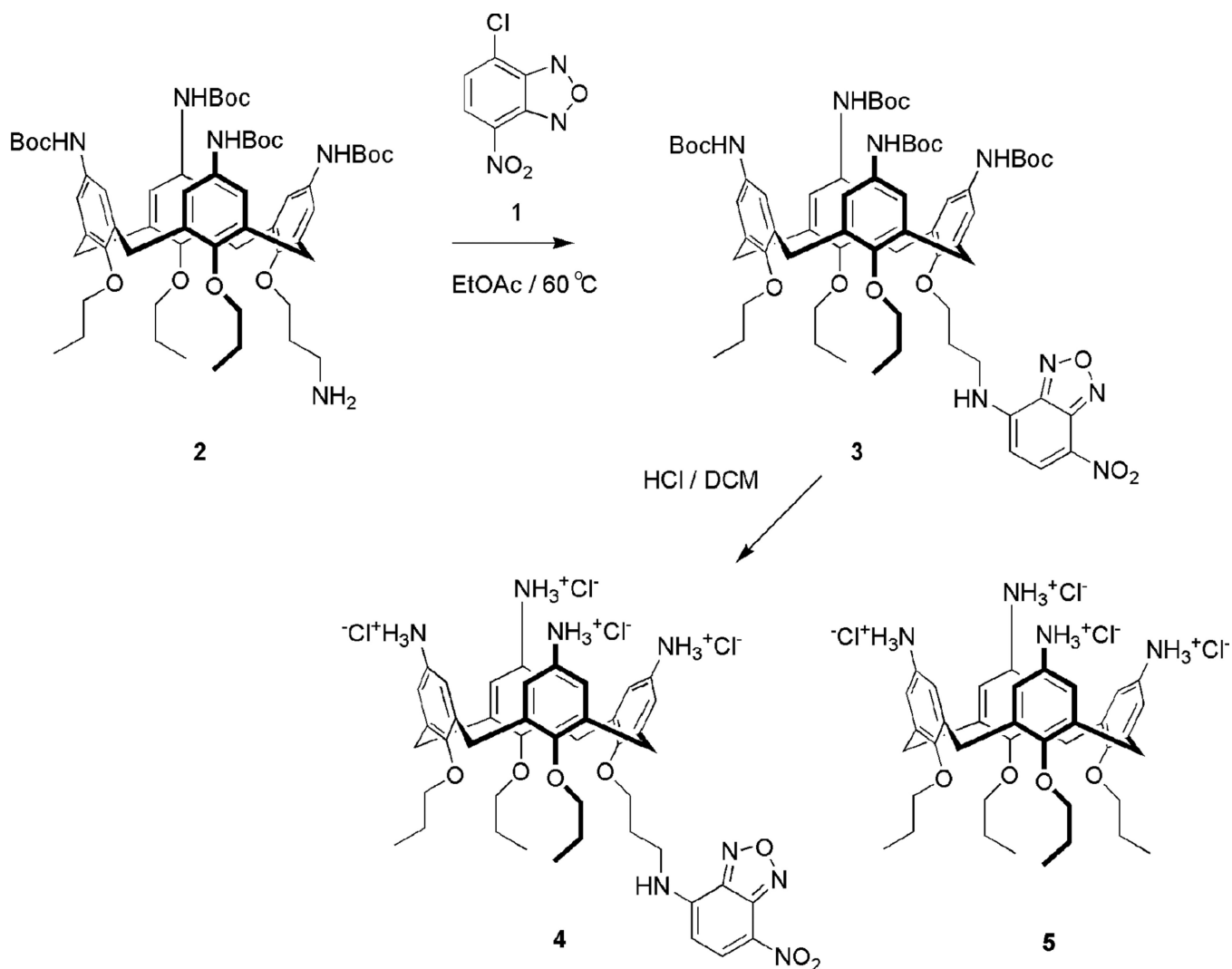
Figure 3. Synthesis of a fluorescent intracellular staining calixarene macrocycle (NBDCalAm)
The final product is labeled 4. Reprinted with permission from reference 182. Lalor, R.;
Baillie-Johnson, H.; Redshaw, C.; Matthews, S.E.; Mueller, A. *J. Am. Chem. Soc.*, **2008**,
130, 2892. Copyright 2008. American Chemical Society.
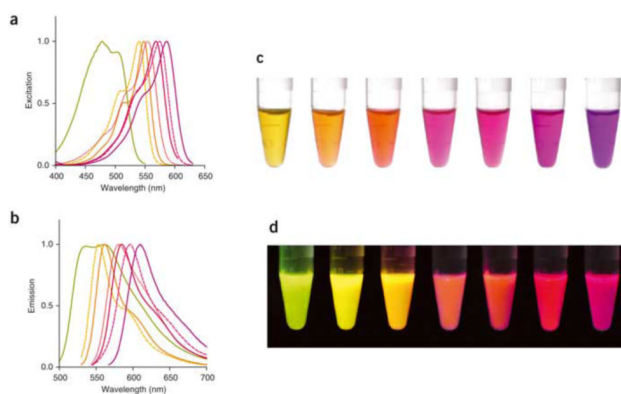
Figure 4. Palate of available fluorescent fusion proteins
A. Excitation spectra. **B**. Emission spectra. **C**. Colors of commercially available fluorescent proteins. **D**. Fluorescent appearance of commercially available proteins. Other conditions are reported in Figure 1 from reference 188. Reprinted with permission from Reference 188. Copyright 2004 Nature Publishing Group.
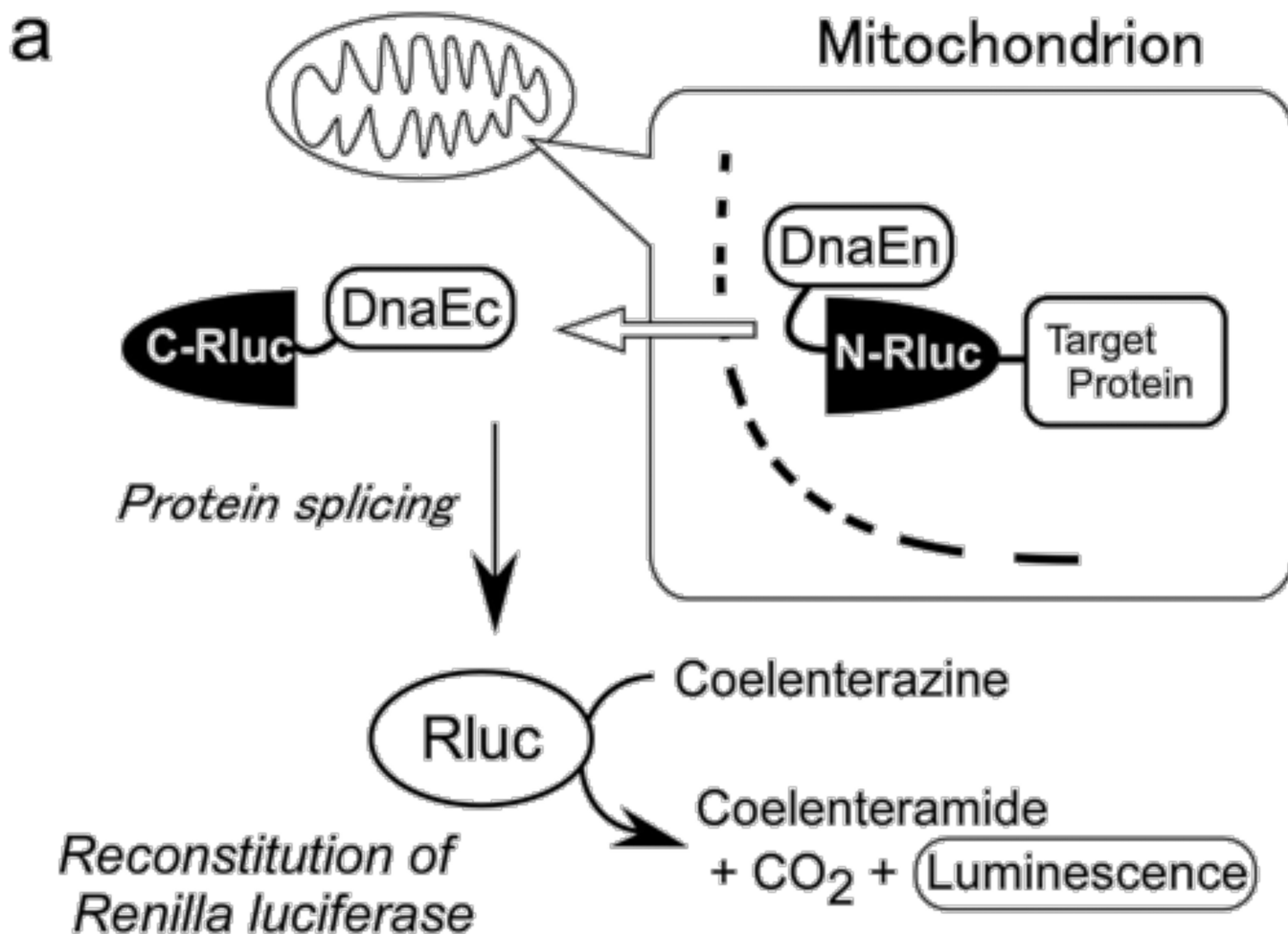
Figure 5. Strategy employed to detect release of proteins from mitochondria
A. Intein-NRluc-Target Protein release from the mitochondrion and its association with the cytosolic CRluc-intein construct. C-Rluc = cytosolic c-terminal luciferase fragment. DnaEc = cytosolic intein fragment. DnaEn = mitochondrial intein fragment. N-Rluc = mitochondrial n-terminal luciferase fragment. Rluc = spliced and active luciferase protein. Additional information reported in Figure 5 from reference 194. Reprinted with permission from Kanno, A.; Ozawa, T.; Umezawa, Y. *Anal. Chem.* **2006**, *78*, 8–76.Copyright 2006. American Chemical Society.
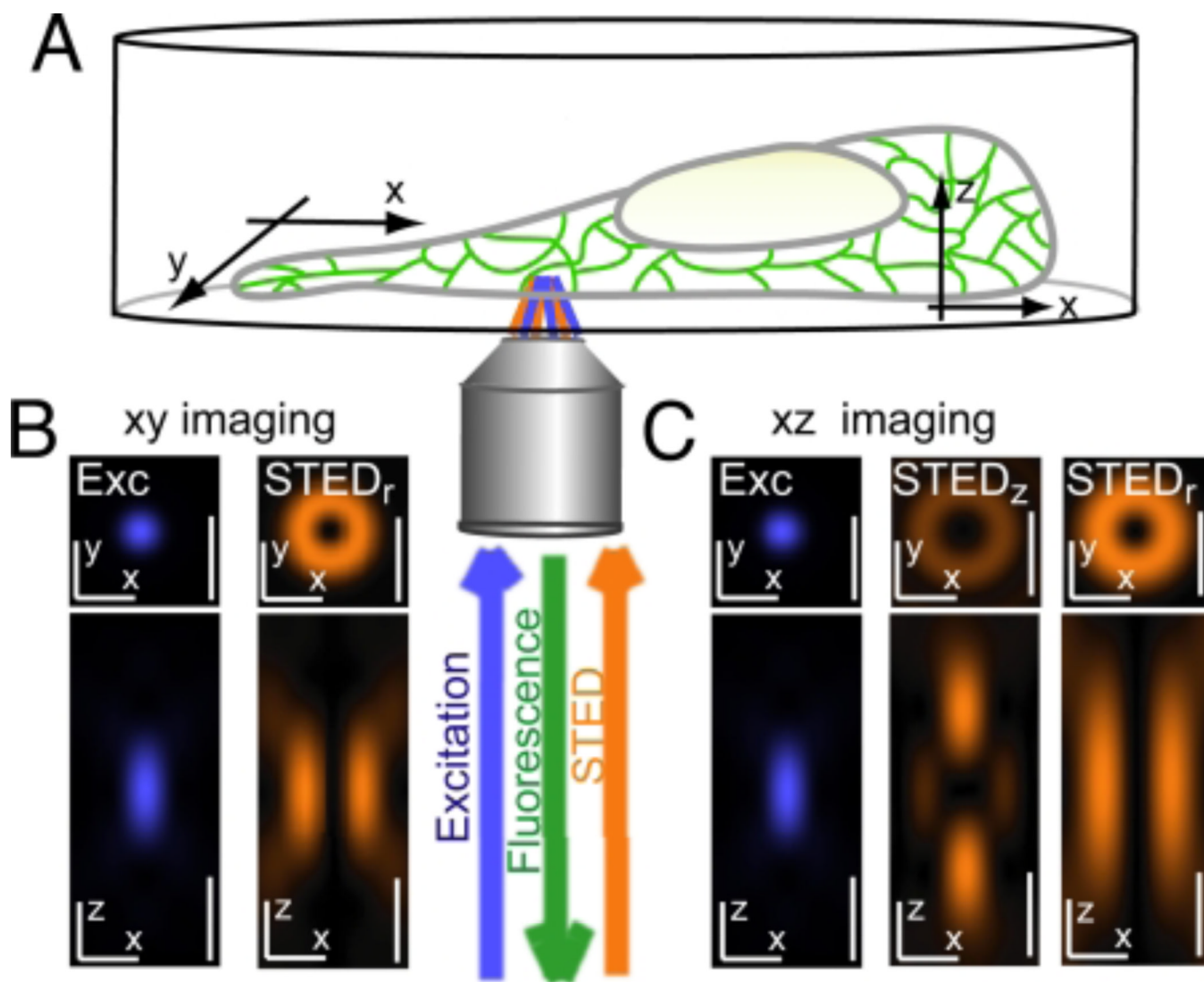
Figure 6. Schematic of 3D-STED imaging of a live cell
A. The excitation and STED beams are focused onto the cell while simultaneously collecting fluorescence. **B**. Excitation and STED beam profiles used in xy-imaging. **C**. Excitation and STED beam profiles used in xz-imaging. Two STED beams are needed both above and below the focal plane to ensure increased resolution. Additional information reported in Figure 1 from reference 203. Reprinted with permission from Reference 203. Copyright 2008 National Academy of Sciences, USA.
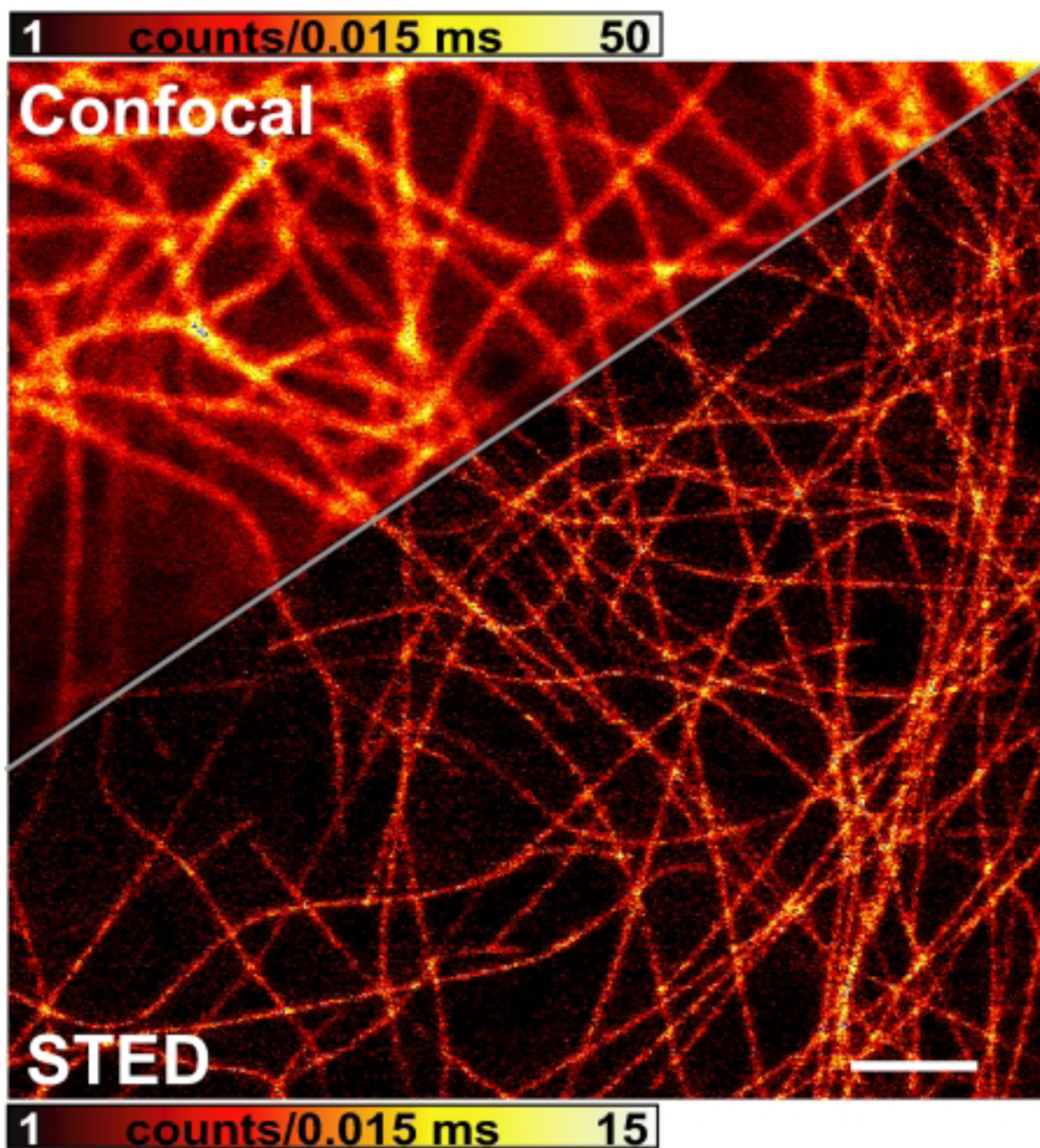
Figure 7. STED imaging of citrine-labeled microtubules
STED provided lateral resolution of 60 nm inside the living cells. This is compared to a
confocal fluorescence microscopy image from the same sample. Other conditions are
reported in Figure 5 from reference 203. Reprinted with permission from Reference 203.
Copyright 2008 National Academy of Sciences, USA.
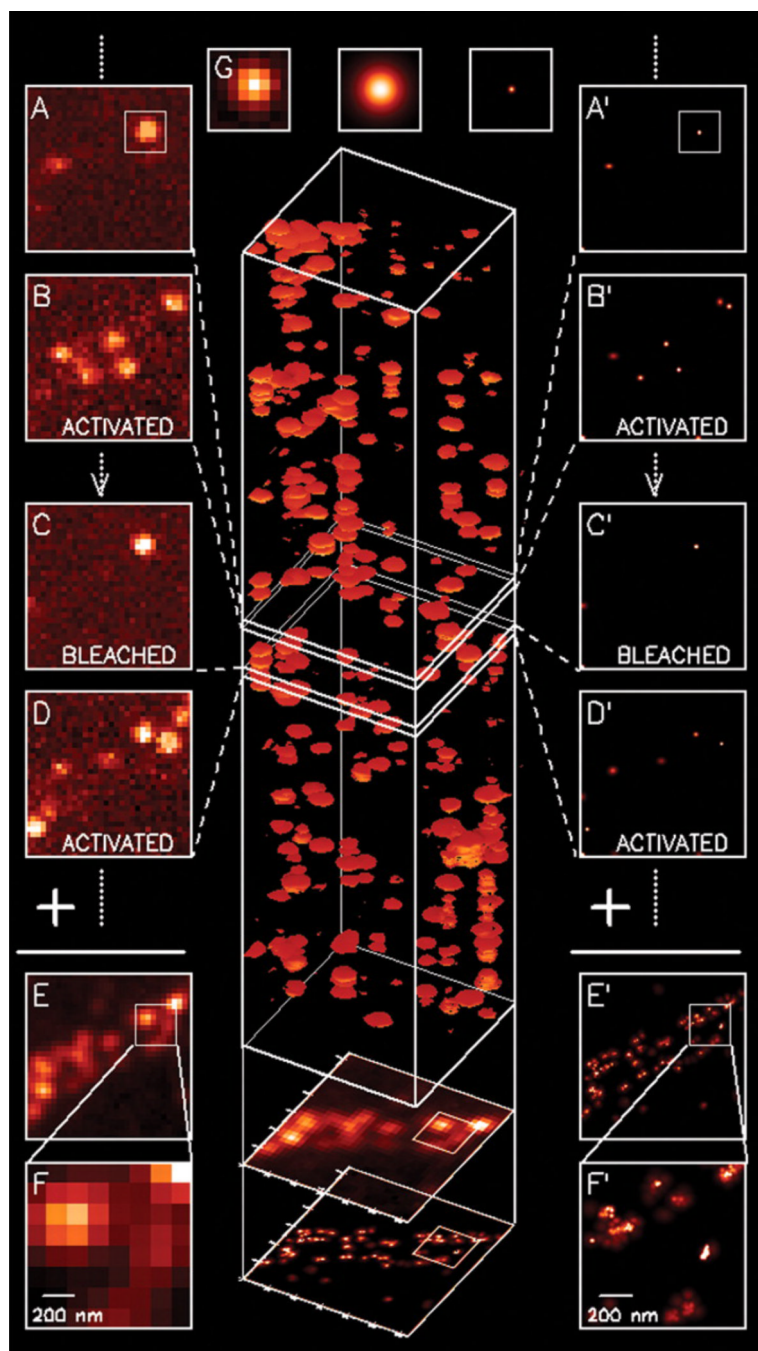
Figure 8. Schematic of FPALM

(A-D) Photo-activatable fluorescent molecules bound to proteins of interest are activated and imaged repeatedly until bleached. The images are combined or summed to provide a diffraction-limited image. (A'-F')-This process can be done for all fluorescent molecules in all microscopy frames to provide a superresolution image. Additional information reported in Figure 1 from reference 199. Reprinted with permission from Reference 199. Copyright 2006 Highwire Press.
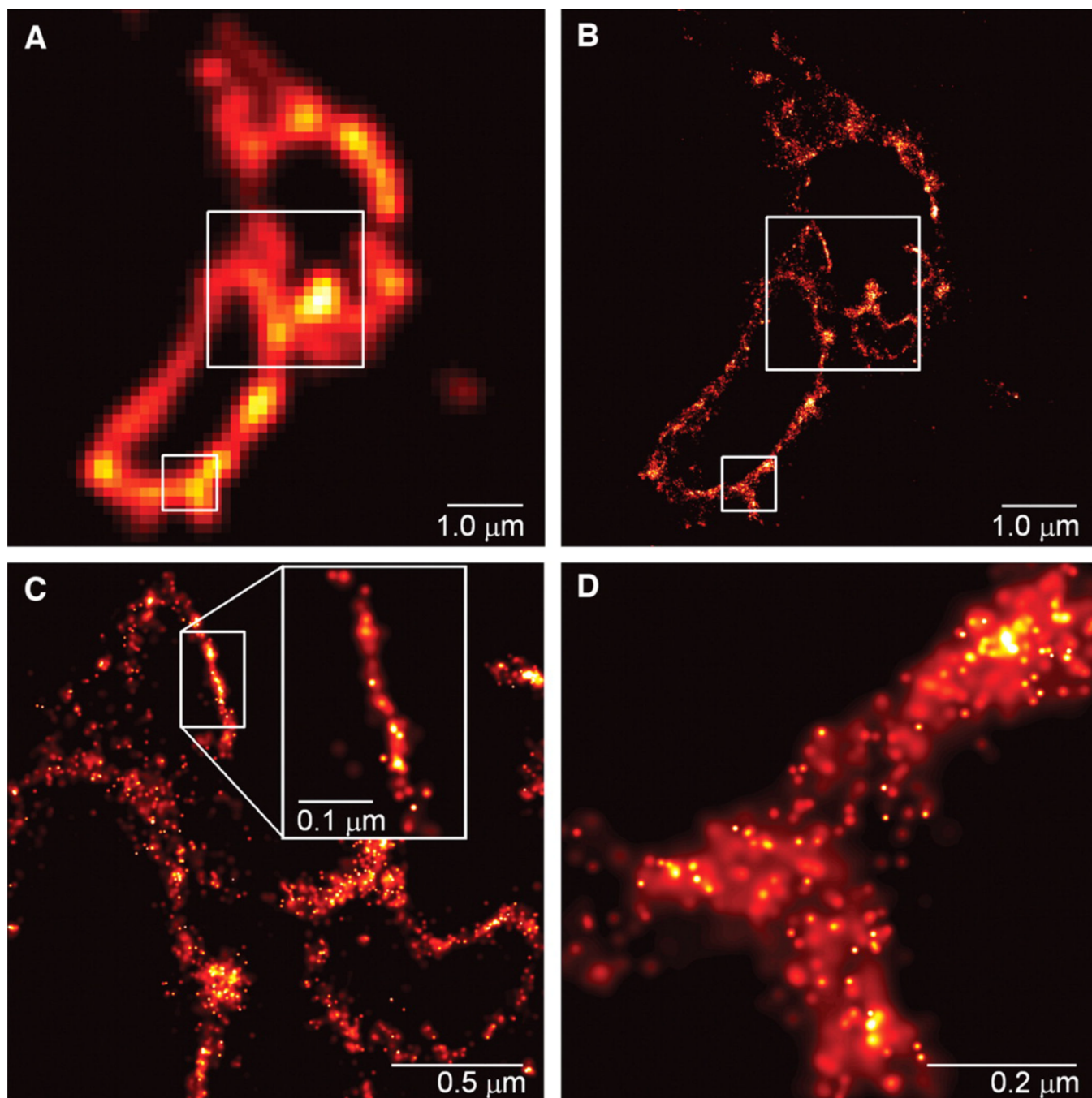
Figure 9. Comparing total internal reflectance fluorescence (TIRF) microscopy with photoactivation localization microscopy (PALM)
A. TIRF image. **B**. PALM image. **C**. Magnification of large box of 'B' has sufficient resolution to observe interacting membranes. **D**. Magnification of small box of 'B' showed the distribution of CD36. Other conditions are reported in Figure 2 from reference 199. Reprinted with permission from Reference 199. Copyright 2006 Highwire Press.
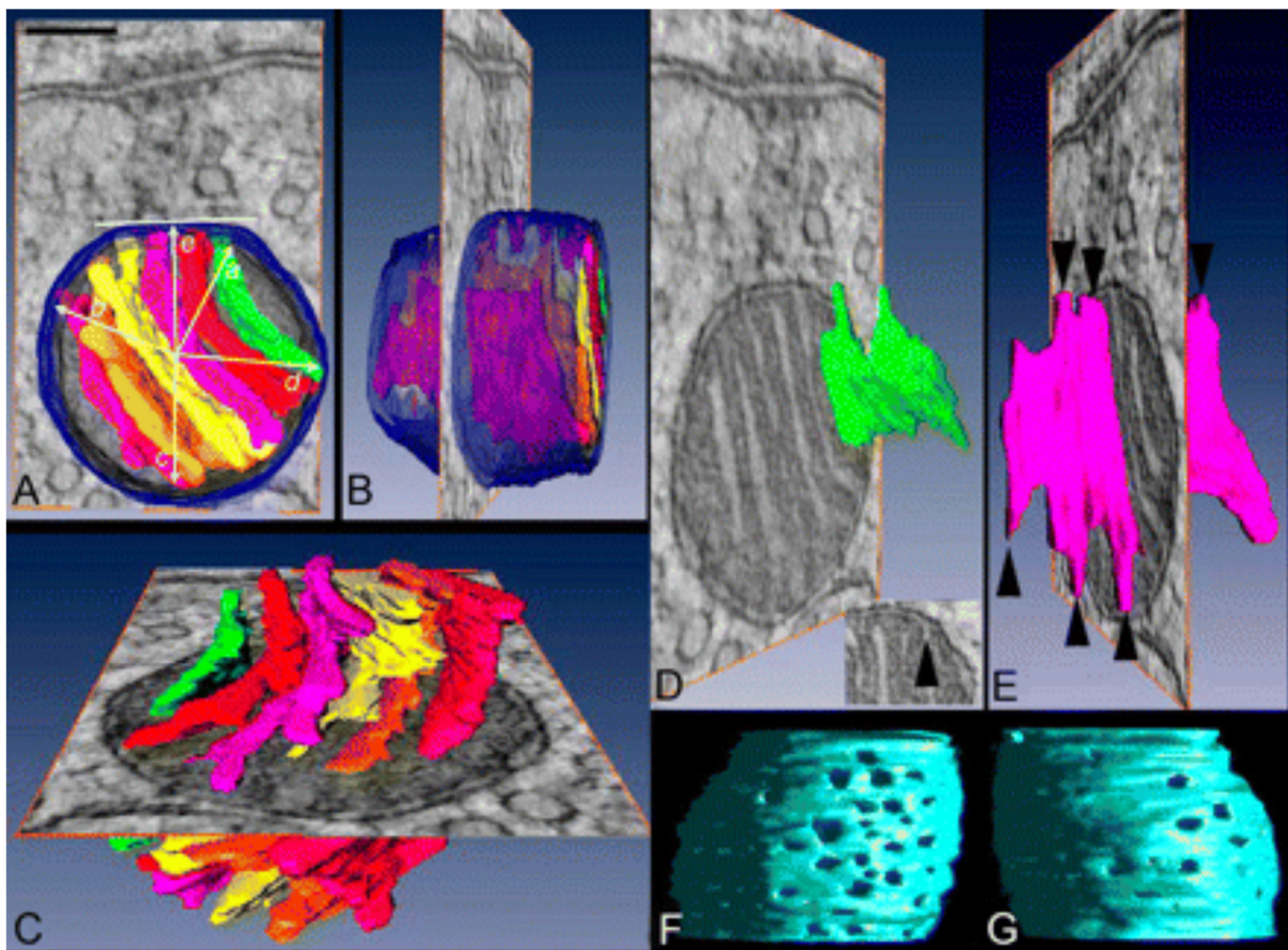
Figure 10. Mitochondrion-associated adherens complex observed by transmission electron tomography

A-E. Different views of Mitochondrion-associated adherens complex. The outer mitochondria membrane is shown in dark/translucent blue with each individual cristae colored differently. Mitochondrion-associated adherens complex have individual lamellar cristae with fingers that connect to the sides of the mitochondria through cristae junctions. **F-G**. The inner mitochondrial membrane with visual distinct cristae junctions. Scale bar is 100 nm. Other conditions are reported in Figure 2 from reference 226. Reprinted with permission from Reference 226. Copyright 2010 Society for Neuroscience.
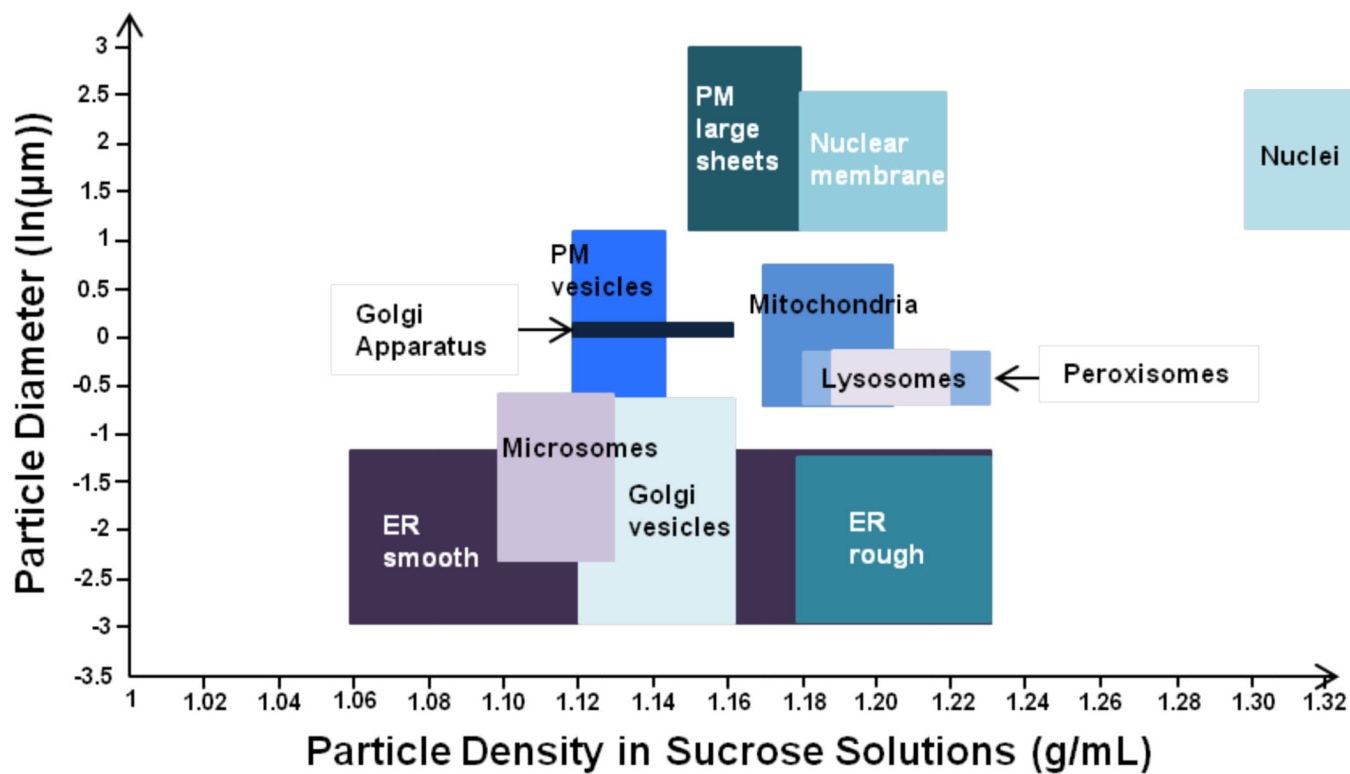
Figure 11. Dimensions of subcellular material prepared by centricollation
Other conditions are reported in Figure 12.3 from reference 270. Reprinted with permission
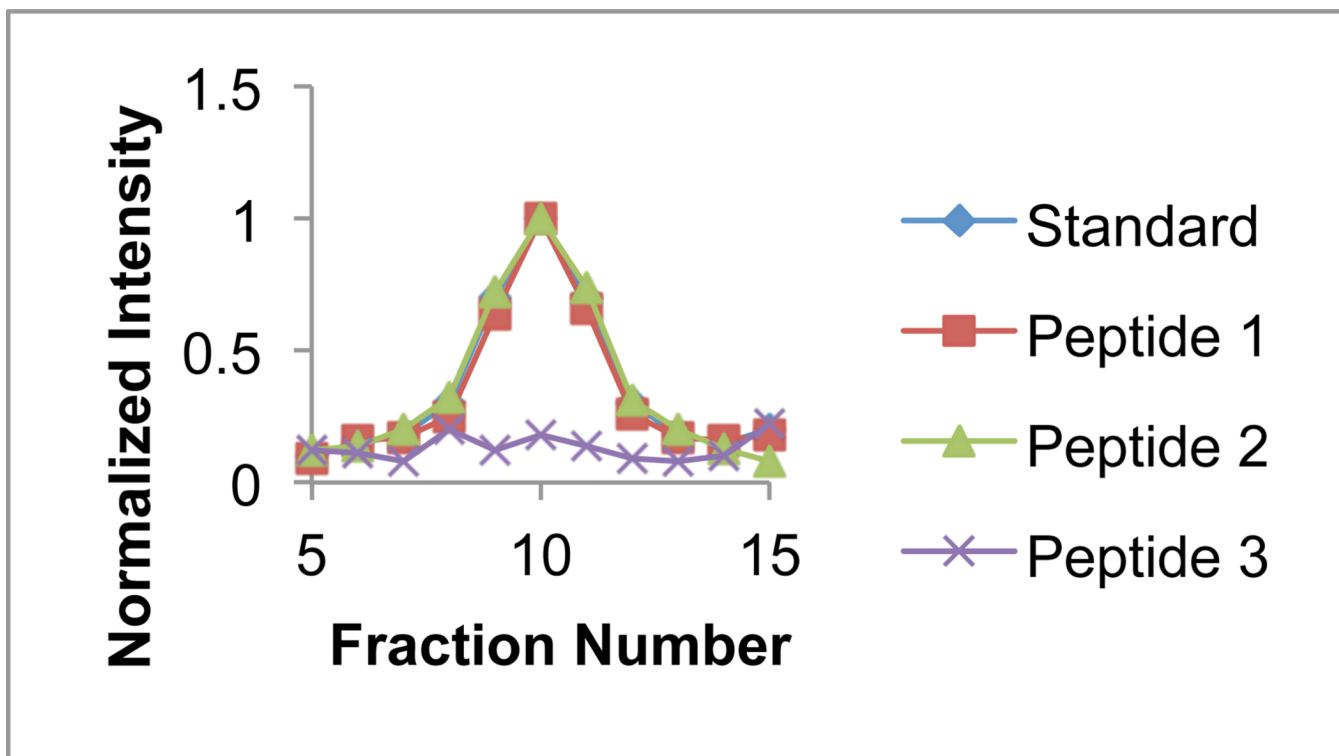from Reference 270. Copyright 2011 Springer Science and Business Media B.V.

Figure 12. Protein Correlation Profiling of a theoretical protein
The "standard" represents what would be a consensus profile, i.e. the profile of proteins known to belong to a given organelle or subcellular component in sucrose density gradient fractions. Peptides 1 and 2 would likely belong to proteins associated with that organelle/ subcellular component while peptide 3 likely belongs to a contaminating protein. For example, if the consensus profile was for a peptide of the LAMP 2 protein, peptides 1 and 2 would correlate with the lysosome. Other conditions are reported in Figure 3 from reference 292a. Adapted with permission from reference 292a. Copyright 2003 Macmillan Publishers Ltd.
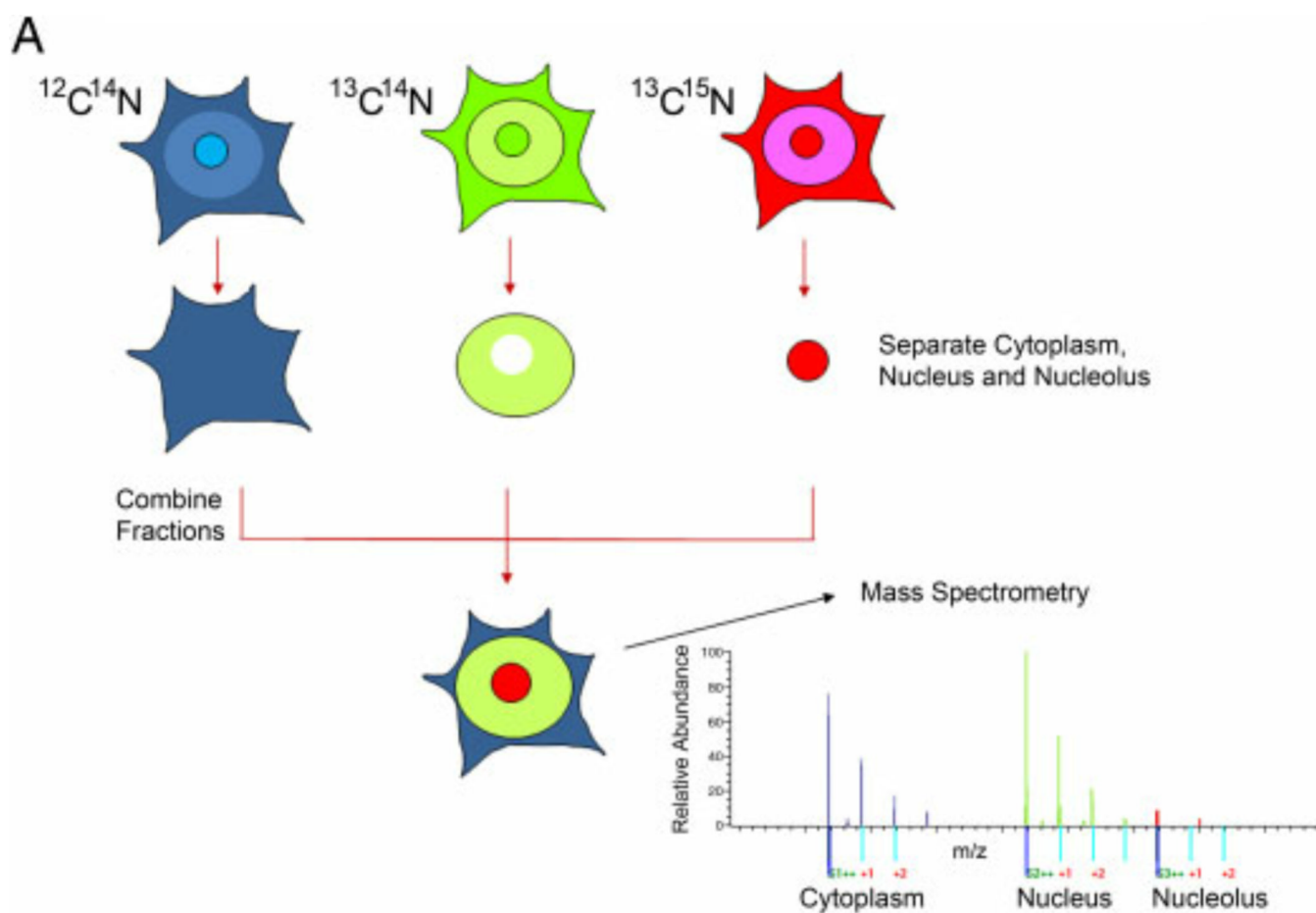
Figure 13. Workflow for Spatial Proteomics
(1) Cells are SILAC labeled in light, medium, or heavy media. (2) Nuclear, nucleolar, and cytoplasmic fractions are isolated from each culture via sucrose density gradient centrifugation. (3) Fractions from each of the cultures are recombined (equal protein amounts) to recreate a whole cell extract containing a subcellular fraction (nuclear, nucleolar, and cytoplasmic) from each of the isotopically labeled cultures. (4) Samples are run on an SDS-PAGE gel and in-gel digested with trypsin. (5) Samples are subjected to LC-MS/MS analysis. Other conditions were reported in Figure 1 from reference 297b. Reprinted with permission from Reference 297b. Copyright 2010 John Wiley and Sons.
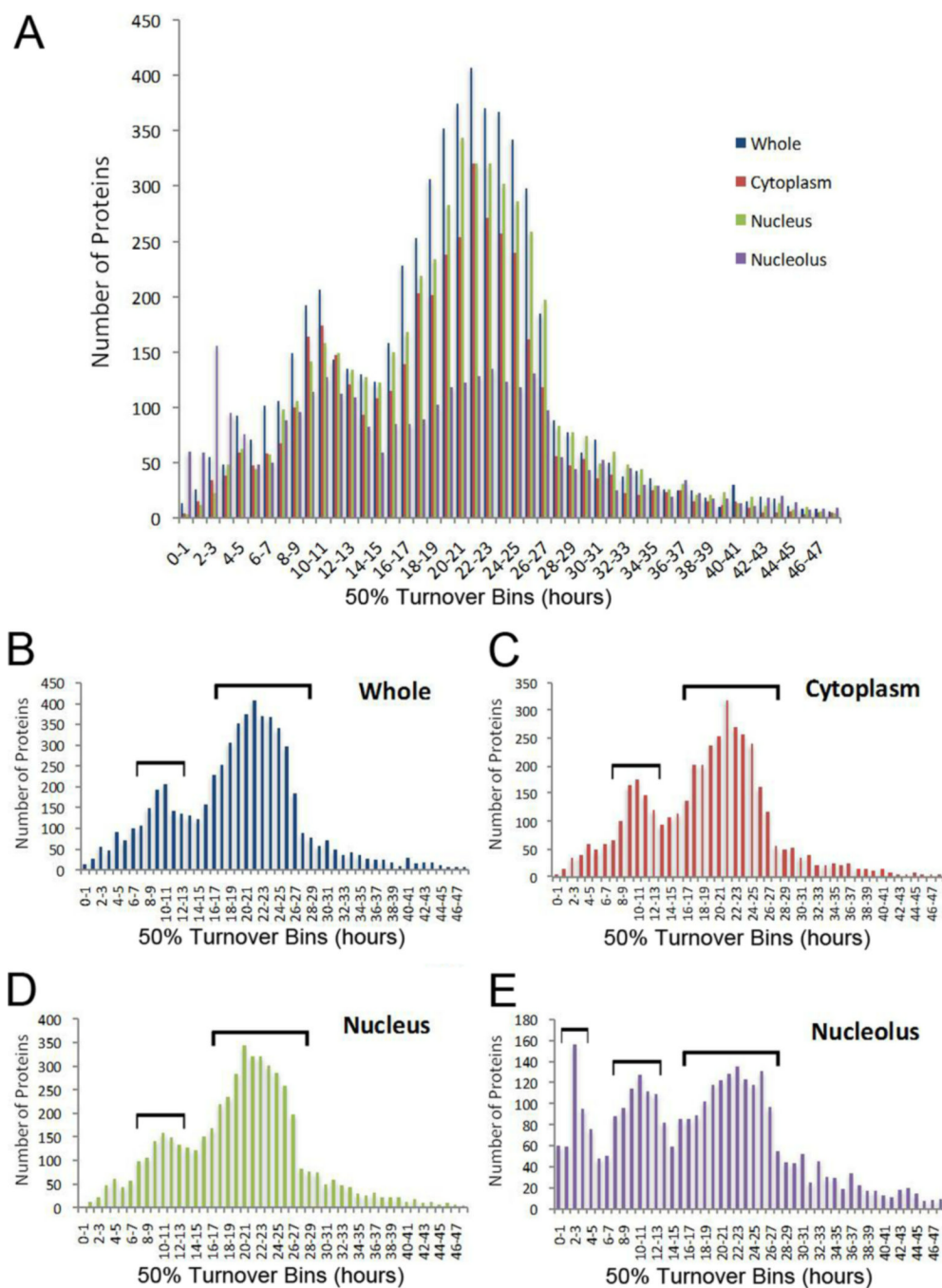
Figure 14. Visualization of protein turnover using PepTracker software
A. Overall of all subcellular fractions. **B**. Whole cell. **C**. Cytosol. **D**. Nucleus. **E**. Nucleolus. The plots show the number of proteins with 50% turnover in each bin (1 bin = 1 hour) The data illustrates that the 50% turnover rates have a bimodal distribution at around 10 and 20 hours in the cytoplasmic and nuclear fractions, with the majority of the 50% turnover at 20 hours. The nucleolar fraction has an additional turnover peak at <6 hours, illustrating a subpopulation of nucleolar proteins that turnover quite rapidly. In addition, the major peak in the nucleolar fraction occurs slightly later around 22–33 hours. Other conditions were

reported in Figure 5 from reference 297b. Reprinted with permission from Reference 297b. Copyright 2010 John Wiley and Sons.
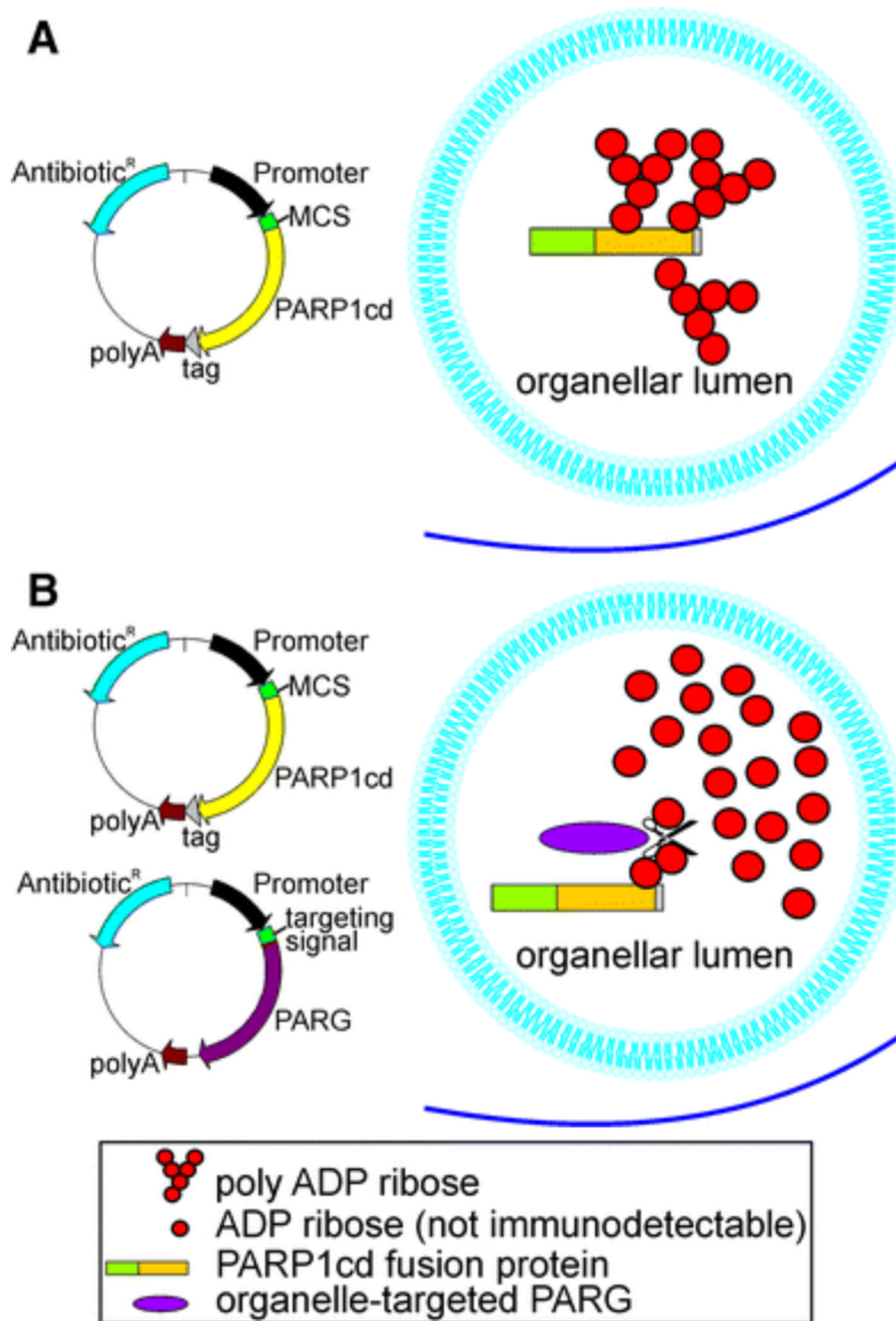
Figure 15. Schematic of the poly-ADP-ribose polymerase assay for visualization of NAD+
A. If NAD+ is present in an organelle, poly-ADP-ribose polymerase will synthesize poly-ADP-ribosee and will be immunodetected. **B**. The enzyme poly-ADP-ribose glycohydrolase can be used to specifically hydrolyze poly-ADP-ribose and confirm fluorescence accumulation in the organelle. Additional information reported in Figure 4 from reference 304. Reprinted with permission from Reference 304. Copyright 2010 Springer.
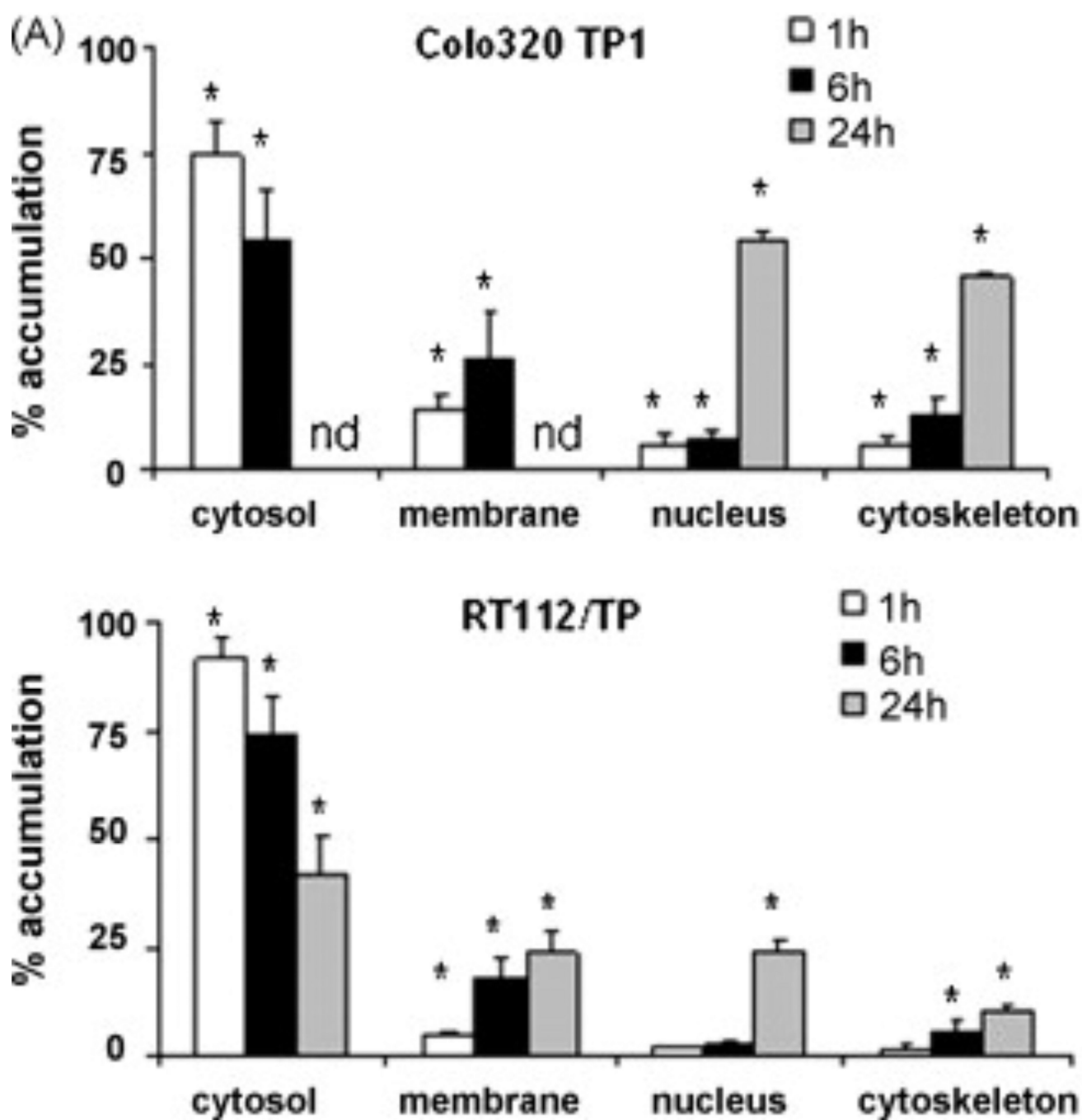
Figure 16. Localization of thymidine derived sugars in enriched subcellular fractions
A. Localization in Colo320 TP1 cells treated with tritium-labeled thymidine derived sugars.
B. Colocalization in RT112/TP cells treated with tritium-labeled thymidine derived sugars.
Values are mean ± standard error of the mean. nd = not detected. Other conditions are
reported in Figure 4 from reference 330. Reprinted with permission from Reference 330.
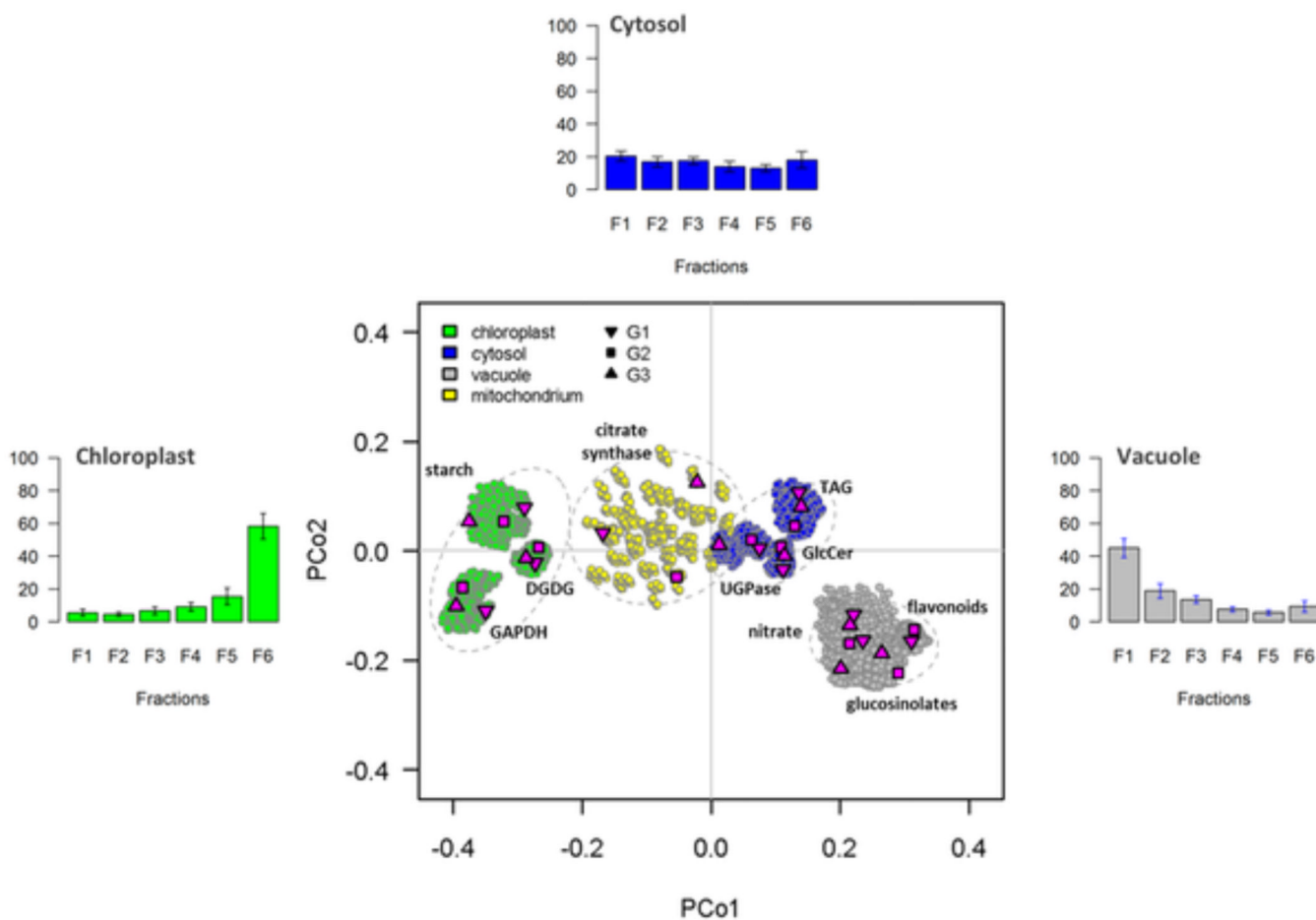Copyright 2010 Elsevier.

Figure 17. Visualization of metabolites in enriched subcellular fractions from *A. thaliana* leaves
The three bar graphs show the relative abundance of organelle markers in each fraction.
These markers are: glyceraldehyde 3-phosphate dehydrogenase (GAPDH) for chloroplasts,
cytosol uridine diphosphate (UDP)-glucose-pyrophosphorylase (UGPase) for cytosol, and
nitrate for vacuole nitrate.. The graph in the middle shows a plot of the first two principal
components in which metabolites are grouped within regions associated with several
organelle markers. Other descriptions and conditions are described in Figure 4 from
reference 306. Reprinted with permission from Reference 306. This is an open-access article
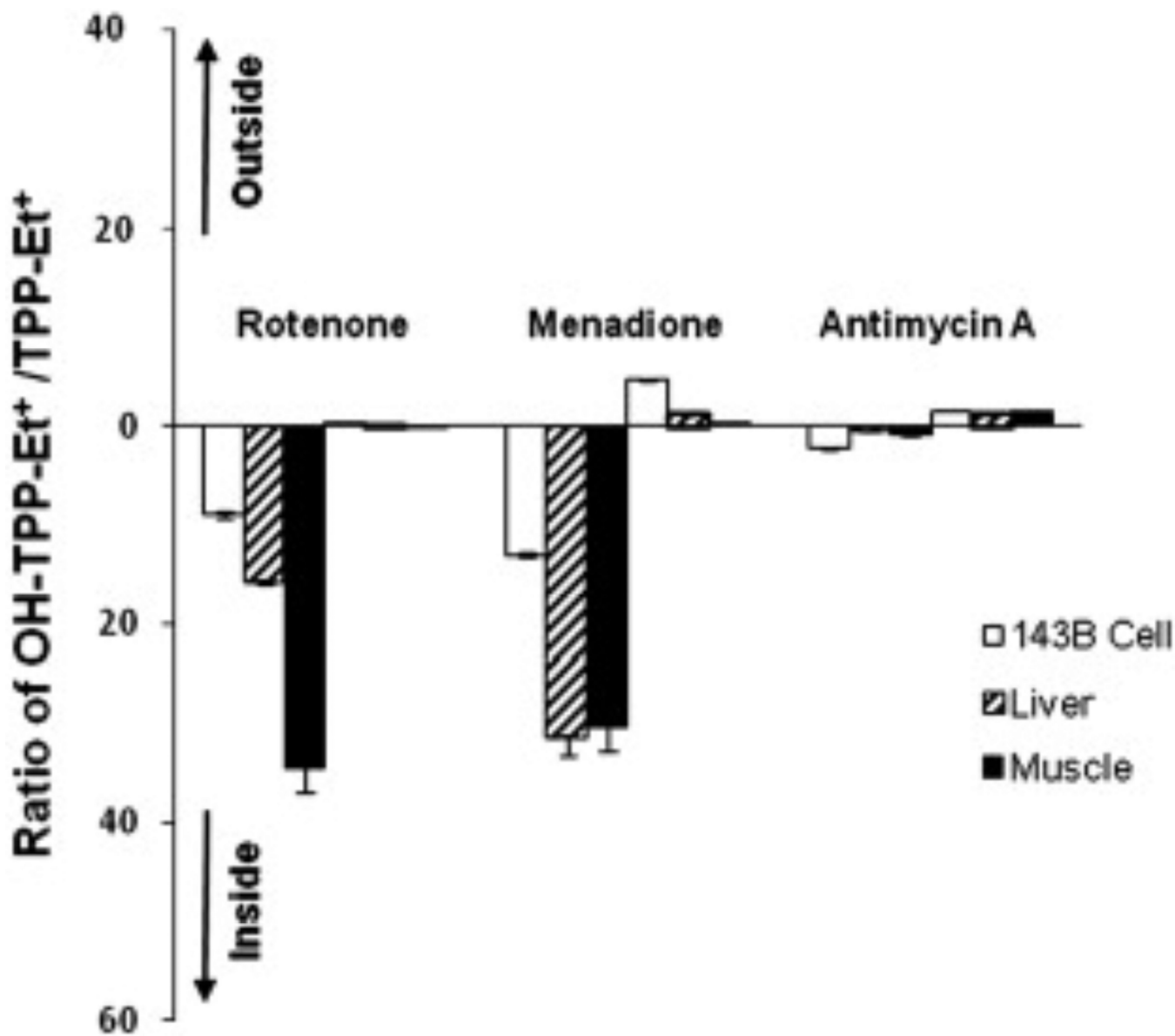distributed under the terms of the Creative Commons Attribution License.

Figure 18. Superoxide-specific and superoxide-independent oxidation in mitochondria from different biological tissues
The bars oriented above x=0 represent MitoSox Red oxidation outside of the inner membrane and the bars oriented below x=0 represent MitoSox Red oxidation in the mitochondrial matrix. Other conditions are reported in Figure 7 from reference 156. Reprinted with permission from Reference 156. Copyright 2009 Elsevier.
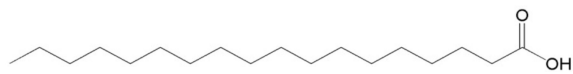
LMFA01010018; Fatty Acyls (FA); ocatdecanoic acid;
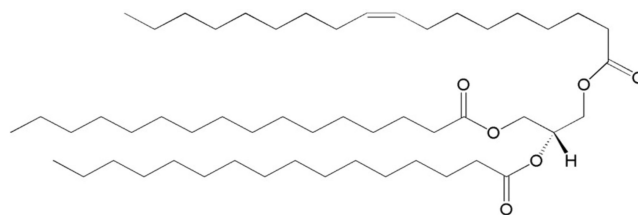
LMGL03010006; Glycerolipid (GL);
1,2-hexadecanoyl-3-(9Z-octadecenoyl)-*sn*-glycerol
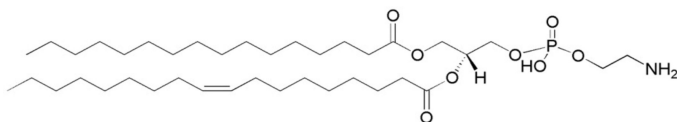
LMGP02010009; Glycerophospholipids (GP);
1-hexadecanoyl-2-(9Z-octadecenoyl)-*sn*-glycero-3-phosphoethanolamine
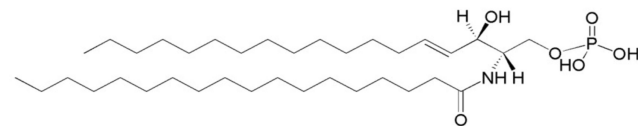
LMSP02050004; Sphingolipids (SP);
N-(octadecanoyl)-sphing-4-enine-1-phosphate
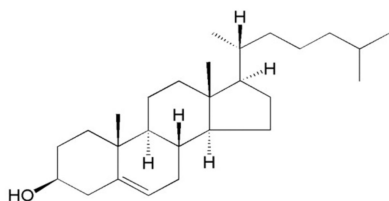
LMST01010001; Sterol Lipids (ST); cholest-5-en-3β-ol
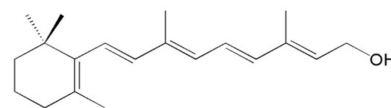
LMPR01040001; Prenol Lipids (PR); Retinol
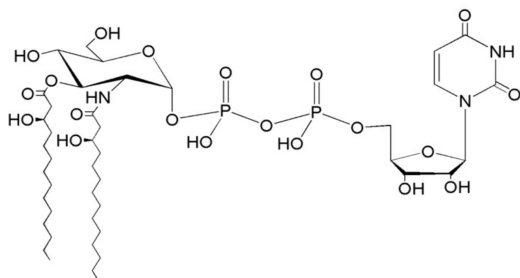
LMSL01020002; Saccharolipids (SL);
UDP-2,3-bis-(3R-hydroxy-tetradecanoyl)-αD-glucosamine
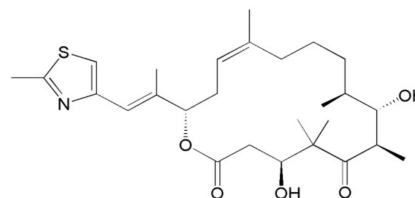
LMPK03000001; Polyketides (PK); epothilone D

Figure 19. Lipid classes as determined by Lipid MAPS
Additional information reported in Figure 1 from reference 322. Reprinted with permission from Reference 322. Copyright 2007 Oxford University Press.
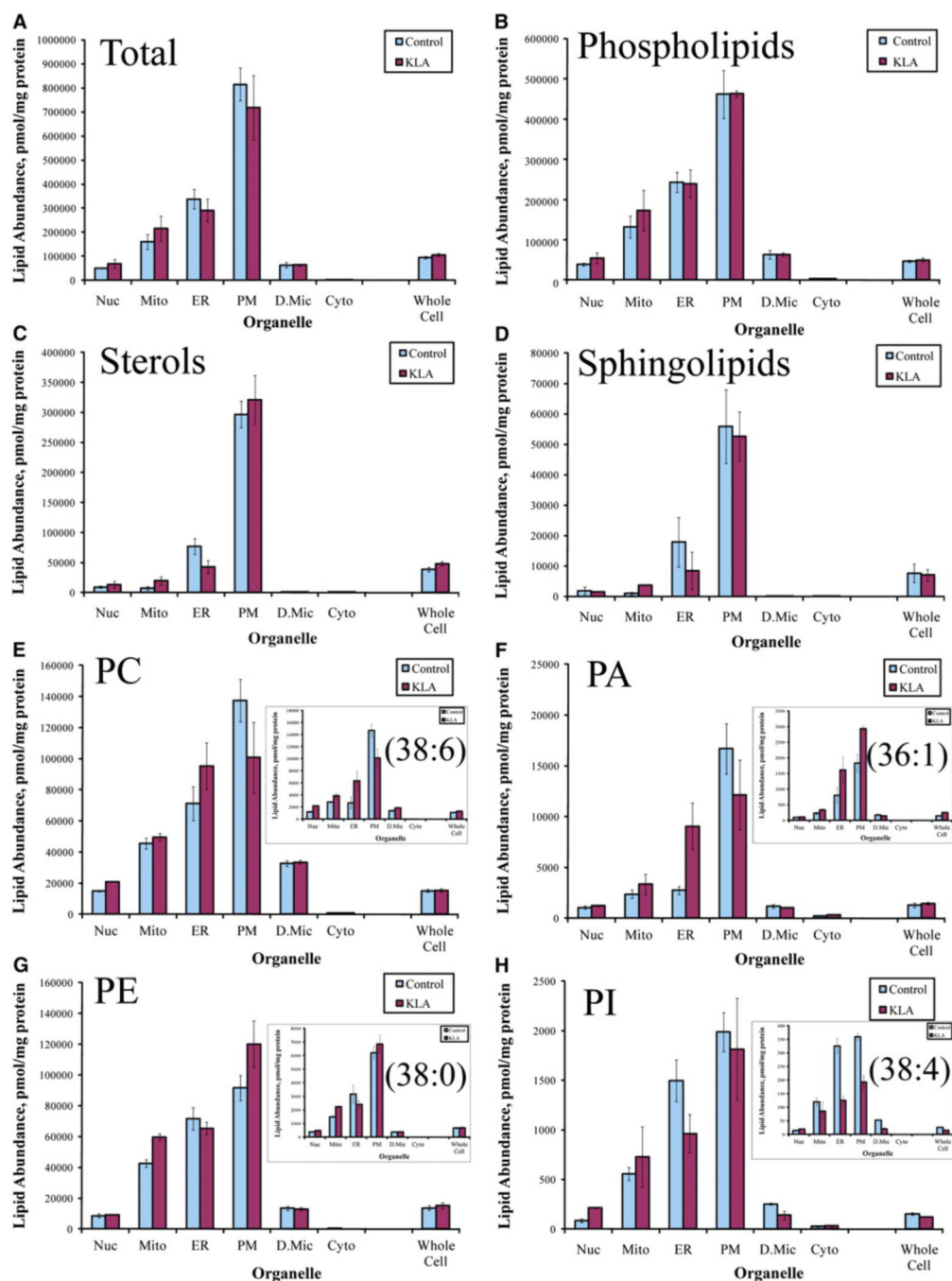
Figure 20. Distribution of lipids in enriched subcellular fractions of RAW264.6 macrophages
When macrophagy was triggered, enriched subcellular fractions had modified distributions of lipids. Kdo$_2$-lipid A (KLA) was used to stimulate subcellular signaling cascades. Nuc = nuclear, Mito = mitochondria, ER = endoplasmic reticulum, PM = plasmalemma, D. Mic = dense microsome, Cyto = cytoplasm, PC = phosphatidylcholine, PA = phosphatidic acid, PE = phosphatidylethanolamine, PI = phosphatidylinositol. Values are mean ± SE, n=3. Other conditions are reported in Figure 2 from reference 343. Reprinted with permission from Reference 343. Copyright 2010 American Sociery for Biochemistry and Molecular Biology Inc.
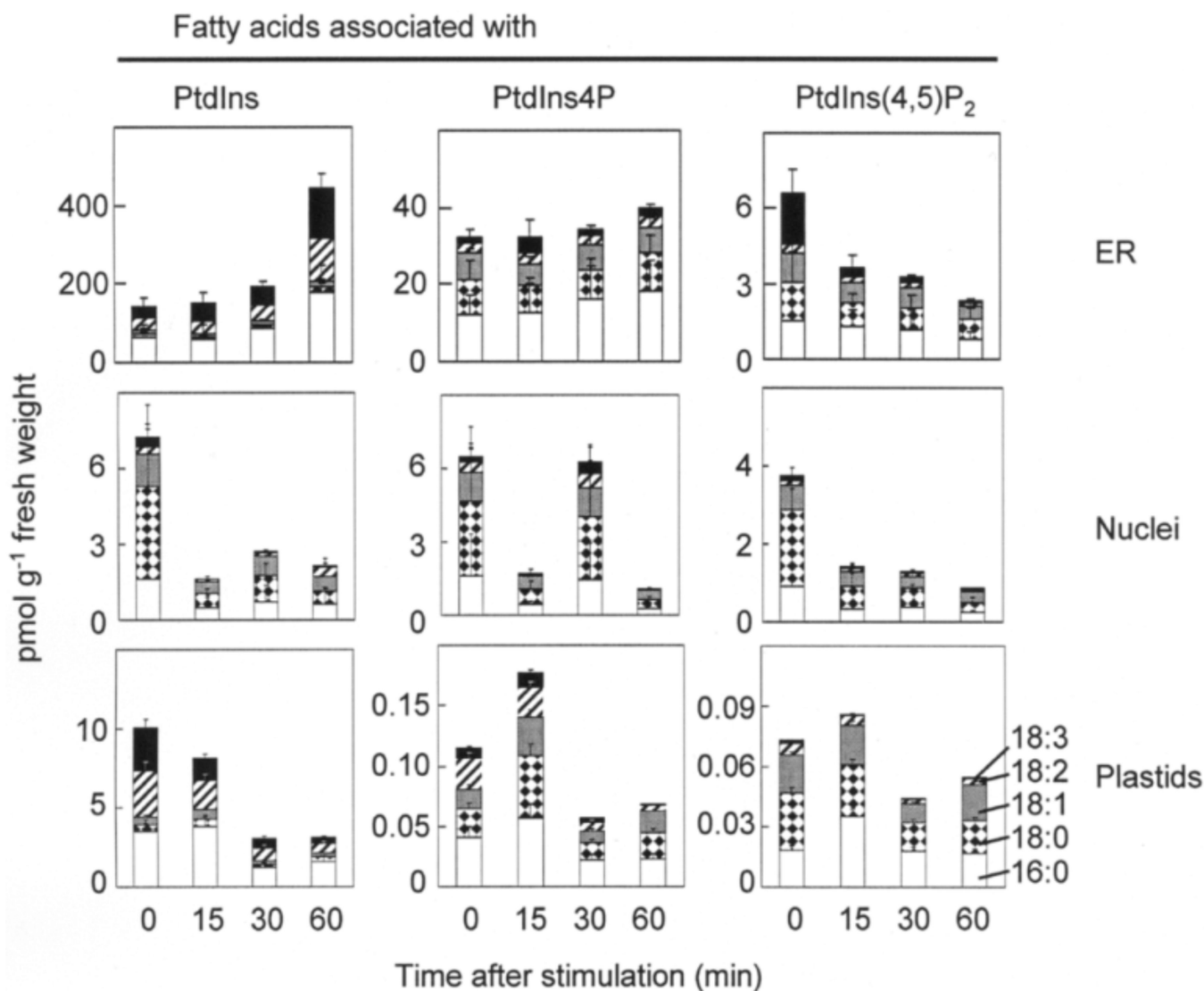
Figure 21. Phosphoinositols in endoplasmic reticulum, nuclei, and plastid enriched from *A. thaliana* leaves
Leaves were exposed to hyperosmotic stress prior to fractionation to determine changes in lipid expression. Each bar is composed of several lipids (e.g. 18:3, 18:2, 18:1, 18:0, and 16:0). PtdIns = phosphatidylinositol, PtdIns4P = phosphatidylinositol 4-phosphate, PtdIns(4,5)P$_2$ = phosphatidylinositol 4,5-bisphosphate, ER = endoplasmic reticulum. Bars are means ± S.D. n=3–5. Other conditions are reported in in Figure 5 from reference 345. Reprinted with permission reference 345. Copyright 2007 The Biochemical Society.
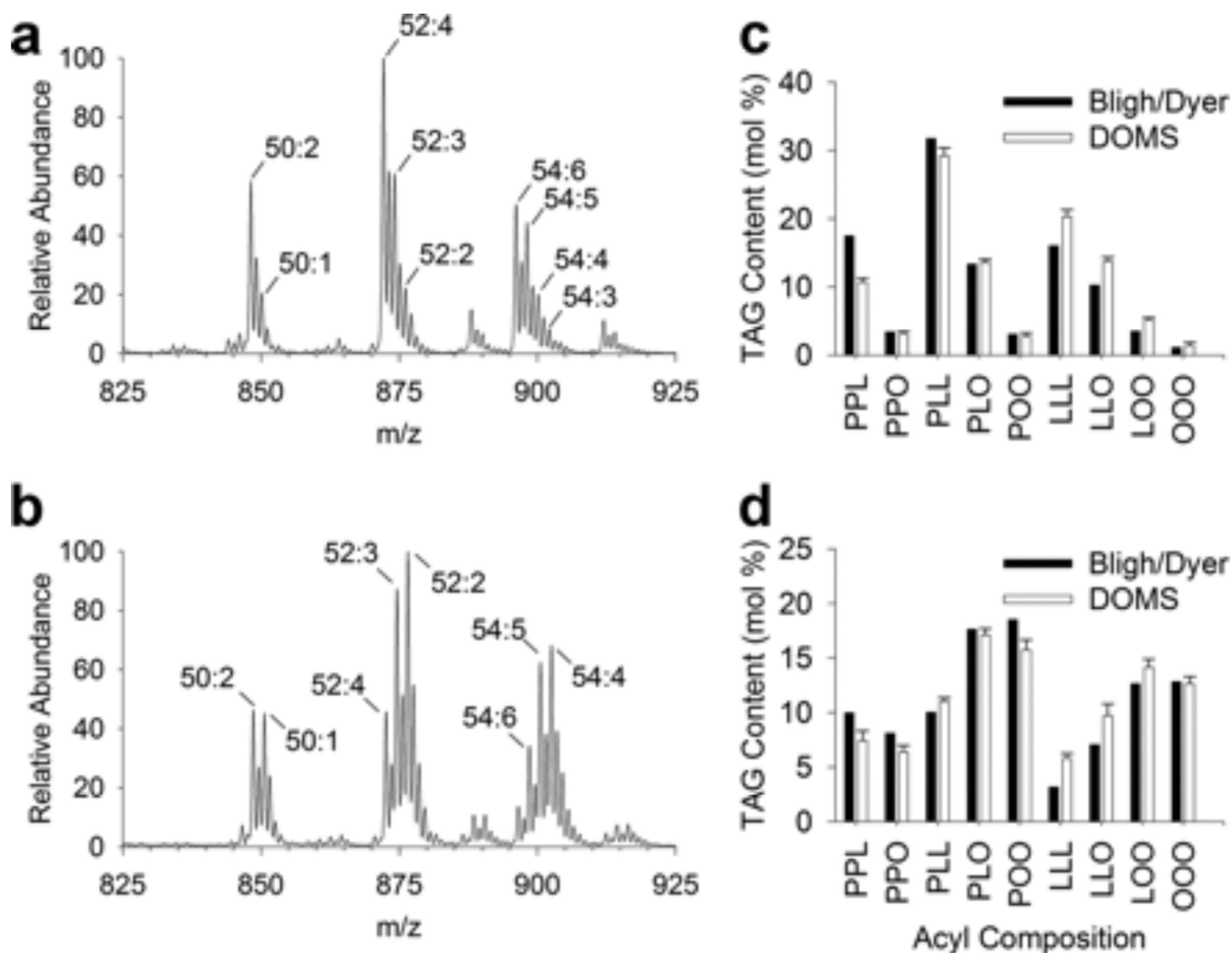
Figure 22. Analysis of enriched lipid droplets with direct organelle mass spectrometry
A. Mass spectra of triacylglycerols from Coker 312 wild type cotton embryos. **B**. Bn*fad2*
embryos. **C**. Triacylglycerol distribution of wild type using direct organelle mass
spectrometry (DOMS) or the Bligh/Dyer lipid extraction. **D**. Triacylglycerol distribution of
Bn*fad2* in DOMS and the Bligh/Dyer lipid extraction. For C-D., n = 10–25 lipid droplets. P
= 16:0-palmitic acid, O = 18:1-oleic acid, L = 18:2-linoleic acid. Three letter code
abbreviations represent the three fatty acids bound to a triacylglyceride (TAG). Other
conditions are reported in Figure 4 from reference 354. Reprinted with permission from
Reference 354. Copyright 2011 American Society for Biochemistry and Molecular Biology,
Inc.
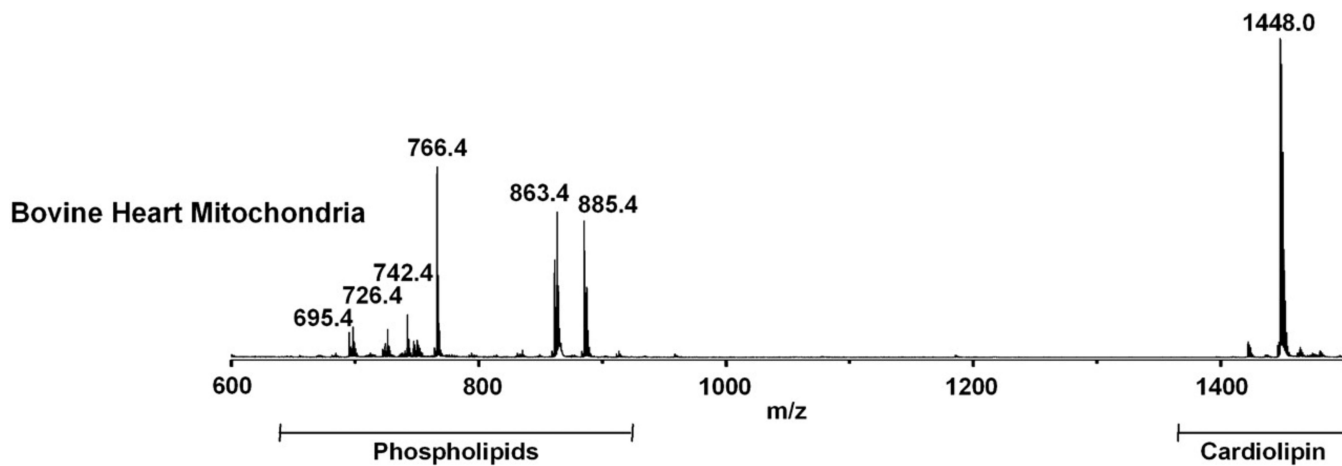
Figure 23. MALDI-TOF mass spectrum of enriched mitochondria from bovine heart
Phosphatidic acid (m/z 695.4), phosphatidylserine (m/z 726.4), phosphatidylethanolamine (m/z 742.4 and 766.4), phosphatidylinositol (m/z 863.4 and 885.4), and cardiolipin (m/z 1448.0) are all shown. Other conditions are reported in Figure 1 from reference 362. Reprinted with permission from reference 362. Copyright 2012 The American Society for Biochemistry and Molecular Biology, inc.
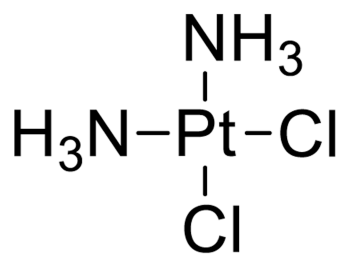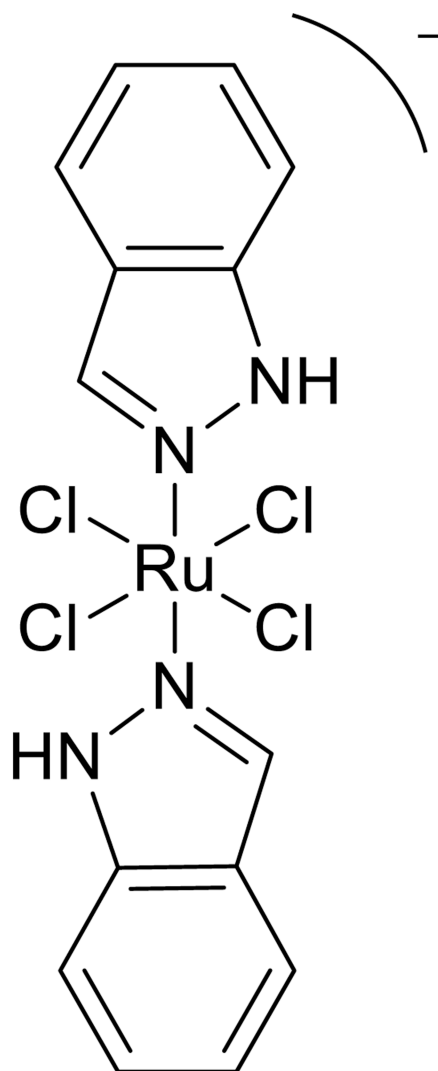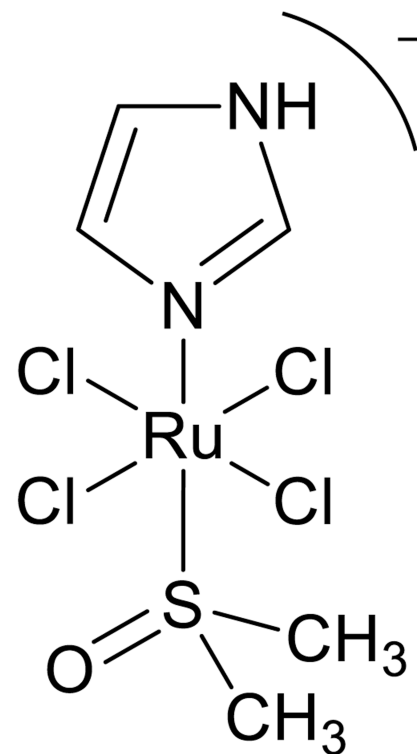
Figure 24. Ruthenium and platinum drugs
For more information on these compounds, see reference 371.
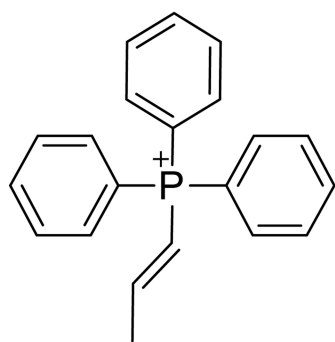
TP187
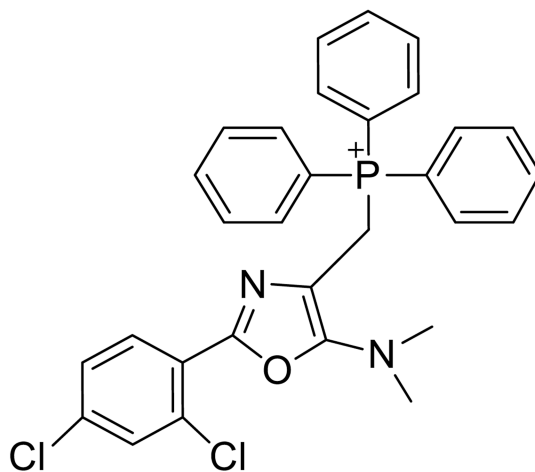
TP197
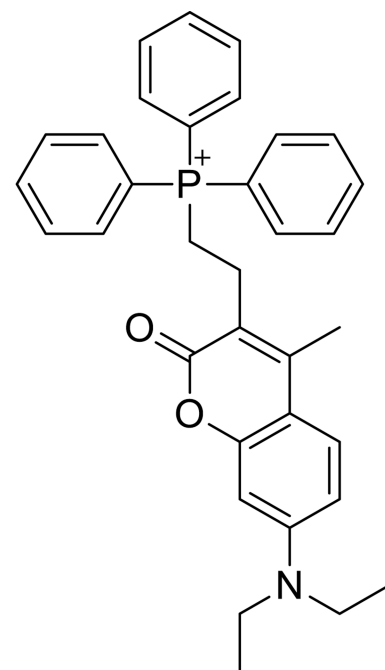
TP421

Figure 25. Triphenylphosphonium compounds
For more information on these compounds, see reference 372.
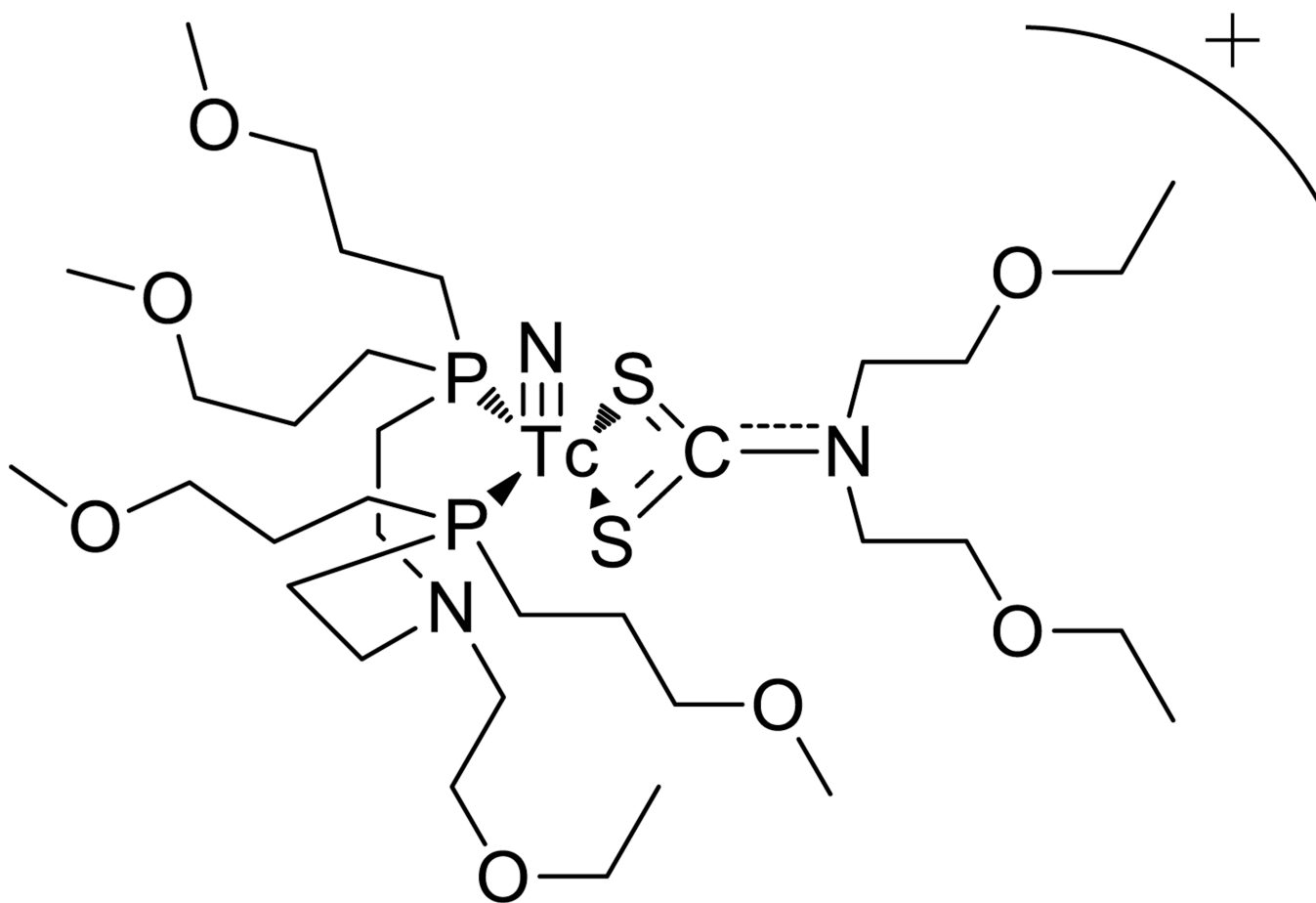
$$^{99m}\text{Tc(N)-DBODC(5)}$$

Figure 26. Technetium-based imaging agents
For more information on these compounds, see reference 377.
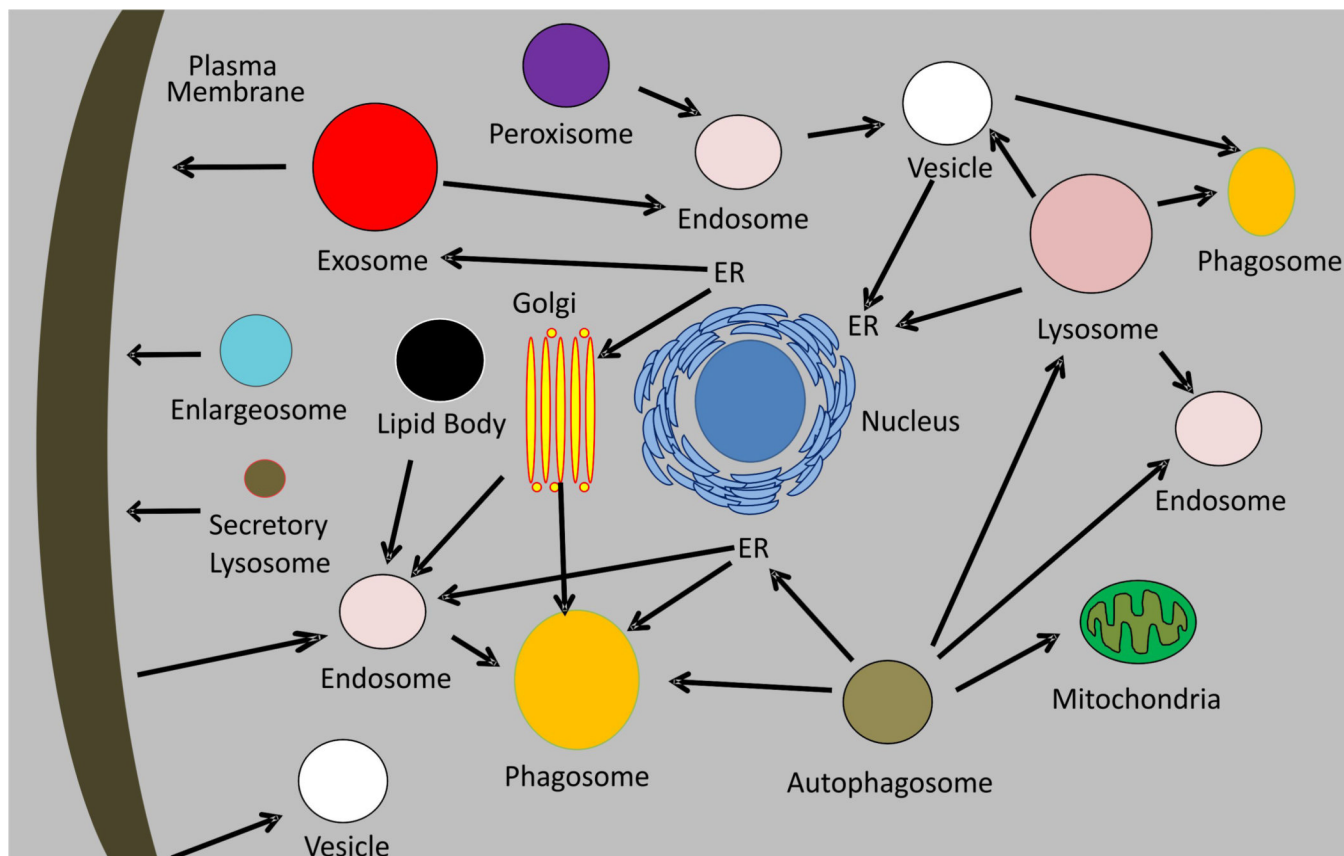
Figure 27. Organelle interactions mentioned in this review
Organelles are not to scale.
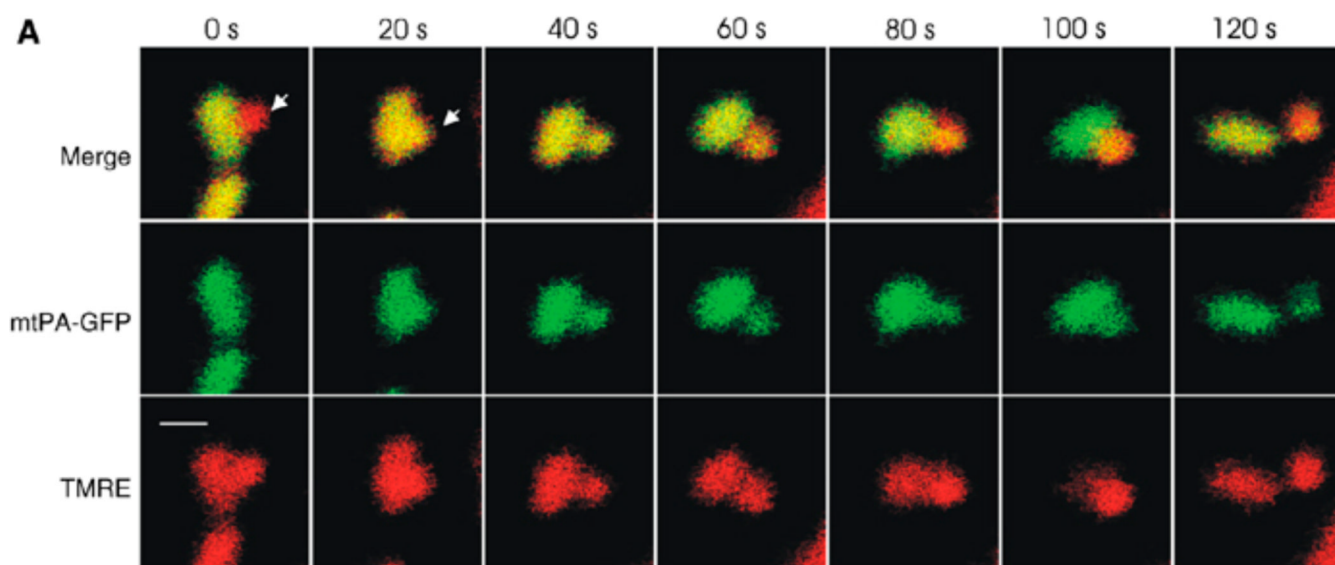
Figure 28. Live imaging of fusion and fission of mitochondria
Inside an INS1 cell, a mtPA-GFP labeled mitochondrion (green) is fusing with a tetramethylrhodamine (TMRE) labeled mitochondrion (red). Fusion occurs in the frame labeled 20 s, mitochondria exchange contents and fission becomes apparent in the frame labeled 60 s. Scale bar, 2 μm. Other conditions are reported in Figure 2 from reference 396. Reprinted with permission from reference 396. Copyright 2008 Macmillan Publishers Ltd.

Figure 29. Cell fusion results in redistribution of fluorescently labeled respiratory complexes in the mitochondrial network

The images are examples of the outcome of cell fusion between cell sub-lines that express constructs of red fluorescent protein with Complexes III (CIII-R) or V (CV-R) or green fluorescent protein with Complexes I, II, III, or V (represented as CI-G, CII-G, CIII-G, or CIV-G, respectively. **Top**: Microscopy images. **Bottom**: Fluorescence intensities along the longitudinal axis of the mitochondrion indicated by a white arrow. The Pearson's cross correlation coefficient for the mitochondrion was determined from these data. **A**. Coexpression of CIII-R and CII-G five days after cell fusion. **B**. Coexpression of CV-R and CV-G five days after cell fusion. **C**. Coexpression of CV-R and CIII-G four hours after cell

fusion. **D**. Coexpression of CI-G and CV-R in mitochondria 4.5 hours after cell fusion. Some mitochondria display only CV-R fluorescence (arrow) because they did not fuse with CI-Gmitochondria. **E**. Coexpression of CI-G and CIII-R five hours after cell fusion. **F**. Coexpression of CI-G and mtDsRed (matrix localization). **G**. Progressive mixing of CI-G and CV-R reveal an increase in homogeneity with time due to ongoing fusion dynamics. **H**. Complex II mixes better with other complexes in co-expressing cells than complex I and V, respectively. Other conditions were reported in Figure5 from reference 394. Reprinted from reference 394. This is an open-access article distributed under the terms of the Creative Commons Attribution License. No Copyright form was needed.
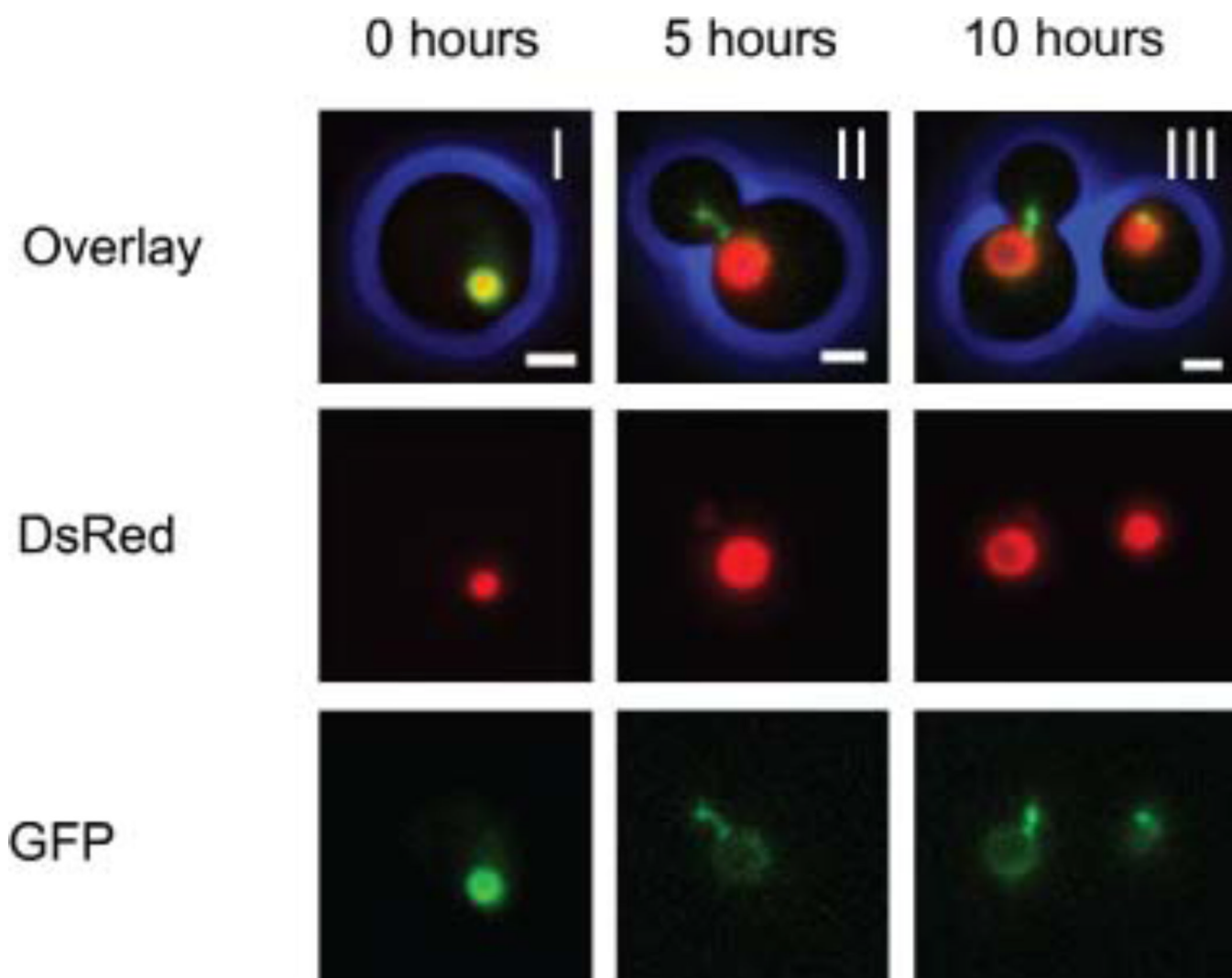
Figure 30. Imaging of peroxisome extension in budding yeast *Hansenula polymorpha*
Cells express the fluorescent constructs Pex25-eGFP and DsRed-SKL of the respective peroxisomal proteins Pex25 and SKL. Precultivated on methanol medium supplemented with methylamine induced synthesis of these proteins. **I**. After 5 h of induction, the cells were shifted to methanol medium with ammonium sulfate to repress the PAMO that controls Pex25-eGFP expression (I). **II**. Five hours after the shift and **III**. Ten hours after the shift Pex25-eGFP is still present at the organelle elongation. Scale bar: 1 μm. Other conditoins were reported in Figure 3 from reference 401. Reprinted with permission from Reference 401. Copyright 2011 John Wiley and Sons.
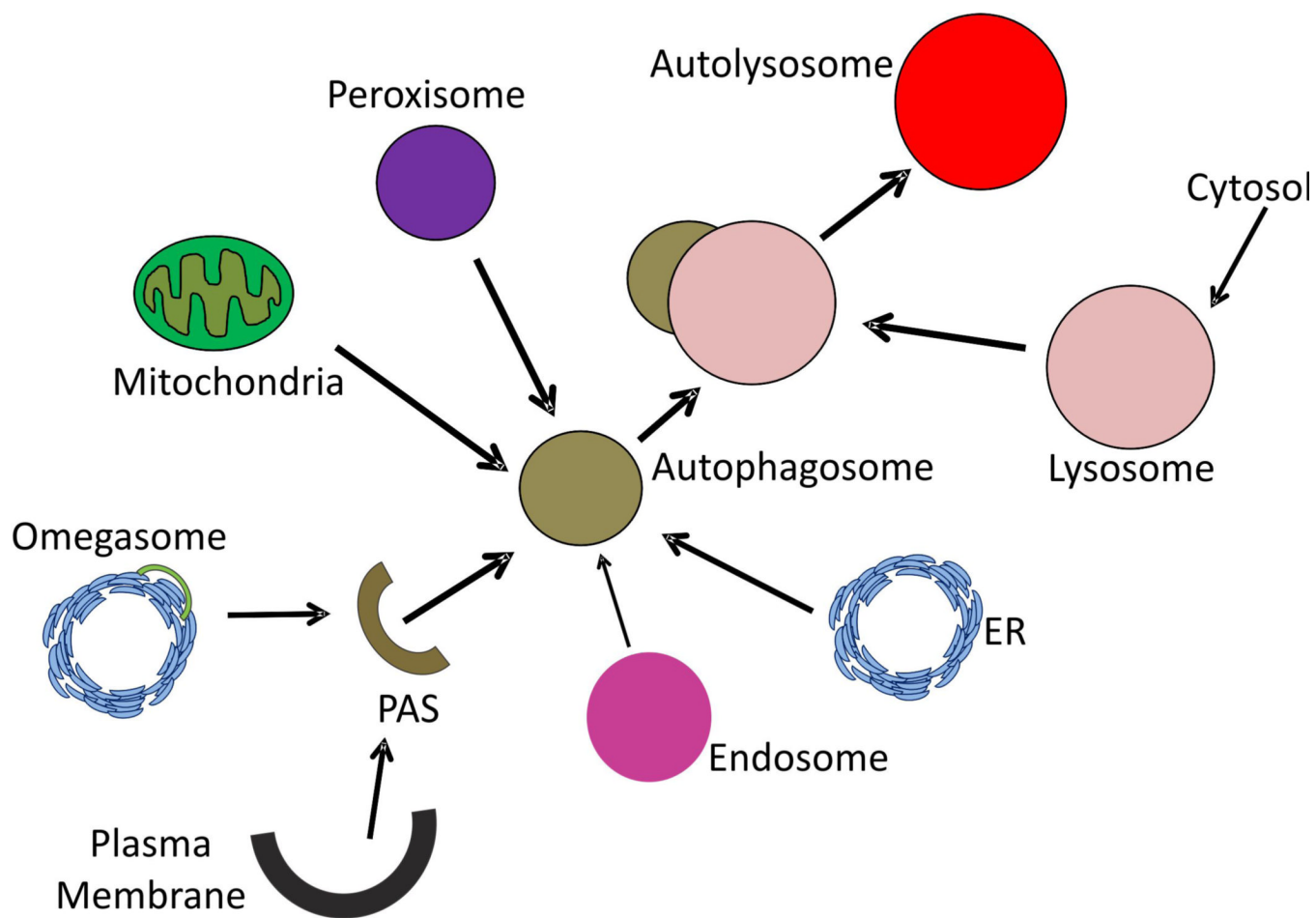
Figure 31. Autophagosome interactions
PAS = preautophagosomal structure.

Figure 32. Different routes of endocytosis and phagocytosis in mammalian cells
These are: macropinocytosis, clathrin-coated vesicles, and caveolae. There are multiple proteins associated with the endocytic organelles such as Rab5 in early endosomes, Rab7 in late endosomes, and LAMP-1 and LAMP-2 in the lysosomes. Additional information shown in Figure 2 from referece 415. Reprinted with permission from reference 415. Copyright 2006 Nature Publishing Group.
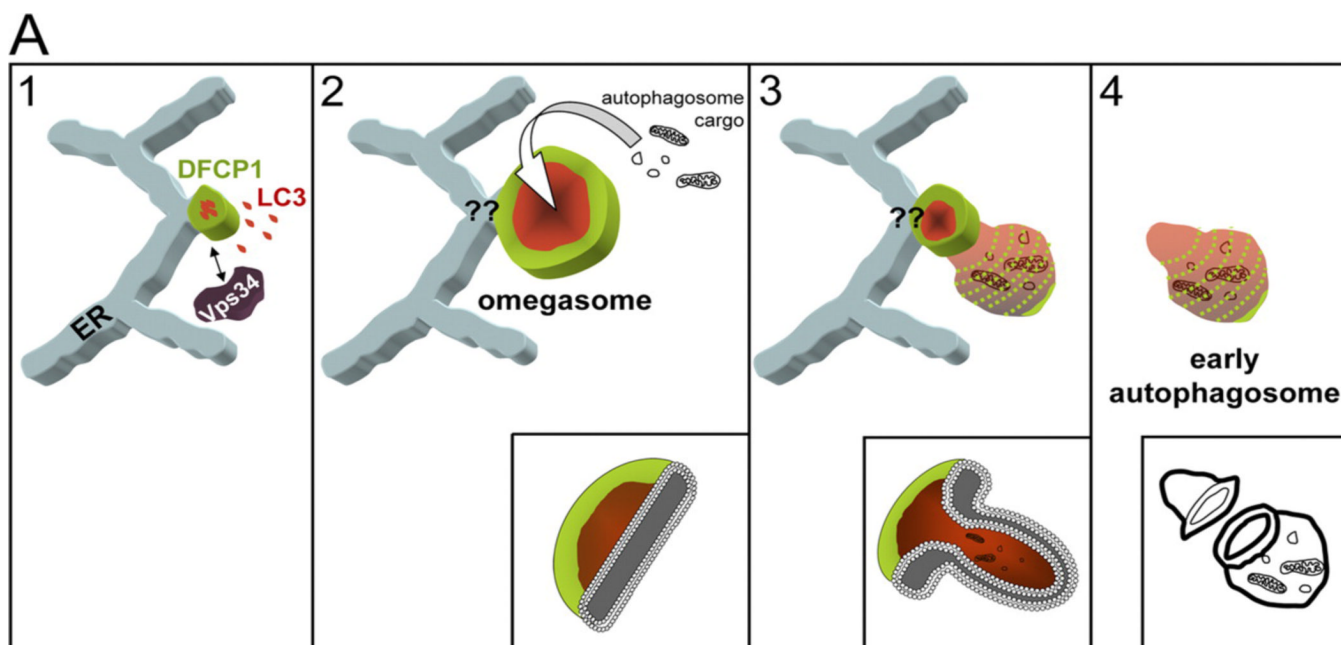
Figure 33. Genesis of the Autophagosome from the omegasome in the endoplasmic reticulum
Additional information shown in Figure 9 from reference 439a. Reprinted with permission from Reference 439a. This is an open-access article distributed under the terms of the Creative Commons Attribution License. No Copyright form was needed.
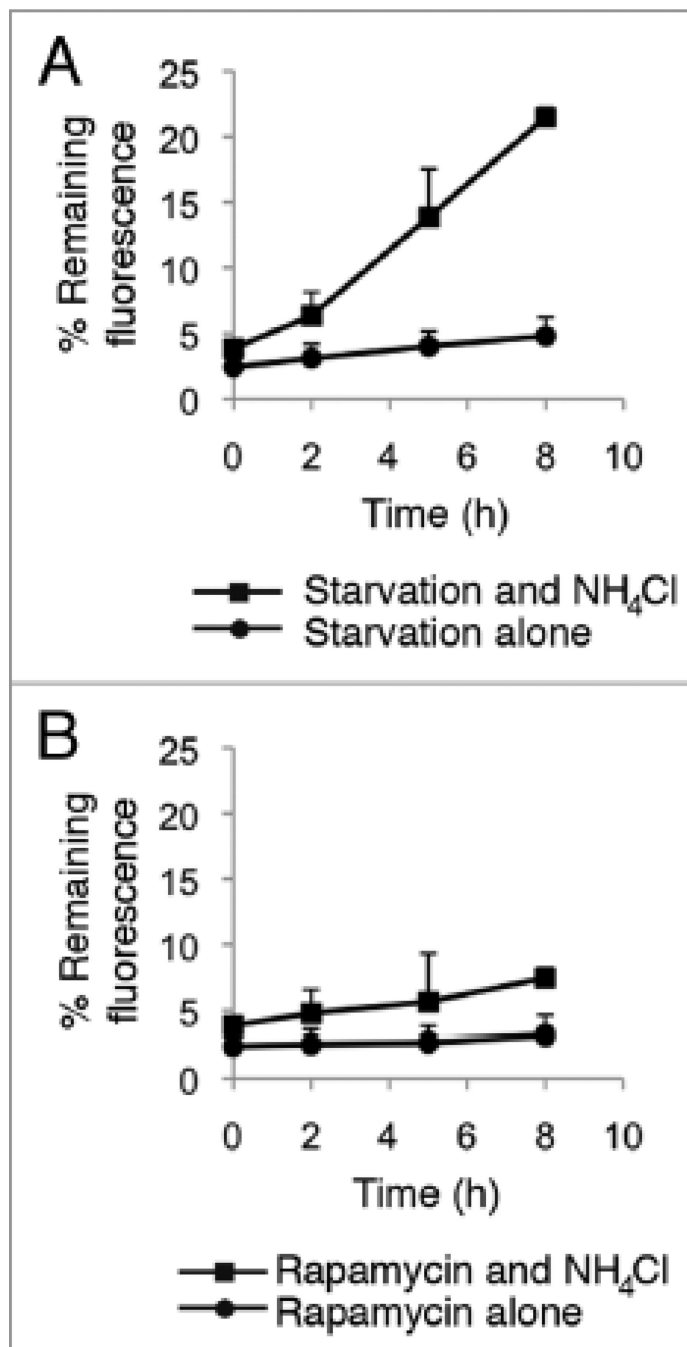
Figure 34. Assessment of autophagic flux by flow cytometry
A. Starvation induces GFP-LC3-II formation. **B**. Rapamycin treatment has minimal effect on GFP-LC3-II formation. The y-axis shows the GFP-LC3-II fluorescence remaining after treating cells with saponin. Ammonium chloride treatment inhibits autophagy progression. Other conditions are reported in Figure 2 from reference 441. Reprinted with permission from reference 441.
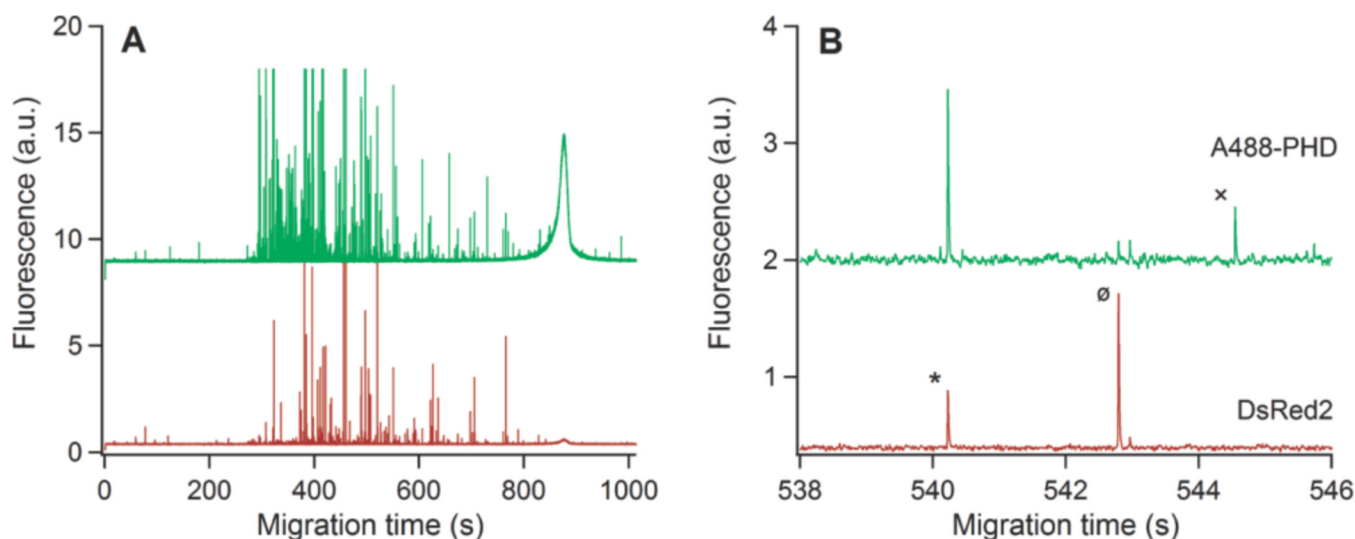
Figure 35. Heterogeneity in the binding of mitochondria and cytoskeleton
A.Capillary electrophoresis with laser induced fluorescence detection showed that isolated organelles appear in an electropherogram as spikes of associated with the highly variable levels of DsRed2 (expressed in mitochondrial matrix) and Alexa488-phalloidin that labes the cytoskeleton (bottom and top, respectively). **B**. The migration time window 538–546 s from part A showing representative individually detected events. The detected events are classified as mitochondria interacting with the cytoskeleton (*), mitochondria without the cytoskeleton (ø), and other organelles interacting with the cytoskeleton (×). Other conditions were reported in Figure 3 from reference 558. Reprinted with permission from Kostal, V.; Arriaga, E.A. *Anal. Chem.* **2011**, *83*, 1822. Copyright 2011. American Chemical Society.

Table 1

Organelles covered in this review.

Organelle	Size	Description
Adiposomes (1990s)	20 nm – 1 μm[1]	This is a recently proposed name for lipid droplets. They consist of lipid core (triacylglycerols) surrounded by a phospholipid monolayer. Several proteins are attached to such monolayer. Besides being lipid storage organelles they are involved in lipid metabolism.
Amphisomes (1980s)	822 ± 37 nm[2]	Formed by fusion of an endosome with an autophagosome. See definitions of these organelles below.
Apicoplasts (1990s)	0.15 – 1.5 μm[3]	Non photosynthetic plastids commonly found in Apicomplexa protozoans.
Autophagosomes (1960s)	0.15 – 1.5 μm[4]	Double membrane organelles that encapsulate subcellular regions or organelles and fuse with lysosomes to form an autolysosome, in which their cargos are degraded. This process is also known as macroautophagy and may take specific names according to the target (e.g. mitophagy refers to autophagy of mitochondria). Autophagosomes are particularly involved in cell growth, development, homeostasis, and nutrient replenishment during starvation.
Chloroplasts (1883)	2 – 10 μm[5]	Double membrane organelles responsible for photosynthesis in plants and other eukaryotes that conduct photosynthesis. It has its own genome that encodes for redox proteins used in electron transport during photosynthesis. It uses light, carbon dioxide, and water to produce oxygen and chemical energy stored as ATP and NADPH.
Enlargeosomes (1990s)	80 – 150 nm[6]	Small vesicles released by regulated exocytosis. These organelles do not dock to the plasma membrane. Release of enlargeosomes is stimulated by Ca^{2+}, some esters, or ATP.
Endosomes (1970s)	78 – 500 nm[2,7]	Involved in the internalization of extracellular components into the cell and traffics components to the lysosome for degradation. However, endosomes also recycle material to the plasma membrane (recycling endosomes) and transfer material to the Golgi. Early endosomes are a dynamic tubular-vesicular network. Upon maturation to late endosomes they become more acidic and vesicles aooear in the lumen becoming multi- vesicular bodies that lack tubules. Late endosomes fuse with lysosomes. In plants, late endosomes can also be referred to as multi-vesicular bodies. Recycling endosomes consist mainly of tubular networks that return receptor molecules to the plasma membrane.
Endoplasmic reticulum (1945)	a	Network of interconnected tubules and membrane sheets held together through cytoskeletal contacts. Its membrane is continuous with the outer membrane of the nucleus. When associated with ribosomes (rough ER) it is involved in the folding of recently synthesized proteins. When devoid of ribosomes (smooth ER), it is involved in lipid synthesis, carbohydrate processing and metabolism, detoxification, and calcium regulation.
Exosomes (1980s)	30 – 100 nm[8]	Vesicles secreted by mammalian cells when multi- vesicular bodies (late endosomes) fuse with the plasma membrane. The biological role of exosomes has not been elucidated.
Golgi apparatus (1897)	a	Consists of several stacks of cysternae (membrane enclosed discs). Each region of the stack contains different enzymes responsible for modification of macromolecules prior to sorting to different intra- and extracellular destinations. Proteins transported from the rough endoplasmic reticulum are glycosylated in this organelle. This organelle is also a major site for carbohydrate synthesis and lipid transport.
Lipid droplets (1970s)	b	Also known as lipid bodies. See entry for adiposomes.
Lysosomes (1955)	0.1 – 1.2 [2,9]	Their interior has an acidic pH that is maintained by proton pumps. They contain hydrolases that digest material originating from the endocytic or the autophagy pathways. They are involved in microautophagy and chaperone-mediated autophagy.
Lysosome related organelles (1950s)	c	This broad classification includes lysosomes, melanosomes, platelet dense granules, and neuromelanin granules. They contain lysosomal proteins and cell-type specific molecules.
Melanosome (1960s)	~500 nm[10]	Organelle containing the pigment melanin. They are found in specialized cells such as melanocytes (producers) and keratinocytes (acceptors). They participate in protection against damaging UV radiation.

Organelle	Size	Description
Mitochondria (1840s)	0.5 – 5 μm[11]	Double membrane organelles that exhibit dynamic processes of fusion and fission. Their inner membrane presents a folded morphology (cristae) and is highly impermeable. The outer membrane has pores that allow for the passage of low molecular weight species. They have their own genome that encodes peptides needed for electron transfer and oxidative phosphorylation. They are involved in fatty acid metabolism, calcium homeostasis, and apoptosis.
Nucleus (1680s)	~10 μm[12]	Double membrane organelle with characteristic nuclear pores that allow for transfer of material in and out of this subcellular region that contains most of the genetic material of the cell. Gene regulation and transcription occur in this organelle; they are typically the largest organelles.
Peroxisomes (1954)	~500 nm[13]	Formed *de novo* from the endoplasmic reticulum or replication by fission. Often it has a crystalloid core. Contains enzymes involved in catabolism of fatty acids, polyamines, and D-amino acids. They are also involved in the synthesis of plasmagen, the most abundant lipid in myelin. They produce hydrogen peroxide that is used by peroxidases to oxidize substrates. In plants, they host enzymes needed in the glyoxylate cycle and photorespiration.
Phagosomes (1960s)	0.9 – 3 μm[14]	Vesicle formed by fusion of the plasma membrane around a particle, which is then brought into the cell. These organelles commonly contain bacteria or foreign objects covered with antibodies.
Secretory granules (1920s)	820 ± 16 μm[15]	These structures are secreted by mammalian cells, delivering material to the extracellular space via the process termed degranulation. Other properties are similar to those of exosomes.
Secretory lysosomes (1980s)	similar to lysosomes[16]	These degrade their contents prior to secretion. Other properties are similar to those of exosomes.
Synaptosomes (1960s)	0.5 – 3 μm[17]	Vesicles that form from isolation of the synaptic terminals of neurons. They retain the molecular machinery involved in neurotransmission.

Year of discovery is given under the organelle name.

[a] size not given due to their unique morphology.

[b] see adiposomes.

[c] not given due to the heterogeneity of the organelle type.

Table 2

Topical specialized reviews of organelles.

Title	Section	Topic	Reference
One core, two shells: bacterial and eukaryotic ribosomes	1	Ribosomes	Melnikov, 2012[18]
The centrosome in cells and organisms	1	Centrosome	Bornens, 2012[19]
Centriolar satellites: busy orbits around the centrosome	1	Centriolar satellites	Barenz, 2011[20]
Biogenesis and function of nuclear bodies	1	Nuclear bodies	Mao, 2011[21]
The cop9 signalosome: more than a protease	1	Signalosome	Wei, 2008[22]
Mammalian cop9 signalosome	1	Singalosome	Kato, 2009[23]
Cell biology of prokaryotic organelles	1	Prokaryotic organelles	Murat, 2010[24]
Bacterial microcompartments: Their properties and paradoxes	1	Prokaryotic organelles	Cheng, 2008[25]
Subcellular localization of RNA and proteins in prokaryotes	1	Prokaryotic organelles	Nevo-Dinur, 2012[26]
The centrosome in cells and organisms	1	Centrosomes	Bornens, 2012[19]
Guidelines for the use and interpretation of assays for monitoring autophagy in higher eukaryotes	3.1	Assays	Klionsky, 2008[27]
Autophagy: assays and artifacts	3.1	Assays	Barth, 2010[28]
Cellular and subcellular imaging in live mice using fluorescent proteins	3.2	Technology	Hoffman, 2012[29]
Methods for imaging and analyses of intracellular organelles using fluorescent and luminescent proteins	3.2	Technology	Takeuchi, 2007[30]
The green fluorescent protein	3.2	Fluorescent proteins	Tsien, 1998[31]
Fluorescent labels for proteomics and genomics	3.2	Fluorescent proteins	Waggoner, 2006[32]
Recombinant aequorin and green fluorescent protein as valuable tools in the study of cell signaling	3.2	Fluorescent proteins	Chisea, 2001[33]
Fluorescent protein FRET: the good, the bad and the ugly	3.2	Fluorescent proteins	Piston, 2007[34]
Fluorescent biosensors of protein function	3.2	Fluorescent proteins	Van Englengberg, 2008[35]
Organelle identification and characterization in plant cells: using a combinatorial approach of confocal immunofluorescence and electron microscope	3.3	Technology	Tse, 2009[36]
Advances in cellular, subcellular, and nanoscale imaging in vitro and in vivo	3.3	Technology	Wessels, 2010[37]
Atomic force microscopy as a multifunctional molecular toolbox in nanobiotechnology	3.3	Technology	Muller, 2008[38]
Force probing surfaces of living cells to molecular resolution	3.3	Technology	Muller, 2009[39]
AFM for structure and dynamics of biomembranes	3.3	Technology	Goksu, 2009[40]
Atomic force microscopy: a versatile tool for studying cell morphology, adhesion, and mechanics	3.3	Technology	Franz, 2008[41]
Plant organelle proteomics: collaborating for optimal cell function	4.1	Proteomics	Agrawal, 2011[42]
Feature extraction techniques for protein subcellular localization prediction	4.1	Proteomics	Gao, 2009[43]
Organelle proteomics experimental designs and analysis	4.1	Proteomics	Gatto, 2010[44]
Complementary methods to assist subcellular fractionation in organellar proteomics	4.1	Technology	Gauthier, 2008[45]
Plant cell organelle proteomics in response to abiotic stress	4.1	Proteomics	Hossain, 2012[46]

Title	Section	Topic	Reference
Proteomics meets cell biology: the establishment of subcellular proteomes	4.1	Proteomics	Jung, 2000[47]
Subcellular fractionation methods and strategies for proteomics	4.1	Technology	Lee, 2010[48]
Creation of an antibody-based subcellular protein atlas	4.1	Technology	Lundberg, 2010[49]
Protein lipid modifications in signaling and subcellular targeting	4.1	Proteomics	Sorek, 2009[50]
Evolution of organelle-associated protein profiling	4.1	Technology	Yan, 2009[51]
Recent progress in predicting protein sub-subcellular locations	4.1	Proteomics	Du, 2011[52]
Prediction of subcellular locations of proteins: where to proceed?	4.1	Proteomics	Imai 2010[53]
Trends in ultrasensitive proteomics	4.1	Proteomics	Altelaar, 2012[54]
Metabolomics of oxidative stress in recent studies of endogenous and exogenously administered intermediate metabolites	4.2	ROS and oxidative stress	Liu, 2011[55]
Biological applications of x-ray fluorescence microscopy: exploring the subcellular topography and speciation of transition metals	4.2	Metal Composition	Fahrni, 2007[56]
Global analysis of cellular lipidomes directly from crude extracts of biological samples by ESI mass spectrometry	4.3	Lipidome	Han & Gross, 2003[57]
Lipidomics in tissues, cells and subcellular compartments	4.3	Lipidome	Horn, 2012[58]
Brain uptake and utilization of fatty acids, lipids, and lipoproteins: application to neurological disorders	4.3	Lipids-brain	Hamilton, 2007[59]
Lipids and lipid domains in the peroxisomal membrane of the yeast *yarrowia lipolytica*	4.3	peroxisome lipids	Bouhk-Viner, 2006[60]
Lipid signaling on the mitochondrial surface	4.3	Mitochondria lipids	Huang, 2009[61]
The dynamic roles of intracellular lipid droplets: from archaea to mammals	4.3	Lipid droplets	Murphy, 2012[62]
Oxidative stress, mitochondrial bioenergetics, and cardiolipin in aging	4.3	Mitochondria lipids	Paradies, 2010[63]
Lipidomics era: accomplishments and challenges	4.3	Lipidomics	Bou Khalil, 2009[64]
MALDI imaging of lipid biochemistry in tissues by mass spectrometry	4.3	Lipidomics	Zemski Berry, 2011[65]
Bioinformatics and systems biology of the lipidome	4.3	Lipidomics	Subramaniam, 2011[66]
Modeling kinetics of subcellular disposition of chemicals	4.4	Xenobiotics	Balaz, 2009[67]
Subcellular neuropharmacology: the importance of intracellular targeting	4.4	Xenobiotics	Miyashiro, 2009[68]
The subcellular distribution of small molecules: from pharmacokinetics to synthetic biology	4.4	Xenobiotics	Zheng, 2011[69]
Subcellular targeting: a new frontier for drug-loaded pharmaceutical nanocarriers and the concept of the magic bullet	4.4	Xenobiotics	D'Souza, 2009[70]
Quantitative analysis of organelle abundance, morphology and dynamics	5	Interactions	van Zutphen, 2011[71]
Dynamic organization of mitochondria in human heart and in myocardial disease	5	Interactions	Hoppel, 2009[72]
Actin dynamics at the Golgi complex in mammalian cells (organelle interactions)	5.3	Interactions	Egea, 2006[73]
Autophagosome formation and molecular mechanism of autophagy	5.6	Autophagy-ER	Tanida, 2011[74]
Vesicular trafficking and autophagosome formation	5.6	Autophagy	Longatti, 2009[75]
Involvement of members of the rab family and related small GTPases in autophagosome formation and maturation	5.6	Autophagy	Chua, 2011[76]

Title	Section	Topic	Reference
Molecular machinery of macroautophagy and its deregulation in diseases	5.6	Autophagy	Wong, 2011[77]
The role of ATG proteins in autophagosome formation	5.6	Autophagy	Mizushima, 2011[78]
Mechanisms of autophagy and pexophagy in yeasts	5.6	Autophagy-peroxisomes	Sibirny, 2011[79]
Peroxisomes as dynamic organelles: autophagic degradation	5.6	Autophagy-peroxisomes	Oku, 2010[80]
Molecular mechanism and physiological role of pexophagy	5.6	Autophagy-perixosomes	Manjithaya, 2010[81]
Mechanisms of mitophagy	5.6	Autophagy-mitochondria	Youle, 2011[82]
Mitophagy	5.6	Autophagy-mitochondria	Tolkovsky, 2009[83]
Chemical microscopy applied to biological systems	7.1	Heterogeneity	Navratil, 2006[84]
Recent advances in the analysis of biological particles by capillary electrophoresis	7.2	Heterogeneity	Kostal, 2008(Kostal, 2008}
Isolation of subcellular organelles	8.2	Technology	Storrie, 1990[85]
Within the cell: analytical techniques for subcellular analysis	8.2	Technology	Olson, 2005[86]
Subcellular fractionation, electromigration analysis and mapping of organelles	8.2	Technology	Pasquali, 1999[87]
Communicating subcellular distributions	8.4	Technology	Murphy, 2010[88]
Cell organizer: image-derived models of subcellular organization and protein distribution	8.4	Technology	Murphy, 2012[89]

Table 3

Traditional organelle-specific enzyme assays

Organelle	Assay	Reference
Autophagosome	Acid phosphatase & cathepsin D	Marzella, 1982[160]
Autophagosome	Lactate dehydrogenase	Kopitz, 1990[161]
Chloroplast	Phosphoenolpyruvate carboxylase	Uedan, 1976[162]
Chloroplast	Chlorophyllase	Arkus, 2006 [*][163]
Endosome	Cathepsin H	Claus, 1998[164]
Endosome	Cathepsin S	Claus, 1998[164]
Endosome	Horseradish Peroxidase	Pool Jr, 1983[165]
ER	BADPH-Cytochrome C Reductase	Sottocasa, 1967[166]
ER	Glucose-6-Phosphatase	Nordlie, 1966[167]
Golgi	Thiamine pyrophosphatase	Cheetham, 1971[168]
Golgi	α-mannosidase II	Pool Jr, 1983[165]
Lysosome	Acid phosphatase	Barret, 1977[158]
Lysosome	β-galactosidase	Pool Jr, 1983[165]
Lysosome	β-hexosaminidase	Barrett, 1977[158]
Lysosome	Lysosome-specific dipeptidyl peptidase 1	Thong, 2011 [*][169]
Mitochondria	Cytochrome c oxidase	Storrie, 1990[85]
Mitochondria	INT reductase	Pennington, 1961[170]
Mitochondria	Succinate dehydrogenase	Alston, 1977[157]
Nucleus	Histone modifying enzymes	Fischle, 2005[171]
Peroxisome	Catalase	Leighton, 1968[159]
Phagosome	(Biotin-LC-Phe-Arg)$_2$-Rhodamine 110	Yates, 2005[172]
Plasma Membrane	5'-nucleotidase	Howell, 1982[173]
Plasma Membrane	Alkaline phosphodiesterase I	Touster, 1970[174]

Topic included in the manuscript are marked with an asterisk (*).

Table 4

Structures and excitation and emission wavelengths for reviewed fluorescent dyes
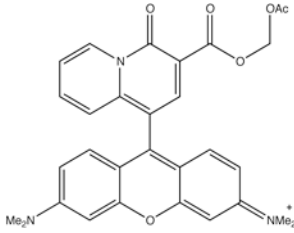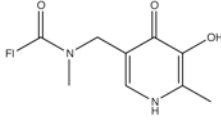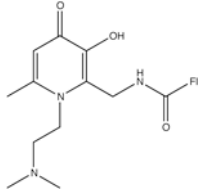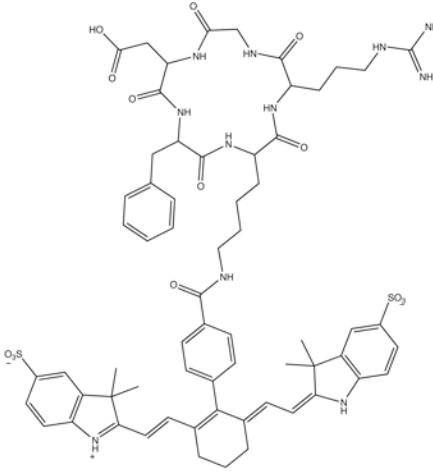
Probe Use	Probe Structure	Excitation (nm)	Emission (nm)	Reference
Mitochondria localized Mg^{+2}		540	590	Shindo, 2011[185a]
Endosome and Lysosome localized Fe^{+3}		494	512	Fakih, 2008[185b]
Endosome and Lysosome localized Fe^{+3}		491	514	Fakih, 2008[185b]
pH-activatable fluorescent probe		785	810	Lee, 2011[184]
Actin imaging	See Figure 2	405	460	Li, 2011[183]
Acidic organelles	See Figure 3	470	525	Lalor, 2008[182]

Table 5

Fluorescent protein properties

Protein name	Excitation maximum (nm)	Emission maximum (nm)	Extinction coefficient (M⁻¹cm⁻¹)	Fluorescent quantum yield	Brightness (% of DsRed)	pK$_a$	Maturation half-life, 37 °C	Photobleaching half-life (s)
DsRed	558	583	75,000	0.79	100	4.7	10 h	ND
T1	555	584	38,000	0.51	33	4.8	<1 h	ND
Dimer2	552	579	69,000	0.69	80	4.9	2 h	ND
mRFP1	584	607	50,000	0.25	21	4.5	<1 h	6.2
mHoney dew	487/504	537/562	17,000	0.12	3	<4.0	ND	5.9
mBanana	540	553	6,000	0.7	7	6.7	1 h	1.4
mOrange	548	562	71,000	0.69	83	6.5	2.5 h	6.4
dTomato	554	581	69,000	0.69	80	4.7	1 h	64
tdTomato	554	581	138,000	0.69	160	4.7	1 h	70
mTangerine	568	585	38,000	0.3	19	5.7	ND	5.1
mStrawberry	574	596	90,000	0.29	44	<4.5	50 min	11
mCherry	587	610	72,000	0.22	27	<4.5	15 min	68

For additional information, please see Table 1 from reference 188. Adapted with permission from reference 188. Copyright 2004 Macmillan Publishers Ltd.

Table 6

STED and PALM imaging used in organelle studies

Organelle	Process studied	Technique	Dye used	Reference
Endosomes	Protein patterns	STED	Atto-532	Donnert, 2006[202]
ER	Dynamics	STED	Citrine FP	Hein, 2008[203]
ER	Integrin receptors	PALM	EosFP	Schtengel, 2008[204]
ER	Morphology	STED	Atto565	Willig, 2006[198]
Lysosomes	Morphology	PALM	Kaede	Betzig, 2006[199]
Mitochondria	Protein clusters	STED	Atto647	Singh, 2012[205]
Mitochondria	Import receptors	STED	Atto532, Atto647	Wurm, 2011[206]
Mitochondria	Cristae	STED	KK114	Schmidt, 2009[207]
Mitochondria	mtDNA nucleoids	STED	Atto532, KK114	Kukat, 2011[208]
Mitochondria	mtDNA nucleoids	PALM	mEos2, Dronpa	Brown, 2011[209]
Mitochondria	Protein complexes	TALM	Halo/TMR	Appelhans, 2011[210]
Mitochondria	Mitochondrial network	3D STORM	A405-Cy5, A488-Cy5, A555-Cy5	Huang, 2008[197b]
Mitochondria	Mitochondrial network	3D PALM	Dronpa	Vaziri, 2008[211]
Mitochondria	Mitochonrial proteins	PALM	mEos, Dronpa, mKikGR, mPA-GFP	Brown, 2010[212]
Mitochondria	Morphology	PALM	dEosFP	Betzig, 2006[199]
Mitochondria	Protein localization	STED, PALM	Citrine, tdEOS, Dendra	Watanabe, 2011[213]
Nucleus	Nuclear lamina	STED	Atto647N	Willig, 2006[198]
Nucleus	Replication foci	STED	Atto647	Cseresnyes, 2009[214]
Nucleus	Protein speckles	STED	Atto-532	Donnert, 2006[202]

Table 7

Proteomic databases relevant to organelle analysis.

Software & Website	Type	Features	Organelles	Reference
LOCATE http://locate.imb.uq.edu.au/	Human and murine subcellular protein localization database	Based entirely on experimental results, MemO (membrane protein prediction), subcellular localization via N-terminal myc tag, and indirect immunofluorescence, Location Proteome (proteins contained within a specific area of the cell based on fluorescence spectroscopy creating a localization tree)	Nucleus, plasma membrane, extracellular, mitochondria, ER, Golgi apparatus, lysosomes, endosomes, cytoplasmic vesicles, peroxisome, cytoskeleton	Sprenger, 2008[262]
iLOC-EUK	Subcellular localization prediction tool for single- or multiple-location eukaryotic proteins	GO (Gene Ontology), SeqEvo (Sequential Evolution) descriptor, Multi-Label KNN (K-Nearest Neighbor) classifier, PseAAC (pseudo amino acid composition)	Acrosome, cell membrane, cell wall, centriole, chloroplast, cyanelle, cytoplasm, cytoskeleton, ER, endosome, extracellular, Golgi apparatus, hydrogenosome, lysosome, melanosome, microsome, mitochondrion, nucleus, peroxisome, spindle pole body, synapse, vacuole	Chou, 2011[263]
Plant-mPLoc http://www.csbio.sjtu.edu.cn/bioinf/plant-multi/	Plant subcellular protein localization prediction tool	GO (Gene Ontology), FunD (Functional Domain) descriptor, SeqEvo (Sequential Evolution) descriptor, OET-KNN (Optimized Evidence-Theoretic K Nearest Neighbor) prediction engine	Cell membrane, cell wall, chloroplast, cytoplasm, ER, Golgi apparatus, mitochondrion, nucleus, peroxisome, plastid, vacuole	Chou, 2010[264]
PepTracker http://www.peptracker.com/	Platform for visualization of the distribution of proteins over subcellular compartments	Storage of quantitative data from MaxQuant, visualization of the data for more efficient data mining, automated analysis of patterns and trends	Nucleus, nucleolus, cytoplasm	Boisvert, 2012[265]

Table 8

Metabolomic databases relevant to organelle analysis.

Database	Focus	Features	Website	Reference
Library and Database of Toxic Compounds	Toxicological substances	Analysis done with LC-QTOF-MS, positive and negative ESI, high accuracy MS; contains over 7500 toxicology-relevant analytes; some standards spiked into either blood or/ and urine matrix	NA	Broecker, 2011[307]
Manchester Metabolomics Database	Serum, urine, yeast intracellular extracts, yeast, placental tissue; overlap with other databases	Accurate ESI-MS spectra, theoretical isotope abundance data, and ion types; 1,065 commercially available compound spectra performed with UPLC-MS and GC-MS; overlap with HMDB, KEGG, LIPID Maps, BioCyc, and DrugBank; provides a total of 42,687 compounds	www.dbkgroup.org/MMD/	Brown 2009[308]
KEGG Database	Encyclopedia of genes and genomics	Provide relevant information on cells, organisms, and organelles; connects gene catalogs to cell function, organism status, and ecosystem; is publically available	www.genome.jp/kegg/	Kanehisa, 2011[309]
FiehnLib GC-MS	Volatile metabolites below 550 Da	Contains GC-MS and some additional LC-MS/MS; it has some overlap with the BioMeta/ KEGG database and the Golm Metabolite Database; supports BinBase	http://fiehnlab.ucdavis.edu/projects/FiehnLib/	Kind, 2009[310]

Database	Focus	Features	Website	Reference
Golm Metabolite Database	Biological active metabolites	GC-MS detection, MS spectra and chromatograms	http://gmd.mpimp-golm.mpg.de/	Kopka, 2004[311]
KNApSAcK	Plant secondary metabolites	Chromatogram peak identification, over 49,000 specie-metabolite relations with over 24,000 metabolites; is publically available	http://kanaya.naist.jp/KNApSAcK/	Oikawa, 2006[312]
BinBase MS Database	Volatile compounds	GC-TOF-MS; contains over 1500 database entries for compounds from 18 species or 3435 samples; links to chemical and biochemical databases; web queries are possible	http://binbase.sourceforge.net	Skogerson, 2011[313]
Yeast Metabolome Database	Yeast small molecules	Contains experimental intracellular and extracellular metabolites detected from both MS and NMR; contains more than 2000 metabolites collected from a literature review of yeast metabolites; mass spectrometry data from over 995 different genes/proteins.	http://www.ymdb.ca/	Jewison, 2012[314]
Plant Metabolome Database	Plant secondary metabolites of plants	Contains primary and secondary metabolites specific to plants; contains more than 1,000 metabolites with three-dimensional structures; chemical information overlap with KEGG and PubChem	http://www.sastra.edu/scbt/pmdb/	Udayakumar, 2012[315]
Chemical Entities of Biological Interest	Small chemical compounds, biological and synthetic	Merger of the IntEnz, Kegg, PDBeChem,	http://www.ebi.ac.uk/chebi/	Degtyarenko, 2008[316]

Database	Focus	Features	Website	Reference
		and ChEMBL databases; contains mass, formulas, structures, and database links; publically available		
Human Metabolome Database	Human metabolites, associated enzymes and transporters, and disease-related properties	Contains metabolites, enzyme responsible for production of metabolites; contains over 6800 entries and 3800 lipids, information pathway, abundance, and disease related properties as well as spectral databases, NMR, LC-MS, and GC-MS data	http://www.hmdb.ca/	Wishart, 2009[317]
National Institute of Standards and Technology	Identify species based on chemical formula	Contains compounds with most prominently electron ionization mass spectrometry data; properties such as thermodynamic data, IR spectrum, mass spectrum, UV/Vis spectrum, and vibrational and electronic energy levels	http://www.nis t.gov/pml/data/index.cfm	Wagner, 2003[318]
METLINE	Endogenous metabolites	Freely accessible database containing high resolution Fourier transform mass spectrometry, tandem mass spectrometry, and LC/MS data	http://metlin.scripps.edu/	Smith, 2005[319]
MASSBANK	Analytes including endogenous metabolites	Contains mass spectral data for many types of compounds; contains primary and secondary metabolites	http://www.massbank.jp/?lang=en	Horai, 2010[320]
Database of Bacterial Lipoproteins	Bacterial lipoproteins	Contains 278 lipoproteins and predicted lipoproteins from bacterial	NA	Babu, 2006[321]

Database	Focus	Features	Website	Reference
		genomes; 773 different lipoproteins from the Swiss-Prot database were identified and grouped into 278 clusters containing protein orthologs; contains information for predicting the molecular function of the lipoprotein.		
LIPIDMaps	Biologically relevant lipids	Contains lipid-associated protein sequences, annotations, and genes associated with lipids; proteins are also classified to associate with the different LIPIDMaps; contains structures, studies from core laboratories, and simulations for appropriate lipids; structures can be searched based on name or structure.	http://www.lipidmaps.org/data/databases.html	Sud, 2007[322]
DrugBank	Drug data and drug information	Contains over 4,100 drugs and 14,000 drug targets; contains drug properties and links to other databases such as PubMed and KEGG	http://www.drugbank.ca/	Wishart, 2006[323]

Table 9

Carbon accumulation in enriched subcellular fractions from barley protoplasts.

Compounds	Total	Cytosol	Chloroplasts	Mitochondria
Glycolate	0.18 ± 0.01	0.17 ± 0.01	0.03 ± 0.01	ND
Glycine	2.38 ± 0.05	1.66 ± 0.09	0.74 ± 0.01	ND
Serine	2.20 ± 0.01	1.68 ± 0.01	0.75 ± 0.13	ND
Malate	1.76 ± 0.01	1.53 ± 0.01	0.06 ± 0.03	0.26 ± 0.04
Aspartate	0.29 ± 0.01	0.17 ± 0.01	0.10 ± 0.01	0.05 ± 0.01
Alanine	0.18 ± 0.01	0.12 ± 0.01	0.07 ± 0.01	ND
Sucrose	1.91 ± 0.11	1.91 ± 0.11	ND	ND
Starch	0.09 ± 0.01	0.02 ± 0.01	0.08 ± 0.01	ND
Other insolubles	0.03 ± 0.01	ND	0.03 ± 0.01	ND
Total	**9.02 ± 0.12**	**7.26 ± 0.14**	**1.86 ± 0.14**	**0.31 ± 0.04**
True photosynthesis	**8.76 ± 0.44**	**ND**	**ND**	**ND**

Values (ng-atom C×(mg choline)$^{-1}$×s^{-1}) are given as average ± SE. For additional information, see Table 3 from reference 324. Reprinted with permission from reference 324. Copyright 2011 Elsevier.

Table 10

Effects of various treatments on mitochondrial function and properties.

Reagent	Oxygen consumption	ROS	Swelling	CC release	SOD1 release	Oxidation of ANT
Ca^{2+}/Pi	+	+	+	+	+	+
Ca^{2+}/Pi + CsA	–	–	–	–	–	–
ADP/Fe^{2+}	+	+	+	+	+	+
ADP/Fe^{2+} + CsA	+	+	+	+	+	+
Valinomycin	+	+	+	+	+	+
FCCP	+	–	–	–	–	–
Arachidonic acid		+	+	+	+	+
Palmitic acid	+	+	+	+	+	+
Rotenone	–	+	–	–	–	–
Antimycin A	–	+	–	–	–	–
KCN	–	+	–	–	–	–

CC = cytochrome c; SOD1 = superoxide dismutase; ANT = adenine nucleotide translocase. For additional information, see Table 1 from reference 333. Reprinted with permission from reference 333. Copyright 2006 Elsevier.

Table 11

Lipid composition of mitochondria from rat brain and cell cultures

Lipid	In vivo (Tissue)			In vitro (Cell Culture)		
	Brain	CT-2A	EPEN	Astrocyte	CT-2A	EPEN
EtnGpl	187.4±12.1	245.9±13.7**	368.4±46.4*	171.4±18.6	163.0±6.5	211.0±16.7
PtdEtn	164.9±10.0	137.3±6.0*	259.4±45.7	85.9±3.4	69.7±3.0**	98.9±2.3*
PlsEtn	22.5±2.2	99.3±7.1**	147.8±21.4**	80.5±15.0	87.5±9.4	106.9±14.4
PakEtn	N.D.	9.3±0.7**	12.4±3.0*	5.0±0.3	5.7±0.1*	5.1±1.1
ChoGpl	129.9±7.7	121.2±3.6	160.0±29.5	168.5±14.2	127.4±13.2*	194.4±15.7
PtdCho	119.6±5.3	81.4±3.4**	127.4±25.4	124.6±10.5	98.1±12.4*	174.3±13.9**
PlsCho	1.2±0.1	19.4±2.1***	11.6±4.8	22.4±4.0	15.8±0.8	9.3±0.8*
PakCho	9.1±3.2	20.4±2.6**	17.0±6.2	21.5±2.1	13.5±0.4*	10.8±1.1**
Cardiolipin	52.7±4.5	26.1±1.0**	13.5±2.7***	28.3±4.3	24.6±3.7	31.1±4.2
PtdIns	9.4±0.8	9.5±2.6	19.4±2.5*	18.5±2.4	18.4±1.6	20.5±3.3
PtdGro	7.1±0.5	9.8±0.5**	16.4±3.6*	7.7±2.6	7.6±1.5	4.7±0.3
CerPCho	5.3±1.2	4.6±0.2	5.8±1.8	9.7±1.4	15.9±3.4	22.1±1.3**
PtdSer	4.6±1.5	9.1±0.6*	10.4±2.0*	17.8±0.4	28.7±5.7	24.1±3.6
LysoPtdCho	2.7±0.6	6.3±0.6**	2.8±0.4	1.5±0.1	2.2±0.4	2.4±0.6
Cer	0.7±0.2	2.3±0.2***	1.7±0.2**	0.9±0.1	1.0±0.5	2.0±0.2**

Healthy brain tissue was isolated from brain C57BL/6J mice. Cancerous tumors were developed by implantation of CT-2A astrocytoma or ependymoblastoma (EPEN) cells in the brain of C57BL/6J mice. Lipid contents are given in nmol/mg of protein (mean ± S.D. n=3. Statistically different values are compared to either brain or astrocyte.

*
$p < 0.05$,

**
$p < 0.01$, and

***
$p < 0.001$.) EtnGpl = ethanolamine glycerosphingolipids, PtdEtn = phosphatidylethanolamine, PlsEtn = plasmenylethanolamine, ChoGpl = choline glycerosphingolipids, PlsCho = plasmenylcholine, PakCho = plasmanylcholine, PtdIns = phosphatidylinositol, PtdGro = phosphatidylglycerol, CerPCho = sphingomyelin, PtdSer = phosphatidylserine, LysoPtdCho = lysophosphatidylcholine, Cer = ceramide. For additional information, please see Table 1 from reference 360c. Reprinted with permission from reference 360c. Copyright 2009 Portland Press Limited.

Table 12

Proteins involved in endocytic organelle interactions

Protein/Compound	Cell Type	Methods	Comments	Ref
Sorting Nexin 27 (SNX27)	HeLa, A431, and NIH 3T3	CFM, WB, KD	Enriched in early endosomes; interacted with *N*-methyl-D-aspartate receptor 2C; knockdown caused decreased endocytosis	Cai, 2011[417]
Vps45, Rab5	C.elegans	CFM, WB, KD	Associated with endosomes; knockdown caused accumulation of morphologically small endosomes; inhibited endocytic flux	Gengyo- Ando, 2007[418]
coatomer protein complex-1, dynamin, actin, anti-retromer subunit antibodies, Rab-GTPases, phosphatidylinositol- 3-phosphate, and early endosomal autoantigen 1	PC12	CFM, STED	Involved in endosome-vesicle fusion and docking along with the sorting/budding of vesicles	Barysch, 2009[419]
Rubicon, Rab7, UV radiation resistance- associated gene protein (UVARG),	293T	CFM, WB, KD	Rubicon expression increase caused a decrease in endosome interactions; rubicon interacted with Rab7 and UVRAG to regulate Rab7 activation	Sun, 2010 [420]
Mucolipin 3	APRE-19	CFM, KD	KD of mucolipin 3 increased calcium concentration, decreased pH, and increased endosome fusion	Lelouvier, 2011[421]
Rab5	COS1,HeLa, rat kidney cells	CFM, KD	Mutation of Rab5 caused three different types of endosomes, one of which were giant endosomes which were stimulated to reform late endosomes and lysosomes; Rab5 may be needed for late endosome and lysosome formation	Hirota, 2007[422]
Rab5	HeLa	CFM	Diphtheria toxin caused increased size of early endosomes by preventing either Rab5 loss or early endosome fusion, increased endosome acidity, and prevented increased size of endosome suggesting that early endosomes were affected	Antignani, 2008[423]
Tre-2/Bub2/Cdcl6-2 (TBC-2)	C. elegans	CFM, KD	TBC-2 is Rab GTPase protein for Rab5 and Rab7 protein; its mutations caused morphologically large Rab57 positive late endosomes; it had the same phenotype as Rab5 mutation; likely it regulated lysosome and late endosome interactions	Chotard, 2010[424]
Cullin-3	A549	CFM, TEM, WB, KD	Cullin-3 KD caused incomplete fusion of late endosomes with other	Huotari,2012[425]

Protein/Compound	Cell Type	Methods	Comments	Ref
			vesicles, and increased numbers of lysosomes and late endosomes; morphologically larger late endosomes, needed for late endosome interaction	
Monl-Cczl	Yeast	CFM, ivFA, WB, KD	Monl-Cczl complex was dependent on Vps21 and Vps8, facilitated late endosome maturation, and worked as a guanine exchange factor specific for Rab7	Nordmann, 2010[426]
D12	NIH3&3 and HEK293	CFM, WB, KD	SNARE protein localized in the ER and vesicles with ER and Golgi properties; D12 suppression caused an increase of lipofuscin granules which were a result of decreased mitophagy; interacted with VAMP7, a known SNARE for endosomes; appeared involved in late endosome-lysosome interactions	Okumura, 2006[427]
Arf-like GTPase 8 (Arl8)	C. elegans	CFM, KD	Decreased Arl8 levels; caused decreased lysosome mobility and caused decreased late endosome-lysosome interactions; produced morphologically smaller late endosomes and lysosomes; may be a SNARE	Nakae, 2010[428]
Vps3 and Vps8	Yeast	CFM, ivFA, KD	Identified as endosome tethering complex included with class C core vacuole/endosome tethering complexes; needed for late endosome and lysosome interactions; mutations caused loss of acidity and lack of fusion	Peplowska, 2007[387]
Late endosome/lysosome membrane adaptor pl8	Mouse embryonic fibroblasts	CFM, WB, KD	KD of pl8 caused defects in endosome dynamics, abnormal morphology of late endosomes and lysosomes, and accumulation of late endosomes; needed for late endosome-lysosome interactions	Takahashi, 2012[429]
Atl8	U937	CFM, FC, WB, KD	KD of Arl8b caused decreased endocytic flux and decrease in lysosome interactions; Arl8b recruited Vps41 HOPS complex likely to facilitate endocytic delivery	Garg, 2011[430]

TEM = Transmission electron microscopy; CFM = Confocal fluorescence microscopy; WB = Western blotting; KD = knock-downs; *ivFA-in vitro* fusion assays; FC = flow cytometry.

Table 13

Proteins involved in autophagosome maturation and interactions.

Protein	Cell type	Techniques	Role	Reference
TECPR1	HER293	TEM, CFM, WB, KD	Recruited Atgl2-Atg5 to the autophagosome membrane; the formed complex then bound to phosphatidylinositol 3-phosphate; the complex was essential for fusion between autophagosomes and lysosomes	Chen, 2012[444]
UVRAG	HeLa and TCT116	TEM &WB, KD	Bound to either Beclinl or C-Vps, stimulated autophagosome interaction with either lysosomes or endosomes, was responsible for Rab7 localization.	Liang, 2008[445]
HDAC6	HDAC6	TEM, CFM, WB, KD	Knockdown of HDAC6 caused accumulation of ubiquitin-labeled protein and an increase in autophagosome formation	Lee, 2010[446]
OTALI	NIH3T3, COS-7, MEF	TEM, CFM, WB, KD	OTAL1 was a GAP protein, bound with Atg8 which is a known autophagosome protein; GFP-OTAL1 was also in the cytosol and Golgi; OTAL1 bound to Rab33b which was required for autophagosome-lysosome interaction	Itoh, 2011[447]
Hsc70	NIH3T3, RALA255-10G	CFM, TEM	Hsc70-positive lysosomes interacted less with autophagosomes; these lysosomes appeared prevalent in CMA; the interaction was also ATP, GTP, temperature, and lysosomal pH-sensitive	Koga, 2010[448]
Vps4, Fabl	*D. melongaster*	CFM, TEM, KD	Vps4 KD resulted in autophagosome accumulation; loss of Fabl functionality resulted in loss of interaction with lysosomes	Rusten, 2007[388a]
B'-COP, β-COP, and α-COP	HeLa, HEK293A	CFM, TEM, WB, KD	COPI protein knockdown (consisting of B'-COP, β-COP, and α-COP) caused decrease in autophagosome-lysosome formation, an increase in autophagosome number, and disruption of endosome pathway	Razi,2009g[388b]

TEM = Transmission electron microscopy; CFM = Confocal fluorescence microscopy; WB = Western blotting; KD = knockdowns.

Table 14

Proteins involved in phagosome interactions.

Protein	Cell Type	Phagocytosed	Methods	Results	Ref
Ezrin and Arp2/3	RAW264.7	Avidin-coated latex beads	TEM, CFM, KD	Dysfunctional Ezrin reduced actin coating; Ezrin regulated phagosome-lysosome fusion and recruited Arp2/3, which was identified as cytoskeleton-associated protein	Marion, 2011[457]
Surface Protein D (SPD)	Human lung macroph ages	*M. tuberculosis* lipoglycan-coated beads	TEM, CFM	SPD increased interactions between lysosomes and phagosomes; it associated with lipoglycan	Ferguson, 2006[458]
Group V secretory phospholipase A2	Mice peritonea 1 macroph ages	*C. albivans*	CFM, KD	Phagosome-lysosome interaction reduced 50–60% in KD	Balestrieri, 2009[459]
Integrin-β-1	Bone marrow macroph ages	FITC-labeled *E. Coli* and *S. aureus*	CFM, WB	Decreased Integrin-β-l concentration caused reduced lysosome-phagosome interaction; associated with decrease in F-actin accumulation; decreased Racl, Rac2, and Cdc42 caused decrease in integrin1	Wang, 2008[460]
CD63	RAW264.7	*M. tuberculosis*	CFM, WB,	CD63 was increased in interacting lysosomes and phagosomes, a lysosome glycoprotein, RILP, was not incorporated during interaction; *M. tuberculosis-containing* phagosomes may fuse with late endosomes and lysosomes	Seto, 2010[461]
Rab and RILP	J774A.1 and RAW264.7	Live bacillus Camille-Guerin (BCG)	CFM	Phagosomes with latex beads were associated with Rab7 and RILP; phagosomes with BCG had reduced Rab7 and RILP levels, and increased levels of a Rab7 GAP inactivating factor	Sun, 2007,[462]
Acid sphingomye linase(ASM)	Peritonea l and mouse embryonic fibroblasts	*L. monocytogenes*	WB, CFM, KD	ASM found in endosomes, lysosomes, and phagosomes; KD of ASM caused decrease in phagosome-lysosome interaction and increased mannose-6-phosphate and Rab7 localization to the phagosome; decreased phagosome acidity	Schramm, 2008[463]
Tyrosine kinase VSK3	*D. discoideu m*	Protein G- labeled beads	CFM, TEM, KD	KD of VSK3 reduced fusion between endocytic organelles	Fang, 2007[464]

Protein	Cell Type	Phagocytosed	Methods	Results	Ref
				and decreased interaction between lysosomes with phagosomes	
Rab7 and Rab- interacting lysosomal protein (RILP)	C57BI.6J	*B. abortus*	CFM, KD	KD of Rab7 and increase of RILP caused decrease in interaction of phagosomes with late endosomes and lysosomes	Starr, 2008[465]
NSF-SNARE	J774E and HeLa	*S.typhimurium*	CFM, KD	Endosome-phagosome interaction required ATP and NSF SNARE; phagosomes contained Rab5 and EEA1	Parashu raman, 2010[466]
LIMP-2	CHO, mouse embryonic fibroblasts	*L. monocytogenes*	CFM, WB, KD,	LIMP2 KD caused decreased phagosome-lysosome interaction	Carrasco-Marin, 2011[467]
Toll-like receptor 2	RAW264.7	BSA-labeled microspheres	CFM, TEM, KD	TLR triggers LC3 recruitment to phagosomes; mediated by Atg5, Atg7, Beclinl, and phosphoinositol-3-kinase; Atg5 and PI3K KD decreased interaction of phagosomes and autophagosomes; TLR protein increase caused increased lysosome-phagosome colocalization	Sanjuan, 2007[468]
Ark and Sar1	U937.1	*L. pneumophilia*	TEM, KD	Phagosome-ER interactions were decreased with knockdown of ADP ribosylation factor protein and Sar1 proteins (a GTPase)	Robinson, 2006[469]

TEM = Transmission electron microscopy; CFM = Confocal fluorescence microscopy; WB = Western blotting; KD = knock-downs; *iVFA- in vitro* fusion assays; FC = flow cytometry.

Reports on organelle function.

Table 15

Enzyme	Function	Organelle	Organism	Analysis	Observations	Reference
Ascorbate oxidase (AAO)	Produces dehydroascorbate	Chloroplast, cytosol, cell walls	C.linumm	TEM		Caputo, 2010[480]
Phenylalanine ammonia-lyase (PAL), cinnamate-4-hydroxylase (C4H), and 4-coumaratexoenzy me A ligase (4CL)	Phenylalanine metabolism	Chloropal st, nucleus, cell wall	A.thaliana	CFM	PAL was found in cell walls, C4H in the chloroplast and nucleus, and 4CL in secondary cell walls.	Chen, 2006[481]
Ethylene-Dependent Gravitropism-Deficient and Yellow-Green 1	Regulated intramembrane proteolysis	Chloroplast	A.thaliana	CFM	new protease observed in chloroplast	Chen, 2012[482]
NADPH thioredoxin reductase C (NTRC)	Regulation of chloroplast 2-Cys peroxiredoxin	Chloroplast	A.thaliana	WB, MS	KD of NTRC caused oxidized 2-Cys peroxiredoxin	Kirchsteiger, 2009[483]
Melanocorin-4 receptor	Trans-membrane G protein	ER	N2A, GT1-7, HEK293	CFM	All four variants of the melanocorin-4-receptor were found in the ER	Granell, 2010[484]
β-mannosidase 1 hydrolases(MANI)	N-glycan modification	ER, Golgi	A.thaliana	CFM	MANIaand MANIb were expressed in the ER-Golgi apparatus	Kajiura, 2011[485]
Phospholipase A_2	Hydrolyzes phospholipids at sn-2	ER, Golgi	Tobacco epiderma l cells	TEM, WB	PLA2 was localized in both the Golgi and ER	Kim, 2011[486]
Aspartate N-acetyltransferase (NAT8L)	Produce N-acetylaspartate	ER	CHO	CFM	irregular colocalization was observed due to the heterogeneity of the ER	Tahay, 2012[487]
Nuclear Respiratory Factor 1 and 2	Leucine zipper protein	ER	COS-7, HeLa, NIH-3T3, 293-HEK	CFM	increased with increased ER stress	Wang, 2006[488]
Cytochrome P450 monooxygenase 1A1	Oxidize organic compounds	Mitochondria	C57GL/6l mice	WB, CFM	CYP1A1 was also present in microsomal fractions; not detected in the cytosol	Dong, 2009[489]
ATP-binding cassette transporters and Cytochrome P450s	Transport of substrates for cytochrome P450	Mitochondria	Humanbrain	TEM, WB	CYP2D6, CYP2J2, CYO2U1, and CYP46A1 were localized mitochondria	Dutheil, 2009[490]
Methionine sulfoxide reductase A(MSRA)	Oxidative stress regulation	Mitochondria, cytosol	Mouse embryonic stem cells	CFM	GFP-MSRA primarily localized in the mitochondria and partly in the cytosol	Jia, 2011[491]
Malate dehydrogenase (MDHs)	Reversibly catalyzes malate to oxaloacetate	Mitochondria, glycosome, cytosol	L.Mexicana promastigotes	CFM		Leroux, 2006[492]
Glutamate dehydrogenase 1 and 2(GDH)	Nitrogen and glutamate metabolism	Mitochondria, ER	COS7, HEK293, 5Y, HeLa, CHO	CFM, WB	GDH 1 and 2 were localized primarily in the mitochondria and partly in the ER	Mastorodemos, 2009[493]
Superoxide dismutase (SOD) dismutase (SOD) xand thioredoxin- dependent peroxidase (TCP)	Antioxidant function	Mitochondria, apicoplast	T. gondii	CFM, TEM		Pino, 2007[494]
MondoA and Max- like BHLHZip	Helix-loop- helix	Mitochondria	K562 and C2C12	CFM, WB	MondoA and Mix were present	Sans, 2006[495]

Enzyme	Function	Organelle	Organism	Analysis	Observations	Reference
	leucine zipper protein				in the outer mitochondrial membrane; MondoA localized between the mitochondria and the nucleus	
Antiquitin	Aldehyde dehydrogenase, oxidative stress response protein	Mitochondria, cytosol	HEK293	CFM, WB		Wong, 2010[496]
Alcohol dehydrogenase (ALCD)and aldehyde dehydrogenase (ALDD)	Convert alcohols to aldehydes or ketones	Mitochondria, cytosol	E. gracillis	Assays	ALCD and ALDD were in the inner membrane of the mitochondrial; they had low levels in the cytosol	Yoval-sanchez 2011[497]
Fatty acid synthase (FAS)and long-chain fatty acyl-CoA synthetase (ASCL)	Synthesize long-chain fatty acids; esterification of long-chain fatty acids	Mitochondria, cytosol, nucleus	M.avellanarius	TEM	FAS levels were higher in the cytosol than in mitochondria or nucleus; ASCL was evenly distributed	Suozzi, 2009[498]
NAD⁺-dependent sorbitol dehydrogenase (NAD-SDH)	Sorbitol metabolism	Chloroplast, cytosol, vacuoles	M. domestic a	WB, CFM	In leaves NAD-SDH was in cytosol, chloroplast, and vacuoles; in the fruit it was in the cytosol and chloroplasts	Wang, 2009[499]
Short-chain dehydrogenase/reductase	Oxidoreductases of sugars, steroids, retinoids, fatty acids, and xenobiotics	Peroxisomes	HEK-293	CFM	C-terminus GFP fusion construct was found in mitochondria	Kowalik, 2009[500]
Metallothionein-3 (MT3)	Neurotransmitter inhibitory factor; supplies zinc	Lysosomes	Mice astrocytes	CFM	KD of MT3 increased glycosylation of lysosomal proteins and autophagy flux	Lee, 2010[501]
Invadolysin	Metalloprotease	Lipid droplets	A375, C32, HCL (human melanoma) cells	CFM		Cobbe, 2009[502]
Protein disulfide isomerase	Isomerizes disulfide bonds; modulates oxidation	ER and Golgi	A.thaliana	CFM, TEM	KD caused enlargement of protein storage vacuoles	Ondzighi, 2008[503]
Tissue Transglutamase	Covalent intra or intermolecular (glutamyl)lysine and (glutamyl)poly amine cross-links	ER	SH-SY5Y	CFM, TEM	Its abundance was doubled in Parkinson's-induced phenotype	Verhaar, 2012[504]
Gupl	Cellular growth	ER and Golgi	S. cerevisiae	CFM, TEM	over-expression caused increased ER localization, caused ER and Golgi expansion	Bleve, 2011[505]
Small heat shock proteins	Accumulate in plants, protect ER proteins from heat-induced damage	ER	Lesculentum	WB	over-expression prevented tunicamycin A- stimulated ER stress	Zhao, 2007[506]
α/β; hydrolases domain-containing protein 5 (Abhd5) and muscle lipid droplet protein (Mldp)	Facilitation of triglyceride storage	Lipid droplets	3T3-L1 and COS-7	CFM	increased interaction between Abhd5 and Mldp observed when cells exposed to oleic acid	Grannemann, 2009[507]
α-ketoglutaric acid dehydrogenase complex, succinate dehydrogenase, malate dehydrogenase	Produce energy from carbohydrate, fat, and protein degradation	Mitochondria	Humanbrain	Assays	In schizophrenia patients, aconitase and KGDHC activity decreased slightly, SDH and MDH activities slightly increased	Bubber, 2011[508]
Complex 1 and Glyceraldehyde 3-phosphate dehydrogenase	NAD oxidation	Mitochondria	A. thaliana	GE, Assays	Inhibition of Complex 1 caused changes in the proteome of mitochondria;	Garnier, 2008[509]

Enzyme	Function	Organelle	Organism	Analysis	Observations	Reference
Peroxisome proliferator- activated receptor γ (PPARγ) cofactor Iα	Impacts muscle metabolism and exercise capacity	Mitochondria	Mouse skeletal muscle	CFM, TEM, assay	had decreased activity of GAPDHand fructose bisphosphate aldolase	Geng, 2010[510]
Peroxisome proliferator- activated receptor γ (PPARγ) cofactor Iα	Impacts muscle metabolism and exercise capacity	Mitochondria	C57BL-6	WB	KD of (PPARγ) cofactor Iα decreased exercise-induced expression of mitochondria cytochrome oxidase IV and cytochrome c, and platelet endothelial cell adhesion molecule 1	Lu, 2010[511]
PTEN-induced putative kinase 1 (PINK)	Phosphorylation of proteins	Mitochondria	Human fibroblasts	CFM, TEM, assay	KD of (PPARγ) cofactor Iα decreased expression of superoxide dismutase 2 and thioredoxin	Grunewald, 2009[512]
F1FO ATP synthase	Synthesis of ATP	Mitochondria	C. reinhardtii	Res, assay	KD of PINK caused changed in activity of Complex I-IV, s wollen mitochondria and more fragmented mitochondria	Lapaille, 2010[513]
His-DHFR tag 2	Histidine triad hydrolase enzyme	Mitochondria	H295	WB, assay, SF	KD of FIFO ATP synthase caused decreased respiration rate and decreased activities of Complex 1 and II	Lenglet, 2008[514]
PsTrxol, Mn- superoxide dismutase (Mn- SOD), peroxiredoxin (PrxII F), alternative oxidase (AOX)	Redox regulation	Mitochondria	P. sativum	WB, Assay	KD of Hint2 caused reduced steroid production and increased calcium flux	Marti, 2011[515]
Purple acid phosphatase 2	Carbohydrate metabolism	Mitochondria, chloroplasts	A. thaliana	CFM, WB, LC-MS	Osmotic stress increased alternative oxidase activity, lipid peroxidation and protein oxidation; increase in thioredoxin activity decreased levels of Mn-SOD, PrxII F, Trxol, and AOX.	Sun, 2012[516]
Hexose kinase II	Maintain concentration gradient for glucose transport	Mitochondria	Mice cardiac muscle	CFM, WB, Res	over-expression increased sucrose and hexose contents in whole cell homogenate	Wu, 2011[517]
Calcium- independent phospholipase A2γ	Conversion of phospholipids to lysophospholipids	Mitochondria	Mice	MS, Res	over-expression lowered the mitochondrial membrane potential	Mancuso, 2007[518]
Sirtuin-2.1	NAD+ histone deacetylase	Nucleus	C. elegans	CFM	KD of this enzyme decreased cardiolipin levels and respiration	Dickinson, 2011[519]
Ataxin Type 3	Transcriptional repressor; deubiquitinase	Nucleus	HEK-293 and HeLa	CFM, WB	Increased expression reduced ROS concentration	Reina, 2010[520]
Cytosolic phospholipase A2α	Cleaves arachidonic acid from membranes	Nucleus	Human cholangio carcinom a cells	WB, Assay	activity was stimulated in response to heat shock and oxidative stress; KD sensitive to heat shock	Han, 2008[521]
Hydroxia-inducible factor	Regulate gene expression	Peroxisomes	Fisher 344 rats and hepatocy te cells	TEM, WB, CFM	activated β-catenin, KD decreased nuclear transcription	Khan, 2006[522]
Caveolin T	Lipid regeneration	Peroxiso mes	Winstar rats	CFM, WB	hypoxia caused localization to peroxisome	Wouden berg, 2010[523]
					KD of caveolin T modified peroxisome morphology	

Enzyme	Function	Organelle	Organism	Analysis	Observations	Reference
Protein kinase c	Protein phosphorylation	Golgi, ER, Nuclear envelope (NE), plasma membrane	MCF-*7* and cos-*7*	WB, CFM	when signal transduction was stimulated, it was present in the plasma membrane and NE; under starvation it was present at the NE	Maissel, 2006[524]
VAMP27	SNARE	Early endosomes and vacuoles	*A.thaliana*	CFM	it interacted with Syp22, Syp51, and VTI11	Ebine, 2008[525]

TEM = Transmission electron microscopy; CFM = Confocal fluorescence microscopy; WB = Western blotting; KD = knock-downs; Assays = Spectrophotometric assays; GE = Gel electrophoresis, Res = respirometry; SF = spectrofluorimetry; GC-FID = gas chromatography coupled to flame ionization detection; LC-MS = liquid chromatography coupled to mass spectrometry detection; MS = mass spectrometry.